UNIVERSITY OF NEUCHÂTEL

CENTRE OF HYDROGEOLOGY

Deterministic models of groundwater age, life expectancy and transit time distributions in advective-dispersive systems

PhD thesis presented to the faculty of Sciences of the University of Neuchâtel
to satisfy the requirements of the degree of Doctor of Philosophy in Science

By

Fabien Cornaton

Thesis Jury Defence Date: 5 December 2003
Public Presentation Date: 6 February 2004

Professor Pierre Perrochet, University of Neuchâtel, Switzerland

Professor Olivier Besson, University of Neuchâtel, Switzerland

Professor Hans-Jörg Diersch, Wasy Institute, Berlin, Germany

Professor Edward Sudicky, University of Waterloo, Ontario, Canada

IMPRIMATUR POUR LA THESE

Deterministic models of groundwater age, life expectancy and transit time distributions in advective-dispersive systems

M. Fabien CORNATON

UNIVERSITE DE NEUCHATEL

FACULTE DES SCIENCES

La Faculté des sciences de l'Université de Neuchâtel, sur le rapport des membres du jury

MM. P. Perrochet (directeur de thèse), O. Besson, H. Diersch (Berlin D) et E. Sudicky (Waterloo Canada)

autorise l'impression de la présente thèse.

Neuchâtel, le 6 janvier 2004

La doyenne:

Martine Rahier

ABSTRACT

The main objective of this dissertation consisted in the elaboration of a methodology to determine reservoir groundwater age, life expectancy, and transit time probability distributions in a deterministic manner, considering advective-dispersive transport in steady velocity fields.

In the first section, it is shown that by modelling the statistical distribution of groundwater age at aquifer scale by means of the classical advection-dispersion equation (ADE) for a conservative and non-reactive tracer, associated to proper boundary conditions, the obtained function corresponds to the density of probability of the random variable age, defined as the time elapsed since the water particles entered the aquifer. In a second step, the evaluation of the life expectancy, being the time remaining before a water particle leaves the aquifer was derived from an adjoint backward model, yielding the life expectancy distribution. The convolution of these two distributions (age and life expectancy) is then shown to correspond to the groundwater total transit time distribution, from inlet to outlet, and is fully defined for the entire aquifer domain. From the ADEs simulating the full distributions of age and life expectancy, moment averaged equations are defined, like e.g. the well-known mean age equation. The mathematical models developed in the first section are illustrated by two-dimensional numerical experiments based on a scaled groundwater simulator model.

In the second section, the focus is directed towards the reservoir theory (RT). An accurate and efficient method is presented to simulate the transit time distribution at discharge zones. It was shown that for systems with a known internal age probability distribution, the application of the RT to advective-dispersive aquifer systems allows full definition of the discharge zone transit time distribution. The RT can also be applied to internal life expectancy probabilities, yielding the recharge zone life expectancy distribution. One-, two-, and three-dimensional theoretical examples are presented to illustrate the application of the RT in advective-dispersive systems, and make inferences on the effect of boundary conditions, aquifer structure, and macro-dispersion on age, life expectancy and transit time distributions. Also, the particular case of vertically averaged forward and backward ADEs is developed.

In the last section, the RT is extended to arbitrary aquifer configurations by subdividing the entire flow system into subsystems, treating each of them as a compartment. Transfer of water fluxes within these compartments from recharge zones to a particular discharge zone could then be considered isolated from any other subsystem. Nevertheless, the effects of mixing and interaction with other compartments and dispersion processes are considered in this approach. In this way, the RT was made applicable to any sub-drainage basin of an aquifer of arbitrary complexity. It was then found that the backward transport of the life expectancy to a specific outlet could predict the forward transport of a contaminant introduced anywhere in space. In other words, the concentration breakthrough curve at any particular outlet, which would result from the transport of a unit mass release at any point can be predicted with only one single realization of the life expectancy field. The usefulness of the elaborated method to deal with environmental settings such as the well-head vulnerability and protection problem, or also the problem of underground storage of high-level nuclear waste, is illustrated on two-dimensional synthetic examples.

Finally the work is concluded with a brief summary and with a critical view on the obtained results, as well as possible directions for future investigations.

RÉSUMÉ

L'objectif principal de cette thèse était d'élaborer une méthodologie permettant de déterminer de manière déterministe la distribution statistique de l'âge, de l'espérance de vie, et du temps de transit des particules d'eau souterraine, en considérant les processus d'advection et de dispersion régissant le transport d'eau et de solutés en milieu souterrain, pour des régimes d'écoulement d'eau permanents.

Dans la première partie de ce travail, on démontre que la distribution statistique de la variable aléatoire 'âge' de l'eau souterraine peut être modélisée à l'échelle de l'aquifère à l'aide de l'équation classique d'advection-dispersion pour le transport un traceur conservatif et non réactif, moyennant un jeu de conditions aux limites approprié. L'âge de l'eau souterraine est considéré comme une quantité relative mesurant le temps écoulé dans le réservoir depuis l'entrée des particules d'eau par les zones de recharge, l'âge étant nul à ces limites. La variable aléatoire 'espérance de vie' de l'eau souterraine est définie comme le temps restant aux particules d'eau avant de sortir de l'aquifère par les zones d'exutoire. La distribution de l'espérance de vie est résolue à l'aide d'une équation adjointe, dite d'advection-dispersion « arrière en temps », dont la principale caractéristique est d'opérer sur un champ de vitesses inversées. Finalement, la distribution statistique de la variable 'temps de transit total' (recharge-exutoire) est évaluée en tout point du réservoir en appliquant le principe de convolution aux distributions des variables 'âge' et 'espérance de vie'. A partir des équations régissant le comportement de ces distributions, des équations de moments sont obtenues, comme par exemple l'équation des âges moyens aujourd'hui bien connue. Les modèles mathématiques développés dans cette partie sont illustrés par des expériences numériques en deux dimensions, sur un modèle réduit de système aquifère.

La deuxième partie de cette thèse est dédiée à la généralisation de la théorie des réservoirs aux systèmes advectifs et dispersifs. Il est montré qu'étant donnée la distribution de fréquence interne des âges de l'eau souterraine, l'application de cette théorie permet de définir de manière raffinée la distribution des temps d'arrivée des particules d'eau à un exutoire donné. Il est également montré que la distribution interne des espérances de vie permet de modéliser la distribution des espérances de vie aux zones de recharge. Des exemples théoriques 1D, 2D et 3D sont utilisés afin d'apprécier l'effet des conditions aux limites, de la structure du réservoir et de la dispersion, sur les distributions internes et aux limites de l'âge, de l'espérance de vie et du temps de transit. Le cas spécifique des équations 2D intégrées verticalement est développé pour les équations 'avant' et 'arrière' d'advection-dispersion.

Dans la dernière partie, les résultats de la théorie des réservoirs sont rendus applicables à tout sous-système d'écoulement d'un aquifère de complexité et configuration quelconques, en traitant chacun des sous-systèmes comme un compartiment du système global d'écoulement qu'est l'aquifère. Tout en permettant des interactions entre compartiments par effets de mélange (dispersion, diffusion), les transferts de flux d'eau au travers de ces unités, des zones de recharge jusqu'à des exutoires spécifiques, peuvent être considérés indépendamment. Dans un deuxième temps, il est montré comment le transport « arrière en temps » de l'espérance de vie des particules d'eau pour atteindre un exutoire donné permet de prédire, avec une seule réalisation, la concentration en soluté à laquelle l'on doit s'attendre à cet exutoire si un polluant s'infiltre à n'importe quelle position de l'espace, polluant pouvant subir désintégration et sorption de premier ordre durant son trajet dans le milieu souterrain. L'efficacité de cette approche à traiter des problèmes environnementaux tels que la vulnérabilité et la protection des zones d'alimentation en eau potable, ou encore la problématique actuelle du stockage souterrain de déchets nucléaires, est illustrée à l'aide d'exemples théoriques bidimensionnels.

Ce travail est clôturé par une conclusion générale incluant quelques aspects critiques sur certaines limitations des modèles développés, ainsi que des directions possibles pour de futurs travaux de recherche.

ACKNOWLEDGEMENTS

The risk of forgetting someone when writing such a paragraph is always pending. I would be tempted to skip it, but many people deserve my sincere gratitude. I hope the list of the people I wish to thank will be exhaustive.

I wish I could some day finally be able to give back to Pierre Perrochet all the things he managed to teach me, although I know this task is impossible. So many hours he spent for discussing with me, explaining to me, listening to me, waiting for positive results, but also laughing at me. He put me along the path of an extremely interesting research subject, from which I hope he got back some satisfaction. Even though he has been the only supervisor I have had, he is so far the best. My gratitude is enormous, and I will always recall those funny long nights delighted by so good wines.

CHYN is really a pleasant working environment, due to the people there. So, I must thank all the collaborators of the Centre of Hydrogeology (which has recently been arbitrarily renamed 'Swiss Centre of Hydrogeology', which abbreviates into SCH, which could mean Swiss Helvetica Community, but it is wrong). I thank the CHYN football team with which I could often let off steam. I hope you will win more often after I've left. I would like particularly to thank Laszlo Kiraly and Pierre-Yves Jeannin for all the good discussions we've had about karstic flow modelling. I must say I started to learn how finite elements work by hurting myself in studying Laszlo Kiraly's codes. I also sincerely thank Ray Flynn for the time he spent for me in carrying out the experiments in the scaled groundwater simulator. I thank Ellen Milnes for long discussions and ideas she had about the subject of this thesis, although I have still not finished thanking her. I am also grateful to François Zwahlen, the Director of CHYN, for his extremely good boss capacity, which is determining in many situations, and for the global dynamic he is able to create. I thank Philippe Renard for his constant and open interest in the subjects of quantitative hydrogeology, and for the fruitful discussions we've had together. Thank you Manuel Da Silva, the sunshine of the Institute, and funny François Gainon who cared with attention that the coffee machine was in order (it was very much appreciated in the last stage of the thesis).

Some have left CHYN, but they have been missing. I think of Ze Paulo Monteiro the 'Porto' and Farid Achour the 'Canadian', with whom so many days and nights (mostly nights) were filled with exiting and funny hydrogeological discussions and non-hydrogeological discussions. I thank Darko Simic who helped me a lot when I arrived at CHYN, and Philippe Jordan for having converted into a 'Frouze', but above all for having so nicely calibrated his flow model of the Seeland aquifer.

I must thank Hans-Jörg Diersch from the WASY Institute in Berlin and Olivier Besson from the Institute of Mathematics of the University of Neuchâtel, for the insights I could get from them about aspects of mathematical modelling. I thank Hervé Jourde from the University of Montpellier II for the collaboration we have on fractured reservoir modelling and for his advices.

I am very grateful to Pierre Tissot, Nicolas Baume and Sylvain Müller from the Computing Centre of the University of Neuchâtel, for their considerable help. An enormous thank to Ellen Milnes for another technical but important aspect: reading the document and correcting the English.

Thanks to the friends from Montpellier, Hervé Jourde and Jean-Christophe Tétu, and from Neuchâtel, Fabienne Vuillemier and Sylvain Dürrenmatt, Marc Pinaud 'noir', and Cédric Egger thanks to whom I could go to El Salvador and don't forget some realities of the field. Thanks to Anne Milnes and Thor the Viking alias 'Gammelpotet' for a nice one-week summer holidays.

Hard times have been changed into sweet times, thanks to Ellen who always cared about me, and who has been the only one that could deal with my bad moods, which have sometimes appeared throughout this work.

Finally, I am very grateful to Professors Hans-Jörg Diersch from Berlin, Olivier Besson from Neuchâtel, and Edward Sudicky from Waterloo, who accepted to be members of the jury.

By the way, I will never forget all the hilarious stories around the famous PC26-34 and his double: *Comprenne qui le pourra*.

TABLE OF CONTENTS

NOMENCLATURE

List of abbreviations

ADE	Advection Dispersion Equation
RT	Reservoir Theory
FRT	Forward Reservoir Theory
BRT	Backward Reservoir Theory
LTG	Laplace Transform Galerkin
FLTG	Forward Laplace Transform Galerkin
BLTG	Backward Laplace Transform Galerkin
pdf	probability density function
cdf	cumulative distribution function

Mathematical symbols

Latin symbols

A	random variable 'age', T
E	random variable 'life expectancy', T
T	random variable 'total transit time', T
C_A	age pdf, T^{-1}
C_E	life expectancy pdf, T^{-1}
C_T	total transit time pdf, T^{-1}
C^r	resident concentration
C^f	flux concentration
G_A	age cdf
G_E	life expectancy cdf
G_T	total transit time cdf
$g_{\mathbf{x}}$	travel distance probability, L^{-3}
g_t	travel time probability, T^{-1}
$\hat{C}$	Laplace transform of the function C
t	variable time, T
s	Laplace variable, T^{-1}
D_{m}	molecular diffusion, L^2/T
R	retardation factor
$\mathbf{x}$	space position vector, L
$\mathbf{q}$	fluid flux vector, L/T
v	pore velocity, L/T
$\mathbf{D}$	tensor of macro-dispersion, L^2/T
$\mathbf{J}_U$	total mass flux vector ($U = A$ or E), L/T^2
$\mathbf{J}_U^d$	dispersive flux vector ($U = A$ or E), L/T^2
$\mathbf{n}$	outward normal unit vector
$\mathbf{I}$	identity matrix
$\langle A \rangle$	mean age, T
$\langle E \rangle$	mean life expectancy, T
$\langle T \rangle$	mean total transit time, T
M_0	aquifer porous volume, L^3
F_0	aquifer steady flow rate, L^3/T
$M_{0,n}$	outlet n drainage basin porous volume, L^3
$F_{0,n}$	outlet n steady flow rate, L^3/T
M_A	cumulative volume of age $\le t$, L^3
M_E	cumulative volume of life expectancy $\le t$, L^3
M_T	cumulative porous volume of transit time $\le t$, L^3
m_A	internal age cdf
m_E	internal life expectancy cdf
m_T	internal transit time cdf
F_A	outlet cumulated flow rate, L^3/T
F_E	inlet cumulated flow rate, L^3/T
f_A	outlet age cdf
f_E	inlet life expectancy cdf
p_n	probability of exit at outlet n
S_d	dispersive source term, T^{-2}
$\mathrm{A}(t)$	volume of age $\le t$ and transit time $> t$, L^3
$\mathrm{B}(t)$	volume of transit time $\le t$, L^3
$\mathrm{C}(t)$	volume of age $> t$, L^3
$\mathrm{O}(t)$	produced volume of transit time $\le t$ at outlet, L^3
Q_{I}	fluid source term, T^{-1}
$f_{X,Y}$	joint pdf of the random variables X and Y
$f_{X\|Y}$	conditional pdf of the random variable X given Y

Greek symbols

Ω	groundwater reservoir
Γ_-	inlet boundary
Γ_+	outlet boundary
Γ_0	impervious boundary
Γ_n	outlet n boundary
∇	operator Nabla
φ	transit time pdf, T^{-1}
ψ_A	internal age pdf, T^{-1}
ψ_E	internal life expectancy pdf, T^{-1}
ψ_T	internal transit time pdf, T^{-1}
$\delta(t)$	time-Dirac delta distribution, T^{-1}
$\mu_n[C]$	n^{th} temporal moment of a function C, T
ϕ	porosity or mobile water content
α_{L}	coefficient of longitudinal dispersivity, L
α_{T}	coefficient of transverse dispersivity, L
α	ratio $\alpha_{\mathrm{L}}/\alpha_{\mathrm{T}}$
λ	decay rate, T^{-1}
τ_0	reservoir turnover time, T
τ_{t}	outlet mean transit time, T
τ_{i}	mean internal age or life expectancy, T
τ_{it}	mean internal total transit time, T
σ_0	reservoir turnover rate, T^{-1}
σ	standard deviation, T

CHAPTER 1

Introduction

1.1. Generalities

Mass transport in aquifers

Among all the preoccupations of hydrogeologists, one of the main questions concerns transport of specific substances in groundwater. Nowadays, the number of substances one can find in groundwater is unfortunately tremendously large, reflecting the generalized problem of aquifer contamination. We can make reference to some classical anthropogenic ones, such as the non-exhaustive list of industrial chemicals that are released in groundwater, or as the well-known pesticides and nitrates issued from intensive agricultural activities. Groundwater contamination can also be of natural origin, e.g. when water flows through geological media such as evaporites, or material enriched in radio-active minerals. One spectacular case of aquifer resources natural contamination is the problem of the flushing by groundwater of the arsenic which occurs naturally in alluvial and deltaic sediments in Bangladesh, and that was found in both shallow and deep wells. The consequences on human health are nowadays enormous, since it is estimated that at least 1.2 million people are exposed to arsenic poisoning, and that the estimated spreading of the substance can potentially still expose 24 million people.

The main processes governing mass transport are commonly classified into two categories. On the one hand, the advection (or convection) processes reflect the carriage of materials and of dissolved substances due to the velocity of the fluid. Advection is generally the dominant process of transport in groundwater. On the other hand, hydrodynamic dispersion and diffusion phenomena reflect the movement of substances in groundwater caused by the concentration gradients, and by the dispersive and diffusive characteristics of the medium. Diffusion is driven by the random motion of particles in groundwater relative to the concentration gradients and the tortuous paths that a substance must follow from one point to another. Mechanical dispersion is induced by the fluid velocity fluctuations, which cause mixing of the substances, and acts like diffusion, although it is generally much faster. Moreover, dispersion effects are known to be space-, and time-scale dependent, and they act in the three direction of space, longitudinally in the flow direction, but also laterally and vertically. They grow with increasing travel distance, and thus with travel time. The result of the combined effects of advection and dispersion leads to a general spreading and mixing of groundwater, and of the contaminants that are transported in it.

One particular entity that is transported in aquifers is the groundwater molecule itself. When water flows out, e.g. at a natural spring, one can see the effect of the movement of groundwater volumes. The flow rate of the spring is generally an easily measurable quantity that indicates the amounts of water that are transferred in time, throughout the aquifer. However, one cannot easily distinguish if each water molecule originates from the same infiltrated water or not, and what the different events are, in terms of travel paths and travel times, that yielded the production of the spring intrinsic outflow. Due to the natural complexity of aquifer structures, and of the processes of transport in groundwater, the water molecules generally follow different paths from recharge zones, where they have infiltrated, to discharge zones, where they exit the aquifer system. The transport of groundwater particles is a first, but fundamental, step for understanding the fate of reactive contaminants in aquifers, which in the contrary to conservative substances can interact with the rock matrix and the multiple phases that can be present in the aquifer medium. Thus, a groundwater molecule can be considered as an ideal conservative tracer.

The concept of groundwater age

Groundwater flow is a particular dynamic and temporal state of the global water cycle on earth. Water particles become groundwater particles at the time when they enter the aquifer system through recharge processes. Therefore, a specific age can be assigned to water molecules. In aquifers, age is classically defined as a reference property with respect to the dynamic system. The age zero, or 'birth' of water molecules in the aquifer system, is commonly assigned to water particles entering the aquifer system by its inlet limits. It is thus dependent on an initial space reference. This reference can be e.g. the water table, or the ground surface if one considers the dynamic underground flow system by including the variably saturated part of it (unsaturated zone). The age of a groundwater molecule is then simply the time elapsed during its travel from an initial point, and is preferentially reserved to describe the increasing time since recharge.

Groundwater particles move along flow paths of varying lengths. The length of the flow paths differs for different types of flow systems, and dictates the time water and rock are in contact. Water molecules can remain only very little time in aquifers, or they can remain very long time. These residence time variations in relation to the possible different path lengths in the groundwater system are illustrated in Fig. 1.1. Depending on the place where water infiltrates, the path lengths will differ, and as a consequence the travel times will of course differ too. These path lengths affect the water chemistry, and the degree of mineralization, but also the nature of groundwater age. The groundwater age transport is equivalent to the water molecules transport, and thus also to the transport of conservative substances in groundwater. For this reason, transporting groundwater age is like tracing water particles in time during their evolution in the aquifer system.

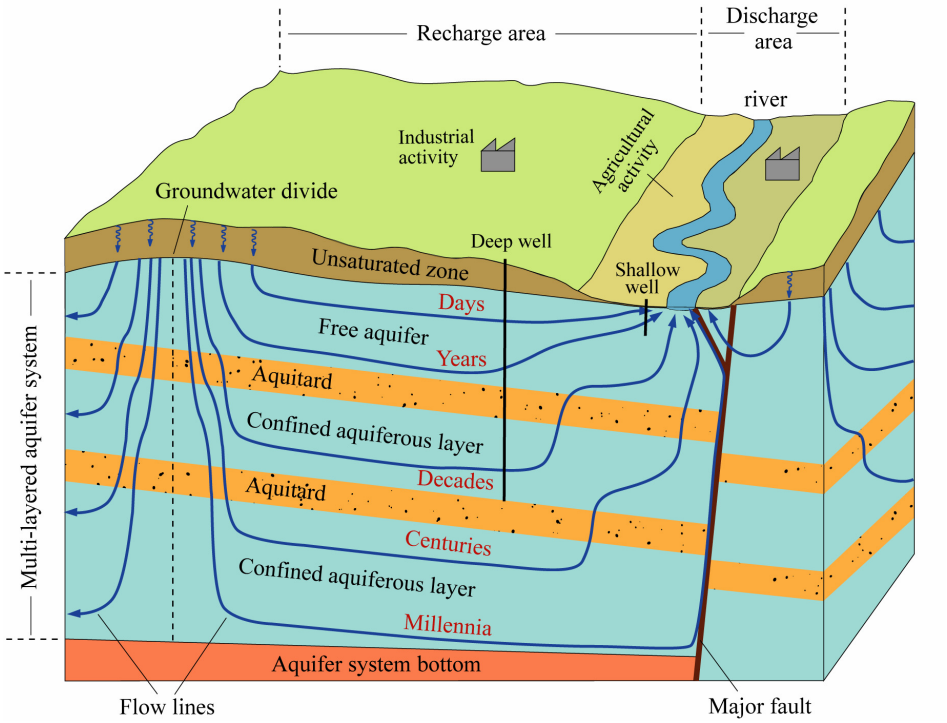

Fig. 1.1. Schematic illustration of a natural hydrological system, showing the different possible flow paths of groundwater particles from the recharge to the discharge area.

Age is a property that is transported in groundwater by advection, but also by dispersion. More precisely, the product of groundwater age with its mass is the conservative quantity that is transported in aquifers. The behaviour of this property in space is very dependent on the aquifer

structure, and on the heterogeneity of the physical parameters and the recharge patterns. The main consequence is that a groundwater sample will generally contain a heterogeneous distribution of ages. In any water sample, the mixture of ages may range between various kinds of extremes, depending on the reservoir nature and hydro-dispersive characteristics. Groundwater age must, therefore, be regarded as a statistical, or probabilistic distribution, rather than considering it as a single absolute, or average, value.

There are different ways of considering the age date with respect to which the spatial reference is chosen. If one reverses the spatial reference for the age evaluation, it is interesting to quantify the age date as the time required by the water molecules for reaching an exit point of the aquifer. In the present dissertation, use will be made of the concept of the life expectancy of groundwater molecules, when focus it put on the knowledge of the dates of 'death' of these molecules, i.e. when they exit the aquifer. The life expectancy is thus a characteristic age date that is nil at the aquifer exit zones. We will also considerer the travel time in a general way, as the time elapsed by water molecules for travelling between two arbitrary points in an aquifer. If these two points are located on inlet and outlet zones, then the age date will be referred to as total transit time within the aquifer system. Age, life expectancy, and total transit time are different age dates that hydrogeologists aim at quantifying, depending on the problem they are interested in. For example, considering Fig. 1.1, we could be interested in knowing the ages of water molecules at a zone within a specific layer, or in the water extracted by a pumping-well. We could also be interested in knowing the time required by the groundwater molecules to travel from a point within a layer to the river outlet.

1.2. Background

The knowledge of groundwater residence and transit time distributions is of prime interest in many environmental issues since they depend on the intrinsic characteristics of the overall transport properties of an aquifer and its sub-systems. For instance, an important fraction of young water within an extracted water sample can often be taken as the signature of a reservoir with good turnover. On the opposite, a considerable component of old water may reflect a poorly recharged aquifer, and/or significant internal mixing processes. The impact of a contamination hazard on groundwater quality is closely linked to the nature of groundwater age, since the age distribution within the aquifer provides direct information on the time required for a water particle, or a conservative tracer, to reach any critical zone that is to be protected. The fate of a solute being transported in groundwater partially depends on the time spent by the water molecules during their migration throughout the aquifer system. Reactive transport of a specific substance is also linked to groundwater age; the time spent flowing through any kind of mineral heterogeneity being a conditional factor for the development of any potential reactions.

Groundwater age can help to evaluate the relative importance of the factors that cause and influence the migration of contaminants through the aquifer. With the age information, inferences can be made on the aquifer physical characteristics, as well as on the chemical transformations that contaminants may suffer. The age can also be of importance for estimating historical aspects related e.g. to the agricultural practices, or the land use of a particular region, which are expected to have lead to groundwater contamination. Since groundwater age can be considered as the most conservative and ideal tracer, the worst scenario with regard to a contamination case is thus chosen by solving the age transport problem.

Groundwater age is a measurable quantity, provided many assumptions. Age dates estimation is a subject of high interest, for which several analytical methods have been developed. Another approach of groundwater age determination is based on mathematical modelling of its evolution in aquifers. Both approaches are complementary, since neither of them can provide absolute answers. The main characteristics of these approaches will be discussed in the following.

Dating methods

The aim of dating methods is the estimation of the age of groundwater after recharge. Since the range of groundwater ages can be highly variable, from less than 1year to thousands of years, or even more than a million years, various methods have been developed, with specific characteristics and possibilities of age estimations. By far the most frequently used dating methods are based on the measurements of natural tracers, such as the isotopes of Radon, Carbon or Oxygen, and on the measurements of man-induced atmospheric concentrations of elements such as Tritium (^{3}H), Chloride (^{36}Cl), Krypton (^{85}Kr), or Chlorofluorocarbons (CFC), which have increased steadily between the 1940s and the early 1990s. Particularly the concentrations of the isotopes ^{3}H and ^{36}Cl increased during late 1950s and early 1960s, as a consequence of the thermonuclear testing, and have been extensively used for dating groundwater in shallow aquifer systems. However, the ^{3}H and ^{36}Cl methods can only accept or reject a recharge event with respect to the time of the nuclear peak in the atmosphere. The most efficient methods for dating recent waters are the ones based on Tritium/Helium ($^{3}H/^{3}He$), ^{85}Kr, and CFC measurements [Solomon *et al.*, 1992; Plummer *et al.*, 1993; Dunkle *et al.*, 1993], which are known to provide age dates over a period of 40years with an accuracy of 20% or less [Cook & Solomon, 1997]. These isotopes are soluble in water, and assuming they can be considered relatively stable in groundwater (e.g. CFC), they can be used to estimate the average age of groundwater by measurement of the concentrations of the dissolved gases [Plummer *et al.*, 1993]. Unfortunately, the decrease of Tritium in groundwater, or of the CFC concentrations in the atmosphere, has the drawback that the date estimates of relatively young waters tend to become less reliable as time passes [Oster *et al.*, 1996].

Old ages dating methods involve that the sampled groundwater is Tritium-free, indicating recharge events older than ~50years, and that the modern components are negligible. The absolute dating techniques involve decay of radio-nuclides in groundwater, for which the ^{14}C, which is transported as dissolved inorganic carbon (DIC) or dissolved organic carbon (DOC), or the ^{36}Cl, are classical elements that are used for dating old groundwater, e.g. in deep and large sedimentary basins.

Generally, the dating methods provide an average value over a water sample, which in theory does not represent hard data. In fact, the mean of an unknown temporal distribution, here the distribution of ages, is not necessarily a reliable value for the most likely of this distribution. As illustration consider the surrounding of the river in Fig. 1.1, where waters of highly contrasted ages can mix. A water sample in this region could contain only small component of young waters with respect to old waters, and the measure of the average age in this water sample could not reflect the right age characteristic of groundwater at this place. Moreover, the estimates of these average age values are also subject to uncertainty. CFC-based groundwater ages are known for having a good resolution for groundwater with relatively young components [Busenberg & Plummer, 1992; Boehlke & Denver, 1996], but they do not account for the time spent by water molecules within the unsaturated zone before they reach the water table. The travel time duration within the unsaturated zone must therefore be estimated. For the case of aquifers with deep water table, this can be a very limiting factor. Young age dating methods, such as the CFC-method, can lead to older estimates of ages: the uncertainty of age estimates increases with age, since older waters corresponding to older recharge events have lower CFC rates, and thus, a greater chance of CFC degradation [Busenberg & Plummer, 1992]. As will be discussed in this work, mixing and dispersion in groundwater are the major factors, which can lead to un-representative mean age measurements.

Age dates are very often used to make inferences on aquifer parameters, groundwater recharge, flow paths and flow velocities. However, with many of these dating methods, the interpretation of age dates is achieved by means of simplified models and fitting the data. This involves significant simplifications of the flow and transport processes, which may lead to erroneous interpretations about e.g. the past release of contaminants in aquifers. Dating methods can however be very useful for calibrating numerical models [see e.g. Reilly et al., 1994; Robertson & Cherry, 1989], which attempt to simulate the flow patterns, the flow rates, and the distribution of ages in groundwater.

Classical mathematical models of groundwater age

To quantify the distribution of ages in aquifers, several types of mathematical models have been developed during the past decades of research in this field. A classical age modelling practise is done by fitting analytical models on measured tracer data, such as the above-mentioned data derived from age dating methods. With these types of models, which are commonly called the analytical lumped-parameter models, the age distributions are more or less arbitrarily chosen, and not deterministically calculated. These models have been extensively used in the simulation of environmental tracer data [e.g. Maloszewski & Zuber, 1982, 1993; Zuber, 1986; Campana & Simpson, 1984; Balderer, 1986; Richter *et al.*, 1993; Amin & Campana, 1996], such as isotopic data, which are commonly interpreted with advective transit time models, although isotope transport does not necessarily undergo advective processes only. Specified transit time distributions describing piston-flow, exponential mixing, combined piston-exponential mixing, or dispersive mixing, are usually chosen to solve the inverse problem by fitting the model on measured tracer output data, with adjustment of some parameters (see Fig. 1.2). This procedure calls for significant simplifications, which can often not be justified, such as for instance neglecting the reservoir structure, as well as the spatial variability of infiltration rates [Campana, 1987] and aquifer flow and transport parameters. Amin & Campana [1996] proposed to model the mixing process effect by means of a three-parameter gamma function which accounts for various states of mixing ranging between no mixing (piston flow model) and perfect mixing (exponential model).

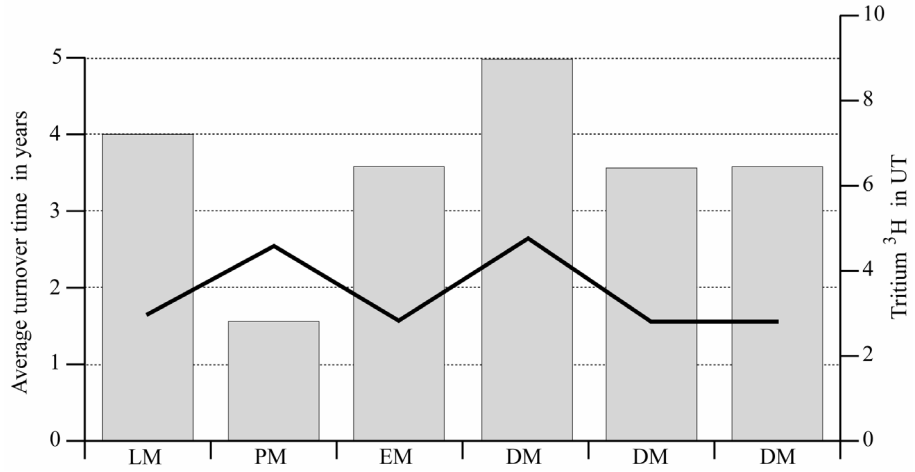

Fig. 1.2. Comparison between different turnover time dates at the Lutry spring (Switzerland), obtained with the piston-flow model (PM), the exponential model (EM), the linear model (LM), and the dispersive model (DM, with different sets of parameters) . The thick solid line indicates the absolute difference between the modelled age and the average age date given by the ^{3}H method (in Tritium units UT). Adapted from Etcheverry [2002].

Lumped-parameter models are often used to make inferences on the flow velocity, the aquifer turnover time, or on past recharge events. However, robust verifications of the applicability of lumped parameter models can hardly be found [e.g. see Haitjema, 1995; Luther & Haitjema, 1998; Etcheverry & Perrochet, 1999]. Haitjema [1995] provided some guidelines for the use of such models, and derived an analytical solution of the exponential model for semi-confined stratified aquifers. Luther & Haitjema [1998] claimed that the conditions on the validity of the theoretical exponential residence time distribution (horizontal, un-stratified and homogeneous aquifer with respect to porosity ϕ, recharge rate I, and saturated thickness H), can be relaxed when specific configurations are encountered, as for example when the parameters ϕ, I, and H vary in a piecewise constant way, such that the ratio $\phi H/I$ remains constant throughout the domain. This ratio indicates the system turnover time, which means that each water sample taken from the reservoir must give a

mean age that is equal to the aquifer mean turnover time. This system configuration and these mean age conditions may hardly be found in nature, and the assumptions of Luther & Haitjema [1998] remain very limiting. Etcheverry [2001] showed that a simple linear variation of the thickness H significantly influences the shape of the theoretical exponential residence time distribution.

Age transport has often been described through a pure advective vision of transport. Transit time distributions are obtained by making the assumption of pure advective motion of the groundwater particles, the particle-tracking technique being the most popular one. Particle-tracking algorithms basically track down a certain amount of released water particles, given a known flow velocity field. This can be done forwards by following the flow lines downstream, or backwards by following the flow lines upstream. These purely kinematic ages ignore the effect of dispersion and mixing on age transport [Davis & Bentley, 1982; Cordes & Kinzelbach, 1992], and often reveal to be ill posed in complex heterogeneous systems [Varni & Carrera, 1998], for which the three-dimensional implementation is subject to severe technical problems. Moreover, particle-tracking does not allow the calculation of transit time distributions, since groundwater volumes are not associated to simulated ages. Nevertheless, the particle tracking method is still widely used to validate dating methods, mainly isotopic methods which consider the disintegration of radioactive isotopes as age index [Smith *et al.*, 1976; Bath *et al.*, 1979]. Use is also made of stable isotopic relations between the isotopes spatial distribution and climatic changes [Sonntag *et al.*, 1979]. In such cases, problems often occur due to dilution and mixing processes, which cannot be taken into account by models based on advection only. In Fig. 1.3a, an example of age dates simulation by particle-tracking is shown. The model represents a simple plan view of an aquifer with a pumping-well. The backward particle-tracking from the well to the ultimate upstream locations gives a purely advective image of the time water particles can spare prior to absorption by the well, by evaluating the velocity over the travel distance (black dots in Fig. 1.3a). Isochrones of life expectancy are then mapped over the system, and they are used to define the well capture zone. Such a capture zone definition is rigid, since water particles situated outside this region are not allowed to enter the capture zone, as well as the particles situated inside are not allowed to diverge from the capture zone. However, it is a well-known fact that dispersion processes will allow water particles to move laterally, and thus to exit or enter the well capture zone. The importance of including age dilution processes such as dispersion and matrix diffusion, when comparison is made between modeled and measured ages, has been pointed out by many authors [Sudicky & Frind, 1981; Maloszewski & Zuber, 1982, 1991].

More elaborated quantitative approaches consider age as a mass that is transported by groundwater through volume-averaged temporal moment equations [e.g. Spalding, 1958; Harvey & Gorelick, 1995; Goode, 1996; Varni & Carrera, 1998; Ginn, 1999], in which the age mass, i.e the product of water mass with the mean age (ρAV, with A the mean age, ρ and V the water density and volume, respectively), is the conserved quantity. These equations are generally formulated with advection-dispersion type equations (ADE). Varni & Carrera [1998] derived a set of recursive temporal moment equations which were compared to radiometric age measurements. Harvey & Gorelick [1995] presented a general framework of temporal moment generated equations for advective-dispersive and reactive transport, which are sequentially solved in order to simulate the breakthrough curves from the n calculated moments. According to Harvey & Gorelick [1995], the first five moments characterizing the accumulated mass, the mean, the variance, the skewness, and the kurtosis of a breakthrough curve, respectively, may provide sufficient information to summarize the entire breakthrough, for the case when the principle of maximum entropy function is applied. Since many natural systems can reveal a multi-modality of the age distribution within the reservoir and at the discharge zones, and since the shape of the distribution is a priori unknown, an infinity of moments would therefore be required to construct the entire distribution. As will be discussed several times in this dissertation, for various reasons mean age calculations do not represent an absolute simulation answer since mean age can be unrepresentative of the entire age distribution. In Fig. 1.3, an example of mean age and mean life expectancy calculations is given, using first moment forms of the ADE. The mean age field in Fig. 1.3b is given by the solution of the mean age equation [Goode, 1996]. The mean life expectancy field in Fig. 1.3c originates from the solution of

an adjoint backward equation, which will be presented in the present work. Both fields include dispersion, and particularly the mean life expectancy field can be compared to the backward particle-tracking solution. However, this type of age date information, as well as the information given by the backward particle-tracking, can hardly provide insight on the entire distributions of age and life expectancy, such as the age distribution for the water extracted at the pumping-well (Fig. 1.3d), although the knowledge of the full distributions is of prime importance.

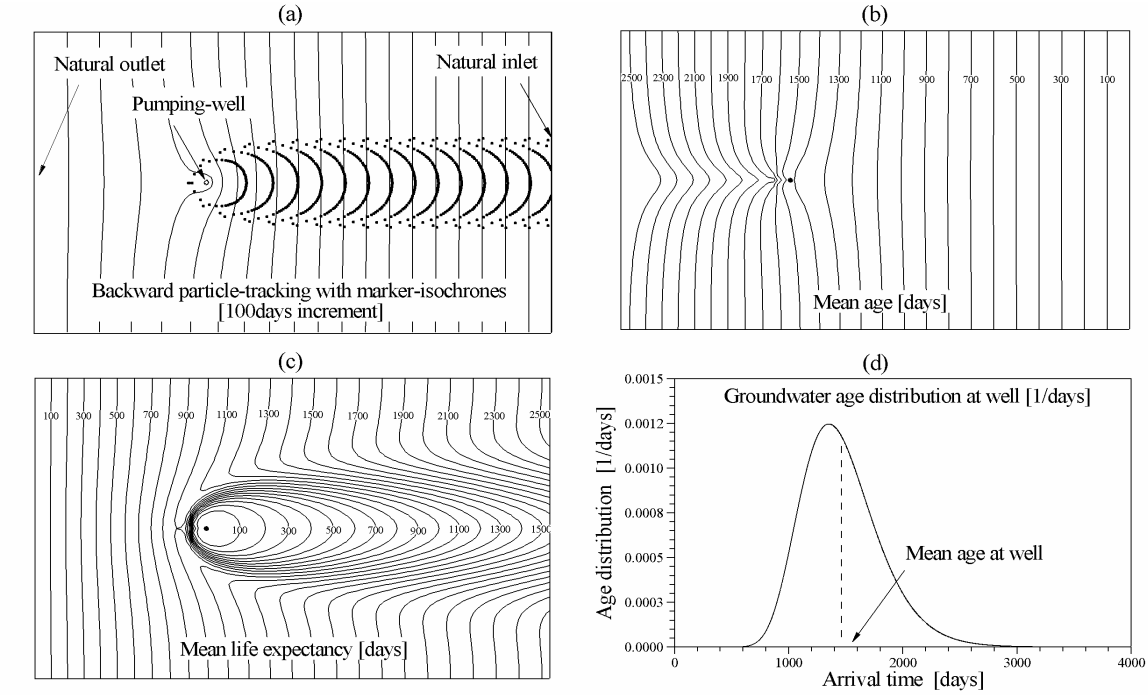

Fig. 1.3. Example of two types of age date simulations in a hydro-dispersive aquifer: (a) The purely advective particle-tracking method (the solid lines represent the hydraulic heads); (b) The advective-dispersive age first temporal moment equation; (c) The advective-dispersive life expectancy first temporal moment equation; (d) The age distribution of the extracted water at the well.

Travel time probabilities have been a subject of high interest in many studies characterizing solute transport in sub-surface hydrology [e.g. Dagan, 1982, 1987, 1989; Jury & Roth, 1990]. The travel time probability is commonly defined as the response function to an instantaneous unit flux impulse [Danckwerts, 1953; Jury & Roth, 1990]. In their transfer function approach of contaminant transport through unsaturated soil units, Jury & Roth [1990] model tracer breakthrough curves with one-dimensional travel time probability functions. Shapiro & Cvetkovic [1988], Dagan [1989], and Dagan & Nguyen [1989] derived the forward travel time probability for a mass of solute by using the Lagrangian concept of particle displacement in porous media. Woodbury & Rubin [2000] combined the Lagrangian solute transport framework with full-Bayesian hydrogeological parameter inference to invert the travel time moments of solutes in heterogeneous aquifers. The method is based on concentration arrival times measured at various points in the aquifer, and inferences on hydraulic parameters are made by inverting travel time moments. A stochastic longitudinal exponential model is imposed for the travel time density function. According to the authors, no scale effect along the travel distance seems to affect the results.

The derivation of forward and backward models for location and travel time probability has become a classical mathematical practice for contaminant transport characterization and prediction [e.g. Uffink, 1989; Van Herwaarden, 1994; Van Kooten, 1995; LaBolle *et al.*, 1998; Neupauer & Wilson 1999, 2001]. The spreading of a contaminant mass is analysed by following the random motion of solute particles, and to do so, the ADE is assimilated to the Fokker-Planck (or forward Kolmogorov) equation. The expected resident concentration of a conservative tracer is taken as the

probability density function for the location of a particle, at any time after having entered the system. LaBolle *et al.* [1998] recall that the standard diffusion theory, which relates the dynamics of a diffusion process to Kolmogorov's equations [1931], may apply to ADEs if porosity and the dispersion tensor are functions varying smoothly in space. They derive general probabilistic definitions for the velocity and dispersion tensor that ensure applicability of the diffusion theory at local scale. Random-walk procedures are very often used to solve the ADEs [see e.g. Uffink, 1989; LaBolle *et al.*, 1998; Weissmann *et al.*, 2002]. The derivation of adjoint state equations of the forward ADE to define backward location and travel time probabilities was recently revisited by Wilson & Liu [1997], and Neupauer & Wilson [1999, 2001], using sensitivity analysis. They derived specific forward and backward probabilities to predict contaminant sources from concentrations measured at monitoring and extraction wells. Compared to the forward modelling approach that helps to predict the future evolution of contamination when the source is known, the backward modelling approach reveals to be useful when the contamination has been detected, and when the possible sources have to be identified.

Eriksson [1961, 1971], followed by Bolin & Rhode [1973], introduced an old theory into the field of environmental problems, namely the reservoir theory (RT), which appeared at the end of the 1940s, and originates from the residence time theory widely used in chemical engineering. The RT is basically an application of the Gauss divergence theorem on a fluid flowing through a given bounded domain. It deals with conservative fluid particles which enter a system and remain in it during a certain period, before exiting the system. The application of the RT to groundwater flow links the internal age statistical distribution to the statistical distribution of transit times at the outlet boundaries of the reservoir. In Eriksson [1961, 1971], the advection is the only process taken into account, and the author mentions that the theory may not hold when mixing processes occur. Etcheverry & Perrochet [1999, 2000], and Etcheverry [2001], developed a mathematical method to directly calculate the groundwater transit time distribution at a reservoir outlet, by combining the mean age approach [Goode, 1996] and the RT. Mean ages were supposed to result from pure advective transport calculations. This approach was validated by means of several analytical developments [Etcheverry & Perrochet, 2000; Etcheverry, 2001], and tested on a few hypothetical two-dimensional structured systems, where dispersion and mixing were neglected. The main interest of the RT is that the age occurrence at the outlet is predicted by using the information on the internal organization of age within the entire reservoir, ensuring that the minimum and maximum ages at outlet are recovered.

1.3. Goals and objectives

The goal of the present work was to develop deterministic mathematical models allowing efficient calculation of age date distributions in reservoir aquifers, as well as at the hydraulic boundaries. To do so, we work with the classical forward advection-dispersion equation, associated to a set of proper boundary conditions. We also make use of the backward modelling approach to solve the problem of the life expectancy. Even if the application of the reservoir theory to purely advective age computations yielded promising results [Etcheverry & Perrochet, 1999, 2000; Etcheverry, 2001], the limiting assumption of no mixing processes, as stated by Eriksson [1971], seems to be equivocal and needs more attention. The authors also restricted the method to systems with single outlet and inlet zones. Therefore, the reservoir theory was further explored within the framework of advective-dispersive transport of conservative tracer, such as age, with the aim of generalizing the theory for application to any kind or aquifer configuration and complexity.

Since research in environmental sciences is only meaningful if it is followed by practical applications, the second goal of this work was to develop numerical tools enabling efficient resolution of the proposed mathematical models.

The specific tasks of this research can be summarized as follows:

- Development of deterministic mathematical models for simulating age, life expectancy and total transit time distributions in arbitrary aquifers, by including diffusion and dispersion processes;
- Generalization of the reservoir theory to hydro-dispersive systems, to characterize the internal organization of age and transit time, and to obtain a refined evaluation of the inlet and outlet transit time distributions;
- Extension and adaptation of the reservoir theory to aquifers of arbitrary configuration and complexity, allowing calculation of the age distribution of a specific outlet, with respect to the age and life expectancy occurrence in its drainage basin;
- Testing the sensibility of the models to the aquifer structure and the transport parameters, such as flow velocity, porosity and dispersion;
- Making the link between the age and the life expectancy probability distribution approach, and the reservoir theory, and the problem of contaminant transport in general;
- Providing numerical tools to solve the mathematical models.

1.4 Structure of the dissertation

In Chapter 2, we set probabilistic definitions for the variables age, life expectancy, and total transit time. General equations and boundary conditions are proposed for calculating the statistical distributions of the three above-mentioned variables. In Chapter 3, we generalize the reservoir theory to systems with significant hydro-dispersive components, and analyze some effects induced by the aquifer structure, and by its transport parameters characteristics, on the age distribution at a reservoir outlet. The effect of the transport boundary conditions on simulated ages is also discussed. In Chapter 4, we extend the reservoir theory to systems with arbitrary configuration and complexity, by using the backward modelling approach to identify aquifer sub-drainage basins corresponding to specific outlets. The utility of the reservoir theory combined with the backward transport approach for dealing with groundwater resources protection problems is shown by providing answers to the definition of the outlet intrinsic vulnerability and protection zones. A theoretical application of large space- and time-scale simulations, which particularly addresses the problem of underground storage of toxic waste repositories, is also presented. Finally, in Chapter 5 the conclusions which have been drawn from this work followed by a critical discussion and suggestions with respect to the possible future investigations are presented.

Throughout the dissertation, some particular sections called ‘Excursus’ are present. They concern specific mathematical developments, which might be skipped by the reader if desired, without losing continuity in the woof.

References

[1] Amin I.E. and Campana M.E. A general lumped parameter model for the interpretation of tracer data and transit time calculation in hydrologic systems. *J Hydrol* 1996;179:1–21.
[2] Balderer W. Signification de l'âge moyen de l'eau souterraine donné par les isotopes radioactifs. *Bulletin du Centre d'Hydrogéologie* 1986;6:43–66.
[3] Bath A.H., Edmunds W.M. and Andrews J.N. Paleoclimatic trends deduced from hydrochemistry of a Triassic sand-stone aquifer, United Kingdom. Int. At. Energy, Vienna 1979. *Isotope Hydrology* 1978;2:545–568.

[4] Boehlke J.K. and Denver J.M. Combined use of groundwater dating, chemical, and isotopic analysis to resolve the history and fate of nitrate contamination in two agricultural watersheds, Atlantic Coastal Plain, Maryland. *Water Resour Res* 1996;31(9):2319–2339.
[5] Bolin B. and Rodhe H. A note on the concept of age distribution and transit time in natural reservoirs. *Tellus* XXV 1973;1:58–62.
[6] Busenberg E. and Plummer L.N. Use of chlorofluoromethanes (CCL3F and CCL2F2) as hydrologic tracers and age-dating tools; The alluvium and terrace system of central Oklahoma. *Water Resour Res* 1992;28(9):2257–2283.
[7] Campana M.E. and Simpson E. Groundwater residence times and recharge rates using a discrete-state compartment model and ^{14}C data. *J Hydrol* 1984;72:171–185.
[8] Campana M.E. Generation of Ground-Water Age Distributions. *Ground Water* 1987;25(1):51–58.
[9] Cordes C. and Kinzelbach W. Continuous groundwater velocity fields and path lines in linear, bilinear, and trilinear finite elements. *Water Resour Res* 1992;28:2903–2911.
[10] Cook P.G. and Solomon D.K. Recent advances in dating young groundwater: chlorofluorocarbons, $^{3}H/^{3}He$ and ^{85}Kr. *J Hydrol* 1997;191:245–265.
[11] Dagan G. Stochastic modelling of groundwater flow by unconditional and conditional probabilities, 2, The solute transport. *Water Resour Res* 1982;18(4):835–848.
[12] Dagan G. Solute transport in heterogeneous porous formations. *J Fluid Mech* 1984;145:151–177.
[13] Dagan G. Theory of solute transport by groundwater. *Ann Rev Fluid Mech* 1987;19:183–215.
[14] Dagan G. Flow and Transport in Porous Formations. Springer, Berlin, Heidelberg, Germany; 1989.
[15] Dagan G. and Nguyen V. A comparison of travel time and concentration approaches to modelling transport by groundwater. *J Contam Hydrol* 1989;4:79–91.
[16] Danckwerts P.V. Continuous flow systems: distribution of residence times. *Chem Eng Sci* 1953;2(1):93–102.
[17] Davis S.N. and Bentley H.W. Dating groundwater, a short review, In *Nuclear and Chemical Dating Techniques*, Ed. Lloyd Curie, Am. Chem. Soc. Symp. Ser. 176, 187–222;1982.
[18] Dunkle S.A., Plummer L.N., Busenberg E., Phillips P.J., Denver J.M., Hamilton P.A., Michel R.L. and Coplen T.B. Chlorofluorocarbons (CCl3F and ClCl2F2) as dating tools and hydrologic tracers in shallow groundwater of the Delmarva Peninsula, Atlantic Coastal Plain, United States. *Water Resour Res* 1993;29:3837–3860.
[19] Eriksson E. Natural reservoirs and their characteristics. *Geofisica International* 1961;1(2):27–43.
[20] Eriksson E. Compartment models and reservoir theory. *Annual Review of Ecology and Systematics* 1971;2:67–84.
[21] Etcheverry D. Valorisation des méthodes isotopiques pour les questions pratiques liées aux eaux souterraines. Isotopes de l'oxygène et de l'hydrogène. *Berichte des BWG*, Serie Geologie 2002; 71 pp.
[22] Etcheverry D. and Perrochet P. Reservoir theory, groundwater transit time distributions and lumped parameter models. IAEA-SM-361/44, Vienna;1999.
[23] Etcheverry D. and Perrochet P. Direct simulation of groundwater transit time distributions using the reservoir theory. *Hydrogeology Journal* 2000;8:200–208.
[24] Etcheverry D. Une approche déterministe des distributions des temps de transit de l'eau souterraine par la théorie des réservoirs. PhD Thesis, Centre of Hydrogeology, University of Neuchâtel, 2001, 118 pp.
[25] Gelhar L.W. and Axness C.L. Three-dimensional stochastic analysis of macro dispersion in aquifers. *Water Resour Res* 1983;19(1):161–180.
[26] Ginn T.R. On the distribution of multicomponent mixtures over generalized exposure time in subsurface flow and reactive transport: Fundations, and formulations for groundwater age, chemical heterogeneity, and biodegradation. *Water Resour Res* 1999;35(5):1395–1407.
[27] Goode D.J. Direct simulation of groundwater age. *Water Resour Res* 1996;32:289–296.
[28] Haitjema H.M. On the residence time distributions in idealized groundwatersheds. *J Hydrol* 1995;172:127–146.
[29] Harvey C.F. and Gorelick S.M. Temporal moment generating equations: Modeling transport and mass transfer in heterogeneous aquifers. *Water Resour Res* 1995;31:1895–1912.
[30] Jury W.A Simulation of Solute transport Using a Transfer Function Model. *Water Resour Res* 1982;18(2):363–368.
[31] Jury W.A. and Roth K. Transfer Functions and Solute Movement Through Soil: Theory and Applications. Birkhauser Boston, Cambridge, Mass, 289 pp.; 1990.
[32] Kolmogorov A.N. Über die analytischen Methoden in der Wahrscheilichkeitsrechnung. *Math Anal* 1931;104:415–458.
[33] LaBolle E.M., Quastel J. and Fogg G.E. Diffusion theory for transport in porous media : Transition-probability densities of diffusion processes corresponding to advection-dispersion equations. *Water Resour Res* 1998;34(7):1685–1693.

[34] Luther K.H. and Haitjema H.M. Numerical experiments on the residence time distributions of heterogeneous groundwatersheds. *J Hydrol* 1998;207:1–17.
[35] Maloszewski P. and Zuber A. Determining the turnover time of groundwater systems with the aid of environmental tracers, 1, Models and their applicability. *J Hydrol* 1982;57:207–231.
[36] Maloszewski P. and Zuber A. Influence of matrix diffusion and exchange reactions on radiocarbon ages in fissured carbonate aquifers. *Water Resour Res* 1991;27:1937–1945.
[37] Maloszewski P. and Zuber A. Principles and practice of calibration and validation of mathematical models for the interpretation of environmental tracer data in aquifers. *Adv Water Res* 1993;16:173–190.
[38] Neupauer R. and Wilson J.L. Adjoint method for obtaining backward-in-time location and travel time probabilities of a conservative groundwater contaminant. *Water Resour Res* 1999;35(11):3389–3398.
[39] Neupauer R. and Wilson J.L. Adjoint-derived location and travel time probabilities for a multidimensional groundwater system. *Water Resour Res* 2001;37(6):1657–1668.
[40] Oster H., Sonntag C. and Munnich, K.O. Groundwater age dating with chlorofluorocarbons. *Water Resour Res* 1996;32(10):2989–3001.
[41] Plummer L.N., Michel R.L., Thurman E.M. and Glynn P.D. Environmental tracers for age dating young ground water. In *Regional ground-water quality* 1993, Ed. Alley W.M., New York, Van Nostrand Reinhold,255–294.
[42] Reilly T.E., Plummer L.N., Phillips P.J. and Busenberg E. The use of simulation and multiple environmental tracers to quantify groundwater flow in a shallow aquifer. *Water Resour Res* 1994;30:421–433.
[43] Richter J., Szymezak P., Abraham T. and Jordan H. Use of combination of lumped parameter models to interpret groundwater isotopic data. *J Contam Hydrol* 1993;14(1):1–13.
[44] Robertson W.D. and Cherry J.A. Tritium as an indicator of recharge and dispersion in a groundwater system in Central Ontario. *Water Resour Res* 1989;25:1097–1109.
[45] Shapiro A.M. and Cvetkovic V.D. Stochastic analysis of solute arrival time in heterogeneous porous media. *Water Resour Res* 1988;24(10):1711–1718.
[46] Smith D.B., Downing R.A., Monkhouse R.A, Otlet R.L. and Pearson F.J. The age of groundwater in the Chalk of the London Basin. *Water Resour Res* 1976;12:392–404.
[47] Solomon D.K., Poreda R.J., Schiff S.L. and Cherry J.A. Tritium and Helium 3 as groundwater-age tracers in the Borden aquifer. *Water Resour Res* 1992;28:741–755.
[48] Sonntag C., Klitzch E., Lohnert E.P., El-Shazly E.M, Munich K.O., Junghans C., Thorweike U., Weistroffer K. and Swailem F.M. Paleoclimatic information from deuterium and oxygen-18 in carbon-14 dated north Saharian groundwaters. *Isotope Hydrology* 1979;2:569–580, Int. At. Energy Agency, Vienna.
[49] Spalding D.B. A note on mean residence-times in steady flows of arbitrary complexity. *Chem Eng Sci* 1958;9:74–77.
[50] Sudicky E.A. and Frind E. Carbon 14 dating of groundwater in confined aquifers: Implication of aquitard diffusion. *Water Resour Res* 1981;17:1060–11064.
[51] Uffink G.J.M. Application of the Kolmogorov's backward equation in random walk simulation of groundwater contaminant transport. In *Contaminant Transport in Groundwater* 1989;ed. H.E. Kobus & Kinzelbach, Balkema, Rotterdam, 283–289.
[52] Van Herwaarden O.A. Spread of pollution by dispersive groundwater flow. *SIAM J Appl Math* 1994;54(1):26–41.
[53] Van Kooten J.J.A. An asymptotic method for predicting the contamination of a pumping well. *Adv Water Res* 1995;18(5):295–313.
[54] Varni M. and Carrera J. Simulation of groundwater age distributions. *Water Resour Res* 1998;34(12):3271–3281.
[55] Weissmann G. S., Zhang Y., LaBolle E. and Fogg G.E. Dispersion of groundwater age in an alluvial aquifer system. *Water Resour Res* 2002;38(10):doi:10.1029/2001WR000907.
[56] Wilson J.L. and Liu J. Field Validation of the Backward-in-Time Advection Dispersion Theory. In P*roceedings of the 1996 HSRC/WERC Joint Conference on the Environment*, Great Plains-Rocky Mountain Hazard. Substance Cent., Manhattan, Kansas;1997.
[57] Woodbury A.D. and Rubin Y. A full-Bayesian approach to parameter inference from tracer travel time moments and investigation of scale effects at the Cape Cod experimental site. *Water Resour Res* 2000;36(1):159–171.
[58] Zuber A. Mathematical models for the interpretation of environmental radioisotopes in groundwater systems. In *Handbook of Environmental Isotope Geochemistry 2*, Fritz P. and Fontes J.-Ch. (Eds);1986.

CHAPTER 2

Groundwater age, life expectancy and total transit time probabilities

Abstract

We present a methodology for determining reservoir groundwater age, life expectancy, and transit time probability distributions in a deterministic manner, considering advective-dispersive transport in steady and divergence free velocity fields. We propose to model the statistical distribution of groundwater age at aquifer scale by means of the classical advection-dispersion equation (ADE) for a conservative and non-reactive tracer, associated to proper boundary conditions. The evaluated function corresponds to the density of probability of the random variable age, defined as the time elapsed since the water particles entered the aquifer. An adjoint backward model is introduced to characterize the life expectancy distribution, the life expectancy being the time remaining before leaving the aquifer. By convolution of these two distributions, groundwater total transit time distributions, from inlet to outlet, are fully defined for the entire aquifer domain. From the full distributions of age, life expectancy and total transit time, moment averaged equations are defined. A two-dimensional example is finally presented to illustrate the proposed mathematical models.

2.1. Definitions

The characterization of groundwater particles with respect to a residence time within an aquifer system is fully dependent on the spatial reference from which this time is 'measured'. Usually the groundwater age is defined as a relative quantity with respect to a starting location where age is assumed to be zero. Following Danckwerts [1953], Jury [1982], Jury & Roth [1990], the travel time probability function at an observation point $\mathbf{x}_o$ can be defined as the unit response function to an instantaneous unit pulse input of solute at an initial point $\mathbf{x}_i$. The resulting breakthrough curve is the probability density function (pdf) for the time required to travel from the initial point to the observation point. By letting $\mathbf{x}_i$ be a point on a recharge limit of a given aquifer, the observed breakthrough curve at $\mathbf{x}_o$ is the age, or residence time pdf of water particles, relative to the travel distance corresponding to the pair $\{\mathbf{x}_i, \mathbf{x}_o\}$. Throughout this work, use will be made of three variations of terminology, in order to characterize the time-span corresponding to a specific travel distance, and in relation to the recharge and discharge areas of a well-defined aquifer system.

We consider an arbitrary groundwater reservoir Ω, bounded by the inlet limit Γ_-, the outlet limit Γ_+, and the impervious limit Γ_0 (see Fig. 2.1). For a given spatial position in the reservoir, the age (A) relates to the time elapsed since the water particles entered the system at the recharge limits. For the same spatial position, the life expectancy (E) is defined as the time required for the water particles to reach an outlet limit of the system. Life expectancy is therefore zero at an outlet. The total transit time (T) is finally considered as the total time required by the same water particles to migrate from an inlet zone ($T = E$), to an outlet zone ($T = A$). The three temporal variables A, E and T are random variables, characterized by probability density functions that can be regarded as the statistical occurrence of water particles with respect to time, which could be observed in a groundwater sample if any analytical procedure would allow such measurements. Throughout this dissertation, the symbol 'A' will always denote the age of groundwater particles, the symbol 'E' the life expectancy of groundwater particles, and the symbol 'T' the total transit time of groundwater particles. They will mostly be used as subscripts, to indicate that a function characterizes one of these three random variables.

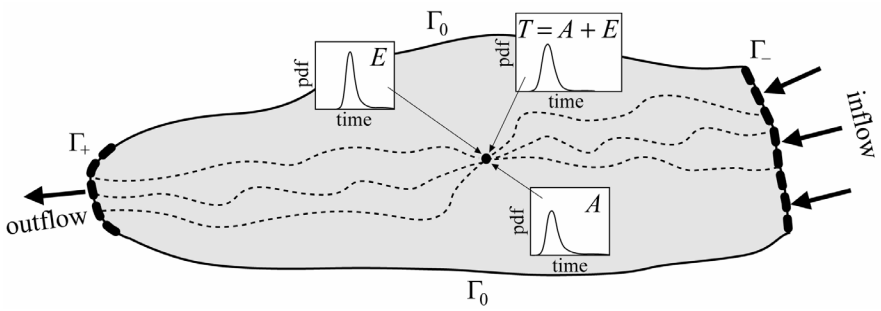

Fig. 2.1. Schematic illustration of a groundwater reservoir with three possible flow lines that pass through an element, showing the random variable total transit time (T) as the sum of the two random variables age (A) and life expectancy (E).

2.1.1 The random variables age, life expectancy, and total transit time

The behaviour of the continuous time random variables A and E can be described by probability density functions and cumulative distribution functions (cdf). Let U be one of these two variables ($U = A$ or $U = E$), with u being the associated values the variable U may take at a given position $\mathbf{x}$ in space. The cdf $G_U(\mathbf{x}, u)$ and the pdf $C_U(\mathbf{x}, u)$ of the variable U are commonly defined as

$$G_U(\mathbf{x},u) = \mathrm{P}\left[-\infty \le U \le u\right] = \int_{-\infty}^{u} C_U(\mathbf{x},\tau)d\tau \tag{2.1}$$

with

$$C_U(\mathbf{x},u) = \frac{\partial G_U(\mathbf{x},u)}{\partial u} \tag{2.2}$$

where P denotes the probability event on U, or number of occurrences with $U \le u$ ratioed to the total number of occurrences, and where τ is a dummy variable for integration. The main properties of the probability functions (2.1) and (2.2) that will be used in this work can be summarized by the following:

$$G_U(\mathbf{x},-\infty) = 0 \tag{2.3a}$$
$$G_U(\mathbf{x},\infty) = 1 \tag{2.3b}$$

For a given position $\mathbf{x}$ in Ω, the pdf C_A measures the density of probability for the groundwater particles of having ages t or less. The same particles are also characterized by the pdf C_E, which measures the density of probability of having life expectancies t or less. Introducing the random variable 'total transit time' T, with density of probability C_T, the water particles can be described by the probability to flow through the system in a time t or less. The variable T is a random variable that corresponds to the sum of the two random variables A and E. Hence, the statistical distribution of T is the pdf of the sum of A and E, $C_T = C_{A+E}$.

In the following, we show that the pdf $C_T(\mathbf{x}, t)$ of the random variable T can be found from the joint pdf $C_{A,E}(\mathbf{x}, t)$ of A and E, which characterizes the joint behaviour of A and E. For the sake of simplicity, the variable position $\mathbf{x}$ will be omitted in the following development. Let us consider the conditional density function $C_{A|E}$ of the random variable A, given that E is fixed at a particular value ϵ. Since $E = \epsilon$, one can write $T = \epsilon + A$, and the conditional distribution of A, given E, is [Benjamin & Cornell, 1970] (see Excursus 2.1):

$$C_{A|E}(\alpha,\epsilon) = \frac{C_{A,E}(\alpha,\epsilon)}{C_E(\epsilon)} \tag{2.4}$$

with α denoting the particular values the random variable A may take. According to Benjamin & Cornell [1970], the density function of a linear function of a single random variable, $Y = a + b\,X$, is

$$C_Y(y) = \left|\frac{1}{b}\right| C_X\left(\frac{y-a}{b}\right) \tag{2.5}$$

where a and b are scalar quantities. Using (2.5) with $b = 1$, the conditional pdf of T, given that $E = \epsilon$, is:

$$C_{T|E}(\omega,\epsilon) = C_{A|E}(\omega-\epsilon,\epsilon) \tag{2.6}$$

with ω denoting the particular values the random variable T may take. Using Eq. (2.4) and replacing A by T, we can express the joint density function of the two random variables T and E by multiplying the conditional pdf of T, given E, with the marginal pdf of E,

$$C_{T,E}(\omega,\epsilon) = C_{T|E}(\omega,\epsilon)\,C_E(\epsilon) \quad , \tag{2.7}$$

and the substitution of (2.6) into (2.7) yields

$$C_{T,E}(\omega,\epsilon) = C_{A|E}(\omega-\epsilon,\epsilon)\,C_E(\epsilon) \tag{2.8}$$

Using again the relationship (2.4) between conditional and marginal distribution functions, (2.8) leads to:

$$C_{T,E}(\omega,\epsilon) = C_{A,E}(\omega-\epsilon,\epsilon) \tag{2.9}$$

Eq. (2.9) reflects the fact that the likelihood that E equals ϵ and that T is the sum of A and E, is equivalent to the likelihood that E equals ϵ and that A equals $\omega - \epsilon$. The marginal distribution of T is found by integrating (2.9) over all values of ϵ:

$$C_T(\omega) = \int_{-\infty}^{+\infty} C_{T,E}(\omega,\epsilon)d\epsilon = \int_{-\infty}^{+\infty} C_{A,E}(\omega-\epsilon,\epsilon)d\epsilon \tag{2.10}$$

The joint quantity $C_{A,E}(\mathbf{x},\alpha,\epsilon)d\alpha d\epsilon$ relates to the probability that A lies in the small interval α to $\alpha + d\alpha$, and that E lies in the small interval ϵ to $\epsilon + d\epsilon$. Assuming that A and E are stochastically independent variables (for the same spatial position, A depends on the initial point while E depends on the end point, and E may not be influenced by the memory of the past evolution), the joint pdf $C_{A,E}$ simplifies in $C_A C_E$ [Benjamin & Cornell, 1970] (see Excursus 2.1). The probability density function $C_T = C_T(\mathbf{x}, t)$ in (2.10) can then be obtained by using the convolution integral:

$$C_T(\mathbf{x},t) = \int_0^t C_A(\mathbf{x},\tau)C_E(\mathbf{x},t-\tau)d\tau \tag{2.11}$$

with τ being a dummy variable for integration. The fact that C_A and C_E are zero for negative values of their arguments allows to apply the convolution integral from 0 to t. Since the pdfs C_A and C_E give the age and life expectancy probability of occurrence at each position $\mathbf{x}$ in Ω, both the maximum age as well as the maximum life expectancy correspond to the maximum total transit

time. Consequently, the time variable t can equivalently refer to all specific values of age, life expectancy, and total transit time. From Eq. (2.11), the cdf of the variable T can be calculated by enforcing Eq. (2.1). The convolution integral (2.11) states that the probability that the variable T lies within a small interval around t is proportional to the product of the probability that the variable A lies in the interval τ to $\tau + d\tau$ and a factor proportional to the probability that the variable E lies in a small interval around $t-\tau$, the value of E ensuring that A and E sum to T. This product is then summed over all possible values of time t (from the minimum age to the maximum age) to yield the total transit time pdf at a position **x** in space.

The derived distribution of $T = A + E$ in Eq. (2.11) can be viewed as a transfer function convolution process, the input distribution being the age pdf C_A, and the signal transferring function being the life expectancy C_E. The field of C_T characterizes the evolution of groundwater particles throughout the aquifer domain by specifying the amount of time from recharge to discharge. In Fig. 2.1, the meaning of the convolution process (2.11) is theoretically illustrated. At a given position in the reservoir (black dot in Fig. 2.1), the temporal evolution of the groundwater particles can be characterized by the three pdfs C_A, C_E and C_T. Each function contains specific information on a time of residence, the nature of which is a function of the spatial references that are chosen for evaluation. For instance, C_A is conditioned by the inlet limit Γ_-, where the variable A is nil, while C_E depends on the outlet limit Γ_+, where the variable E is nil. For the variable T, the pdf C_T is conditioned by the fact that $T = A$ at outlet, and that $T = E$ at inlet.

Excursus 2.1: Joint, marginal, and conditional distributions.

The joint pdf and cdf characterize the behaviour of jointly distributed random variables X and Y. The probability that X is in the interval $[x, x+dx]$ and that Y is in the interval $[y, y+dy]$ is given by $C_{X,Y}(x,y)dxdy$, where $C_{X,Y}(x,y)$ is the joint pdf of X and Y. The pdf $C_{X,Y}(x,y)$ must satisfy the conditions:

$$\int_{-\infty}^{+\infty}\int_{-\infty}^{+\infty} C_{X,Y}(x,y)dxdy = 1 \quad , \quad C_{X,Y}(x,y) = \frac{\partial^2}{\partial x \partial y} G_{X,Y} \geq 0 \tag{E2.1.1}$$

with $G_{X,Y}(x,y)$ being the joint cdf. The probability of the joint occurrence of X and Y in a region of the sampled space is determined by the integration of the joint pdf over that region:

$$\mathrm{P}[(x_1 \leq X \leq x_2) \text{ and } (y_1 \leq Y \leq y_2)] = \int_{x_1}^{x_2}\int_{y_1}^{y_2} C_{X,Y}(x,y)dydx \tag{E2.1.2}$$

The marginal pdf of the variable X is obtained by eliminating the consideration of the variable Y for the evaluation of the behaviour of X. This pdf is thus found by integrating the joint pdf $C_{X,Y}(x,y)$ over all values of Y:

$$C_X(x) = \int_{-\infty}^{+\infty} C_{X,Y}(x,y)dy = \frac{\partial}{\partial x} G_{X,Y}(x,y) \tag{E2.1.3}$$

With (E2.1.3), the symmetrical result for the marginal pdf of Y is valid.

The conditional pdf of the variable X, given a value of Y is defined by:

$$C_{X|Y}(x,y) = \frac{C_{X,Y}(x,y)}{C_Y(y)} \tag{E2.1.4}$$

and the corresponding conditional cdf is:

$$G_{X|Y}(x,y) = \mathrm{P}[X \leq x | Y = y] = \int_{-\infty}^{x} G_{X|Y}(u,y)du \tag{E2.1.5}$$

If the random variables X and Y are supposed to be stochastically independent, the following properties hold:

$$C_{X|Y}(x,y) = C_X(x) \quad \text{and} \quad C_{Y|X}(x,y) = C_Y(y) \tag{E2.1.6}$$

$$C_{X,Y}(x,y) = C_X(x)C_Y(y) \tag{E2.1.7}$$

$$G_{X|Y}(x,y) = G_X(x) \quad \text{and} \quad G_{Y|X}(x,y) = G_Y(y) \tag{E2.1.8}$$

$$G_{X,Y}(x,y) = G_X(x)G_Y(y) \tag{E2.1.9}$$

2.1.2. Resident and flux concentrations versus travel distance and travel time probabilities

In section 2.1.1 we have introduced the random variables A, E and T by defining their respective pdf and cdf. However, no process model has been developed for the physical processes that condition these probabilities in the aquifer system. Transport of conservative solutes in aquifer systems is mainly characterized by advective and dispersive phenomena. In the following, we will progressively approach an advective-dispersive process representation of the transport of C_A, C_E and C_T. Firstly, we briefly recall two definitions of the solute concentration in groundwater, and show their link with age and life expectancy probabilities.

The most common definition of a solute concentration in groundwater is the one that relates the mass of the solute per unit fluid volume, or porous volume, at a given position (Fig. 2.2). This concentration is called the resident concentration C^r. The resident concentration is the dependent variable that participates in the balance of solute mass for an element of volume in the reservoir, $\partial\phi C^r/\partial t = \nabla \cdot \mathbf{J}$, where $\mathbf{J}$ is the solute mass flux, and ϕ is porosity or mobile water content. The travel distance probability $g_{\mathbf{x}}$, or location probability, is related to the resident concentration [Kreft & Zuber, 1978; Dagan, 1987; Jury & Roth, 1990], and describes the position of water particles at a given time after their release into the system [Dagan, 1982, 1987, 1989; Jury & Roth, 1990; Neupauer & Wilson, 1999, 2001]:

$$g_{\mathbf{x}}(\mathbf{x},t) = \frac{C^r(\mathbf{x},t)}{\int_\Omega \phi(\mathbf{x}) C^r(\mathbf{x},t=0^+)\,d\Omega} \tag{2.12}$$

where the domain integral in the denominator of (2.12) normalizes the resident concentration by the total injected mass in the system. The travel distance probability is thus defined as a normalized resident concentration.

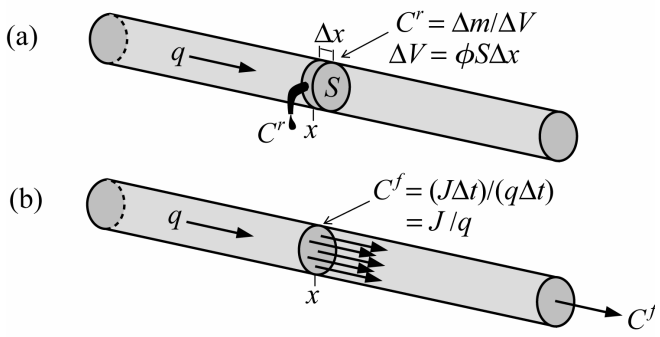

Fig. 2.2. Resident concentration (a) versus flux concentration (b). The vector q denotes the fluid flux, J denotes the total mass flux, and Δm is the solute mass in the fluid volume ΔV. After Kreft & Zuber [1986].

A second type of concentration to be distinguished from C^r is the flux concentration C^f, which is defined by the solute mass flux per unit water flux (Fig. 2.2), at a given time [Kreft & Zuber, 1978; Parker & van Genuchten, 1984]. The travel time probability g_t is related to the flux concentration [Kreft & Zuber, 1978; Jury, 1982; Shapiro & Cvetkovic, 1988; Jury & Roth, 1990; Neupauer & Wilson, 1999, 2001], and characterizes at a position $\mathbf{x}$ the amount of time spent by the water particles within Ω since they entered the system [Jury, 1982; Jury *et al.*, 1986; Dagan, 1989; Dagan & Nguyen, 1989]:

$$g_t(\mathbf{x},t) = \frac{F(\mathbf{x})C^f(\mathbf{x},t)}{m} = \frac{C^f(\mathbf{x},t)}{\int_0^\infty C^f(\mathbf{x},t)dt} \tag{2.13}$$

where m is the released mass, C^f is the flux concentration, and $F(\mathbf{x})$ is the flow rate passing through the section area across which C^f is evaluated. For conservative tracers, the time-integral in the denominator of the right-hand side of (2.13) is equivalent to the flow rate divided by the released mass. The travel time probability is thus defined as a normalized flux concentration.

The multi-dimensional relation between flux and resident concentrations can be found in Sposito & Barry [1987], and is formally the projection of the mass flux vector **J** onto the flow velocity direction:

$$C^f = \frac{\mathbf{J}\cdot\mathbf{q}}{\|\mathbf{q}\|^2} = C^r + \frac{\mathbf{J}_d\cdot\mathbf{q}}{\|\mathbf{q}\|^2} = C^r - \frac{\mathbf{D}\nabla C^r\cdot\mathbf{q}}{\|\mathbf{q}\|^2} \tag{2.14}$$

with $\mathbf{J}^d = -\mathbf{D}\nabla C$ being the dispersive part of the solute mass flux $\mathbf{J} = \mathbf{q}C^r + \mathbf{J}^d$, **q** being the water flux vector, and **D** being the dispersion tensor. Accordingly, the flux concentration form of the random variable age is:

$$C_A^f = \frac{\mathbf{J}_A\cdot\mathbf{q}}{\|\mathbf{q}\|^2} = C_A^r - \frac{\mathbf{D}\nabla C_A^r\cdot\mathbf{q}}{\|\mathbf{q}\|^2} \tag{2.15}$$

with $\mathbf{J}_A$ denoting the total age mass flux:

$$\mathbf{J}_A = \mathbf{q}C_A^r - \mathbf{D}\nabla C_A^r \tag{2.16}$$

With Eq. (2.16), it is supposed that the standard model of solute mass flux that corresponds to a decomposition of $\mathbf{J}_A$ into an advective part and a dispersive part, is adopted. Dispersion can be classically modelled as Fickian diffusion, by means of a tensor of macro-dispersion **D**.

By analogy, the flux concentration form of the variable E can be defined as

$$C_E^f = -\frac{\mathbf{J}_E\cdot\mathbf{q}}{\|\mathbf{q}\|^2} = C_E^r + \frac{\mathbf{D}\nabla C_E^r\cdot\mathbf{q}}{\|\mathbf{q}\|^2} \tag{2.17}$$

with $\mathbf{J}_E$ the total life expectancy mass flux:

$$\mathbf{J}_E = -\mathbf{q}C_E^r - \mathbf{D}\nabla C_E^r \tag{2.18}$$

Following Parker & van Genuchten [1984], a flux concentration is the physical representation of the mean of the microscopic fluid concentrations weighted by the associated microscopic fluid velocities. If as an example we consider the random variable A for a given position **x**, the age distribution C_A, which characterizes the probability per unit time for the time spent since recharge (t is a random variable), should be defined in terms of flux concentration ($C = C^f$). The resident concentration of age ($C = C^r$) will rather characterize a volume-averaged age density function, which describes the density of probability of finding water particles at the position **x** (**x** is a random variable), at time t.

If C_A and C_E are resident concentrations, so is C_T. If C_A and C_E are flux concentrations, so is C_T. Applying a Laplace transform (see Excursus 2.2) to Eqs. (2.15) and (2.17) and convoluting, the total transit time resident and flux concentrations are found to be linked by the following relation:

$$\begin{aligned}\hat{C}_T^f &= \hat{C}_A^f \hat{C}_E^f = \hat{C}_T^r + \frac{1}{\|\mathbf{q}\|^2}[\hat{C}_E^r \hat{\mathbf{J}}_A^d - \hat{C}_A^r \hat{\mathbf{J}}_E^d - \frac{(\hat{\mathbf{J}}_A^d \otimes \hat{\mathbf{J}}_E^d)\mathbf{q}}{\|\mathbf{q}\|^2}] \cdot \mathbf{q} \\ &= \hat{C}_A^f \hat{C}_E^r + \hat{C}_A^r \hat{C}_E^f - \hat{C}_T^r - \frac{(\hat{\mathbf{J}}_A^d \otimes \hat{\mathbf{J}}_E^d)\mathbf{q}}{\|\mathbf{q}\|^4} \cdot \mathbf{q}\end{aligned} \tag{2.19}$$

where $\hat{C}_U(\mathbf{x}, s)$ denotes the s-transform state of the function $C_U(\mathbf{x}, u)$, with $U = A, E$ or T. Eq. (2.19) shows that the total transit time flux concentration is dependent on the total transit time resident concentration, but also on the tensor product between the age and the life expectancy dispersive fluxes, and on the convolution product of the age and life expectancy flux and resident concentrations. For a zero dispersion case, $C^f = C^r$ for the three random variables A, E and T.

Excursus 2.2: Conventions used for the Laplace transforms.

The Laplace transform L of a function $f(t)$, for $0 \le t < \infty$, is defined as

$$\hat{f}(s) = \mathrm{L}\{f(t)\} = \int_0^\infty e^{-st} f(t)\, dt \tag{E2.2.1}$$

where s is Laplace variable [T^{-1}], and $\hat{f}(s)$ is the s-transformed state of $f(t)$. The inverse transform to return into the time domain is

$$f(t) = \mathrm{L}^{-1}\left\{\hat{f}(s)\right\} = \frac{1}{2\pi i}\int_{\gamma - i\infty}^{\gamma + i\infty} e^{st} \hat{f}(s)\, ds \tag{E2.2.2}$$

with $i = \sqrt{-1}$ and where γ is a positive constant chosen large enough, with the result that all singularities of the s-transformed function $f(t)$ in the Bromwich contour integral (E2.2.2) lie to the left of the line drawn normal to the real axis through the point γ. The superscript $\hat{}$ will be used throughout this work to denote the s-transformed state of a temporal function.

We only give some useful properties of the Laplace transform, with respect to Eqs. (2.1), (2.2) and (2.11). The Laplace transform of the derivative of a function is:

$$\mathrm{L}\left\{\frac{\partial f(t)}{\partial t}\right\} = s\hat{f}(s) - f(t=0) \tag{E2.2.3}$$

The Laplace transform of the integral of a function is:

$$\mathrm{L}\left\{\int_0^t f(u)du\right\} = \frac{\hat{f}(s)}{s} \tag{E2.2.4}$$

The convolution theorem in the Laplace domain is:

$$\langle f * g \rangle = L\left\{\int_0^t f(u)g(t-u)du, t, s\right\} = \hat{f}(s)\hat{g}(s) \tag{E2.2.5}$$

The double Laplace transform L^2 of a function $f(x,t)$ can be defined as

$$\tilde{f}(r,s) = \mathrm{L}^2\{f(x,t)\} = \int_0^\infty e^{-rx}\hat{f}(x,s)dx = \int_0^\infty\int_0^\infty e^{-rx-st} f(x,t)dxdt \tag{E2.2.6}$$

2.2. Basic equations for age and life expectancy probabilities

The typical heterogeneity of aquifer systems involves strongly varying flow velocity fields, with multi-scale coherence lengths. The existence of various levels of uncertainty in characterizing this heterogeneity leads to difficulties in the prediction of solute movement in such fields. The spatial variability of velocity and transport parameters induces a spreading of the contaminant mass. The advection-dispersion equation (ADE) is a classical model of contaminant transport in groundwater. It requires the pre-solution of velocity fields at a sufficiently small scale, e.g. at a refinement level of 10m over a 1000m aquifer extension. The tensor of macro-dispersion in the ADE accounts for the uncertainty in the transport prediction induced by mixing. Various studies relate to how the ADE is limited by the impact of physical and chemical heterogeneities on solute transport, so that up-scaling is not always satisfactory [e.g. Dagan, 1984; Sudicky, 1986; Gelhar & Axness, 1983]. If such heterogeneities are present at aquifer scale the transport parameters should be time-dependent, but this time dependency may be relaxed when the correlation scales of the transport parameter random fields are finite [Gelhar & Axness, 1983; Neumann *et al.*, 1987]. The ADE with time-independent parameters holds only when the solute particles have enough time to be distributed by dispersion between the flow lines. Solving the ADE using 'large-scale' velocity fields to predict transport phenomena at a smaller-scale is thus an assumption that may not always be valid, and one must keep in mind the pragmatic question of what equation is to be used and at which scale [Gelhar, 1993].

In this work, we are interested in solving the age transport problem at aquifer scale. Consequently, we make the assumption that the ADE with time-independent transport parameters (the parameters have reached their asymptotic values) can model the evolutional transport of the groundwater age and life expectancy distributions under steady-flow conditions.

2.2.1. Age pdf by forward advective – dispersive transport modelling

Let us consider an aquifer domain Ω in the three-dimensional space, with hydraulic recharge boundary Γ_- and discharge boundary Γ_+, and impervious boundary Γ_0, as illustrated in Fig. 2.1 or Fig. 2.3. The flow field is considered divergence free ($\nabla \cdot \mathbf{q} = 0$). The age pdf at a position $\mathbf{x}$ in Ω can be evaluated by solving the ADE when a unit pulse of conservative tracer is uniformly applied on the recharge area Γ_-. As already said before, the resulting breakthrough curve is the probabilistic age distribution [Danckwerts, 1953; Jury & Roth, 1990]. Making use of this property, we propose to model the groundwater age pdf by the forward advection-dispersion equation. The age pdf at a given position $\mathbf{x}$ is a solution of the following forward boundary-value problem:

$$\frac{\partial \phi C_A}{\partial t} = -\nabla \cdot \mathbf{q} C_A + \nabla \cdot \mathbf{D} \nabla C_A \qquad \text{in} \quad \Omega \qquad (2.20)$$

$$C_A(\mathbf{x}, 0) = C_A(\mathbf{x}, \infty) = 0 \qquad \text{in} \quad \Omega \qquad (2.21)$$

$$C_A(\mathbf{x}, t) = \delta(t) \qquad \text{on} \quad \Gamma_- \qquad (2.22)$$

$$\mathbf{J}_A(\mathbf{x}, t) \cdot \mathbf{n} = \mathbf{q} \cdot \mathbf{n}\, \delta(t) \qquad \text{on} \quad \Gamma_- \qquad (2.23)$$

Implicit Neumann condition on Γ_+ (2.24)

$$\mathbf{J}_A(\mathbf{x}, t) \cdot \mathbf{n} = 0 \qquad \text{on} \quad \Gamma_0 \qquad (2.25)$$

where $C_A(\mathbf{x}, t)$ is the transported age probability distribution, $\mathbf{x}$ is the vector of Cartesian coordinates, t is time, ϕ is porosity or mobile water content, $\mathbf{q}$ is the water flux vector, $\mathbf{D}$ is the tensor of macro-dispersion, $\mathbf{n}$ is a normal outward unit vector, and $\delta(t)$ is the time-Dirac delta function, which ensures a pure impulse on Γ_-. The age flux vector $\mathbf{J}_A$ has been defined in Eq. (2.16). The tensor of macro-dispersion $\mathbf{D}$ is defined as

$$\mathbf{D} = (\alpha_{\mathrm{L}} - \alpha_{\mathrm{T}}) \frac{\mathbf{q} \otimes \mathbf{q}}{\|\mathbf{q}\|} + \alpha_{\mathrm{T}} \|\mathbf{q}\| \mathbf{I} + \phi D_{\mathrm{m}} \mathbf{I} \tag{2.26}$$

where α_{L} and α_{T} are the longitudinal and transversal coefficients of dispersivity, respectively, D_{m} is the coefficient of molecular diffusion, and $\mathbf{I}$ is the identity matrix.

In Eq. (2.20), the classical homogeneous Neumann boundary condition $\mathbf{D}\nabla C \cdot \mathbf{n} = 0$ at the outlet limit is not used, in order to allow a natural age gradient on Γ_+. Instead, the dispersive flux projection is evaluated implicitly at outflowing boundaries, with the consequence that the concentration gradient is not forced to be zero, but is equal to an unknown function. This kind of boundary condition, which is referred to as *Implicit Neumann* condition, enables a total flux continuity at outlet. As discussed by Nauman & Buffham [1983], Parker & van Genuchten [1984], Kreft & Zuber [1986], and Bear & Verruitj [1987], a total mass flux continuity at outlet permits upgradient solute movement by dispersion from Γ_+. The *Implicit Neumann* condition is not prescribed since the dependent variable is unknown, but the operator $\mathbf{D}\nabla()$ is implicitly formulated. Since the age problem requires total flux continuity at the inlet and outlet boundaries, this condition is of prime importance. The effects of this particular boundary condition on the calculated age pdf will be discussed in detail in Chapter 3. The technical computation of this boundary condition within the framework of the finite element method is developed in Appendix B.

The first-kind Dirichlet type boundary condition (2.22) and the third-kind Cauchy type boundary condition (2.23) are both expressed since these two conditions appear to be the most meaningful to simulate the age problem. However, the choice between the first-kind and the third-kind condition has to be made with careful attention to the nature of the dependent variable C_A, although we may be tempted to claim that the third-kind condition is best suited to deal with the age problem in multidimensional domains. The Cauchy-type boundary condition (2.23) is homogeneous at $t > 0$ (zero flux), and prevents solute from moving upstream and exiting the system by the inlet limits. The Dirichlet type condition is also homogeneous at $t > 0$, but however it does not prevent the backward movement of water particles at inflowing limits, when dispersion is significant. This point will be elaborated in detail in Chapter 3. The Cauchy type condition also ensures that the dependent variable C_A is related to resident concentration ($C = C^r$), from which the flux concentration can be derived enforcing Eq. (2.15). It also ensures that the mass flux at outlet corresponds to the transit time response to an instantaneous mass flux input at inlet.

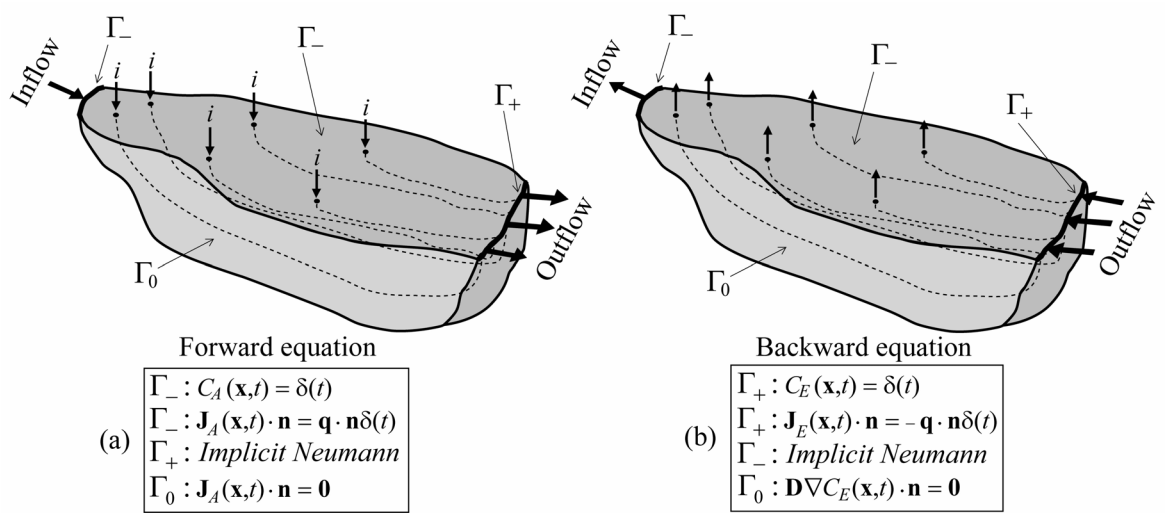

Fig. 2.3. Schematic illustration of a groundwater reservoir in the 3D space, with inlet zone Γ_- (*i* denotes an areal infiltration rate), outlet zone Γ_+, and no-flow boundary Γ_0: (a) Boundary conditions for the age problem; (b) Boundary conditions for the life expectancy problem.

Since the released mass at inlet is unity, whenever the third-kind boundary condition is used at inlet, the function $C_A(\mathbf{x}, t)$ is directly the pdf for the location of the water particles at time t after recharge (see Eq. (2.12)). When the first-kind boundary condition is used, the function $C_A(\mathbf{x}, t)$ reflects the pdf for the travel time t from the recharge zone to a point in the reservoir (see Eq. (2.13)). Therefore, since concentration can be modelled by ADE, then age probability can also be modelled by the ADE.

2.2.2. Life expectancy pdf by backward advective – dispersive transport modelling

The life expectancy probability as defined in section 2.1.1 characterizes the time that water particles will experience from a point in the reservoir until an exit zone. If we conceptualize the water particles following the streamlines from an exit zone in the upstream direction, then the life expectancy at a given point can be considered as the time counted backwards from the nil initial time at the exit zone. To evaluate such a probability, a backward equation is required. The life expectancy probability distribution $C_E(\mathbf{x}, t)$ satisfies the adjoint backward model of Eq. (2.20), and may be defined as a solution of the following boundary-value problem:

$$\frac{\partial \phi C_E}{\partial t} = \nabla \cdot \mathbf{q} C_E + \nabla \cdot \mathbf{D} \nabla C_E \qquad \text{in} \quad \Omega \qquad (2.27)$$

$$C_E(\mathbf{x}, 0) = C_E(\mathbf{x}, \infty) = 0 \qquad \text{in} \quad \Omega \qquad (2.28)$$

$$C_E(\mathbf{x}, t) = \delta(t) \qquad \text{on} \quad \Gamma_+ \qquad (2.29)$$

$$\mathbf{J}_E(\mathbf{x}, t) \cdot \mathbf{n} = -\mathbf{q} \cdot \mathbf{n}\, \delta(t) \qquad \text{on} \quad \Gamma_+ \qquad (2.30)$$

Implicit Neumann condition on Γ_- (2.31)

$$\mathbf{D} \nabla C_E \cdot \mathbf{n} = 0 \qquad \text{on} \quad \Gamma_0 \qquad (2.32)$$

where $\mathbf{J}_E$ is the life expectancy flux vector having been defined in Eq. (2.18). As in the forward problem (2.20), the life expectancy gradient on Γ_- is not assumed to be zero, and the *Implicit Neumann condition* is used at the inlet boundaries.

Eq. (2.27) is the formal adjoint of Eq. (2.20) [Garabedian, 1964; Arnold, 1974], the so-called "backward-in-time" equation [Uffink, 1989; Wilson & Liu, 1997; Weissmann *et al.*, 2002]. It describes how the dependent variable depends on the initial position $\mathbf{x}$ [Gardiner, 1983, p. 128; Uffink, 1989], with the density of probability $C_E(\mathbf{x}, t)$ for the past location $\mathbf{x}$, given that the future position is known. In this case, the final position is Γ_+.

To characterize the probability for the position of water particles at a time t after recharge, the forward ADE (2.20) has been assimilated to the Fokker-Planck equation (or forward Kolmogorov equation), which analyses the random motion of water particles [Uffink, 1989]. The backward equation (2.27) must be related to the backward Kolmogorov equation. Briefly, the forward Kolmogorov equation in standard diffusion theory corresponds to a diffusion process governed by the Ito stochastic differential equation, $d\mathbf{x}(t) = \boldsymbol{A}(\mathbf{x}, t)dt + F(\mathbf{x}, t)d\boldsymbol{W}(t)$ [Gardiner, 1983, p. 144]. The term $A(\mathbf{x}, t)$ is a drift vector, and the term $F(\mathbf{x}, t)d\boldsymbol{W}(t)$ accounts for the stochastic displacement of the particles due to dispersion, with $\boldsymbol{W}(t)$ representing independent Wiener processes, and with $\boldsymbol{F}(\mathbf{x}, t)$ being an amplitude tensor related to the dispersion tensor, $F_{ik}F_{jk} = 2D_{ij}$ [Uffink, 1989]. LaBolle *et al.* [1998] recall that the standard diffusion theory, which relates the dynamics of a diffusion process to Kolmogorov's equations [1931], may apply to ADEs if porosity and dispersion tensor are functions varying smoothly in space. They derived general probabilistic definitions for the velocity and dispersion tensor that ensure applicability of the diffusion theory at local scale.

Given the forward equation, the backward equation is technically obtained by reversing the sign of the flow field, and by adapting the boundary conditions [Wilson & Liu, 1997; Neupauer & Wilson, 1999, 2001; Weissmann *et al.*, 2002]. The advection term is known to be not self-adjoint (it should be written in the form $\mathbf{q}\cdot\nabla C_E$ in Eq. (2.27)) unless flow is divergence free [Weissmann *et al.*, 2002]. Note that on the impermeable boundary Γ_0, a Cauchy type condition (third-kind) in the forward equation becomes a Neumann type condition (second-kind) in the backward equation. A second-kind condition in the forward model would also become a third-kind condition in the backward model [see Gardiner, 1983, pp. 146]. The classical forward ADE is useful to predict the future position of the water particles. On the other hand, the backward-in-time ADE is well-suited for solving transport problems when the ultimate position is known, and when the past positions are to be predicted. This modelling method was used by Neupauer & Wilson [1999, 2001] to detect the possible sources of contamination which was observed at a monitoring well or an extraction well.

We have seen that the age flux pdf C_A is comparable to the travel time probability from inlet to a given point in the reservoir. The pdf C_E gives a measure at the same point of the time water particles will still have to travel to a downgradient outlet. Once the spatial distributions of C_A and C_E are known, the function C_T can be post-processed at all points by enforcing Eq. (2.11), to obtain the total transit time pdf from inlet to outlet.

2.2.3. Total transit time equation

Combining Eq. (2.20) and Eq. (2.27) after a Laplace transform, the following equation can be obtained:

$$\mathbf{q}\cdot\nabla\hat{C}_T = \hat{S}_d \tag{2.33}$$

with

$$\hat{S}_d = \hat{C}_A\nabla\cdot\hat{\mathbf{J}}_E^d - \hat{C}_E\nabla\cdot\hat{\mathbf{J}}_A^d \tag{2.34}$$

Eq. (2.33) is the total transit time pdf differential equation. It is of steady-state kind, with a source term that accounts for the divergence of the age and life expectancy dispersive fluxes. For the pure advective case Eq. (2.33) simplifies in $\mathbf{q}\cdot\nabla C_T(\mathbf{x}, t) = 0$, i.e. the fluid flux vector $\mathbf{q}$ is orthogonal to the gradient vector ∇C_T. The resolution of Eq. (2.33), which is of hyperbolic kind, is linked to technical difficulties, e.g. for the evaluation of the source term S_d over the domain, and is not beneficial since the pdfs C_A and C_E must be evaluated in a preliminary step.

2.2.4. Temporal moments of the pdfs and moment equations

Regardless of the nature of the function $C_U(\mathbf{x}, u)$, with $U = A$, E, or T, the average values of the probability density functions C_A, C_E and C_T are defined by their first order temporal moment, the n^{th} moment μ_n being

$$\mu_n[C_U] = \int_{-\infty}^{+\infty} u^n C_U(\mathbf{x},u)\,du \tag{2.35}$$

or after a Laplace transform

$$\mu_n[C_U] = (-1)^n \frac{\partial^n \hat{C}_U(\mathbf{x}, s=0)}{\partial s^n} \tag{2.36}$$

Applying the convolution theorem in the Laplace domain results in the transformed Eq. (2.11), $\hat{C}_T(\mathbf{x},s) = \hat{C}_A(\mathbf{x},s)\hat{C}_E(\mathbf{x},s)$. Accounting for the transformed pdf property (2.3b), $\hat{C}_U(\mathbf{x},s=0)=1$, and enforcing Eq. (2.36) for $n = 1$ yields

$$\mu_1[C_T] = -\hat{C}_A(\mathbf{x},s=0)\frac{\partial \hat{C}_E(\mathbf{x},s=0)}{\partial s} - \hat{C}_E(\mathbf{x},s=0)\frac{\partial \hat{C}_A(\mathbf{x},s=0)}{\partial s} = \mu_1[C_A] + \mu_1[C_E] \tag{2.37}$$

Using a similar procedure for $n = 2$, it can also be shown that the second moment of C_T is

$$\mu_2[C_T] = \mu_2[C_A] + \mu_2[C_E] + 2\,\mu_1[C_A]\,\mu_1[C_E] \ , \tag{2.38}$$

and that the variance of C_T is

$$\sigma^2[C_T] = \sigma^2[C_A] + \sigma^2[C_E] \tag{2.39}$$

The average age and average life expectancy of a water sample sum up to the average total transit time. The variances of the age and life expectancy pdfs also sum up to the variance of the total transit time pdf. Note that this simple sum in Eq. (2.39) comes from the fact that the variables A and E are supposed to be stochastically independent.

The temporal moments have a real physical meaning if they are related to flux concentration functions, while spatial moments must characterize resident concentration functions [Kreft & Zuber, 1978, 1986; Parker & van Genuchten, 1984, 1986; Sposito & Barry, 1987]. Therefore, the dependent variable in (2.35) is to be related to flux concentration.

Using the operator in (2.36), Eqs. (2.20) and (2.27) can be transformed into their n^{th} normalized moment form. The recursive application of (2.36) to (2.20) and (2.27) yields

$$-\nabla\cdot\mathbf{q}\mu_n[C_A] + \nabla\cdot\mathbf{D}\nabla\mu_n[C_A] + \phi n\mu_{n-1}[C_A] = 0 \tag{2.40}$$

for the forward moment ADE, and

$$\nabla\cdot\mathbf{q}\mu_n[C_E] + \nabla\cdot\mathbf{D}\nabla\mu_n[C_E] + \phi n\mu_{n-1}[C_E] = 0 \tag{2.41}$$

for the backward moment ADE. The n^{th} moment forms of the ADEs (2.20) and (2.27) are only dependent on the $(n-1)^{\text{th}}$ moment μ_{n-1}. For instance, since $\mu_0[C_A] = 1$ and $C_A(\mathbf{x},0) = 0$, the first moment form of Eq. (2.20) corresponds to the mean age equation as defined by Goode [1996, 1998], in which the mean age is the average over a sample of water molecules of the time elapsed since recharge:

$$-\nabla\cdot\mathbf{q}\langle A\rangle + \nabla\cdot\mathbf{D}\nabla\langle A\rangle + \phi = 0 \tag{2.42}$$

with $\langle A\rangle = \mu_1[C_A]$. With $\langle E\rangle = \mu_1[C_E]$, $\mu_0[C_E] = 1$ and $C_E(\mathbf{x},0) = 0$, the first moment form of Eq. (2.27) gives the adjoint backward equation for mean life expectancy:

$$\nabla\cdot\mathbf{q}\langle E\rangle + \nabla\cdot\mathbf{D}\nabla\langle E\rangle + \phi = 0 \tag{2.43}$$

The boundary value problems (2.20) and (2.27) involve that the finite moments of the age and life expectancy pdfs exist for homogeneous boundary conditions. By definition, the mean groundwater age in a steady-flow reservoir, or mean residence time, can be determined from the average of the normalized flux concentration response to a narrow flux input uniformly applied on the recharge limits (see Eq. (2.13)), since this breakthrough curve corresponds to the water particles residence

time distribution [Danckwerts, 1953; Kreft & Zuber, 1978; Jury, 1982; Jury & Roth, 1990]. The mean groundwater age can then be calculated by prescribing at all inflow boundaries a solute mass that is proportional to the water flux [Harvey & Gorelick, 1995]. Consequently, Eqs. (2.42) and (2.43) are solved by assigning $\langle A \rangle = 0$ on the inlet limits Γ_-, and $\langle E \rangle = 0$ on the outlet limits Γ_+, respectively. The mean age and the mean life expectancy are continuously generated during groundwater flow, since porosity acts as a source term in both equations (2.42) and (2.43). This source term indicates that groundwater is aging one unit per unit time, in average. The mean age and mean life expectancy equations can be easily handle by numerical codes that solve the ADE, by distributing a source term equal to porosity, and by reversing the velocity field for the case of Eq. (2.43). Dirichlet type conditions can be used for letting $\langle A \rangle$ be nil on the inlet limits Γ_-, and $\langle E \rangle$ be nil on the outlet limits Γ_+. These technical procedures are nowadays already available in commercial simulators, as e.g. in the FEFLOW software package [Diersch, 2002].

The mean total transit time equation is deduced by subtracting (2.42) and (2.43):

$$\mathbf{q} \cdot \nabla \langle T \rangle = \langle S_d \rangle \tag{2.44}$$

with $\langle T \rangle = \mu_1[C_T] = \langle A \rangle + \langle E \rangle$, and $\langle S_d \rangle = \nabla \cdot \mathbf{D} \nabla \langle A \rangle - \nabla \cdot \mathbf{D} \nabla \langle E \rangle$. Eq. (2.44) requires the boundary conditions $\langle T \rangle = \langle E \rangle$ on Γ_-, and $\langle T \rangle = \langle A \rangle$ on Γ_+.

The pure advective form of Eq. (2.42),

$$-\nabla \cdot \mathbf{q} \langle A \rangle + \phi = 0 \quad , \tag{2.45}$$

yields a solution similar to a forward particle-tracking solution, as stated by Goode [1996, 1998]. Consequently, the pure advective form of Eq. (2.43),

$$\nabla \cdot \mathbf{q} \langle E \rangle + \phi = 0 \quad , \tag{2.46}$$

yields a solution similar to a backward particle-tracking solution. Finally, if dispersion is nil, the solution of Eq. (2.44), $\mathbf{q} \cdot \nabla \langle T \rangle = 0$, yields a solution comparable to the stream lines in a flow model, and associates to each line the advective total transit time from inlet to outlet.

2.2.5. One-dimensional example

If we consider a semi-infinite 1D domain of characteristic length L (the outlet is supposed at the position $x = L$) and uniform velocity v along the x-axis, the age flux pdf at the position x is obtained as the solution of the one-dimensional form of Eq. (2.20) with the boundary condition (2.22) at $x = 0$. The age resident pdf is obtained as the solution of Eq. (2.20) with the boundary condition (2.23) at $x = 0$. These solutions are given in Excursus 2.3, under their dimensionless form, and show the trivial fact that for a one-dimensional flow configuration, the total transit time flux pdf is unique and independent on the spatial coordinate, as illustrated in Fig. 2.4a. For example, the age flux pdf at one quarter of the column (dimensionless distance X = 1/4 in Fig. 2.4a) is equal to the life expectancy flux pdf at three quarters of the column (X = 3/4 in Fig. 2.4a), and the convolution of both distributions gives the total transit time flux pdf, which equals the age flux pdf at outlet (X = 1) and the life expectancy flux pdf at inlet (X = 0). The average age x/v and the average life expectancy $(L-x)/v$ sum to the average total transit time L/v, which is independent on the x-position in a rectilinear flow line.

In a similar way, the age resident pdf at the position X equals the life expectancy resident pdf at the position 1 – X, as shown in Fig. 2.4b. For a fixed value of time, the total transit time resident pdf is constant. This shows that, in 1D, the intensity of probability of finding water particles at any

position in the domain that transit at time t or less, given that t is fixed, is always identical, $C_T^r(x,t=u)=C_T^r(u)$. The total transit time resident pdf gives the intensity of probability for the spatial position of water particles, for a given value of total transit time. In 1D, this intensity of probability is uniform since the trajectory is unique. The resident age and life expectancy curves show the typical apparent discontinuity in concentration at inlet (resident pdf of A) and at outlet (resident pdf of E), as shown in Fig. 2.4b. These discontinuities have a drawback on the total transit time resident pdf, which is not necessarily equal to the age resident pdf at outlet, and equivalently not necessarily equal to the life expectancy resident pdf at inlet. This can be attributed to dispersion effects at the boundaries. Since the Cauchy condition is homogeneous at $T = 0^+$, at inlet for the age pdf problem, and at outlet for the life expectancy pdf problem, backward movement of water particles by dispersion (i.e. at the reserved direction of velocity) is put down by non-zero age and life expectancy resident concentrations at the boundaries, the magnitude of which is higher, the higher the dispersivity. If we consider e.g. the inlet boundary (at X = 0 in Fig. 2.4b), the age and life expectancy concentrations are both not nil. The convolution of both pdfs is, therefore, not equal to any of them (age pdf at outlet, life expectancy pdf at outlet) since both concentrations can have a significant value at inlet and outlet at the same time.

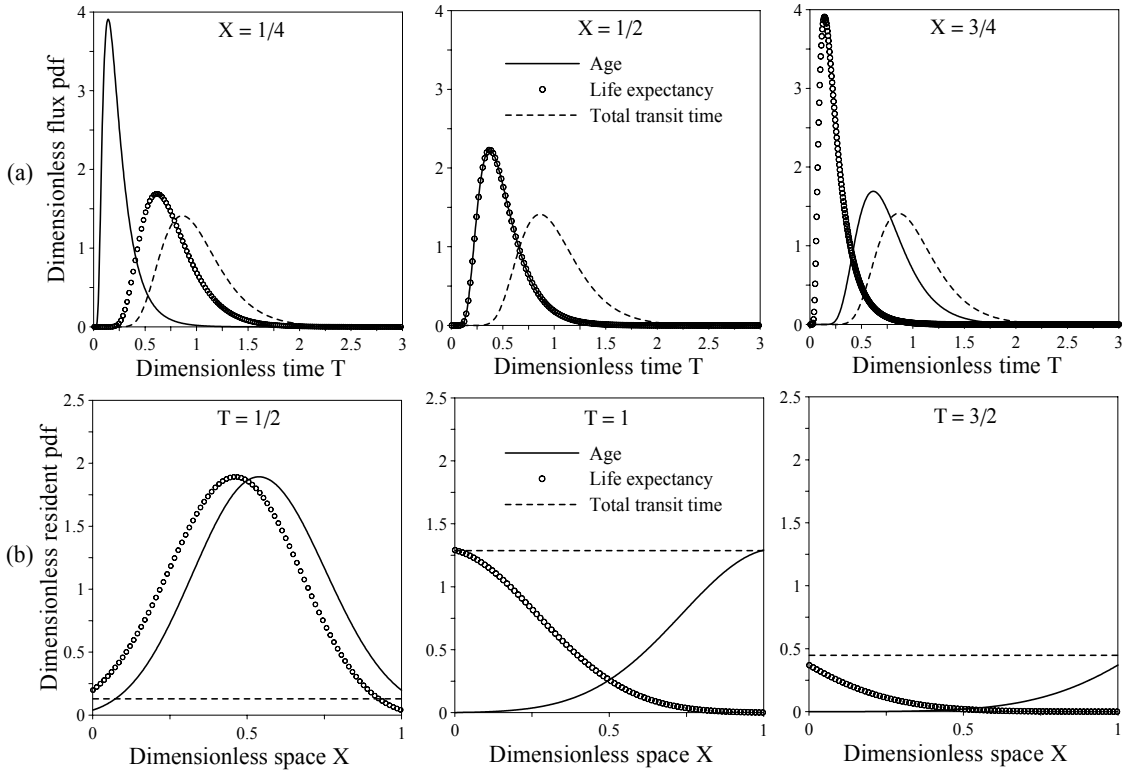

Fig. 2.4. Age, life expectancy and total transit time dimensionless pdfs in a 1D domain for a Péclet number Pe = Lv/D = 20: (a) Flux concentration pdfs; (b) Resident concentration pdfs.

Excursus 2.3: 1D semi-infinite flow domain.

The age resident concentration is found by solving the one-dimensional ADE with the Cauchy type condition $vC_A^r(0,t)-D\partial C_A^r(0,t)/\partial x=v\delta(t)$, and with a zero concentration gradient at a point at infinity. This solution is e.g. given in Jury & Roth [1990]:

$$C_A^r(x,t)=\frac{v}{\sqrt{\pi Dt}}\exp\left(-\frac{1}{4}\frac{(x-vt)^2}{Dt}\right)-\frac{v^2}{2D}\exp\left(\frac{vx}{D}\right)\operatorname{erfc}\left(\frac{x+vt}{2\sqrt{\pi Dt}}\right) \qquad \text{(E2.3.1)}$$

When divided by v, the solution (E2.3.1) is explicitly equivalent to the solution of the initial value problem with the initial condition $\delta(x)$, which defines the resident pdf [Jury & Roth, 1990], or location probability $g_{\mathbf{x}}(x,t)$ as defined in Eq. (2.12). The age flux concentration corresponding to the resident concentration (E2.3.1) is

$$C_A^f(x,t) = C_A^r(x,t) - \frac{D}{v}\frac{\partial C_A^r(x,t)}{\partial x} = \frac{x}{2\sqrt{\pi D}t^{3/2}}\exp\left(-\frac{1}{4}\frac{(x-vt)^2}{Dt}\right) \quad , \tag{E2.3.2}$$

which corresponds to the solution of the 1D ADE using the boundary condition $C_A^f(0,t) = \delta(t)$. The age flux concentration in Eq. (E2.3.2) is the age flux pdf, or travel probability $g_t(x,t)$ as defined in Eq. (2.13). Using the dimensionless variables

$$\mathrm{X} = \frac{x}{L} \qquad \mathrm{T} = \frac{t}{\tau_0} = \frac{vt}{L} \qquad \mathrm{Pe} = \frac{vL}{D}$$

where L is a characteristic length defining the supposed outlet position, and where Pe is the Péclet number, Eqs. (E2.3.1) and (E2.3.2) become

$$C_A^r(\mathrm{X},\mathrm{T}) = \frac{\sqrt{\mathrm{Pe}}}{\sqrt{\pi \mathrm{T}}}\exp\left(-\frac{\mathrm{Pe}(\mathrm{X}-\mathrm{T})^2}{4\mathrm{T}}\right) - \frac{\mathrm{Pe}}{2}\exp(\mathrm{XPe})\,\mathrm{erfc}\left(\frac{\sqrt{\mathrm{Pe}}(\mathrm{X}+\mathrm{T})}{2\sqrt{\mathrm{T}}}\right) \tag{E2.3.3}$$

$$C_A^f(\mathrm{X},\mathrm{T}) = \frac{\mathrm{X}\sqrt{\mathrm{Pe}}}{2\sqrt{\pi}\mathrm{T}^{3/2}}\exp\left(-\frac{\mathrm{Pe}(\mathrm{X}-\mathrm{T})^2}{4\mathrm{T}}\right) \tag{E2.3.4}$$

The life expectancy flux and resident concentrations can be deduced from (E2.3.3) and (E2.3.4) by substitution of X by $1-\mathrm{X}$:

$$C_E^r(\mathrm{X},\mathrm{T}) = \frac{\sqrt{\mathrm{Pe}}}{\sqrt{\pi \mathrm{T}}}\exp\left(-\frac{\mathrm{Pe}(1-\mathrm{X}-\mathrm{T})^2}{4\mathrm{T}}\right) - \frac{\mathrm{Pe}}{2}\exp([1-\mathrm{X}]\,\mathrm{Pe})\,\mathrm{erfc}\left(\frac{\sqrt{\mathrm{Pe}}(1-\mathrm{X}+\mathrm{T})}{2\sqrt{\mathrm{T}}}\right) = C_A^r(1-\mathrm{X},\mathrm{T}) \tag{E2.3.5}$$

$$C_E^f(\mathrm{X},\mathrm{T}) = \frac{(1-\mathrm{X})\sqrt{\mathrm{Pe}}}{2\sqrt{\pi}\mathrm{T}^{3/2}}\exp\left(-\frac{\mathrm{Pe}(1-\mathrm{X}-\mathrm{T})^2}{4\mathrm{T}}\right) = C_A^f(1-\mathrm{X},\mathrm{T}) \tag{E2.3.6}$$

The total transit time flux concentration is calculated by direct application in the time domain of the convolution integral in Eq. (2.11):

$$C_T^f(\mathrm{X},\mathrm{T}) = \int_0^{\mathrm{T}} C_A^f(\mathrm{X},\mathrm{T}')C_E^f(\mathrm{X},\mathrm{T}-\mathrm{T}')d\mathrm{T}' = \frac{\sqrt{\mathrm{Pe}}}{2\sqrt{\pi}\mathrm{T}^{3/2}}\exp\left(-\frac{\mathrm{Pe}(1-\mathrm{T})^2}{4\mathrm{T}}\right) = C_A^f(1,\mathrm{T}) = C_E^f(0,\mathrm{T}) \tag{E2.3.7}$$

We can see that the total transit time flux concentration in Eq. (E2.3.7) could have been obtained by substitution of X by 1 in Eq. (E2.3.4), or by substitution of X by 0 in Eq. (E2.3.6). The total transit time resident concentration is found by convoluting (E2.3.3) and (E2.3.5) in the Laplace domain. The Laplace transform of Eqs. (E2.3.3) and (E2.3.5) are:

$$\hat{C}_A^r(\mathrm{X},s) = \frac{2}{1+\gamma}\exp\left(\frac{\mathrm{XPe}}{2}[1-\gamma]\right) \tag{E2.3.8}$$

$$\hat{C}_E^r(\mathrm{X},s) = \frac{2}{1+\gamma}\exp\left(\frac{(1-\mathrm{X})\mathrm{Pe}}{2}[1-\gamma]\right) \tag{E2.3.9}$$

with $\gamma = \sqrt{(1+4s/\mathrm{Pe})}$. The total transit time resident concentration is given by the convolution product:

$$\hat{C}_T^r(\mathrm{X},s) = \hat{C}_A^r(\mathrm{X},s)\hat{C}_E^r(\mathrm{X},s) = \frac{4}{(1+\gamma)^2}\exp\left(\frac{\mathrm{Pe}}{2}[1-\gamma]\right) \tag{E2.3.10}$$

The inversion of Eq. (E2.3.10) yields

$$C_T^r(\mathrm{X},\mathrm{T}) = C_T^r(\mathrm{T}) = \mathrm{Pe}\left(1+\frac{\mathrm{Pe}(1+\mathrm{T})}{2}\right)\exp(\mathrm{Pe})\,\mathrm{erfc}\left(\frac{\mathrm{Pe}(1+\mathrm{T})}{2\sqrt{\mathrm{PeT}}}\right) - \frac{\mathrm{Pe}^2\mathrm{T}}{\sqrt{\pi\,\mathrm{PeT}}}\exp\left(-\frac{\mathrm{Pe}(1-\mathrm{T})^2}{4\mathrm{T}}\right) \tag{E2.3.11}$$

where use has been made of the shifting theorem

$$\mathrm{L}^{-1}\{f(as+b)\} = \frac{e^{-\frac{bt}{a}}}{a}f\left(\frac{t}{a}\right) \quad , \tag{E2.3.12}$$

and of the following inverse Laplace transform:

$$\mathrm{L}^{-1}\left\{\frac{\exp(-c\sqrt{s})}{(b+\sqrt{s})^2}\right\} = (1+bc+2b^2t)\exp(b^2t+bc)\,\mathrm{erfc}\left(\frac{c}{2\sqrt{t}}+b\sqrt{t}\right) - \frac{2bt}{\sqrt{\pi t}}\exp\left(-\frac{c^2}{4t}\right) \tag{E2.3.13}$$

In 1D, the age flux concentration at the position X always equals the life expectancy flux concentration at the position $1-\mathrm{X}$, and the total transit time flux and resident concentrations are independent on the spatial position X. In a similar way, for a given value of dimensionless time T, the age resident concentration at the position X is equal to the life expectancy resident concentration at the position $1-\mathrm{X}$, and the total transit time resident concentration is a constant in space.

The mean of the pdfs (E2.3.4), (E2.3.6) and (E2.3.7) read

$$\mu_1[C_A^f] = \mathrm{X} \qquad \mu_1[C_E^f] = 1-\mathrm{X} \qquad \mu_1[C_T^f] = 1 \tag{E2.3.12}$$

and the corresponding variances are

$$\sigma^2[C_A^f]=\frac{2\mathrm{X}}{\mathrm{Pe}} \qquad \sigma^2[C_E^f]=\frac{2(1-\mathrm{X})}{\mathrm{Pe}} \qquad \sigma^2[C_T^f]=\frac{2}{\mathrm{Pe}} \tag{E2.3.13}$$

The mean transit time is the first moment of the age flux pdf at outlet, and is independent on dispersion.

The n spatial moments χ_n of the resident concentrations (E2.3.8), (E2.3.9) can be calculated from

$$\chi_n[C^r]=\int_0^\infty \mathrm{X}^n C^r(\mathrm{X},\mathrm{T})d\mathrm{X}=\int_0^\infty \mathrm{X}^n \hat{C}^r(\mathrm{X},s)d\mathrm{X} \quad , \tag{E2.3.14}$$

and by using the general indefinite integral of Abramowitz & Stegun [1970]

$$\int_0^\infty x^n e^{-ax}dx=\frac{n!}{a^{1+n}} \quad ,$$

to give

$$\hat{\chi}_n[C_A^r]=\hat{\chi}_n[C_E^r]=\frac{2^n n!}{s(\mathrm{Pe}[\gamma-1])^n} \tag{E2.3.15}$$

The spatial moments of (E2.3.11) are undefined since the total transit time resident concentration is independent on the spatial position for the special 1D case. The spatial moments of the age and life expectancy resident concentrations can be inverted. We give the first two moments:

$$\chi_1[C_A^r]=\sqrt{\frac{\mathrm{T}}{\pi\,\mathrm{Pe}}}e^{-\frac{\mathrm{Pe}t}{4}}-\frac{1}{2\,\mathrm{Pe}}\mathrm{erfc}\left(\frac{\sqrt{\mathrm{Pe\,T}}}{2}\right)+\frac{1+\mathrm{Pe\,T}}{2\,\mathrm{Pe}}\mathrm{erfc}\left(-\frac{\sqrt{\mathrm{Pe\,T}}}{2}\right) \tag{E2.3.16}$$

$$\chi_2[C_A^r]=\frac{2}{\mathrm{Pe}}\sqrt{\frac{\mathrm{T}}{\pi\,\mathrm{Pe}}}(1+\frac{\mathrm{Pe\,T}}{2})e^{-\frac{\mathrm{Pe}t}{4}}+\frac{1}{\mathrm{Pe}^2}\mathrm{erfc}\left(\frac{\sqrt{\mathrm{Pe\,T}}}{2}\right)+\left(\frac{2\mathrm{T}}{\mathrm{Pe}}+\frac{\mathrm{T}^2}{2}-\frac{1}{\mathrm{Pe}^2}\right)\mathrm{erfc}\left(-\frac{\sqrt{\mathrm{Pe\,T}}}{2}\right) \tag{E2.3.17}$$

where use has been made of the shifting theorem (E2.3.12), and of the inverse Laplace transforms

$$\mathrm{L}^{-1}\left\{\frac{1}{(s-a^2)(\sqrt{s}+a)}\right\}=\frac{t}{\sqrt{\pi t}}+\frac{e^{a^2t}}{4a}\mathrm{erfc}(-a\sqrt{t})-\left(\frac{1+4a^2t}{4a}\right)e^{a^2t}\,\mathrm{erfc}(a\sqrt{t}) \tag{E2.3.18}$$

$$\mathrm{L}^{-1}\left\{\frac{1}{(s-a^2)(\sqrt{s}+a)^2}\right\}=-\frac{(t+2a^2t^2)}{2a\sqrt{\pi t}}+\frac{e^{a^2t}}{8a^2}\mathrm{erfc}(-a\sqrt{t})+(8a^2t+8a^4t^2-1)\frac{e^{a^2t}}{8a^2}\mathrm{erfc}(a\sqrt{t}) \tag{E2.3.19}$$

For large values of T, the asymptotic behaviour of Eqs. (E2.3.16) and (E2.3.17) is

$$\chi_1^a[C_A^r]\approx\frac{1}{2\,\mathrm{Pe}}+\frac{\mathrm{T}}{2} \tag{E2.3.20}$$

$$\chi_2^a[C_A^r]\approx\frac{2\mathrm{T}}{\mathrm{Pe}}+\frac{\mathrm{T}^2}{2}-\frac{1}{\mathrm{Pe}^2} \tag{E2.3.21}$$

From Eqs. (E2.3.16) and (E2.3.17), one can define the effective velocity of the mass centre of the plume of resident age concentration, $v_e=\partial\chi_1/\partial\mathrm{T}$, as well as the effective dispersion, $D_e=0.5\,\partial\mathrm{var}_\mathbf{x}/\partial\mathrm{T}$, with the variance $\mathrm{var}_\mathbf{x}=\chi_2-(\chi_1)^2$. They are plotted in Fig. 2.5. The effective velocity v_e, and the effective dispersion D_e are varying in time, showing the effect of the Cauchy condition at inlet. Since this condition becomes homogeneous at $\mathrm{T}=0^+$, it prevents the upgradient diffusion of water particles and disturbs the symmetry of the fickian diffusion process, with the consequence that the movement of the mass centre is faster at early times, while the effective dispersion is bigger at large times.

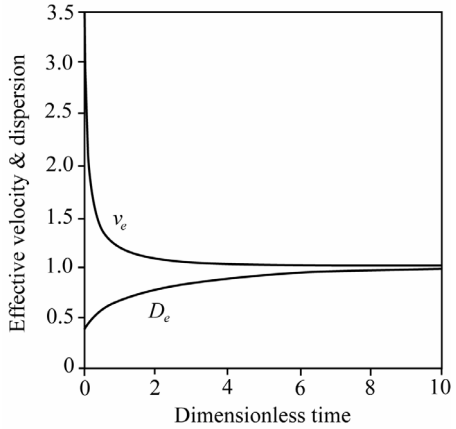

Fig. 2.5. Effective velocity (v_e) and dispersion (D_e) evaluated with the spatial moments of the age resident pdf, for a Péclet number Pe = 1.

2.3. Illustrative example

We present an experimental groundwater model, which has been used for performing tracer tests and numerical experiments. This scaled groundwater simulator (Fig. 2.6) has been designed by the Crystal Scientific Company (Michigan, United States). The system is similar to a 2D vertical stratified porous aquifer (thickness 2.5cm, height 28cm and length 49.5cm). Three main sandy layers with different granulometry are present, ranging from a lower coarse sand confined unit, an intermediate medium-coarse sand semi-confined unit, and an upper fine sand unconfined unit is located. At the top of the intermediate medium-coarse sand unit is a thin horizon of more permeable sand. The presence of some thin clay lenses (mixture of bentonite and carbonate debris) produces local but marked heterogeneities. A persistent horizontal clay lens confines the lower coarse sand unit. The main outlet of the system is schematized by a stream. At the top, a draining lake can be simulated if a two-outlet system is desired. The recharge zone is situated at the top right of the model, steadily stroked by a constant flow rate. The resulting flow in the system is in stable steady-state regime. A vertical column of coarse sand allows water to flow vertically down to the extreme lower right corner, in order to recharge the lower confined unit. Since the granulometry of this column is exactly the same as the one within the confined unit, it acts as an injection pump with respect to the lower unit. Eight piezometers allow measuring the hydraulic potential (piezometers P1 to P8 in Fig. 2.6), piezometers P7 and P8 possibly acting as artesian wells.

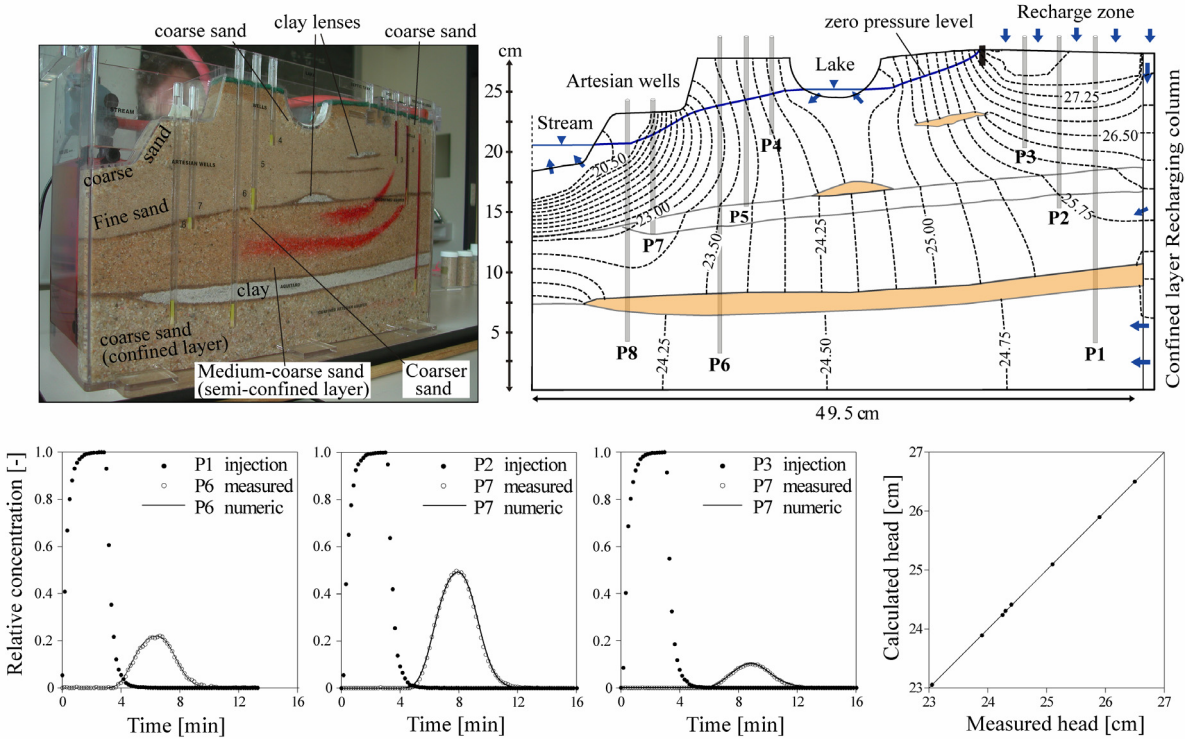

Fig. 2.6. Top: Photography of the scaled groundwater model during a qualitative tracer test using red dye, geometric drawing with super-imposed calculated hydraulic heads (in cm), and position of the water table (thick blue solid line); Bottom: Measured versus simulated uranine concentration breakthrough curves and hydraulic heads.

An equivalent 2D vertical finite element model was built and calibrated using the measured water levels, as well as the data issued from uranine tracer tests, to identify the flow and transport parameters. Flow is variably saturated, and the van Genuchten parametric model is used for the unsaturated zone. The clay lenses are considered as impermeable throughout the duration of the experiment, and therefore are not included within the finite element mesh. The recharge zone on top is simulated with prescribed fluxes, and a water level is assigned at the stream. The steady flow rate

is 1.28 litres per minute. In a preliminary step, the hydraulic conductivities were calibrated manually. After attaining a good level of agreement with the measured potentials, an inverse procedure was employed to refine the calibration. The resulting hydraulic conductivities (K) are given in Table 1.

To identify the transport parameters, solute transport experiments were carried out by passing a step-pulse of fluorescent solute tracer (Uranine – Fluka AG) through the system, the tracer release occurring alternatively in piezometer P1, P2 and P3. The lake was deactivated during the tracer tests to ensure a maximum mass recovery at the monitoring wells. On-line fluorometers GGUN-FL30 [Schnegg & Doerfliger, 1997] measured tracer concentrations in the injection piezometers P1 to P3 and in the observation piezometers P4 to P8 at 10-second intervals throughout the duration of the experiment. Both fluorometer signals were sent to a data logger and converted to concentrations using a metre-specific calibration curves. Regular readings of the effluent electrical conductivity and pH taken throughout the experiment verified that the hydro-chemical conditions remained constant. Regular discharge measurements also verified that the pumping rate remained constant. The results of the tracer tests are plotted in Fig. 2.6 and compared with numerical simulations. Note the quasi-perfect fickian-look of the breakthrough curves, which can be assimilated to Gaussian curves. The flow pattern in the model is shown in Fig. 2.7, via its numerical representation. One can see that the vertical component of velocity is important in the upper fine sand unit, showing the draining effect of the intermediate unit, where flow is generally horizontal, as in the lower confined unit. The tracer tests are not reliable for estimating the transport parameters of the upper fine sand unit, which were therefore calibrated manually. The estimated porosities (ϕ), coefficients of longitudinal dispersivity (α_L), and coefficients of transverse dispersivity (α_T) are given in Table 1.

Table 1. Calibrated flow and transport parameters (units in meters and seconds). The coefficient of molecular diffusion (D_m) was used for the simulation of the uranine tracer tests.

Parameter	Lower layer	Intermediate layer	Upper layer
K [L/T]	9.45×10^{-3}	8.62×10^{-4} and 1.16×10^{-3} (upper horizon)	3.35×10^{-4}
ϕ [-]	0.1425	0.16 and 0.1725	0.0625
α_L [L]	3.5×10^{-3}	5.0×10^{-3} and 6.5×10^{-3}	1.0×10^{-3}
α_T [L]	2.0×10^{-4}	1.0×10^{-4} and 1.25×10^{-4}	1.0×10^{-4}
D_m [L^2/T]	2.0×10^{-8}	2.0×10^{-8}	2.0×10^{-8}

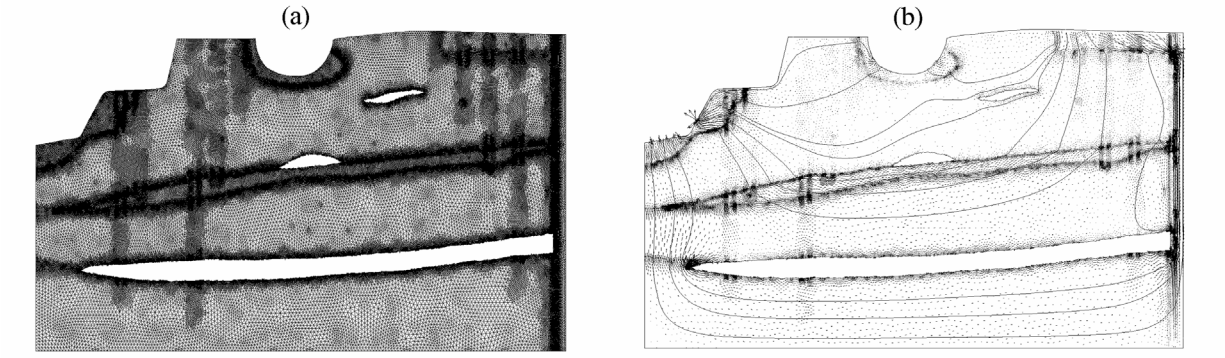

Fig. 2.7. (a): Finite element mesh (211'144 linear triangles, 107'904 nodes); (b) Flow pattern with pore velocities and path lines.

The presented numerical solutions for the moment equations (Eqs. (2.42) and (2.43)) are performed by using the classical Galerkin finite element method. The average total transit time is calculated by post-processing the mean age and mean life expectancy fields according to Eq. (2.37). The numerical solutions of Eqs. (2.20) and (2.27) are performed by using the Laplace Transform Galerkin technique (LTG) [Sudicky, 1989]. The convolution in Eq. (2.11) is realized in the Laplace

domain by enforcing (E2.2.5). For specific technical details about the numerical codes, the reader is referred to Appendices A and B. The set of parameters given in Table 1 was used, except the coefficient of molecular diffusion which was neglected. The flow boundary conditions are modified from the conditions of the tracer tests, by including the lake at the top of the model. Thus, the aquifer has two recharge zones, and two discharge zones, since the left side of the lake is infiltrating while the right part is exfiltrating.

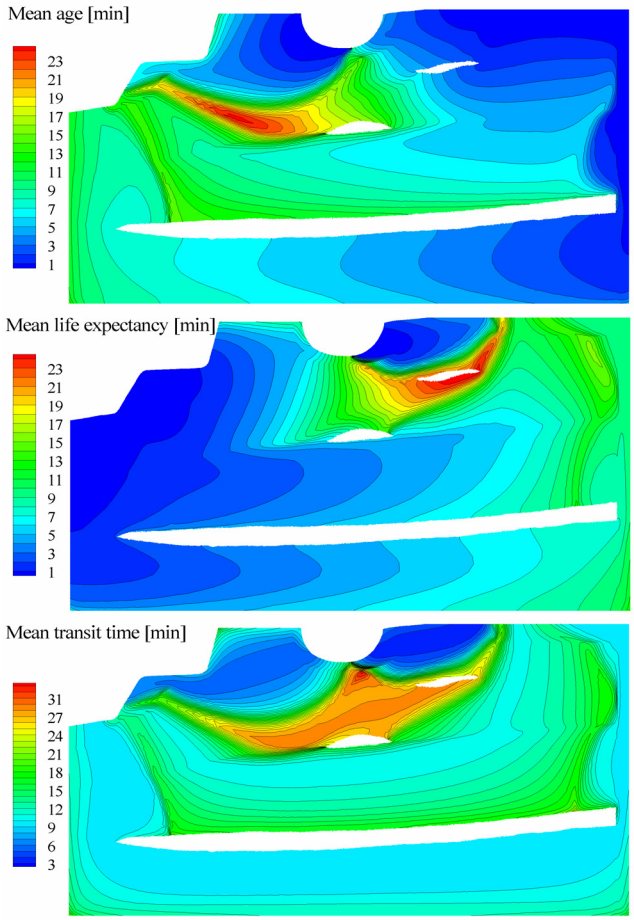

Fig. 2.8. Moment equations resolution in the scaled groundwater model.

The calculated mean age field $\langle A \rangle$ and mean life expectancy field $\langle E \rangle$ reveal complementary distributions (Fig. 2.8). The total transit time field solution $\langle T \rangle$ in Fig. 2.8 accounts for both information on age and life expectancy. The field $\langle T \rangle$ allows direct visualization of the groundwater volumes that are transferred throughout the aquifer, providing a space-time image of the transport dynamics in the aquifer with localization in space of 'streams of time', or 'flow tubes of time'. These streams of time follow continuously the directions of the flow field all the way to the outlets. Qualitatively, the field $\langle T \rangle$ gives a close image of the velocity field (Fig. 2.7b), and can be compared to a streamline model, but with the additional information on total transit time from inlet to outlet. Such a distribution integrates fundamental information about groundwater flow paths and travel duration, allowing an easier and time-integrated visualization of aquifer volumes concerned by high and low velocities. The very low velocity zone within the upper fine sand unit is well apparent. This zone is situated at middle travel from the recharge area to the stream, above the draining intermediate unit and under the circulations concerned by the inflowing and outflowing lake.

The fields $\langle A \rangle$ and $\langle E \rangle$ are affected by dispersion, even if the dispersion magnitude is relatively small. The mean ages at the outlets, as well as the mean life expectancies at the inlets, show the

typical mixing of water particles in the neighbourhood of these limits, due to the mixing of converging fluxes. Therefore, the maximum mean age is not found at the outlet, as well as the maximum mean life expectancy is not found at the inlet. The field $\langle T \rangle$ is, consequently, even more affected by dispersion, since it is derived from the sum of $\langle A \rangle$ and $\langle E \rangle$. The isolines of mean total transit, which are expected to join the points of the inlet to the points of the outlet, can close. These observations point out to the fact that the mean of the global distributions of age and life expectancy can be rapidly un-representative, and can thus be misleading if inferences on the aquifer parameters, such as the pore velocity, are to be made.

The mean fields shown in Fig. 2.8 can be compared to the results of the simulation of the entire distributions at each point in the aquifer, according to Eqs. (2.20) and (2.27). In Fig. 2.9a to 2.9f, the spatial distribution of the age, life expectancy, and total transit time pdfs and cdfs at time $t = 5$min is given. The age pdf distribution (Fig. 2.9a) gives the intensity of probability for the position of the water particles 5 minutes after they have entered the system. The corresponding cdf distribution (Fig. 2.9b) gives the probability of having an age of 5 minutes or less, and is equivalent to the classical transport solution for a conservative tracer when a relative concentration of one is prescribed at inlet. The isolines of life expectancy pdf (Fig. 2.9c) give the intensity of probability for the position of water particles 5 minutes prior to absorption by an outlet, while the isolines of life expectancy cdf (Fig. 2.9d) give the probability that the water particles will reach an outlet before time $t = 5$min. The spatial distribution of the total transit time pdf and cdf for a given time is very valuable for visualization on the same image of the travel paths and the associated travel times. Fig. 2.9e indicates at any position the intensity of probability that the water particles transit through the system with a transit time of 5 minutes. The total transit time cdf in Fig. 2.9f gives the probability that water particles transit through the system in a maximum of 5 minutes. The corresponding zone in space can be easily identified, and mostly corresponds to the upper outlet at the lake. Same distributions are given in Fig. 2.9g and 2.9h for a total transit time of 9 minutes.

The comparison of the average values at the piezometers P1 – P8 with the corresponding density of probability (normalized by the maximum intensity of the distribution) is given in Table 2. Generally, for the adopted set of parameters, the mean of the distributions give a quite good representation in relation to the relative low level of dispersion. The short travel paths and the big velocities (around 4 cm/min in the lower and intermediate units) may not permit dispersion to increase significantly with distance and time. At P1, P4 and P5, the average values are however less representative of the global distributions. Particularly, the age density of probability at the time equal to the mean age at P1 is small. The age pdf at P1 shows an important proportion of very young ages (the mode of the curve is at 1.2min), but the curve presents considerable tail (standard deviation of 8.835min) and asymmetry (positive skewness coefficient of 132.95), with the result that the mean is shifted towards older ages. The young ages fraction at P1 is caused by the very rapid movement of water particles within the vertical recharging column of the lower confined unit, which also collects a significant amount of water particles having travelled vertically through the upper and intermediate units (see the streamlines in Fig. 2.10a). The mean life expectancy is, however, well representative of the global distribution, in relation to the fact that downstream of P1, no mixing of waters can occur because of the persistent and confining clay lens that isolates the lower unit from the rest of the aquifer. At piezometer P4, very young water particles infiltrated at the lake are collected, but also older particles which have infiltrated at the recharge area. The mean of the age distribution is thus shifted towards older time values, as attested by the tail of the curve in Fig. 2.10b. Same processes may affect P5, with even more pronounced mixing effects, as shown by the important tails of the age and total transit time pdfs in Fig. 2.10b and 2.10d. The strong tailing effect in the total transit time pdf at P5 attests of important mixing of water particles with contrasted travel times, in relation to the drainage of the upper unit by the intermediate unit. The mean total transit time at P5 also corresponds to a relative low intensity of probability.

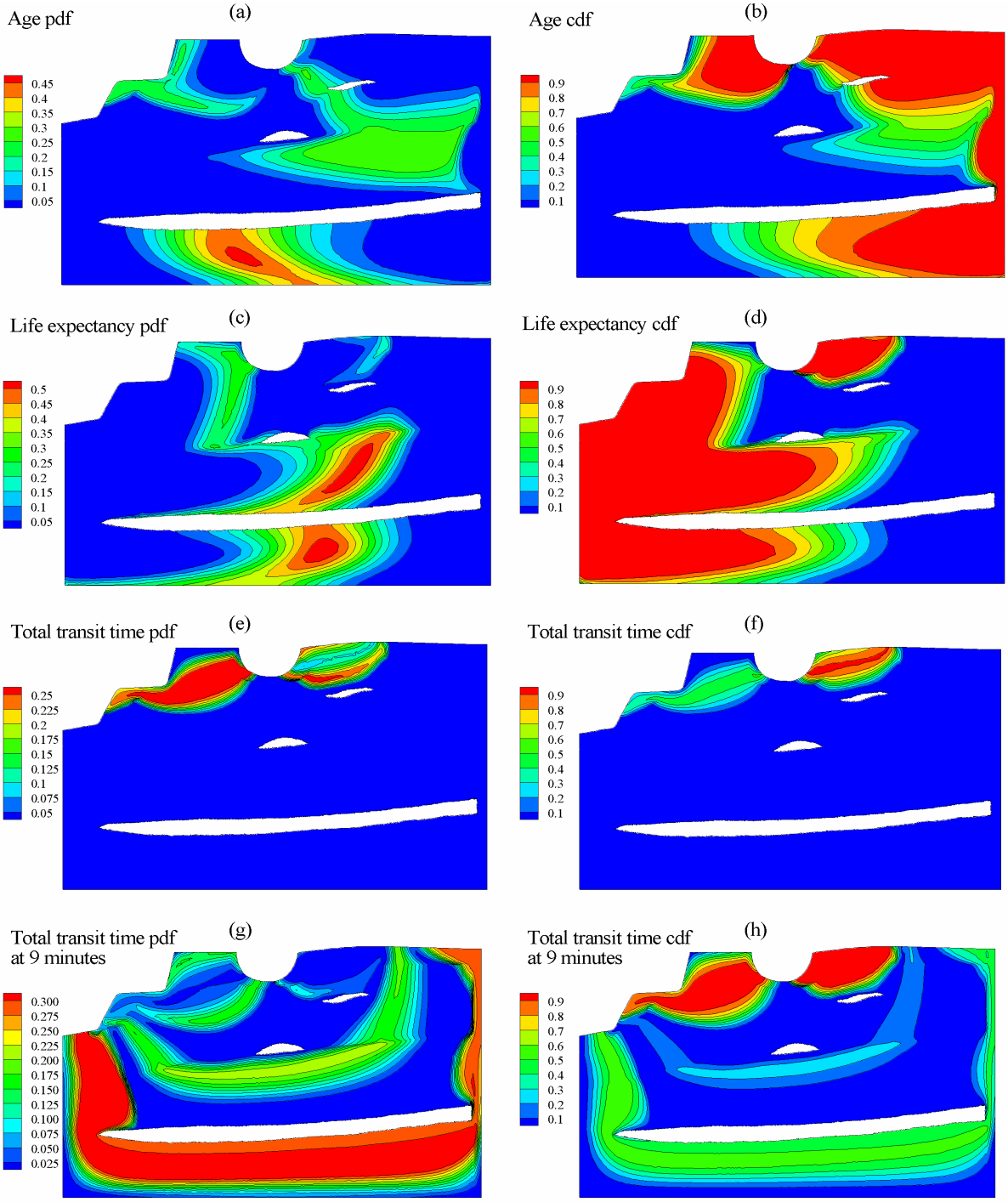

Fig. 2.9. Age, life expectancy and total transit time pdf (in min^{-1}) & cdf fields at time $t = 5\text{min}$: (a) Age pdf; (b) Age cdf; (c) Life expectancy pdf; (d) Life expectancy cdf; (e) Total transit time pdf; (f) Total transit time cdf; (g) Total transit time pdf at time $t = 9\text{min}$; (h) Total transit time cdf at time $t = 9\text{min}$.

Piezometers P5 and P7 are very close in space, but the three pdfs C_A, C_E and C_T show very different behaviours. Piezometer P5 has a far more pronounced tailing than P7. This can be explained by the fact that, on the one side, the more transmissive upper part of the intermediate layer, where P7 is, transports water particles with comparable ages, and on the other side, mixing of water particles with contrasted ages occurs at P5 (here particles infiltrated at the lake can mix with particles infiltrated at the recharge area).

Generally, when the observation points are located near a hydraulic boundary, the pdfs are more affected by dispersion, which tends to create long tails. This is the case e.g. for P3 and P4, which are located just downgradient a recharge zone, and that already show important tailing effects in their life expectancy pdf. The divergence of the water particles pathways is the principal consequence for the dispersion of the life expectancy pdfs of points located in the neighbourhood of recharge zones, as attested by the path lines in Fig. 2.10a. Note finally that the total transit time pdfs at P1, P6 and P8 are quite similar, as well as the total transit time pdfs at P2 and P7, in relation to the uniform and horizontal nature of the flow within the lower and intermediate units, but also because of the impossible mixing with the upper sand units caused by the presence of the impermeable clay unit.

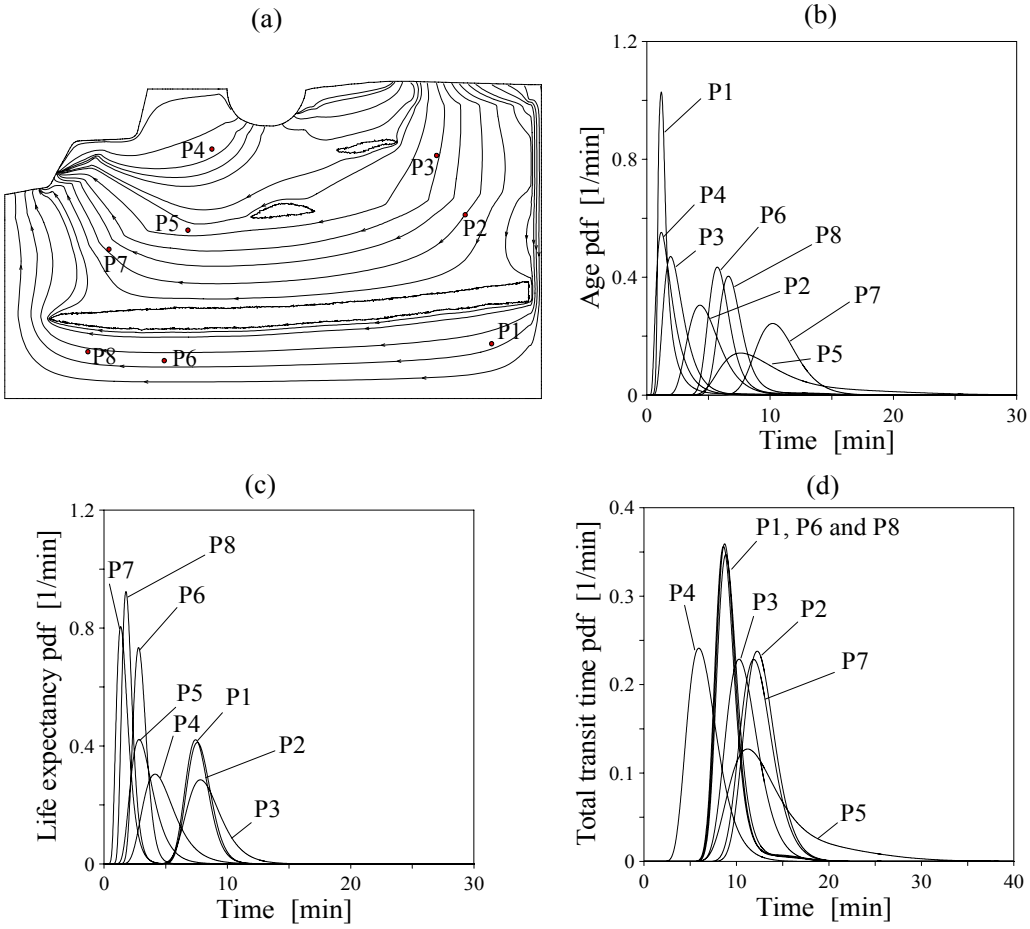

Fig. 2.10. Age, life expectancy and total transit time flux pdfs & cdf, observed at the piezometers P1 – P8: (a) Path lines (the small arrows indicate the travel distance from inlet) and observation points location; (b) Age pdfs; (c) Life expectancy pdfs; (d) Total transit time pdfs.

Table 2. Mean age, mean life expectancy and mean total transit time at the observation points P1 – P8 (in minutes), compared to the density of probability of the corresponding pdfs, ratioed to the maximum intensity.

Piezometer	$\langle A \rangle$	$C_A/\max\{C_A\}$ [%]	$\langle E \rangle$	$C_E/\max\{C_E\}$ [%]	$\langle T \rangle$	$C_T/\max\{C_T\}$ [%]
P1	1.727	**38.05**	7.664	96.65	9.391	88.76
P2	4.972	88.50	7.784	97.35	12.756	95.38
P3	2.517	80.85	8.391	91.95	10.908	94.30
P4	1.876	**68.50**	4.824	87.82	6.700	90.45
P5	10.578	**60.14**	3.384	85.78	13.962	**67.71**
P6	6.279	82.25	2.974	93.99	9.253	88.33
P7	10.761	94.65	1.642	85.60	12.403	95.60
P8	7.224	81.88	1.971	90.90	9.195	85.95

2.4. Flux and resident pdfs mass balance equations

To close this chapter, we present the mass balance equations that link the age, and life expectancy, flux and resident pdfs. Together considering Eqs. (2.15) and (2.16), the age mass flux $\mathbf{J}_A$ can then be defined as the product between the age flux concentration and the velocity vector:

$$\mathbf{J}_A = \mathbf{q}C_A^f - \left(\mathbf{I} - \frac{\mathbf{q} \otimes \mathbf{q}}{\|\mathbf{q}\|^2} \right) \mathbf{D} \nabla C_A^r \tag{2.47}$$

where the first term on the right-hand side of (2.47) relates to the component of the flux along the direction of the water velocity vector, and where the second term on the right-hand side of (2.47) relates to the component of the flux along the direction perpendicular to the direction of the water velocity vector. Similarly, considering Eqs. (2.17) and (2.18), the life expectancy mass flux $\mathbf{J}_E$ reads

$$\mathbf{J}_E = -\mathbf{q}C_E^f - \left(\mathbf{I} - \frac{\mathbf{q} \otimes \mathbf{q}}{\|\mathbf{q}\|^2} \right) \mathbf{D} \nabla C_E^r \tag{2.48}$$

Inserting Eqs. (2.47) and (2.48) into Eqs. (2.20) and (2.27), respectively, yields

$$\frac{\partial \phi C_A^r}{\partial t} = -\nabla \cdot \mathbf{q}C_A^f + \nabla \cdot \left(\mathbf{I} - \frac{\mathbf{q} \otimes \mathbf{q}}{\|\mathbf{q}\|^2} \right) \mathbf{D} \nabla C_A^r \tag{2.49}$$

$$\frac{\partial \phi C_E^r}{\partial t} = \nabla \cdot \mathbf{q}C_E^f + \nabla \cdot \left(\mathbf{I} - \frac{\mathbf{q} \otimes \mathbf{q}}{\|\mathbf{q}\|^2} \right) \mathbf{D} \nabla C_E^r \tag{2.50}$$

Eqs. (2.49) and (2.50) are generalized mass balance relationships between the resident and flux concentration forms of C_A and C_E, respectively. One can verify that in one-dimension, the second terms on the right-hand side of (2.49) and (2.50) vanish. For instance, the one-dimensional form of Eq. (2.49) yields the relation given by Parker & van Genuchten [1984].

2.5. Summary

In this Chapter, it was proposed to evaluate the probability distributional evolution of groundwater age and life expectancy by means of forward and backward transient advection-dispersion type equations, according to proper boundary conditions. For a given position in space, the age and life expectancy pdfs are complementary distributions. A direct application of the principle of superposition to these distributions results in an integrated distribution of total transit times, which characterizes the probability of having a given transit time from the recharge zone to the discharge zone, together with the quantities associated to that transit time. The total transit time pdf is simply the convolution integral of the age pdf and the life expectancy pdf, and tells about the entire history of water particles since recharge until discharge. Age, life expectancy, and total transit time pdfs provide different kind of information, and each of them can reveal to be more advantageous than the other one depending on the hydrogeological insights to be provided. For instance, life expectancy and total transit time distributions are well suited for intrinsic vulnerability assessment problems, and they allow the mapping of different regions within a recharge zone, in terms of residence time in the aquifer and associated properties.

The presented ADEs and boundary-value problems for solving the age and life expectancy pdfs and cdfs at aquifer scale are the basis for the derivation of the reservoir theory for hydro-dispersive systems, developed in the next two chapters.

References

[1] Abramowitz M., Stegun I.A. Handbook of Mathematical Functions. Dover Publishing Co., New-York, 1970.

[2] Arnold L. Stochastic Differential Equations: Theory and Applications. New York: John Wiley, 228 pp.; 1974.

[3] Bear J. and Verruitj A. Modeling Groundwater Flow and Pollution. Kluwer Academic Publ., 414 pp.; 1987.

[4] Benjamin J.R. and Cornell C.A. Probability, Statistics, and Decision for Civil Engineers. New York: McGraw-Hill Book Co.; 1970.

[5] Dagan G. Stochastic modelling of groundwater flow by unconditional and conditional probabilities, 2, The solute transport. *Water Resour Res* 1982;18(4):835–848.

[6] Dagan G. Solute transport in heterogeneous porous formations. *J Fluid Mech* 1984;145:151–177.

[7] Dagan G. Flow and Transport in Porous Formations. Springer, Berlin, Heidelberg, Germany; 1989.

[8] Dagan G. and Nguyen V. A comparison of travel time and concentration approaches to modelling transport by groundwater. *J Contam Hydrol* 1989;4:79–91.

[9] Danckwerts P.V. Continuous flow systems: distribution of residence times. *Chem Eng Sci* 1953;2(1):93–102.

[10] Diersch H.-J. An efficient method for computing groundwater residence times. FEFLOW Software White Papers Vol. 1, 2002, WASY GmbH Berlin, 137–145.

[11] Garabedian P.R. Partial Differential Equations. New York: John Wiley, 672 pp.; 1964.

[12] Gardiner C.W. Handbook of Stochastic Methods for Physics, Chemistry and Natural Sciences. Berlin: Springer, 672 pp.; 1983.

[13] Gelhar L.W. and Axness C.L. Three-dimensional stochastic analysis of macro dispersion in aquifers, *Water Resour Res* 1983;19(1):161–180.

[14] Gelhar L.W. Stochastic Subsurface Hydrology, Prentice-Hall, Inc., Englewood Cliffs, NJ, 1993.

[15] Goode D.J. Direct simulation of groundwater age. *Water Resour Res* 1996;32:289–296.

[16] Goode D.J. Ground-water age and atmospheric tracers: Simulation studies and analysis of field data from the Mirror Lake site, New Hampshire. Ph.D. thesis, Princeton University, Department of Civil Engineering and Operations Research, 1998, 194 pp.

[17] Harvey C.F. and Gorelick S.M. Temporal moment generating equations: Modeling transport and mass transfer in heterogeneous aquifers. *Water Resour Res* 1995;31:1895–1912.

[18] Jury W.A. Simulation of Solute transport Using a Transfer Function Model. *Water Resour Res* 1982;18(2):363–368.

[19] Jury W.A., Sposito G. and White R.E. A Transfer Function Model of Solute Transport through Soil, 1, Fundamental Concepts. *Water Resour Res* 1986;22(2):243–247.

[20] Jury W.A. and Roth K. Transfer Functions and Solute Movement Through Soil: Theory and Applications. Birkhauser Boston, Cambridge, Mass, 289 pp.; 1990.

[21] Kolmogorov A.N. Über die analytischen Methoden in der Wahrscheilichkeitsrechnung. *Math Anal* 1931;104:415–458.

[22] Kreft A. and Zuber A. On the physical meaning of the dispersion equation and its solutions for different initial and boundary conditions. *Chem Eng Sci* 1978;33:1471–1480.

[23] Kreft A. and Zuber A. Comments on "Flux-Averaged and Volume-Averaged Concentrations in Continuum Approaches to Solute Transport" by J. C. Parker and M. Th. van Genuchten. *Water Resour Res* 1986;22(7):1157–1158.

[24] Nauman E.B. and Buffham B.A. Mixing in Continuous Flow Systems. John Wiley, New York, 1983.

[25] Neumann S.P., Winter C.L. and Newman C.M. Stochastic theory of field-scale Fickian dispersion in anisotropic porous media. *Water Resour Res* 1987;23:453–466.

[26] Neupauer R. and Wilson J.L. Adjoint method for obtaining backward-in-time location and travel time probabilities of a conservative groundwater contaminant. *Water Resour Res* 1999;35(11):3389–3398.

[27] Neupauer R. and Wilson J.L. Adjoint-derived location and travel time probabilities for a multidimensional groundwater system. *Water Resour Res* 2001;37(6):1657–1668.

[28] Parker J.C. and van Genuchten M. Th. Flux-averaged and volume-averaged concentrations in continuum approaches to solute transport. *Water Resour Res* 1984;20(7):866–872.
[29] Parker J.C. and van Genuchten M. Th. Reply. *Water Resour Res* 1986;22(7):1159–1160.
[30] Schnegg P. and Doerfliger N. An inexpensive flow-through field fluorometer. *Proceedings of the 6th 'Colloque d'hydrologie en pays calcaire et milieu fissuré'*, Chaux-de-Fonds, August, 1997.
[31] Shapiro A.M. and Cvetkovic V.D. Stochastic analysis of solute arrival time in heterogeneous porous media. *Water Resour Res* 1988;24(10):1711–1718.
[32] Spalding D.B. A note on mean residence-times in steady flows of arbitrary complexity. *Chem Eng Sci* 1958;9:74–77.
[33] Sposito G. and Barry D.A. On the Dagan model of solute transport in groundwater: Foundational aspects. *Water Resour Res* 1987;23(10):1867–1875.
[34] Sudicky E.A. A natural-gradient experiment on solute transport in a sand aquifer: spatial variability of hydraulic conductivity and its role in the dispersion process. *Water Resour Res* 1986;22:2069–2082.
[35] Sudicky E.A. The Laplace transform Galerkin technique: A time-continuous finite element theory and application to mass transport in groundwater. *Water Resour Res* 1989;25(8):1833–1846.
[36] Uffink G.J.M. Application of the Kolmogorov's backward equation in random walk simulation of groundwater contaminant transport. In *Contaminant Transport in Groundwater* 1989;ed. H.E. Kobus Kinzelbach, Balkema, Rotterdam, pp. 283–289.
[37] Van Kooten J.J.A. An asymptotic method for predicting the contamination of a pumping well. *Adv Water Res* 1995;18(5):295–313.
[38] Weissmann G. S., Zhang Y., LaBolle E. and Fogg G.E. Dispersion of groundwater age in an alluvial aquifer system. *Water Resour Res* 2002;38(10):doi:10.1029/2001WR000907.
[39] Wilson J.L. and Liu J. Field Validation of the Backward-in-Time Advection Dispersion Theory. In *Proceedings of the 1996 HSRC/WERC Joint Conference on the Environment*, Great Plains-Rocky Mountain Hazard. Substance Cent., Manhattan, Kansas;1997.

CHAPTER 3

Generalized Reservoir Theory

Abstract

An accurate and efficient method is introduced to simulate the transit time distribution at discharge zones. By applying the reservoir theory (RT) to advective-dispersive aquifer systems, we demonstrate that the discharge zone transit time distribution is fully defined if the internal age probability distribution is known. The RT also applies to internal life expectancy probabilities yielding the recharge zone life expectancy distribution. The particular case of vertically averaged forward and backward ADEs is developed. One-, two-, and three-dimensional theoretical examples are presented to illustrate the application of the RT in advective-dispersive systems, and make inferences on the effect of boundary conditions, aquifer structure, and macro-dispersion on age, life expectancy and transit time distributions.

3.1. Background

3.1.1. The Reservoir Theory

The reservoir theory (RT) initially originates from the residence time theory [Danckwerts, 1953, 1958; Zwietering, 1959], and at first was popular in chemical engineering to evaluate the time substances remain in contact within a chemical reactor. The residence time theory aims at characterizing the dynamic process of fluid particles that enter a system, travel within it, and finally exit the system (Fig. 3.1). By attributing an identical property to the fluid particles, i.e. the residence time of these particles counted with reference to the initial time when they entered the system, the residence time theory formulates a fundamental relationship between the occurrence of that property within the reservoir and the occurrence of the same property at the exit limit of the reservoir. The RT was later introduced in the Earth Sciences domain by Eriksson [1961, 1971], after having attempted to quantify the relationships between the carbon quantities and fluxes in nature by assuming a simple linear relation [Eriksson & Welander, 1956]. The RT corresponds to the application of the residence time theory to natural reservoirs, such as atmosphere, superficial water reservoirs, or groundwater systems.

The first basic concept of the RT is related to the statistical description of the age (or residence time) occurrence within the considered reservoir. The reservoir internal age distribution is a characteristic function of the RT. Throughout this work, this function will be denoted by $\psi(t)$. The second concept of the RT is related to the statistical description of the age occurrence at the outlet limit of the reservoir. This function, which will be denoted by $\varphi(t)$, characterizes the statistical distribution of the arrival times, or transit times, at the reservoir outlet. The RT formulation makes the link between the internal age distribution ψ and the outlet transit time distribution φ by the following fundamental relationship:

$$\varphi(t) = -\frac{V}{Q}\frac{\partial \psi(t)}{\partial t} = -\frac{1}{Q}\frac{\partial^2 M(t)}{\partial t^2} \tag{3.1}$$

In the RT formulation (3.1), V is the reservoir volume, Q is the steady-state flow rate throughout the reservoir, and the function $M(t)$ characterizes the cumulated amount of elements within the reservoir having an age t or less. This simple relation translates the natural fact that an increase of age mass per unit time within the reservoir (first derivative of ψ) is balanced by the number of fluid particles per unit time that leave the system by the outflow (function φ).

The principal assumptions of the residence time theory [see e.g. Neuman & Buffham, 1983], or of the RT [see e.g. Eriksson, 1971; Bolin & Rhode, 1973], which constrain the domain of validity of the theories, can be formalized by the following. The reservoir must be open and its geometry must be well defined, such that at any time the knowledge of whether a particle is in the reservoir or at the outside of it must be unequivocal. The choice for the limits of the reservoir must be done in a way that they enclose a group of objects with similar property. Each particle that entered the system must definitively leave the system sooner or later. This excludes the possibility of nil velocities within the domain. The system must be under steady-flow conditions, and in stationary state, such that its basic physical characteristics are not varying in time. The fluid can transport conservative elements during flow through the reservoir. The RT is thus applicable to fluids, but also to conservative tracers. It is also assumed that no mixing may occur within the reservoir [Eriksson, 1971].

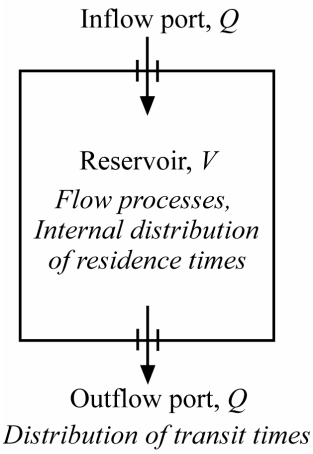

Fig. 3.1. Schematic physical reservoir of volume V with one entry port where the flow rate Q enters, and with one exit port where the same flow rate exits.

3.1.2. Reservoir Theory in Hydrogeology

The application of the RT in the field of groundwater was first attempted by Etcheverry & Perrochet [1999, 2000] and Etcheverry [2001]. Etcheverry [2001] showed that the RT can be seen as a result of the divergence theorem, when applied to the fluid mass conservation equation in open and bounded aquifer systems, considered in steady flow regime. These authors developed a mathematical method to directly calculate the groundwater transit time distribution at a reservoir outlet, by combining the RT with the mean age approach [Goode, 1996, 1998]. By considering hydrogeological systems under steady-state flow regimes, the pure advective solution of the mean age equation (see Eq. (2.45) in Chapter 2) is used to evaluate the internal age distribution ψ, by integration of the mean ages over the aquifer domain. A direct application of the RT formulation (3.1) permits the evaluation of the function φ for the aquifer outlet, given V the total porous volume of the aquifer, or total amount of mobile water, and Q the steady-state flow rate at outlet and inlet.

This approach was validated by means of several analytical developments [Etcheverry & Perrochet, 2000; Etcheverry, 2001], and tested on a few hypothetical two-dimensional structured systems, where dispersion and mixing were neglected. The main interest of the RT is that the age occurrence at the outlet is predicted by using the information on the internal organization of age

within the entire reservoir, ensuring that the minimum and maximum ages at outlet are recovered. Etcheverry & Perrochet [1999, 2000] and Etcheverry [2001], restricted their analysis to systems with single recharge and discharge zones. For arbitrary reservoirs with multiple inlets and outlets, the application of the method provides information on the transit time distribution relative to the ensemble of all outlets. Therefore, the method is very limited since the transit time distribution φ is instructive only when a specific outlet is characterized independently of any other outlet.

In this Chapter, we generalize the RT to aquifer systems with significant hydro-dispersive components. Chapter 4 will be dedicated to the adaptation of the RT to systems of arbitrary configuration, thus allowing the treatment of individual outlets.

3.2. Generalized Reservoir Theory

3.2.1. Global reservoir characteristics

When a specific age distribution is assigned to each elementary water volume in the reservoir, the volume of mobile water can be classified in a cumulative manner with respect to the age occurrence in the reservoir. Let $M = M_A(t)$ be the cumulated amount of water particles in the reservoir with an age inferior or equal to a particular value t, and let $m = m_A(t)$ be the corresponding probability function, or reservoir internal age cdf. The function $m_A(t)$ is the porous volume normalized function $M_A(t)$, which is evaluated by integrating over Ω the probability G_A of finding water particles with an age t or less, assuming that each particle has entered the system on Γ_-:

$$m_A(t) = \frac{M_A(t)}{M_0} = \frac{1}{M_0}\int_\Omega \phi\, G_A(\mathbf{x},t)\, d\Omega = \frac{1}{M_0}\int_\Omega \phi \left(\int_0^t C_A(\mathbf{x},\tau) d\tau \right) d\Omega \tag{3.2}$$

with M_0 being the total amount of mobile water, or aquifer porous volume. In Eq. (3.2), the age pdf must be under its resident concentration form ($C = C^r$), since the function $m_A(t)$ cumulates the probability of finding water particles which have travelled to a position $\mathbf{x}$ prior to time t. The function $M_A(t)$ is zero at the origin and tends towards the total porous volume M_0 at infinity. The internal age frequency distribution function $\psi = \psi_A(t)$ is the pdf associated to $m_A(t)$, and from Eq. (2.2) it follows

$$\psi_A(t) = \frac{\partial m_A(t)}{\partial t} = \frac{1}{M_0}\int_\Omega \phi\, C_A(\mathbf{x},t)\, d\Omega \tag{3.3}$$

The function $\psi_A(t)$ gives the density of probability of finding elements in Ω that have reached the age t, and $\psi_A(t)dt$ is the probability that A lies within the interval $[t, t+dt]$. Thus, the quantity $M_0\,\psi_A(t)$ represents the number of elements per unit time (or flow rate fraction) that are within the interval $[t, t+dt]$. Following Eriksson [1971], $\psi = \psi_A(t)$ is a monotonically decreasing function, and $m = m_A(t)$ is an increasing function with monotonically decreasing increments. These typical behaviours are illustrated in Fig. 3.2. The pdf ψ_A and the cdf m_A are the characteristic probability functions of the reservoir theory formalized by Eriksson [1971] and Bolin & Rhode [1973]. We similarly define the internal life expectancy cdf $m = m_E(t)$ and pdf $\psi = \psi_E(t)$:

$$m_E(t) = \frac{M_E(t)}{M_0} = \frac{1}{M_0}\int_\Omega \phi\, G_E(\mathbf{x},t)\, d\Omega = \frac{1}{M_0}\int_\Omega \phi \left(\int_0^t C_E(\mathbf{x},\tau) d\tau \right) d\Omega \tag{3.4}$$

$$\psi_E(t) = \frac{\partial m_E(t)}{\partial t} = \frac{1}{M_0}\int_\Omega \phi\, C_E(\mathbf{x},t)\, d\Omega \tag{3.5}$$

The function $m_E(t)$ cumulates the probability that a water particle in the reservoir will reach the outlet prior to time t. As will be shown in the next section 3.2.2, the internal life expectancy pdf ψ_E is equivalent to the internal age pdf ψ_A. The function $\psi = \psi_E(t)$ is thus also monotonically decreasing, and the function $m = m_E(t)$ increases with monotonically decreasing increments.

We finally consider the internal distribution of the groundwater particles total transit time pdf C_T as deduced from the convolution integral in Eq. (2.11), to introduce the functions $m_T(t)$ and $\psi_T(t)$ as the internal total transit time cdf and pdf, respectively:

$$m_T(t) = \frac{M_T(t)}{M_0} = \frac{1}{M_0}\int_\Omega \phi\, G_T(\mathbf{x},t)\, d\Omega = \frac{1}{M_0}\int_\Omega \phi \left(\int_0^t C_T(\mathbf{x},\tau) d\tau \right) d\Omega \tag{3.6}$$

$$\psi_T(t) = \frac{\partial m_T(t)}{\partial t} = \frac{1}{M_0}\int_\Omega \phi\, C_T(\mathbf{x},t)\, d\Omega \tag{3.7}$$

The function $M_T(t)$ corresponds to the mass of mobile water in the reservoir having a total transit time inferior or equal to t. The function $\psi_T(t)$ characterizes the density of probability of finding water particles within the reservoir that have the total transit time t, and the quantity $M_0\, \psi_T(t)dt$ gives the amount of water particles that travel through Ω within the time interval $[t, t + dt]$. The behaviour of the cdf m_T and of the pdf ψ_T is arbitrary, although at infinity ψ_T must vanish while m_T must be one, as illustrated in Fig. 3.2. The pdfs ψ_A, ψ_E and ψ_T integrate to unity.

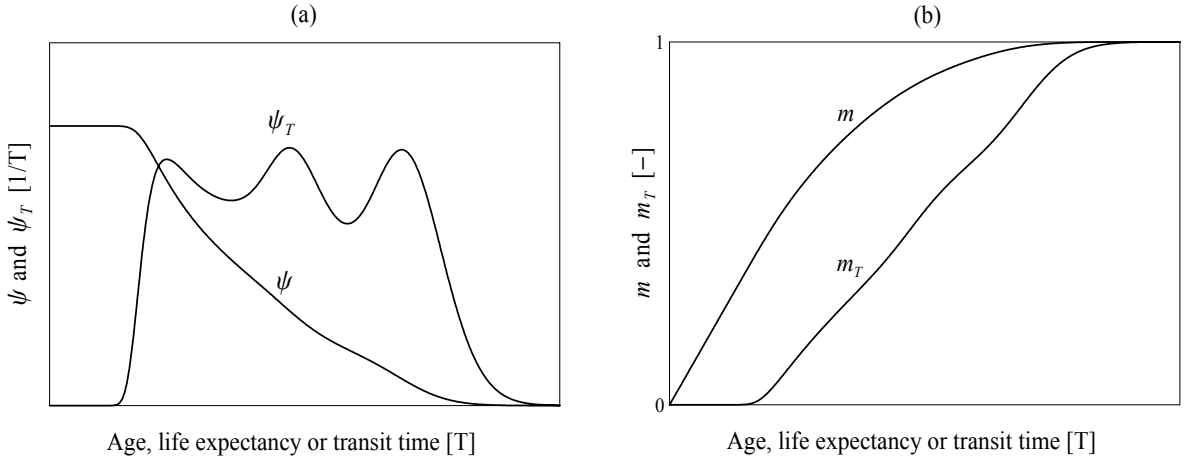

Fig. 3.2. Theoretical shape of the characteristic reservoir internal distributions for a heterogeneous reservoir: (a) Internal age pdf ψ and internal total transit time pdf ψ_T; (b) Internal age cdf m and internal total transit time cdf m_T. The functions ψ and m can equivalently correspond to age or life expectancy.

3.2.2 The discharge zone and recharge zone transit time pdf

A reservoir discharge zone is a particular portion of finite size, which intercepts the groundwater particles that contribute to the outflow rate passing through this limit. These water particles have different arrival times that converging water fluxes mix together before flowing out. At a given point of the discharge boundary, the total transit time flux pdf is the age flux pdf. To characterize the contribution of each flux event on an outflow boundary, in terms of transit time probability, it is convenient to average the age probability fluxes on Γ_+. Under steady-flow regime, the representative transit time distribution $\varphi_A(t)$ of the reservoir outlet zone can be defined as the flow rate-normalized sum on Γ_+ of the total mass flux response function $\mathbf{J}_A$ which results from the unit flux impulse on Γ_-:

$$\varphi_A(t) = \frac{1}{F_0}\int_{\Gamma_+} \mathbf{J}_A \cdot \mathbf{n}\, d\Gamma = \frac{1}{F_0}\int_{\Gamma_+} [\mathbf{q}C_A - \mathbf{D}\nabla C_A]\cdot \mathbf{n}\, d\Gamma \tag{3.8}$$

where F_0 represents the total steady-state discharge throughout the bounded domain, $\mathbf{n}$ is an outward normal unit vector, and C_A is under its resident concentration form ($C = C^r$). While flux concentrations are defined with respect to a control plane orthogonal to the velocity vector, the outlet transit time probability function in Eq. (3.8) is defined by the projection of the total age flux on the arbitrary-shaped boundary Γ_+. Inserting the age flux concentration definition (Eq. (2.15)) into Eq. (3.8) produces the equivalent relation:

$$\varphi_A(t) = \frac{1}{F_0}\int_{\Gamma_+} [\mathbf{q}C_A^f - \left(\mathbf{I} - \frac{\mathbf{q}\otimes\mathbf{q}}{\|\mathbf{q}\|^2}\right)\mathbf{D}\nabla C_A]\cdot \mathbf{n}\, d\Gamma \tag{3.9}$$

With Eq. (3.9), one can see that, if the velocity vector $\mathbf{q}$ points in the direction of the outward normal unit vector $\mathbf{n}$, which is the case in one-dimension, then the dispersive term vanishes, and the pdf $\varphi_A(t)$ is proportional to the sum on the outlet limit of the flux-weighted age flux concentration pdfs.

The discharge flow rate can also be described as a cumulative function of the transit time values at outlet. We introduce the function $f_A(t)$ as the transit time cdf of the reservoir outlet, i.e. $f_A(t)$ is the probability that the particles flow out with a transit time t or less, such that it corresponds to the normalized cumulated outflow function $F_A(t)$:

$$f_A(t) = \frac{F_A(t)}{F_0} = \int_0^t \varphi_A(\tau) d\tau \tag{3.10}$$

From the pdf-cdf relationship (2.2), of course we have $\varphi_A(t) = \partial f_A(t)/\partial t$. Similar forms of Eq. (3.10) have been employed for the measurement of the travel time pdf [e.g. Jury & Roth, 1990; Varni & Carrera, 1995], since the function $f_A(t)$ can also be viewed as the integral on Γ_+ of the mass flux evaluated from the resident concentration solution of the forward ADE (2.20) for a unit step-flux input on Γ_-.

By analogy, the life expectancy pdf and cdf of the reservoir inlet Γ_- can similarly be defined as

$$\begin{aligned}\varphi_E(t) = \frac{\partial f_E(t)}{\partial t} &= \frac{1}{F_0}\int_{\Gamma_-} \mathbf{J}_E \cdot \mathbf{n}\, d\Gamma = -\frac{1}{F_0}\int_{\Gamma_-} [\mathbf{q}C_E + \mathbf{D}\nabla C_E]\cdot \mathbf{n}\, d\Gamma \\ &= -\frac{1}{F_0}\int_{\Gamma_-} [\mathbf{q}C_E^f + \left(\mathbf{I} - \frac{\mathbf{q}\otimes\mathbf{q}}{\|\mathbf{q}\|^2}\right)\mathbf{D}\nabla C_E]\cdot \mathbf{n}\, d\Gamma\end{aligned} \tag{3.11}$$

where use has been made of the life expectancy flux concentration definition in Eq. (2.17). The dispersive term in Eq. (3.11) also vanishes when velocity is parallel to the boundary normal unit vector.

Eq. (2.19) in Chapter 2 indicates that the total transit time flux pdf equals both the life expectancy flux pdf at inlet, and the age flux pdf at outlet. As a matter of fact, assuming neither addition nor subtraction of mass during transport, steady-flow conditions and stationary state, then, theoretically, every probability flux $\mathbf{J}_A$ on Γ_+ would have an identical counterpart $\mathbf{J}_E$ on Γ_- and vice-versa. Therefore, Eqs. (3.8), (3.9) and (3.11) relate to the same and unique function, $\varphi = \varphi_A = \varphi_E$, and thus $f = f_A = f_E$. In fact, each element added in the reservoir at the inlet must exit at some position $\mathbf{x}_o$ of the outlet sooner or later. Each element added at the position $\mathbf{x}_o$ at the outlet must travel the same

distance upstream, and thus spend the same time-span within the reservoir, backward in time, before reaching a position somewhere at the inlet limit.

At the reservoir outlet, the arrival times C_A are distributed along the discharge boundary, implying mixing and superposition of the information carried by each breakthrough curve. Moreover, within the reservoir mixing processes can also be important, and the true minimum and maximum ages can be diluted. To characterize an outlet representative transit time distribution, we must ensure that the minimum and the maximum ages are captured. Technical problems can often occur when solving Eq. (3.8) or Eq. (3.11), because mass flux line/surface integration is required. If the outlet is of small size, then the capture of breakthrough curves, or the identification of particle arrivals, is easily ill-posed, mainly because of the loss of information due to the numerical mixing of converging fluxes. Hence, numerical methods will generally require a high level of refinement in the neighbourhood of these integration limits, which rapidly becomes a computational limiting factor. Due to the fact that the transit time pdf φ representative of the inlet limit is identical for the outlet limit, discretization methods imply that the number of observation nodes should be the same at the inlet and at the outlet, in order to be able to recover the same breakthrough curves. In other words, the temporal resolution of the curve, when a counting of the individual arrival times is performed, is a direct function of the spatial refinement in the vicinity of exit zones. The same restriction affects other simulation methods, such as the random-walk procedure.

Therefore, we propose in the following an alternative approach that is relaxed from the above-mentioned practical problems. The ADEs (2.20) and (2.27) in Chapter 2 are considered to simulate the age and life expectancy probability distributions in the reservoir Ω, which is bounded by the recharge limit Γ_-, the discharge limit Γ_+, and the impervious limit Γ_0. Flow is still assumed to be divergence-free, $\nabla \cdot \mathbf{q} = 0$. We first consider the ADE model of Eq. (2.20), associated to a Cauchy type condition at inlet, to calculate the age resident pdf $C_A(\mathbf{x}, t)$:

$$\frac{\partial \phi C_A}{\partial t} = -\nabla \cdot \mathbf{q} C_A + \nabla \cdot \mathbf{D} \nabla C_A \qquad \text{in} \quad \Omega \tag{3.12}$$

$$C_A(\mathbf{x}, 0) = C_A(\mathbf{x}, \infty) = 0 \qquad \text{in} \quad \Omega$$

$$\mathbf{J}_A(\mathbf{x}, t) \cdot \mathbf{n} = 0 \qquad \text{on} \quad \Gamma_0$$

$$\mathbf{J}_A(\mathbf{x}, t) \cdot \mathbf{n} = \mathbf{q} \cdot \mathbf{n}\, \delta(t) \qquad \text{on} \quad \Gamma_-$$

Implicit Neumann condition on Γ_+

Integrating Eq. (3.12) over the domain Ω, and making use of the divergence theorem ($\int_\Omega \nabla \cdot \mathbf{F}\, d\Omega = \int_\Gamma \mathbf{F} \cdot \mathbf{n}\, d\Gamma$) results in

$$\int_{\Gamma_+} [\mathbf{q} C_A - \mathbf{D} \nabla C_A] \cdot \mathbf{n}\, d\Gamma + \frac{\partial}{\partial t} \int_\Omega \phi C_A\, d\Omega = -\int_{\Gamma_-} [\mathbf{q} C_A - \mathbf{D} \nabla C_A] \cdot \mathbf{n}\, d\Gamma \tag{3.13}$$

Normalizing Eq. (3.13) by the steady flow rate F_0 and accounting for Eqs. (3.3) and (3.8), Eq. (3.13) can be re-arranged into the following form:

$$\varphi_A(t) + \tau_0 \frac{\partial \psi_A(t)}{\partial t} = -\frac{1}{F_0} \int_{\Gamma_-} [\mathbf{q} C_A - \mathbf{D} \nabla C_A] \cdot \mathbf{n}\, d\Gamma \tag{3.14}$$

with the quantity τ_0 being the turnover time commonly defined at steady state as the ratio of porous volume to flow rate:

$$\tau_0 = \frac{M_0}{F_0} \tag{3.15}$$

We now considerer the ADE model of Eq. (2.27), associated to a Cauchy type condition at outlet, to calculate the life expectancy resident pdf $C_E(\mathbf{x}, t)$:

$$\begin{aligned}
&\frac{\partial \phi C_E}{\partial t} = \nabla \cdot \mathbf{q} C_E + \nabla \cdot \mathbf{D} \nabla C_E && \text{in} \quad \Omega \\
&C_E(\mathbf{x}, 0) = C_E(\mathbf{x}, \infty) = 0 && \text{in} \quad \Omega \\
&\mathbf{D} \nabla C_E \cdot \mathbf{n} = 0 && \text{on} \quad \Gamma_0 \\
&\mathbf{J}_E(\mathbf{x}, t) \cdot \mathbf{n} = -\mathbf{q} \cdot \mathbf{n} \, \delta(t) && \text{on} \quad \Gamma_+ \\
&\textit{Implicit Neumann condition} && \text{on} \quad \Gamma_-
\end{aligned} \tag{3.16}$$

Similarly, following the procedure from (3.12) to (3.14), the integration of Eq. (3.16) yields

$$-\int_{\Gamma_-} [\mathbf{q} C_E + \mathbf{D} \nabla C_E] \cdot \mathbf{n} \, d\Gamma + \frac{\partial}{\partial t} \int_\Omega \phi C_E \, d\Omega = \int_{\Gamma_+} [\mathbf{q} C_E + \mathbf{D} \nabla C_E] \cdot \mathbf{n} \, d\Gamma \tag{3.17}$$

Normalizing Eq. (3.17) by F_0 and accounting for Eqs. (3.5) and (3.11) yields

$$\varphi_E(t) + \tau_0 \frac{\partial \psi_E(t)}{\partial t} = \frac{1}{F_0} \int_{\Gamma_+} [\mathbf{q} C_E + \mathbf{D} \nabla C_E] \cdot \mathbf{n} d\Gamma \tag{3.18}$$

The boundary integrals on the right-hand side of Eqs. (3.14) and (3.18) can be simplified by accounting for the Cauchy boundary conditions at inlet and outlet. For instance, inserting the Cauchy boundary condition at Γ_- into Eq. (3.14) reduces the boundary integral to $-F_0 \delta(t)$, and inserting the Cauchy boundary condition at Γ_+ into Eq. (3.18) reduces the boundary integral to $F_0 \delta(t)$. Consequently, Eqs. (3.14) and (3.18) become:

$$\varphi_A(t) + \tau_0 \frac{\partial \psi_A(t)}{\partial t} = \delta(t) \tag{3.19}$$

$$\varphi_E(t) + \tau_0 \frac{\partial \psi_E(t)}{\partial t} = \delta(t) \tag{3.20}$$

With Eq. (3.19) we have recovered the reservoir theory formulation. Eq. (3.20) is an equivalent formulation which relates the recharge boundary life expectancy distribution to the internal life expectancy distribution. With respect to the forward and backward ADEs from which Eqs. (3.19) and (3.20) are issued, we will refer to the formulation (3.19) as "forward reservoir theory" (FRT), and to the formulation (3.20) as "backward reservoir theory" (BRT).

To obtain the FRT and BRT formulations, the inlet and outlet boundaries have been considered as two entities on which the mass boundary conditions have been applied. These two boundaries may be continuous, or may represent the ensemble of several inflowing or outflowing boundary portions. In both cases, the functions φ_A and φ_E are global distributions, representative of the entire outlet limit, and of the entire inlet limit, respectively. In such a case, the function φ can be assimilated to the transfer function of the considered system. Since $\varphi_A = \varphi_E$, from Eqs. (3.19) and (3.20) we set $\psi = \psi_A = \psi_E$, and synthesize the above formulations to:

$$\varphi(t) + \tau_0 \frac{\partial \psi(t)}{\partial t} = \delta(t) \tag{3.21}$$

Eq. (3.21) corresponds to the RT formulation of Eriksson [1971], in which the outlet zone transit time pdf $\varphi(t)$ is proportional to the first derivative of the internal age pdf $\psi(t)$. It generalizes the reservoir theory to advective-dispersive solute transport processes, and is valid for both age and life expectancy. If dispersion is set to zero, the function $\psi = \psi_A(t)$ can be evaluated with Eq. (3.3) by using the first moment of the breakthrough curve $C_A(\mathbf{x}, t) = \delta(t - \langle A(\mathbf{x}) \rangle)$ as proposed by Etcheverry and Perrochet [1999, 2000]. Similarly, the function $\psi = \psi_E(t)$ can be evaluated according to Eq. (3.3), by integration of the field $C_E(\mathbf{x}, t) = \delta(t - \langle E(\mathbf{x}) \rangle)$, as it has also been proposed by Etcheverry [2001]. Since $\psi = \psi_A = \psi_E$, it follows from Eq. (2.1) that the functions m_A and m_E are equal, $m = m_A = m_E$, and consequently with (3.2) and (3.4) $M = M_A = M_E$.
This points out to the importance of allowing age and life expectancy dispersive fluxes to cross naturally the outlet and inlet boundary portions, as guaranteed by the *Implicit Neumann condition* in (3.12) and (3.16). The use of the homogeneous Neumann condition on Γ_+ and Γ_- may lead to different results for ψ, and thus for φ, if contrasted boundary configurations and flow conditions exist. This will be illustrated later in section 3.5.2. The third-kind boundary condition (Cauchy-type) for the forward and backward ADEs is the correct condition for solving the age and life expectancy problems with the aim of applying the reservoir theory, since it appears naturally in both Eqs. (3.14) and (3.18). This condition ensures a pure pulse total flux input entering the system at inlet for the age problem, and at outlet for the life expectancy problem. It becomes homogeneous for $t > 0$, which inhibits backward mass losses by dispersion. As will be discussed in section 3.5.1, these mass losses by dispersion can occur if one makes use of a Dirichlet type condition, leading to a possibly incorrect solute mass balance.

The fundamental relation between the outlet transit time cdf $f(t)$ and the internal age pdf $\psi(t)$ given by the RT is obtained after integration of Eq. (3.21):

$$f(t) + \tau_0 \psi(t) = 1 \tag{3.22}$$

or

$$F_0 - F(t) = M_0 \psi(t) = \frac{\partial M(t)}{\partial t} \tag{3.23}$$

These equations indicate that the outflow of water particles leaving the system through Γ_+ with an age inferior or equal to t is balanced by the number of elements per unit time within Ω that reach the age t. In other words, the flow rate fraction of age t or less at the outlet is a function of the spatial occurrence of water particles of age t or less within the system. The same considerations can be made for $f = f_E$ and $\psi = \psi_E$. Since the function $f(t)$ is zero at the origin, it follows that $\psi(0) = \sigma_0 = 1/\tau_0$ (σ_0 is the mean turnover rate), independently of the level of dispersion. Since $f(t)$ is a cumulative function, $\psi(t)$ must be monotonically decreasing and $M(t)$ must be an increasing function with monotonically decreasing increments. The pdf $\psi(t)$ is constant from zero to the minimum age at outlet $t_{\min}$, with $\psi(0,\ldots,t_{\min}) = \sigma_0$, which throws light on the fact that the probability per unit time of finding elements in Ω that have reached the age $t \le t_{\min}$ is certain. From Eq. (3.23) it follows that $M(t)$ has a constant derivative equal to $M_0 \psi(0) = F_0$, until the minimum age $t_{\min}$ is reached at outlet.

From the internal organisation of the age or life expectancy occurrence, it is possible to predict the transit time distribution of a reservoir outlet (or equivalently the life expectancy distribution of a reservoir inlet), without the need of 'counting' the arrivals of the water particles at a boundary of finite size. Eq. (3.21) permits simulation of a transit time response at a boundary resulting from a pure total flux input, by integration of the resident concentration throughout the reservoir. The information that can be lost when $\varphi(t)$ is directly evaluated at the reservoir exit zone (or inlet zone)

is recovered with Eq. (3.21). Thus, the pdf $\varphi(t)$ defined in Eqs. (3.8) or (3.11) as a pure boundary property becomes a property of the reservoir internal structure and hydro-dispersive characteristics. A far more accurate evaluation of $\varphi(t)$ is thereby achieved, for which the main operation (domain integrals (3.3) and (3.5)) is easily implemented for one-, two- and three-dimensional systems.

A convenient way to compute Eqs. (3.21) and (3.22) is to work in the Laplace space, since it allows to handle all time-dependent quantities in a quasi-analytical way. Using Eq. (E2.2.3), and accounting for the initial condition $\psi(0) = 1/\tau_0$, the Laplace transform of Eq. (3.21) reads

$$\hat{\varphi}(s) + s\tau_0\hat{\psi}(s) = 2 \tag{3.24}$$

Fig. 3.3 illustrates in 1D the outlet (or inlet) transit time pdf, the internal age (or life expectancy) pdf, and the internal total transit time pdf resulting from the analytical resolution of Eqs. (3.3), (3.7) and (3.21) (see Excursus 3.1). Recall that for pure convective transport conditions (dashed lines in Fig. 3.3), the function $\varphi(t)$ equals the piston-flow transit time pdf $\delta(t-\tau_0)$, and the function $\psi(t)$ is the Heaviside function $\mathrm{H}(\tau_0 - t)/\tau_0$, such that $\psi(t) = \psi(0) = 1/\tau_0$ until $t_{\min} = \tau_0$, and $\psi(t) = 0$ after $t_{\min}$. The first temporal moment of the pdf $\varphi(t)$ (average transit time at outlet τ_t) is dispersion-independent, and equals the turnover time τ_0, $\tau_t = \tau_0 = 1$, while the average internal total transit time τ_{it} and the average internal age τ_i (first temporal moment of ψ_T and ψ) are dispersion dependent, with $\tau_{it} = 2\tau_i = 1 + 2/\mathrm{Pe}$ (Pe denotes the Péclet number). Increasing longitudinal dispersion (low Péclet numbers) generates short arrival times and tailing effects (see the variances of the pdfs in Excursus 3.1), and thus old arrival times at the outlet as well as old ages within the domain, which are visible on the three functions $\varphi(t)$, $\psi(t)$ and $\psi_T(t)$ for a range of Péclet numbers. The function $\psi(t)$ is constant from 0 until the minimum age at outlet. Since the Cauchy type condition prevents backward losses by dispersion at $x = 0$, the value of $\psi(t)$ at the origin is always $1/\tau_0$ for any Péclet number (Fig. 3.3b).

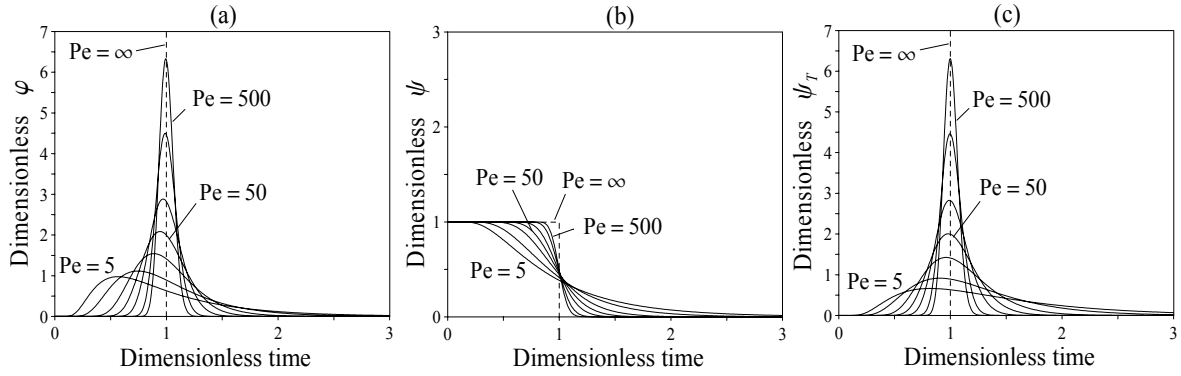

Fig. 3.3. Reservoir theory pdfs for a 1D semi-infinite flow domain, as a function of the Péclet number (Pe) for Pe = 5, 10, 25, 50, 100, 250 and 500: (a) Outlet (or inlet) transit time pdf; (b) Internal age (or life expectancy) pdf; (c) Internal total transit time pdf. Time is normalized by the average turnover time $\tau_0 = L/v$, x by the characteristic length L (supposed outlet position), and $\mathrm{Pe} = Lv/D$.

3.2.3 Temporal moments of the reservoir theory probability density functions

A direct consequence of the RT is that the average transit time τ_t at outlet or inlet (first temporal moment of the transit time pdf $\varphi(t)$) is equal to the reservoir mean turnover time τ_0. In effect, multiplying Eq. (3.21) by t and integrating by parts, accounting from the pdf property (2.3b) yields

$$\tau_t = \int_0^{+\infty} t\,\varphi(t)dt = -\tau_0\left(\left[t\psi(t)\right]_0^{+\infty} - \int_0^{+\infty}\psi(t)dt\right) = \tau_0 = \frac{M_0}{F_0} \tag{3.25}$$

Since the reservoir is considered under steady flow conditions, internal average time characteristics can be defined. Moreover, the temporal moments of the global distributions $\psi_A(t)$, $\psi_E(t)$ and $\psi_T(t)$ have physical significance since resident concentrations have been integrated in space. The mean internal age τ_{ia} (also called mean residence time), the mean internal life expectancy τ_{ie}, and the mean internal total transit time τ_{it}, are deduced from the first temporal moments of the functions $\psi_A(t)$, $\psi_E(t)$ and $\psi_T(t)$, respectively. Because $\psi_A = \psi_E$, we set $\tau_{ia} = \tau_{ie} = \tau_i$:

$$\begin{aligned}\tau_i &= \int_0^{+\infty} t\psi_A(t)dt = \frac{1}{M_0}\int_\Omega \phi\langle A\rangle d\Omega \\ &= \int_0^{+\infty} t\psi_E(t)dt = \frac{1}{M_0}\int_\Omega \phi\langle E\rangle d\Omega\end{aligned} \tag{3.26}$$

with $\phi = \phi(\mathbf{x})$, and with $\langle U\rangle = \langle U(\mathbf{x})\rangle$ denoting the mean of the random variable A or E, i.e. the mean age and the mean life expectancy. Using Eqs. (3.7) and (2.37), the average internal total transit time τ_{it} is found to be equal to twice the value of τ_i:

$$\tau_{it} = \int_0^{+\infty} t\psi_T(t)dt = \frac{1}{M_0}\int_\Omega \phi\langle T\rangle d\Omega = 2\tau_i \tag{3.27}$$

with $\langle T\rangle = \langle T(\mathbf{x})\rangle = \mu_1[C_T]$ being the mean total transit time. Using Eqs. (3.21) and (3.27), the second temporal moment and the variance of the distribution $\varphi(t)$ reveal themselves as being functions of τ_0, τ_i and τ_{it} only:

$$\mu_2[\varphi] = \int_0^{+\infty} t^2\varphi(t)dt = 2\tau_0\tau_i = \tau_0\tau_{it} \tag{3.28}$$

$$\sigma^2[\varphi] = \tau_0(2\tau_i - \tau_0) = \tau_0(\tau_{it} - \tau_0) \tag{3.29}$$

The second temporal moments of the distributions $\psi_A(t)$, $\psi_E(t)$ and $\psi_T(t)$ are

$$\mu_2[\psi] = \frac{1}{M_0}\int_\Omega \phi\,\mu_2[C_A]d\Omega = \frac{1}{M_0}\int_\Omega \phi\,\mu_2[C_E]d\Omega \tag{3.30}$$

$$\mu_2[\psi_T] = \frac{1}{M_0}\int_\Omega \phi\,\mu_2[C_T]d\Omega = 2\left(\mu_2[\psi_{U=A,E}] + \frac{1}{M_0}\int_\Omega \phi\langle A\rangle\langle E\rangle d\Omega\right) \tag{3.31}$$

and the variance of $\psi_T(t)$ is

$$\sigma^2[\psi_T] = 2\left(\sigma^2[\psi_{U=A,E}] + \frac{1}{M_0}\int_\Omega \phi\langle A\rangle\langle E\rangle d\Omega - \tau_i^2\right) \tag{3.32}$$

According to Bolin & Rhode [1973], from the first moments of $\varphi(t)$ and $\psi(t)$ some particular cases can be drawn. The first considerations correspond to the case for which the turnover time (or average transit time) and the mean residence time (or average internal age) are identical. Using Eqs. (3.25) and (3.26), the condition for $\boldsymbol{\tau_t = \tau_0 = \tau_i}$ is

$$\tau_t = \tau_i \Rightarrow \int_0^{+\infty} t[\varphi(t) - \psi(t)]dt = 0 \tag{3.33}$$

for which a sufficient condition is

$$\varphi(t) = \psi(t) = \frac{1}{\tau_0}\exp\left(-\frac{t}{\tau_0}\right) \tag{3.34}$$

The value at origin of ψ in Eq. (3.34) is effectively $1/\tau_0$. This exponential form is a direct consequence of Eq. (3.21): if one of the two pdfs $\varphi(t)$ and $\psi(t)$ has an exponential form, then the other must be identical. This is the exponential model, often termed the well-mixed model, which is mathematically equivalent to the unit response function of a well-mixed reservoir. In chemical engineering, this model is used for reactors inside which the age distribution of the elements is uniform, i.e. there is a perfect mixing of the elements. Although the exponential model is widely used by hydrogeologists to simulate isotopic data, its application in aquifer systems must be handled carefully, since it involves a large number of poorly realistic assumptions on the aquifer structure and recharge conditions.

Eriksson [1958] interpreted the exponential distribution of ages in groundwater as a consequence of an exponential decrease of porosity and permeability with depth. Luther & Haitjema [1998] argued that the conditions on the validity of the theoretical exponential residence time distribution in porous media (horizontal, un-stratified and homogeneous aquifer with respect to porosity ϕ, recharge rate I, and saturated thickness H), can be relaxed if the parameters ϕ, I, and H vary in a piecewise constant way, such that the ratio $\phi H/I$ remains constant throughout the domain. This ratio characterizes the system turnover time, which means that each water sample taken from the reservoir must lead to a mean age that equals the aquifer mean turnover time. In nature however, such system configurations and conditions on mean age may hardly be found.

Etcheverry [2001] showed that a simple linear variation of the thickness H significantly influences the shape of the theoretical exponential residence time distribution. The conceptual interpretation of the exponential model is subject to controversies. Some scientists may reject the validity of the exponential model because ideal mixing cannot occur in aquifers, whereas others may interpret good matching of data with the model as good mixing conditions. However, both approaches should consider that the main assumption underlying Eq. (3.34) as residence time distribution is that no particle exchange occurs between flow lines [Eriksson, 1958], and consequently no mixing takes place.

We now consider the case for which the average transit time τ_t is superior to the mean residence time τ_i, $\boldsymbol{\tau_t = \tau_0 > \tau_i}$. This case corresponds to the situation for which only few water particles leave the aquifer rapidly after having entered. This situation is for example the one illustrated in Fig. 3.3, where the outlet transit time pdf $\varphi(t)$ is small or nil for young ages, attesting the existence of a minimum date for travelling from inlet to outlet. Confined aquifer conditions and/or very distant recharge and discharge zones are typical settings leading to these features.

Finally, the case $\boldsymbol{\tau_t = \tau_0 < \tau_i}$ is considered. It could correspond to the situation for which important amounts of water particles enter the aquifer and flow out relatively rapidly, while sufficient amounts of water stay long enough to increase the value of τ_i. For such a configuration, $\varphi(0)$ must be bigger than $\psi(0)$, and the two curves must both decrease and cross each other at a certain date, after which ψ is higher than φ. This situation may be encountered when the source and sink zones are close to each other, or when superficial recharge is uniformly distributed, such that the fraction of young water is important at outlet, but when the heterogeneity of the velocity distribution is such that long travel paths might lead to old ages within the domain. As will be illustrated in section 3.3.2, karstic systems are typical media where this case ($\tau_t < \tau_i$) is encountered, in relation to the effect of the high velocities in karstic network, which can carry water particles more or less independently of the surrounding low permeability matrix.

Excursus 3.1: RT for a 1D semi-infinite domain.

The internal age, internal life expectancy and internal total transit time pdfs can be obtained from Eqs. (3.3), (3.5) and (3.7) by using the pdfs of Eqs. (E2.3.3), (E2.3.5) and (E2.3.11):

$$\psi_U(\mathrm{T}) = \int_0^1 C_U^r(\mathrm{X},\mathrm{T})d\mathrm{X} = \frac{1}{2}\left(\operatorname{erfc}\left(\frac{\sqrt{\mathrm{Pe}}(\mathrm{T}-1)}{2\sqrt{\mathrm{T}}}\right) - \exp(\mathrm{Pe})\operatorname{erfc}\left(\frac{\sqrt{\mathrm{Pe}}(\mathrm{T}+1)}{2\sqrt{\mathrm{T}}}\right)\right) \tag{E3.1.1}$$

$$\psi_T(\mathrm{T}) = \int_0^1 C_T^r(\mathrm{X},\mathrm{T})d\mathrm{X} = \mathrm{Pe}\left(1+\frac{\mathrm{Pe}(1+\mathrm{T})}{2}\right)\exp(\mathrm{Pe})\operatorname{erfc}\left(\frac{\mathrm{Pe}(1+\mathrm{T})}{2\sqrt{\mathrm{PeT}}}\right) - \frac{\mathrm{Pe}^2\mathrm{T}}{\sqrt{\pi\,\mathrm{PeT}}}\exp\left(-\frac{\mathrm{Pe}(1-\mathrm{T})^2}{4\mathrm{T}}\right) \tag{E3.1.2}$$

with U denoting the random variable A or E. The 1D reservoir theory is equivalent to the mass conservation relation between flux and resident concentrations given by Jury & Roth [1990]:

$$\varphi(\mathrm{T}) = -\frac{\partial\psi_U(\mathrm{T})}{\partial\mathrm{T}} = -\frac{\partial}{\partial\mathrm{T}}\int_0^1 C_U^r(\mathrm{X}',\mathrm{T})d\mathrm{X}' = \frac{\sqrt{\mathrm{Pe}}}{2\sqrt{\pi}\mathrm{T}^{3/2}}\exp\left(-\frac{\mathrm{Pe}(1-\mathrm{T})^2}{4\mathrm{T}}\right) = C_A^f(1,\mathrm{T}) = C_E^f(0,\mathrm{T}) \tag{E3.1.3}$$

The dimensionless outlet transit time pdf is simply the age flux pdf at X = 1, or equivalently the life expectancy flux pdf at X = 0 (see Eqs. (E2.3.4) and (E2.3.6)). The mean of the pdfs φ, ψ_U, and ψ_T are

$$\tau_\mathrm{t} = \mu_1[\varphi] = 1 \qquad \tau_\mathrm{i} = \mu_1[\psi_U] = \frac{1}{2}+\frac{1}{\mathrm{Pe}} \qquad \tau_\mathrm{it} = \mu_1[\psi_T] = 1+\frac{2}{\mathrm{Pe}} = 2\tau_\mathrm{i} \tag{E3.1.4}$$

and the spreading of these pdfs is measured by their variance:

$$\sigma^2[\varphi] = \frac{2}{\mathrm{Pe}} \qquad \sigma^2[\psi_U] = \frac{(\mathrm{Pe}+6)^2}{12\,\mathrm{Pe}^2} \qquad \sigma^2[\psi_T] = \frac{2\mathrm{Pe}+6}{\mathrm{Pe}^2} \tag{E3.1.5}$$

3.2.4. Internal groundwater volumes

The functions $M_A(t)$, $M_E(t)$ and $M_T(t)$ correspond to the classification of internal groundwater volumes with respect to age, life expectancy and total transit time (see Eqs. (3.2), (3.4) and (3.6)). Each of them is zero at the origin, and tends towards the porous volume M_0 at the maximum age, life expectancy or total transit time. These functions allow the quantification of the internal amounts of water and how they transit within the system. In the following, we complete the framework of the RT by analyzing the outlet transit time cdf $f(t)$ (or inlet life expectancy cdf), to show how such complex aquifer porous volumes can be directly quantified as a function of age, life expectancy, and total transit time. In Fig. 3.4, the theoretical shape of the cumulated outflux function $F(t) = F_0 f(t)$ (or cumulated influx function) is represented. The areas A, B, C and O in Fig. 3.4a characterize different groundwater volumes that can be defined as functions of time t (Fig. 3.4b). The area $\mathrm{A} = \mathrm{A}(t)$ represents the total groundwater volume V in Ω of age inferior or equal to t but of total transit time superior to t:

$$\mathrm{A}(t) = V_\Omega\left\{A \le \mathrm{t} \text{ and } T > t\right\} = t[F_0 - F(t)] = tM_0\psi(t) \tag{3.35}$$

In Eq. (3.35), the pdf $\psi(t)$ is expressed given the relationship (3.23) between $\psi(t)$ and $F(t)$. Since $\mathrm{A}(t)$ is the integral over the domain of the amount of water particles having an age t or less and a total transit time superior to t, it is a function of the joint pdf of the variables T and A, which may be written as:

$$\mathrm{A}(t) = \int_\Omega \phi\,\mathrm{P}[(t \le T) \text{ and } (A \le t)]\,d\Omega = \int_\Omega \phi\left(\int_t^{+\infty}\int_0^t C_{T,A}(\mathbf{x},u,v)dvdu\right)d\Omega \tag{3.36}$$

with $C_{T,A}(\mathbf{x}, \omega, a)$ being the joint pdf of T and A at the position $\mathbf{x}$ (see Excursus 2.1). If the minimum transit time $t_{\min}$ is not nil, the function $\mathrm{A}(t)$ can be sub-divided into the volume of age inferior or equal to time $t_{\min}$, corresponding to the area $\mathrm{A}_1(t) = t_{\min}(F_0 - F(t))$, and the volume of age inferior or equal to t and superior to time $t_{\min}$, which is the area $\mathrm{A}_2(t) = (t - t_{\min})(F_0 - F(t))$.

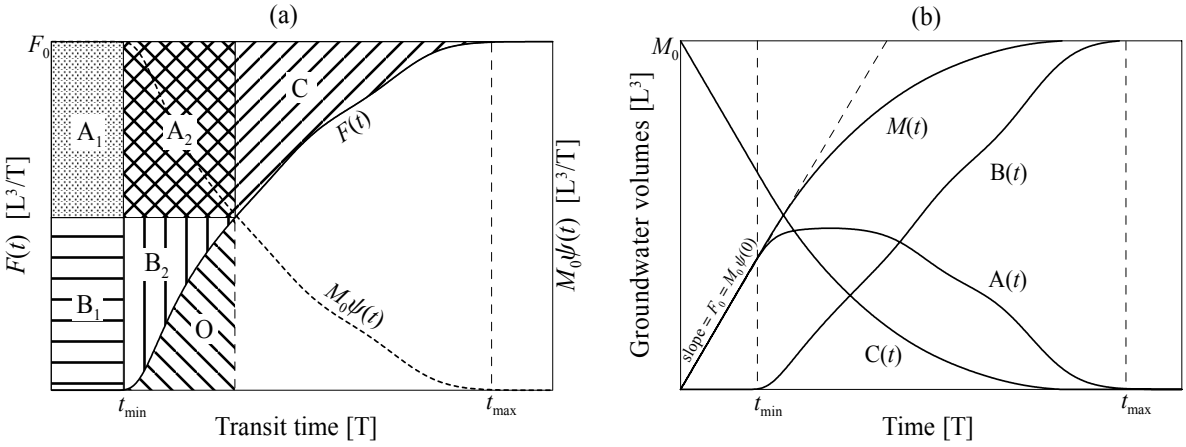

Fig. 3.4. Theoretical cumulated outflow function, internal age pdf (scaled by the porous volume) and internal groundwater volume functions: (a) Cumulated outflow distribution of transit times $F(t)$, with the indicated areas A, B, C representing characteristic internal groundwater volumes relative to a value of time, and porous volume-scaled internal age pdf $M_0\psi(t)$; (b) Aquifer porous volumes A, B, M and C as a function of age (or life expectancy) and transit time.

The area $\mathrm{B} = \mathrm{B}(t)$ in Fig. 3.4a is the volume of groundwater that flows through Ω with a transit time t or less:

$$\mathrm{B}(t) = V_\Omega\{T \le t\} = tF(t) - \mathrm{O}(t) \tag{3.37}$$

with the area $\mathrm{O} = \mathrm{O}(t)$ being the produced amount of water on Γ_+ with a transit time t or less:

$$\mathrm{O}(t) = V_{\Gamma_+}\{A \le t\} = \int_0^t F(u)du = tF_0 - M(t) \quad , \tag{3.38}$$

for which use has been made of Eqs. (3.3) and (3.15) to express the function $M(t)$. The quantity $tF(t)$ in Eq. (3.37) is the total amount of groundwater water in Ω that reaches the age t or less on Γ_+, plus the volume flowing out with an age t or less. The amount of groundwater $\mathrm{B}(t)$ is nil until the minimum transit time $t_{\min}$ is reached, and equals the total porous volume at the maximum transit time $t_{\max}$. The function $\mathrm{B}(t)$ reflects the volume of age inferior or equal to time $t_{\min}$, which is the area $\mathrm{B}_1(t) = t_{\min}F(t)$ in Fig. 3.4a, and the volume of age superior to time $t_{\min}$, which is the area $\mathrm{B}_2(t) = (t - t_{\min})F(t) - \mathrm{O}(t)$ in Fig. 3.4a. Note also that the total amount of groundwater of age $t_{\min}$ or less is given by the sum $\mathrm{A}_1 + \mathrm{B}_1 = t_{\min} F_0$.

Since the amount of groundwater $\mathrm{B}(t)$ is the internal volume that will leave the reservoir up to time t, it equals the function $M_T(t)$, which represents a fraction of the function $M(t)$. The complementary part is the amount of groundwater of age t or less and of transit time superior to t, namely the function $\mathrm{A}(t)$ defined in Eq. (3.35):

$$M(t) = V_\Omega\{A \le t\} = \mathrm{A}(t) + \mathrm{B}(t) \tag{3.39}$$

Finally, we can consider the area C = C(t), which relates the total amount of groundwater in the reservoir of age superior to time t:

$$\mathrm{C}(t) = V_\Omega\left\{A > t\right\} = (t_{\max} - t)F_0 - \int_t^{t_{\max}} F(u)du \tag{3.40}$$

The value at the origin of C(t) must equal the aquifer porous volume, C(0) = M_0. The sum of A(t) and C(t) gives the total amount of groundwater in the reservoir transiting at a time superior to t. Since the sum A + B + C is constant for all t, and since A(t) and B(t) sum to M(t), then M(t) and C(t) sum up to M_0. Consequently, C(t) must be decreasing with monotonically increasing increments. With Eq. (3.39), one can express A(t) as the difference between two increasing functions that both tend towards the porous volume M_0 at infinity. The function A(t) is thus zero at the origin and at infinity. Since B(t) is zero until the minimum transit time $t_{\min}$, A(t) must equal M(t) between 0 and $t_{\min}$. During this time-span, which can be taken as the signature of badly recharged and/or advection-dominated systems for significant values of $t_{\min}$, these two functions have a constant derivative (see Fig 3.4b) equal to the steady flow rate $F_0 = M_0\,\psi(0)$. The behaviour of this function (number of peaks, compared durations of increasing and decreasing parts) is instructive as to the volumetric proportions of groundwater remaining a long time in the system, or flowing quickly to the outlet. The time after which the function A(t) starts to decrease gives information on the importance of the water volumes in the aquifer with long or short transit times. If this time is relatively young, then the aquifer may present a good turnover property, and vice-versa.

Note that if F(t) characterizes the inlet cumulated inflow rate, i.e. $F(t) = F_0 f_E(t)$, then each aquifer porous volume defined above as a function of age becomes a function of life expectancy. By analyzing the system outlet transit time cdf, the quantification of complex one-, two- or three-dimensional groundwater volumes with respect to age, life expectancy, and transit time, is straightforward, and provides important practical system insights. An obvious application is in the field of groundwater resources protection and vulnerability assessments. The underground storage of toxic waste also requires the knowledge of groundwater volumes that could be contaminated, and assumptions on the time spent by these volumes within the reservoir until they reach an outlet area.

Example 1: Two-dimensional aquifer with uniform or localized recharge

The case of an aquifer with a good turnover property (Fig. 3.5a) is compared to the case of an aquifer with distant sink and source zones (Fig. 3.5b). For the model of Fig. 3.5a, the transit time pdf $\varphi(t)$ is a quasi-exponential function (Fig. 3.5c). The average transit time τ_t and the average internal age τ_i are more or less equal, as well as the functions $\varphi(t)$ and $\psi(t)$ (see section 3.2.3). The functions A(t) and M(t) diverge rapidly, indicating the existence of minimum transit times at outlet approaching zero. For the model of Fig. 3.5b, $\varphi(t)$ is nil until the minimum transit time is reached, and τ_t is nearly twice as big as τ_i, which correspond to the case $\tau_t > \tau_i$ discussed in section 3.2.3. The functions A(t) and M(t) remain identical until the minimum transit time is reached. After this date, the decrease of A(t) is immediate, reflecting the fact that after the shortest travel distance from source to sink has been covered, the outflow of older water particles is concentrated over a short time-span, relating the relative uniformity of the travel distances within the system (see Fig. 3.5b). A narrow triangle-shaped function A(t) is typical of aquifers with significant minimum transit times and bad turnover property. For the aquifer with good turnover property, A(t) shows a far more longer tail, relating the different travel distances from recharge to discharge (see Fig. 3.5a).

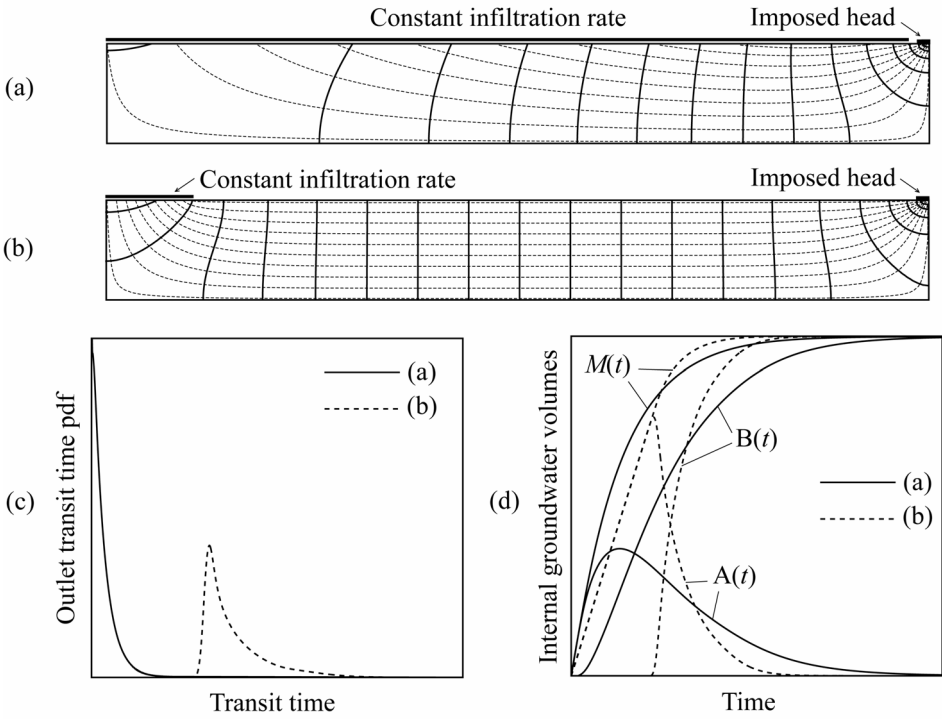

Fig. 3.5. Groundwater volume functions as indicators of the aquifer recharge conditions: (a) Vertical model of a uniformly recharged aquifer with hydraulic heads distribution (solid) and flow lines (dashed); (b) Vertical model of an aquifer with distant source and sink zones; (c) Outlet transit time pdf for the two models; (d) Aquifer porous volumes A, B, and *M* for the two models.

Example 2: Two-dimensional single flow-system aquifer

A 2D half-circular reservoir is used to simulate a single-flow system aquifer, homogeneous with respect to the porosity ϕ and the hydraulic conductivity K. A positive head difference $\Delta H = H_2 - H_1$ is applied between the recharge area and the discharge area (Fig. 3.6a). This geometry is well suited for the derivation of analytical solutions [Etcheverry & Perrochet, 2000]. Due to homogeneity and symmetry, the flow lines remain parallel to each other, flow being one-dimensional along the flow line coordinate. The spatial distributions of mean age and mean life expectancy are thus symmetric (Fig. 3.6a). According to Eq. (2.37), the spatial distribution of the mean total transit times is given by the sum $\langle T(\mathbf{x})\rangle = \langle A(\mathbf{x})\rangle + \langle E(\mathbf{x})\rangle$, as illustrated in Fig. 3.6b. The analytical derivation for $\langle A\rangle$, $\langle E\rangle$ and $\langle T\rangle$ is given in Excursus 3.2. For this example, when lateral dispersion is set to zero, then each isoline of mean total transit time can be assimilated to a flow line, but with the supplementary information on the mean total transit time from inlet to outlet associated to each line.

The porous volumes A, B, *M*, and C can easily be identified in Fig. 3.6a and b, by using the mean age and the mean total transit time isochrones. Note that the special case of this theoretical aquifer allows a good representation of the groundwater internal volumes with the mean values $\langle A\rangle$, $\langle E\rangle$ and $\langle T\rangle$. These groundwater volumes are plotted in Fig. 3.7b as a function of time, for the case of pure advective transport conditions. The minimum age at outlet, i.e. the minimum total transit time, can be identified in Fig. 3.7b by the time value at which the functions $M(t)$ and $\mathrm{A}(t)$ diverge. The function $\mathrm{A}(t)$ shows a maximum, a short time after $t = \tau_t$, indicating that after this date the groundwater volumes concerned by ages superior to τ_t will have a tendency to leave the system more or less rapidly, according to the definition of $\mathrm{A}(t)$. The function $\mathrm{B}(t)$ is a straight line from the minimum transit time t_{min} to the maximum transit time t_{max}, indicating that for a unit increase of transit time, the aquifer volumes remain constant (the aquifer volumes between two iso-contours in Fig. 3.6b are all equal).

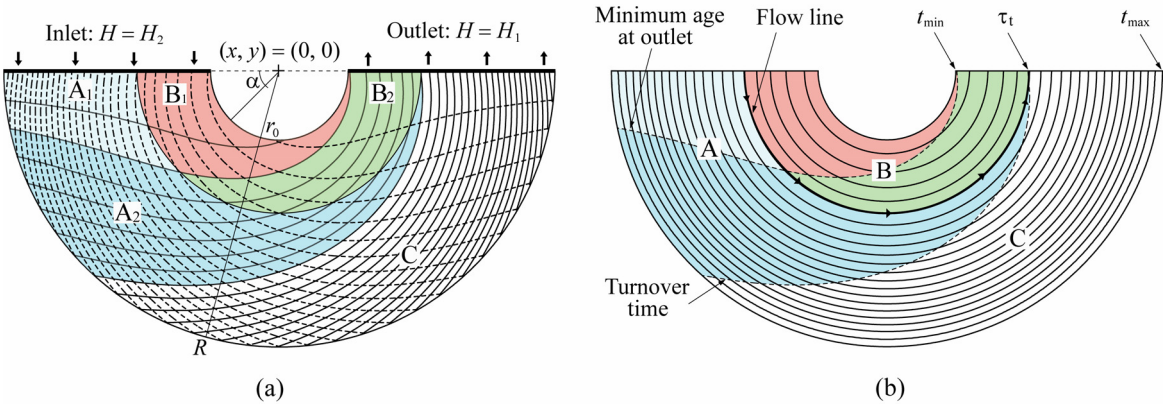

Fig. 3.6. Mean age, mean life expectancy and mean total transit time for the 2D vertical half-circular aquifer (Eq. (E3.2.1)): (a) Mean age (solid lines) and mean life expectancy (dashed lines) isochrones with 100days increment; (b) Mean total transit time isochrones (solid lines) with 100days increment. Parameters: $\Delta H = H_2 - H_1 = 100$m, $K = 10^{-4}$ m/s, $\phi = 0.2$, inner radius $r_0 = 250$m, outer radius $R = 1000$m, $t_{min} = 143$days, $t_{max} = 2285$days and $\tau_t = \tau_0 = 772.5$days.

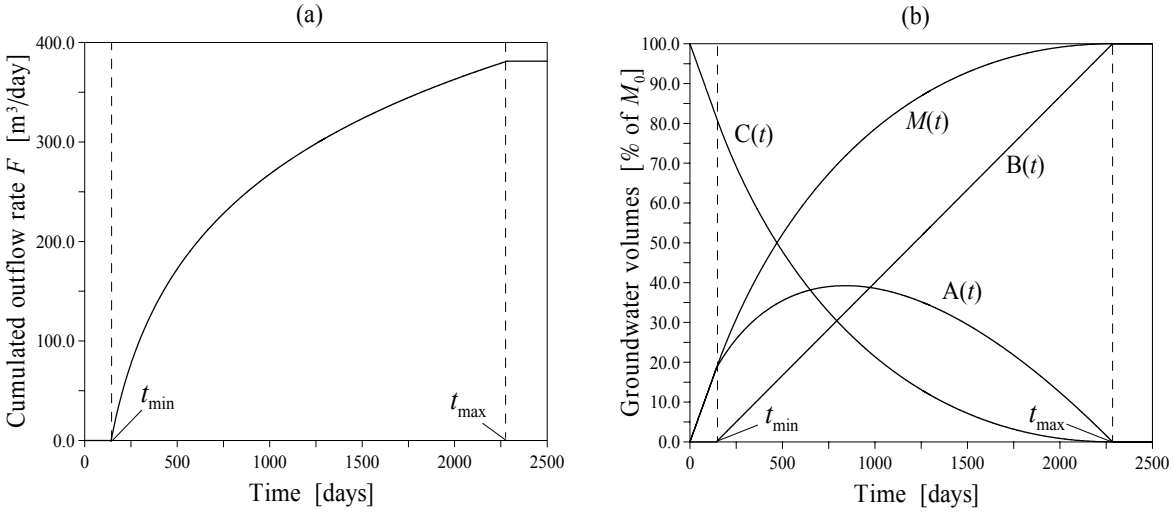

Fig. 3.7. 2D vertical half-circular aquifer under pure advective transport conditions: (a) Cumulated outflow distribution of transit times $F(t)$; (b) Groundwater volume functions.

3.3 Illustrative examples

3.3.1. Groundwater simulator

In this first example, we give the numerical solutions of the characteristic functions of the FRT and BRT by using the scaled groundwater simulator presented in Chapter 2 (see Fig. 2.6). The two types of flow conditions the scaled model can handle are simulated. The first case (case1) corresponds to the single inlet and single outlet configuration, i.e. that the lake is totally impermeable. In the second flow configuration (case2), the lake is activated. Since the lake is draining by its right side, which creates a local flow system, and infiltrating by its left side, the system has then two inlets and two outlets. In Fig. 3.8, the probability functions of the FRT and BRT are presented for case1. The peak of the stream-outlet transit time pdf is followed by an important tail, caused by the late arrival times related to the low velocity zones that occur in the

system (see Fig. 2.7). Case2 is given in Fig. 3.9. The transit time distribution shows the two modes that correspond to the two distinct outlet (or inlet) zones. The interest of the RT to evaluate outlet or inlet transit time distributions becomes clear, when the results are compared to the direct evaluation of the functions at inlet or outlet. The differences between the evaluation of the transit time pdf φ by solving the RT formulation (3.21) and by solving Eqs. (3.8) and (3.11) directly at outlet and inlet are very important. For example, the outlet corresponding to the stream is simulated by means of some nodes where a hydraulic head is imposed. The flux-weighted sum of the age mass fluxes monitored at these nodes suffers from a loss of information induced by the mixing of converging fluxes at the stream surroundings. With the RT, this information is recovered.

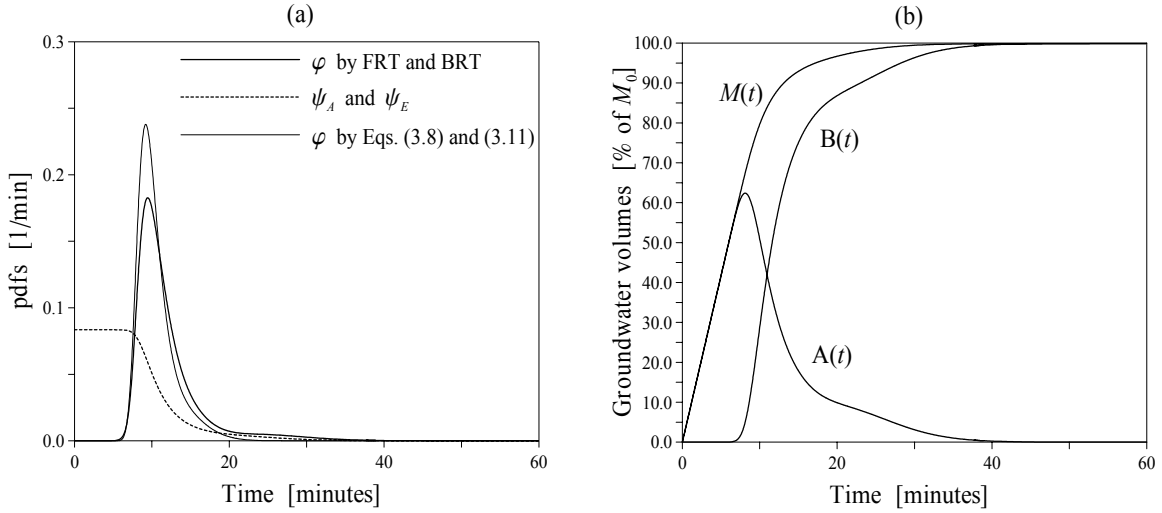

Fig. 3.8. FRT and BRT in the scaled groundwater model, with single inlet and outlet zones: (a) Distributions φ and ψ; (b) Groundwater volume functions.

For case1, the equality of $M(t)$ and A(t) until $t \sim 7.25$min (minimum transit time) attests of the important travel paths water particles must follow until they reach the outlet (the turnover time $\tau_0 = \tau_t$ is $\sim 12\text{min} = 2\tau_i$). The function A($t$) shows the same tailing effects as the transit time pdf φ. Since A(t) characterizes the internal water volumes of age t or less which transit at a time superior to t, the effect of low velocities induced long travel times must effectively be distinguishable through the behaviour of this function. For case2, this minimum transit time is reduced by the short travel distances from the recharge area to the intermediate outlet at the lake.

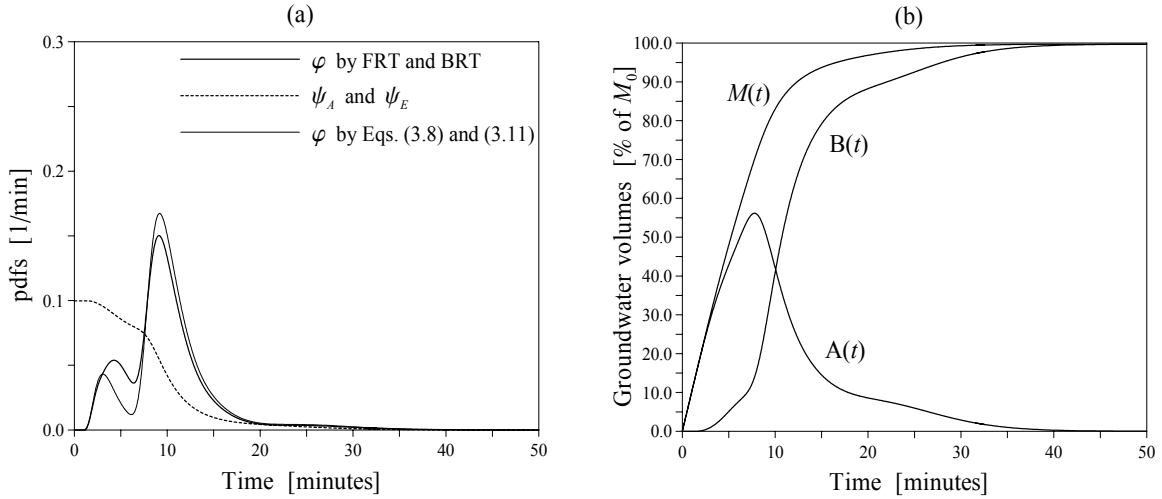

Fig. 3.9. FRT and BRT in the scaled groundwater model, with dual inlet and outlet zones: (a) Distributions φ and ψ; (b) Groundwater volume functions.

3.3.2. Column experiment

A column was designed to carry out solute and particle tracer test experiments [Flynn, 2003; Flynn *et al.*, 2003], and consists of a porous matrix made of spherical soda lime glass beads (Potters Industries, Europe) of varying sizes. The column was packed with a matrix that becomes progressively finer moving towards the centre. The resulting structure is graded, by means of a set of concentric layers of uniform grain-size distribution (Fig. 3.10b), giving the structure an onion-like aspect. The heterogeneity in the column is found along the transition between each sand unit. The water and solute inflow is applied at the bottom of the column through an entrance surface of finite size (Fig. 3.10a). The transport of uranine and viruses resulting from a step-like input has been monitored at the outlet using the same on-line fluorometer GGUN-FL30 as the one described in section 2.3. Analytical and finite element solutions have been carried to fit the experimental data [Flynn *et al.*, 2003]. We present here the application of the FRT to solve a conservative solute transport process by using a transfer function model approach, as described earlier by Jury [1982], Jury *et al.* [1986], White *et al.* [1986], Sposito *et al.* [1986], or Jury & Roth [1990].

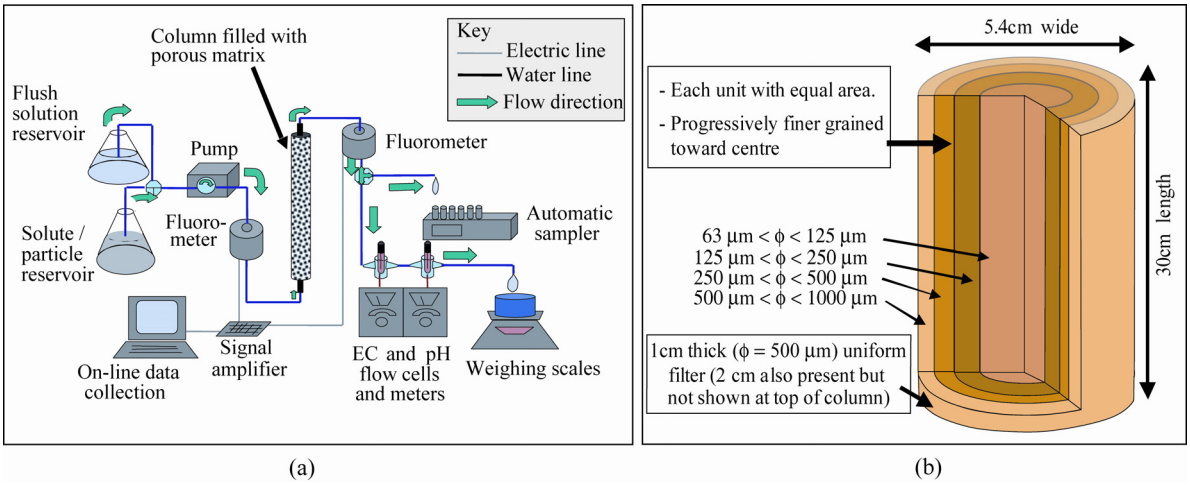

Fig. 3.10. Schematic illustration of column apparatus used during uranine tracer test: (a) Experiments with detail of graded column apparatus; (b) Column structure and granulometry (single bead size: 25cm long × 1.9cm in diameter). Modified after Flynn [2003].

The hydraulic conductivity for each sand unit was evaluated by granulometric analysis. Porosity and dispersion coefficients were obtained by calibration of a numerical solution. Fig. 3.11 gives a representation of a 3D finite element model of the experimental column, and of the calculated hydraulic head distribution. Due to the symmetry of the column, the transport simulations were carried out with a 2D vertical axisymmetric finite element model, allowing working with a finer level of mesh refinement than in 3D. Fig. 3.12 shows the distribution of the pore velocity and dispersive parameters, and the results of classical transport simulations, to give an idea of the transport dynamics in the column. The effect on solute transport of the increase of permeability towards the external radius of the column is well-marked.

The transfer function model of solute transport, which predicts the outflow concentration by convoluting the system transfer function with the inflow concentration, can be written as:

$$C_{\text{out}}(t) = \int_0^t \varphi(u)\, C_{\text{in}}(t-u)\, du \tag{3.41}$$

where C_{in} and C_{out} are the inflow and outflow concentrations, respectively. The functions C_{in} and C_{out} have been monitored at 10-second intervals throughout the duration of the experiments. The convolution (3.41) was performed in the Laplace domain, following Eq. (E2.2.5). The simulation results for two distinct experiments are given in Fig. 3.13. They show a good fit of the experimental data, except in the last part of the tail of the curves. The CPU-time is about ten times smaller with the transfer function approach using the LTG scheme [Sudicky, 1989], than with the classical ADE resolution with a time-stepping procedure. The RT is well-suited for such types of simulations, for which the parameter calibration procedure often requires many successive runs.

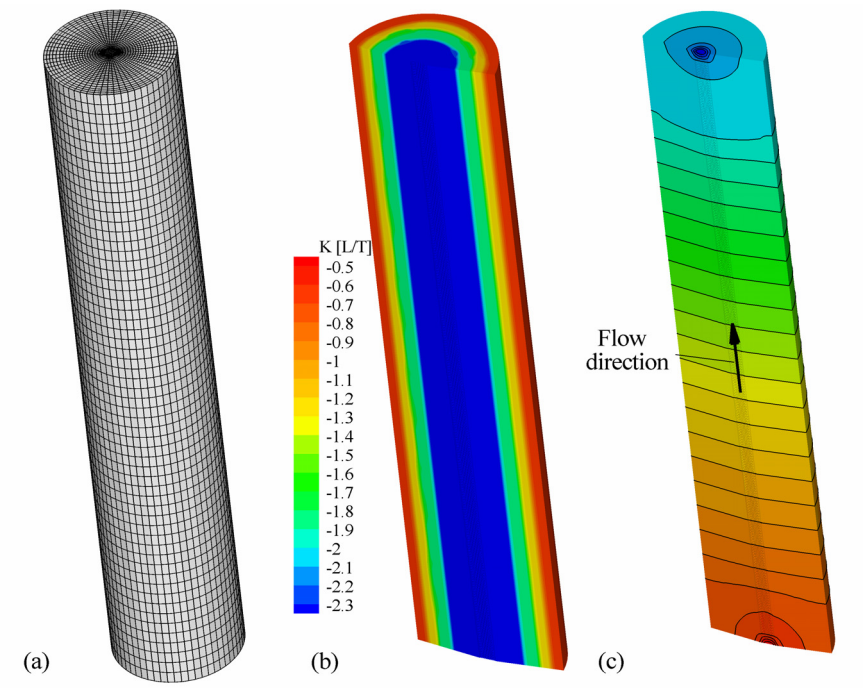

Fig. 3.11. Numerical model of the column experiment: (a) Finite element mesh (92476 nodes, 89100 brick elements); (b) Hydraulic conductivity distribution ($\log_{10}K$ in m/s); (c) Simulated hydraulic heads pattern.

In Fig. 3.14 the flux concentration solutions at some observation points within the column (which have not been monitored during the tracer tests), evaluated by convolution of the calculated age flux pdfs with the step-input function, are plotted. As predicted by the distribution of resident concentration in time (Fig. 3.12) the breakthrough curves monitored at the middle height of the column, and near the centre of the column, are very delayed with respect to the breakthrough of the outflow (e.g. points 1 to 3 in Fig. 3.14), although the travel distance to outlet is twice as long. The central unit (lowest permeability) is responsible for the oldest arrival times at the outlet. This unit generates the long tail of the outflow concentration curve. If we transpose this experiment from the local scale to a natural aquifer, one can imagine the same phenomenon occurring during a tracer test between three piezometers more or less aligned in the large-scale flow direction. Some particular preferential pathways could easily create earlier arrival times at a monitoring piezometer located further from the injection location than at a monitoring piezometer located in between the injection location and the last monitoring piezometer. Fitting such tracer test data with analytical one-dimensional solutions of the ADE would, therefore, yield erroneous interpretations on the transport parameters.

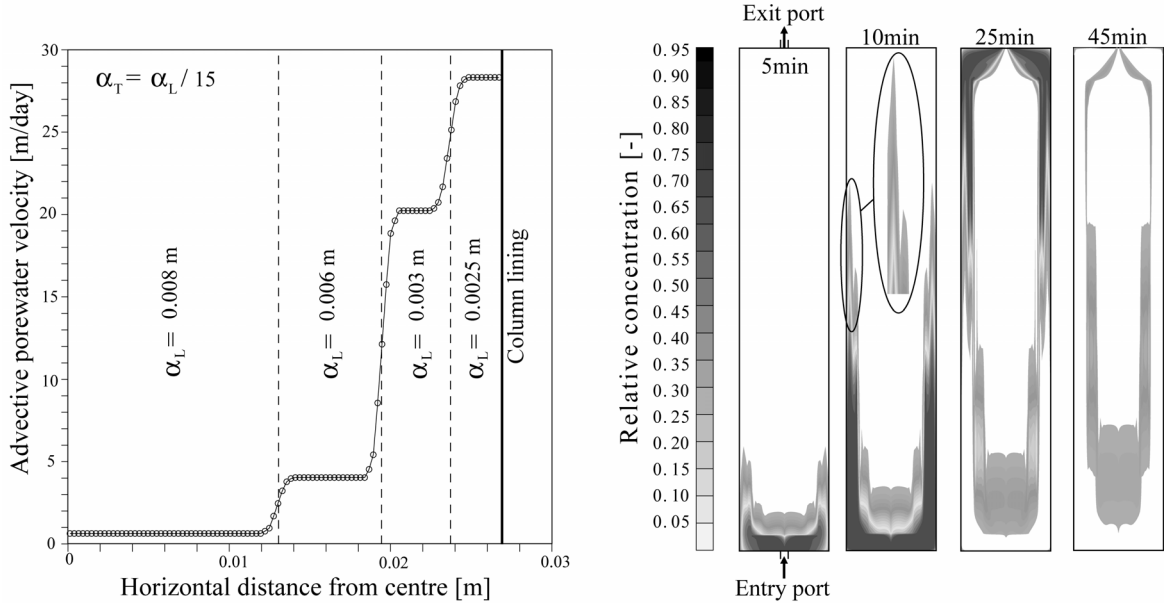

Fig. 3.12. Transport parameter distribution and plots of resident concentration at various times. The finite element model is 2D vertical axisymmetric, and consists of 69'600 linear quadrangles (height 0.5mm, width 0.25mm).

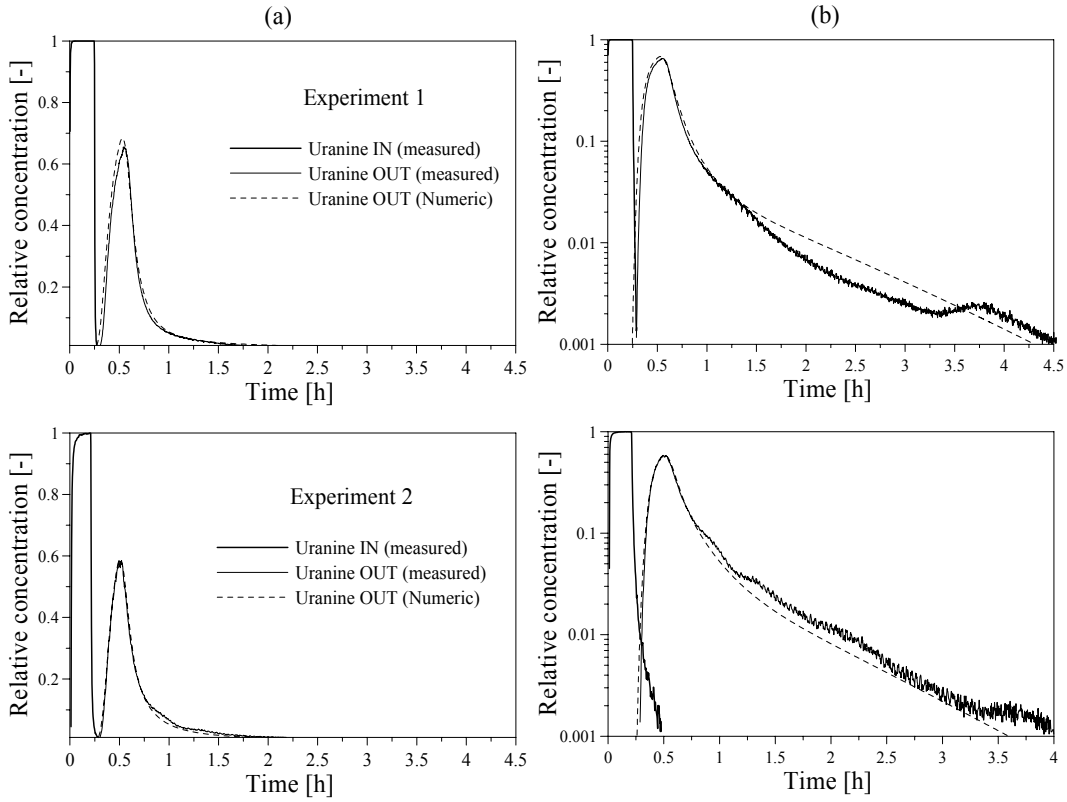

Fig. 3.13. Measured versus modelled effluent concentration: (a) Linear scale; (b) Semi-logarithmic scale.

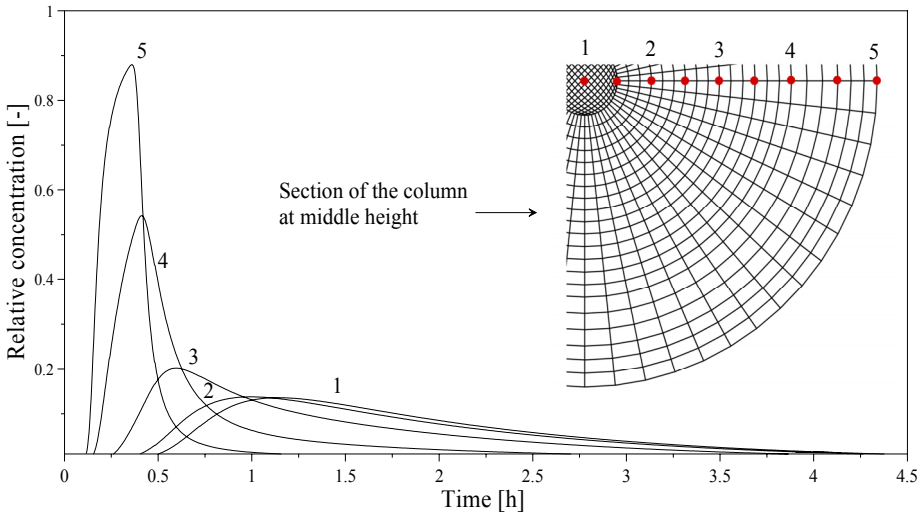

Fig. 3.14. Simulated flux concentrations, observed at middle height of the column.

3.3.3. Three-dimensional heterogeneous aquifer with discrete feature elements

In this last example we consider a 3D synthetic, finite element aquifer, which was used to simulate karstic spring hydrographs [Cornaton & Perrochet, 2002]. The reservoir consists of a highly transmissive network of 2-noded pipe elements embedded in a low hydraulic conductivity matrix body made of homogeneous 8-noded brick elements (Fig. 3.15a). Both the 1D and the 3D elements have a size of 25m. Recharge is separated into a diffuse infiltration (80%) on top of the model, and a concentrated infiltration (20%) imposed directly into the pipe network at the summit of sinkholes. A single spring zone is simulated by means of an imposed water level. Flow in the matrix is confined and of darcean kind. Within the pipe network, the law of Manning-Strickler is used to simulate laminar/turbulent flow conditions. The steady-state flow solution is represented in 3D in Fig. 3.15b by means of three hydraulic head iso-surfaces, and shows the high drainage effect of the pipe network.

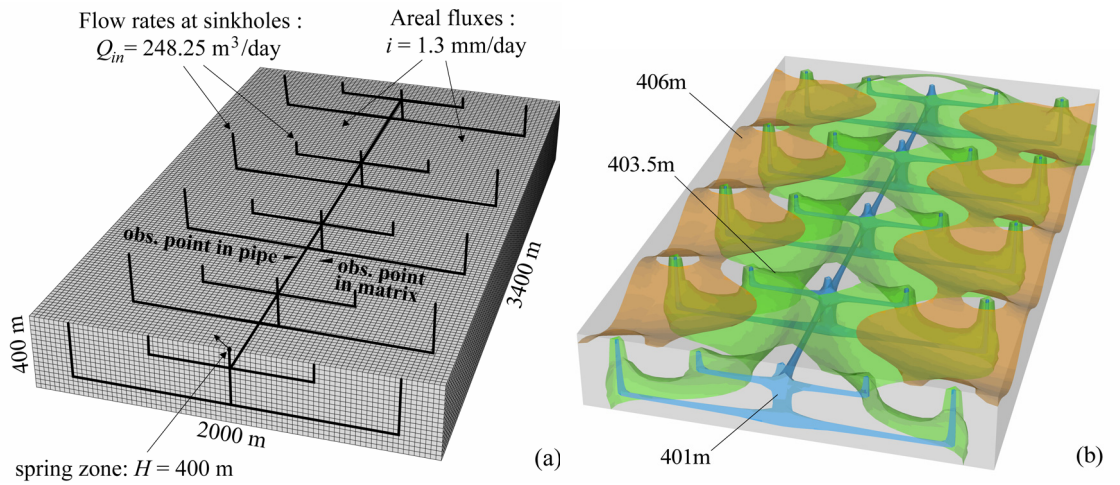

Fig. 3.15. Theoretical model of a karstic basin: (a) 3D model body and flow boundary conditions. The pipe network is schematized by the black thick solid lines; (b) Simulated hydraulic heads. The maximum head is 408.25m, and the minimum head is 400m at the spring.

The spring transit time distribution and temporal capture zone have been simulated in order to demonstrate the robustness and efficiency of the RT method, even when high parameter and geometric contrasts are taken into account. In the 3D matrix, the hydrodynamic dispersion tensor is classically defined by Eq. (2.26). For the pipe elements, the dispersion tensor follows Taylor's analysis of diffusion in laminar and turbulent flow [1953, 1954]. The spring capture zone relative to a particular time t_{ref} corresponds to the field of probability that the water particles will have a life expectancy t_{ref} or less before exiting at the spring. This particular aspect of capture zone delineation will be developed more specifically in Chapter 4. Such a probability is given by the value at t_{ref} of the cdf G_E of the random variable E, which is, following Eq. (2.1), the time integral of the function $C_E(\mathbf{x}, t)$. This operation is straightforward in the Laplace domain, since the Laplace inversion for the single time value t_{ref} of the function $\hat{G}_E = \hat{C}_E(\mathbf{x}, s)/s$ yields the desired probability for a water particle being at the position $\mathbf{x}$ to reach the spring before time t_{ref}, $\mathrm{P}(\mathbf{x}, E \le t_{ref} \mid \Gamma_+, 0)$. Thus, Eq. (3.16) is solved by assigning the Cauchy type condition at the spring, and the spring capture zone is then designed by post-processing the field $\mathrm{P}(\mathbf{x}, E \le t_{ref} \mid \Gamma_+, 0)$.

The calculated spring one-month and one-year capture zones are given in Fig. 3.16, which represents the field of probability that the water particles will reach the spring before one month and one year, respectively. The one-month capture zone remains very close to the pipe network, showing that most of the water particles that need one month or less for reaching the spring transit by the pipe network. The one-year capture zone significantly penetrates the matrix, showing that travel times up to one year are common within the matrix.

Table 1
Geometrical characteristics, hydraulic and transport parameters, CPU time (INTEL® processor, 1.2Ghz), and calculated statistics for the 3D simulation example of Fig. 3.15.

Geometry		**Statistics**	
8-noded bricks	174'080	τ_t (y)	2.513
2-noded pipes	1048	τ_i (y)	5.453
Nodes	188'649	τ_{it} (y)	10.903
Matrix volume (m^3)	2.720×10^9	$\sigma^2[\varphi]$ (y)	21.160
Pipe network volume (m^3)	6.503×10^2	$\langle A \rangle$ (pipe, y)	2.220
Model area (m^2)	6.800×10^6	$\sigma^2[C_A]$ (pipe, y)	13.785
M_0 (m^3)	1.366×10^7	$\langle A \rangle$ (matrix, y)	1.247
$\Delta\mathbf{x}$ (m)	25.0	$\sigma^2[C_A]$ (matrix, y)	7.645
Flow parameters		**Transport parameters**	
K_{matrix} (isotropic, m/y)	31.557	ϕ (matrix)	5.0×10^{-3}
Pipes radius (m)	1.0	α_L (matrix, m)	25.0
Hydraulic radius (m)	0.5	α_T (matrix, m)	1.0
Friction ($m^{1/3}/s$)	20.0	D_m (matrix, m^2/y)	3.15×10^{-2}
Diffuse areal infiltration (m^3/y)	0.64	D_m (pipes, m^2/y)	3.15×10^{-2}
Concentrated recharge (m^3/y)	1.087×10^6	Kin. viscosity (pipes, m^2/y)	31.557
F_0 (m^3/y)	5.436×10^6	Discrete Laplace variables	20
CPU (min)	1.844	CPU (min)	21.377

The spring transit time pdf, as well as the observed age pdf in the pipe network and in the surrounding matrix, are given in Fig. 3.17. The well-known duality of karstic aquifers (rapid flow in the pipe network, low flow and high storage in the matrix), which has also often been compared to a dual-porosity behaviour for flow and mass transport, is apparent on the simulated age and transit time pdfs. The very early peak at the spring (14.5days) is followed by a very long tail (the maximum age within the domain is ~250years). The observed age pdf at the observation point in the pipe network (see Fig. 3.15a for its location) is more or less the same curve as the spring transit time pdf (peak at 13.31days), because of the mixing of the overall ages in the network. Within the

surrounding matrix (at 100m from the pipe), the age pdf is in contrast highly delayed, with the peak of the curve appearing around 140days.

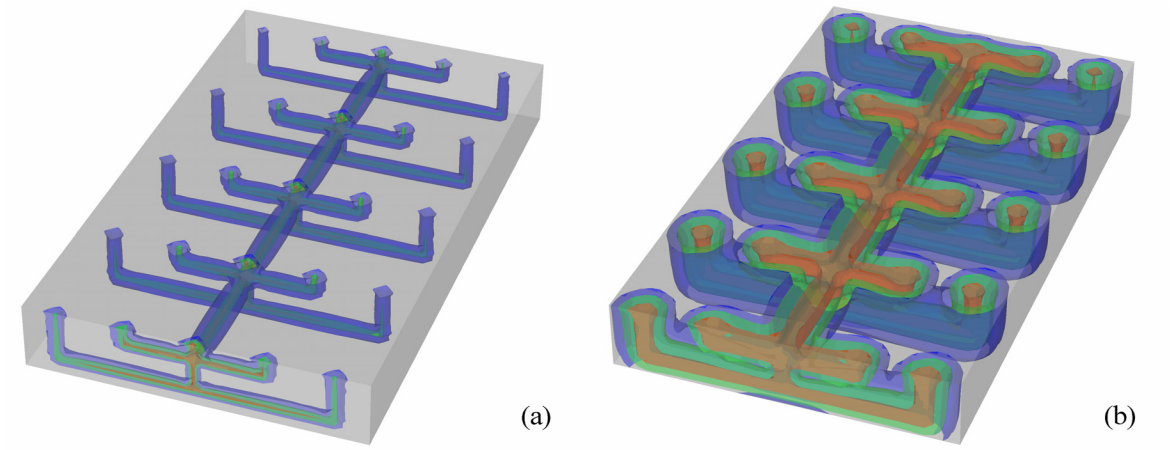

Fig. 3.16. Karstic spring probabilistic capture zones: (a) One-month capture zone; (b) One-year capture zone. Iso-surfaces of probability 0.1 – 0.5 – 0.9 (blue = 0.1; green = 0.5; red = 0.9).

The mean age observed in the pipe network is older than the mean age observed in the surrounding matrix (Table 1), partly because of the high mixing and contribution of the old matrix waters which are continuously drained by the pipe network. Not only does the drainage of old waters by the pipe network drastically increases the mean of the age pdf in the pipes, but it also generates very long tails, the variance of the age pdf in the pipe being nearly twice as big as the variance of the age pdf in the matrix (Table 1). Since the pipe network collects each infiltrated water particle, it contains the entire age spectrum, from the minimum age to the maximum age. However, the median of the observed age pdf in the pipe network (t_{50} = 288.8days) is smaller than the median of the observed age pdf in the surrounding matrix (t_{50} = 370.6days), showing that the major contribution to the flow rate at the spring is related to ages younger than one year. With reference to section 3.2.3, note that the mean residence time τ_i is bigger than the outlet average transit time τ_t, in relation to the 'short-circuit' of old waters by very young waters carried by the pipe network.

These observations are of high importance, considering the classical approach of turnover time determinations with the aid of environmental tracers and lumped-parameter models. Maloszewski & Zuber [1991] demonstrated the effects of matrix diffusion and exchange reactions on ^{14}C movement and groundwater age in fractured rocks. The organization of the flow pattern, like e.g. here with a highly transmissive conduit network draining each water molecule of the entire aquifer, can by itself be responsible of consequent aging effects at a spring, without the need of matrix diffusion and exchanges.

By applying the RT to calculate an outlet transit time pdf, each age occurrence within the domain is accounted for. As a matter of fact, the transit time pdf calculations are carried out with refined accuracy. In this example with high velocity contrasts and discrete features, it is clear that the distribution of ages in the reservoir could never be calculated with the same accuracy by temporal moments or particle-tracking techniques. Moreover, by using the LTG technique to solve the ADEs, the simulations turn to be relatively quick (see CPU time in Table 1), and simulations over hundreds of years or more are not constrained by the temporal resolution since the LTG technique does not undergo any time-stepping procedure.

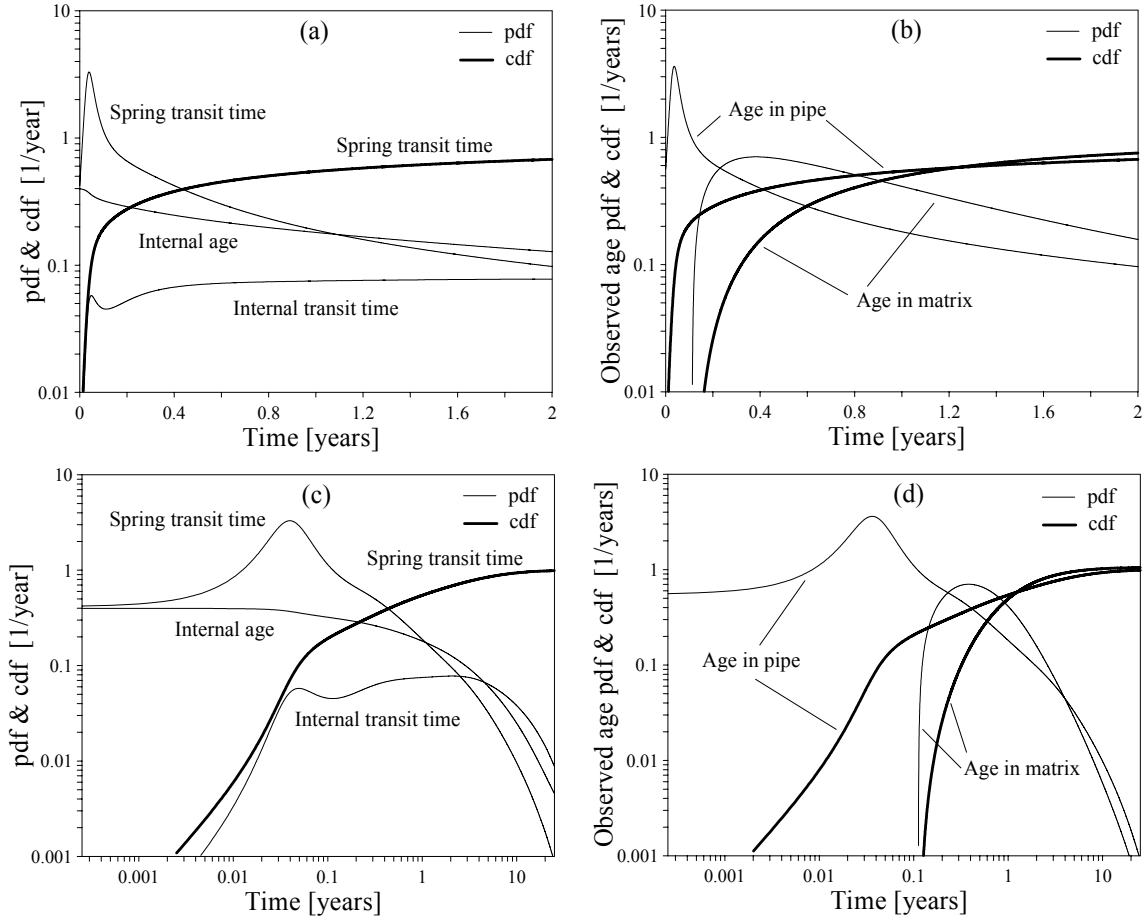

Fig. 3.17. Simulated age and transit time pdfs and cdfs in the theoretical karstic basin: (a) Spring transit time pdf and cdf, and reservoir internal age and total transit time pdfs; (b) Age pdf and cdf observed in the pipe network and in the surrounding matrix (see Fig. 3.15a for the location of the observation points). (c) and (d) give the same functions as (a) and (b), respectively, using a log-log representation.

3.4. Analysis of the outlet transit time pdf under dispersion processes

To analyze the sensibility of the transit time pdf φ under dispersion processes, we present some simulations of 2D vertical theoretical reservoirs.

3.4.1. Two-dimensional single flow-system aquifer

The 2D half-circular reservoir of section 3.2.4 is used to simulate the outlet transit time pdf under varying dispersivity. For the pure advective case, $\varphi(t)$ is proportional to $1/t$, $\psi(t)$ is proportional to the logarithm of $1/t$, between the minimum and the maximum transit time, and $\psi_T(t)$ is a constant from the minimum to the maximum transit time.

The case $\alpha_T = 0$ in Fig. 3.18a is analysed by means of analytical solutions (Excursus 3.2) for the functions $\varphi(t)$, $\psi(t)$, and $\psi_T(t)$. These advective-dispersive solutions are based on the assumption that flow is one-dimensional along the flow line coordinate, and thus they only take longitudinal dispersion into account. For this system, the pdfs $\varphi(t)$, $\psi(t)$, and $\psi_T(t)$ show generally moderate fluctuations with respect to longitudinal dispersion. The main effect of the α_L coefficient can be seen in the increase of the spreading of the probability distributions. The outlet transit time pdf shows younger arrival times when α_L increases, but also a longer tail. The internal age pdf and the internal total transit time pdf are affected the same way by dispersion. The average internal age τ_i

and the average internal total transit time τ_{it} are dispersion dependent; they increase linearly with α_L, indicating that dispersion leads to a higher average age of the system. The variability of age and transit time within the aquifer increases proportionally with the square of α_L (see the second moments of $\psi(t)$ and $\psi_T(t)$ in Excursus 3.2), while the variance of the outlet transit time pdf $\varphi(t)$ increases linearly with α_L.

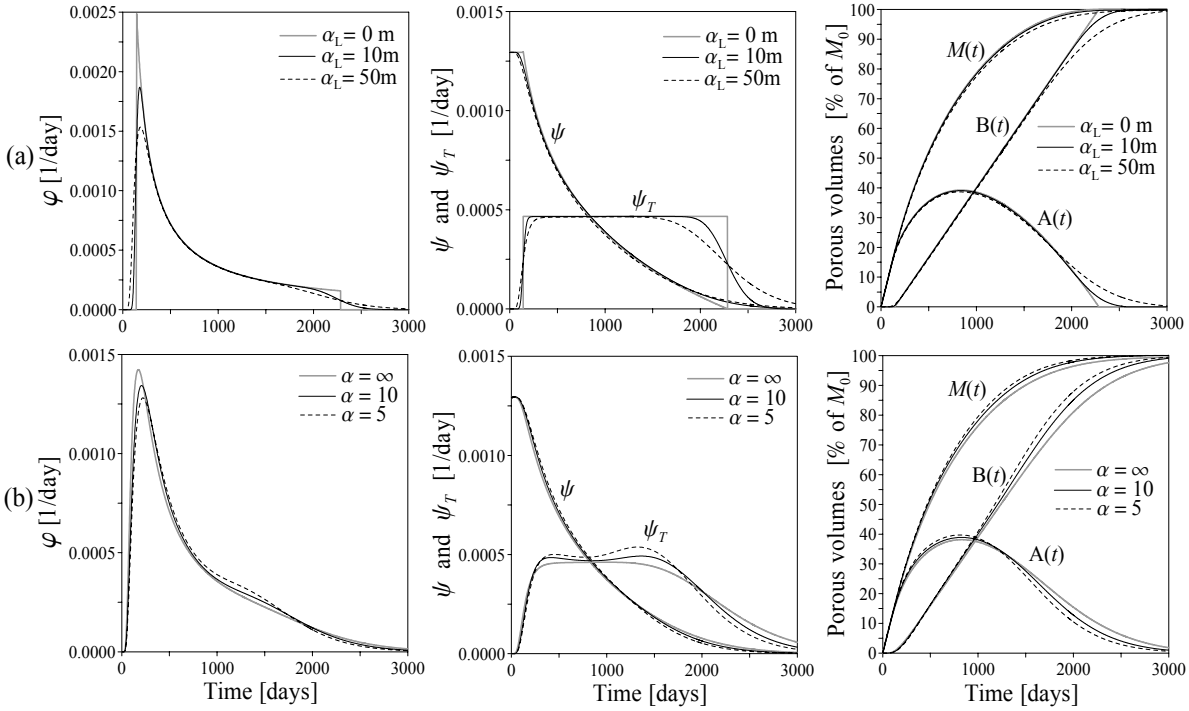

Fig. 3.18. RT solutions for the 2D vertical half-circular aquifer: (a) Analytical solutions (see Excursus 3.2) for the pdfs φ, ψ, and ψ_T, and for the internal groundwater volume functions A, B, and M, as a function of the α_L coefficient ($\alpha_T = D_m = 0$); (b) Same functions as (a), as a function of the ratio $\alpha = \alpha_L/\alpha_T$ (α_L = 50m).

Contrasted behaviour appears when the coupled effect of longitudinal and lateral dispersivity is taken into account (Fig. 3.18b). The case $\alpha_T \neq 0$ was analysed using numerical solutions, by increasing the ratio $\alpha = \alpha_L/\alpha_T$. The tailing effect decreases from a starting situation ($\alpha = \infty$ in Fig. 3.18b) with increasing values of lateral dispersivity (decrease of α ratio in Fig. 3.18b), which causes the mixing of ages, old water particles moving laterally between the flow lines and replacing younger particles, and vice-versa.

The pdf $\psi_T(t)$ is instructive for the characterization of the internal organization of total transit times. When longitudinal dispersivity increases, the uniformity of the advective internal total transit time organization is modified, and the probability of having larger transit times increases, as shown by the long tails of the curves. For the case $\alpha = 5$, the pdf $\psi_T(t)$ shows a tendency in the individualization of water volumes with respect to transit time, due to the effect of lateral exchanges of water particles. The internal groundwater volume functions also attest of the above-mentioned dispersion effects. For example, the function A(t) shows long tails for large values of α_L, reinforcing the observed behaviour at outlet of the transit time pdf for old ages. The internal increase of water volumes which require long transit times to exit the aquifer due to an increase of α_L has of course its consequence at outlet with older arrival times. As with the pdfs $\varphi(t)$, $\psi(t)$, and $\psi_T(t)$, this tailing effect decreases when lateral dispersion is added.

Excursus 3.2: Reservoir theory for the 2D half-circular aquifer.

In the crown-shaped aquifer geometry in Fig. 3.6, the flow lines remain parallel to each other in the entire aquifer domain. Therefore, we assume a 1D transport process at each point $x = \alpha r$ on the flow line coordinate. The total porous volume is $M_0 = \phi\pi(R^2 - r_0^2)/2$, the steady flow rate is $F_0 = K\Delta H \ln(R/r_0)/\pi$, the dispersion coefficient is $D(r) = \alpha_L v(r)$, and the pore velocity $v(r) = q(r)/\phi = K\Delta H/\phi\pi r$. The age resident and flux pdfs are deduced from Eqs. (E2.3.1) and (E2.3.2), by substituting x by αr, and the life expectancy resident and flux pdfs are deduced from the same equations by replacing x by $(\pi - \alpha) r$. The total transit time flux pdf is finally obtained by replacing x by πr in Eq. (E2.3.1), and the total transit time resident pdf is calculated by convolution of the age resident pdf with the life expectancy resident pdf, according to Eq. (2.11). The average age, life expectancy and total transit time are given by the first moment of the corresponding flux pdfs:

$$\langle A(\alpha,r)\rangle = \frac{\phi\alpha\pi r^2}{K\Delta H} \quad , \quad \langle E(\alpha,r)\rangle = \frac{\phi(\pi-\alpha)\pi r^2}{K\Delta H} \quad , \quad \langle T(r)\rangle = \langle A(\alpha,r)\rangle + \langle E(\alpha,r)\rangle = \frac{\phi\pi^2 r^2}{K\Delta H} \tag{E3.2.1}$$

Since on the outlet line ($\alpha = \pi$) velocity points in the direction of the outward unit vector, the discharge zone transit time pdf φ can be evaluated by averaging the age flux pdfs on the outlet line, or equivalently by averaging the life expectancy flux pdfs on the inlet line ($\alpha = 0$). The internal age (or life expectancy) pdf ψ, and the internal total transit time pdf ψ_T are calculated following the domain integration in Eqs. (3.3), (3.5) and (3.7), by integrating between the inner radius r_0 and the outer radius R, and by integrating from 0 to π (see Fig. 3.6):

$$\psi_U(t) = \frac{1}{M_0}\int_0^{\pi}\int_{r_0}^{R} \phi C_U^r(x = \alpha r, t) r\, dr\, d\alpha \tag{E3.2.2}$$

$$\psi_T(t) = \frac{1}{M_0}\int_0^{\pi}\int_{r_0}^{R} \phi C_T^r(x = \pi r, t) r\, dr\, d\alpha \tag{E3.2.3}$$

with $U = A$ or E. The outlet transit time pdf φ can be deduced from the flow rate normalized sum of each flux-weighted age flux pdf at outlet:

$$\varphi(t) = \lim_{\alpha=\pi}\frac{1}{F_0}\int_{r_0}^{R} q(r) C_A^f(\alpha r, t)\, dr = \lim_{\alpha=\pi}\frac{1}{F_0}\int_{r_0}^{R} [q(r) C_A^r(\alpha r, t) - D(r)\frac{\partial C_A^r(\alpha r, t)}{r\partial\alpha}]\, dr \tag{E3.2.4}$$

The average transit time τ_t equals the turnover time τ_0:

$$\tau_t = \tau_0 = \frac{M_0}{F_0} = \frac{\phi\pi^2(R^2 - r_0^2)}{2K\Delta H\xi} \quad , \quad \xi = \ln\left(R/r_0\right) \tag{E3.2.5}$$

The average internal age (or life expectancy) τ_i and internal total transit time τ_{it} vary linearly with α_L:

$$\tau_i = \mu_1[\psi_U] = \frac{\phi\pi}{12K\Delta H(R^2 - r_0^2)}[8(R^3 - r_0^3)\alpha_L + 3\pi(R^4 - r_0^4)] \quad , \quad \tau_{it} = \mu_1[\psi_T] = 2\tau_i \tag{E3.2.6}$$

as well as the variance of φ:

$$\sigma^2[\varphi] = \frac{\phi^2\pi^2}{12K^2\Delta H^2\xi^2}[8\pi(R^3 - r_0^3)\xi\alpha_L + 3\pi^2(R^4 - r_0^4)\xi - 3\pi^3(R^2 - r_0^2)^2] \tag{E3.2.7}$$

The second temporal moments of the internal age and internal total transit time pdfs have a parabolic form with respect to α_L:

$$\mu_2[\psi_U] = \frac{\phi^2\pi^2}{45K^2\Delta H^2(R^2 - r_0^2)}[90(R^4 - r_0^4)\alpha_L^2 + 36\pi(R^5 - r_0^5)\alpha_L + 5\pi^2(R^6 - r_0^6)] \tag{E3.2.8}$$

$$\mu_2[\psi_T] = \frac{\phi^2\pi^2}{15K^2\Delta H^2(R^2 - r_0^2)}[75(R^4 - r_0^4)\alpha_L^2 + 36\pi(R^5 - r_0^5)\alpha_L + 5\pi^2(R^6 - r_0^6)] \tag{E3.2.9}$$

3.4.2 Vertical multi-layered aquifer

In this second theoretical example, we consider a four-layered vertical aquifer system, as illustrated in Fig. 3.19. From the top to the bottom of the model, the layers have decreasing thicknesses and increasing pore velocities. The domain is discretized into 30'000 homogeneous bilinear quadrangles. The total porous volume M_0 is 65312.5m^3. A constant input flow rate F_0 of 402.5m^3/day enters the system along the left limit, using imposed fluxes of varying intensity proportional to the different layers hydraulic conductivities. The system turnover time is then $\tau_t = \tau_0 = 162.267$days. The outlet is simulated at the top of the right side by a constant hydraulic head H along a relatively small zone of 15m. The permeability-porosity couples have been set in a way that the pore velocity contrasts (velocities v_i in Fig. 3.19a) involve specific ages within each layer. In the neighbourhood of the outlet zone, due to its small size, fluxes converge and high mixing of arrival times is expected. This mixing at the outlet surrounding is illustrated in Fig. 3.19b, where the average age distribution is plotted. The fact that the layers thickness diminishes with depth, while the influx intensity increases, is meant to create arrival time peaks at outlet of comparable orders of magnitude.

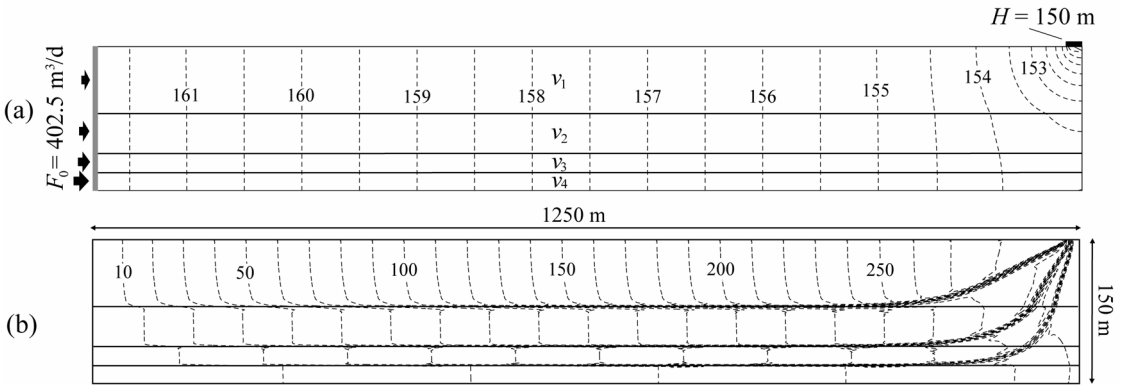

Fig. 3.19. 2D vertical multi-layered aquifer: (a) Boundary conditions and Laplacian flow field in meters; (b) Mean age isochrones in days, illustrating the pore velocity contrast effect on age transport ($\alpha_L = \Delta\mathbf{x} = 2.5$m, $\alpha_T = 0$, $D_m = 0$). Average pore velocities: $v_1 = 4.0$m/day, $v_2 = 6.5$m/day, $v_3 = 10.5$m/day, $v_4 = 23.5$m/day.

The temporal moments τ_i and τ_{it} are good indicators of the dynamics of the global system. Because they are volume-averaged quantities, their magnitude will depend on the water quantities of contrasted age and transit time, which are directly related to the flow and transport dynamics. For this example, τ_i and τ_{it} show only small variations with respect to dispersion (Table 2), because even if velocities between layers are contrasted, flow in the system is generally rapid. Longitudinal dispersion has the effect of making the system older, by creating long tails that can be observed at the reservoir outlet, but also on the internal age and internal total transit time distributions (Fig. 3.20a and b). Spreading in the direction of velocity is of course the main cause for this. Lateral dispersion presents the property of homogenising the ages by mixing water particles of different ages. For a given level of longitudinal dispersion, increasing the ratio $\alpha = \alpha_L/\alpha_T$ (Fig. 3.21) makes the system younger, with diminishing tailing, and diminishing values of the mean internal age τ_i and the mean internal total transit time τ_{it} (Table 2). Longitudinal dispersion induces spreading of solute particles, and thus variability around the plume centre of gravity. When lateral dispersion is added, the mixing of particles between flow lines homogenises the concentrations. When longitudinal spreading is important, the exchange surface along the plume body is extended, and mixing can then be expected to be of high magnitude.

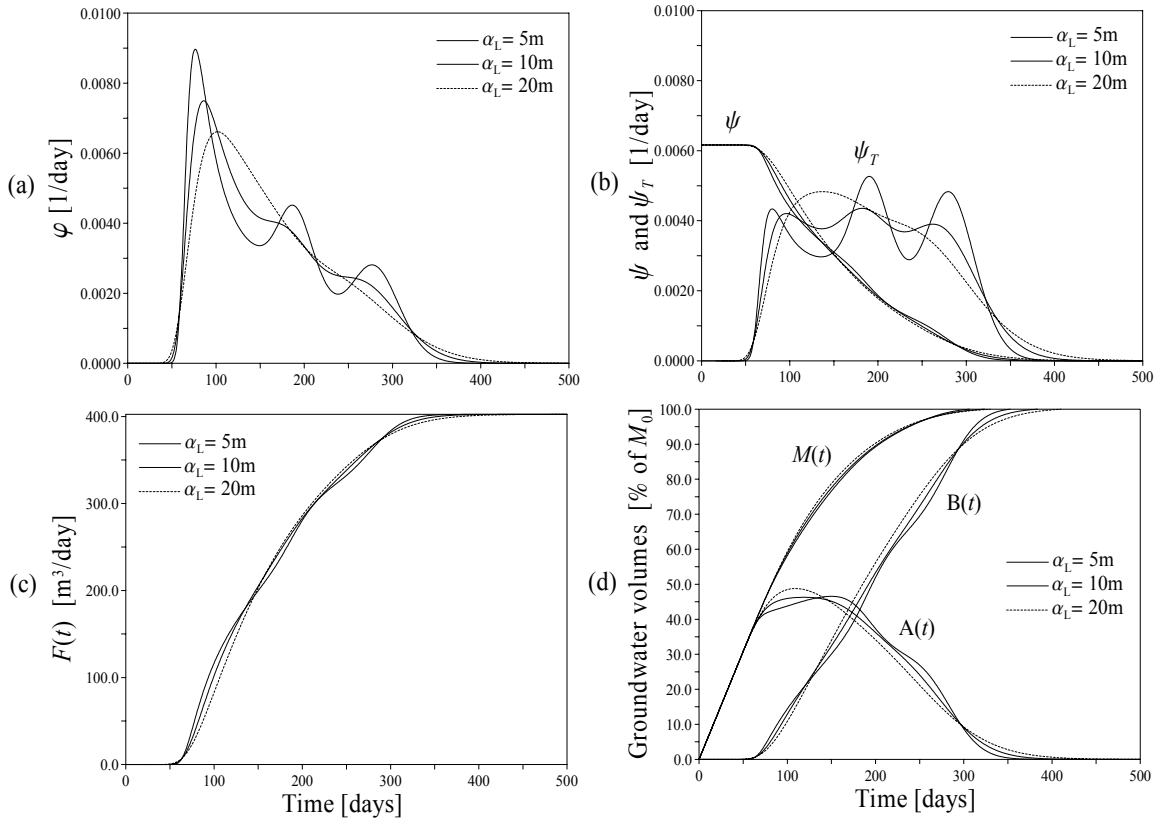

Fig. 3.20. Calculated pdfs, cdfs and groundwater volumes for the 2D vertical multi-layered aquifer as a function of dispersion, for the ratio $\alpha = \alpha_L/\alpha_T = 10$: (a) Outlet transit time pdf; (b) Internal age pdf and internal total transit time pdf; (c) Outlet transit time cdf (scaled by F_0); (d) Groundwater volumes versus time.

The internal total transit time pdf $\psi_T(t)$ is of large interest for the characterization of the internal organisation of the flow dynamics. Its shape and particularly the number of modes it shows has a direct consequence on the shape of the outlet transit time pdf. If we take the example of the case $\alpha = \infty$ ($\alpha_T = 0$) in Fig. 3.21, the function $\psi_T(t)$ exhibits as many peaks as the outlet transit time pdf $\varphi(t)$. However, the magnitudes of these peaks with respect to each other are different for the two functions. The peak of maximum intensity is the first one for $\varphi(t)$, and the third one for $\psi_T(t)$. If we look at the time value corresponding to the first peak of $\varphi(t)$, say t_1, then inside the domain the density of probability that the water particles have a total transit time equal to t_1 is smaller than the same density of probability at the reservoir outlet. This is due to the fact that $\psi_T(t)$ deals with volume-averaged probabilities while $\varphi(t)$ deals with flux-averaged probabilities.

The four consecutive peaks of the outlet transit time pdf, which can be well identified for the case $\alpha = \infty$ (Fig. 3.21a), correspond to the four families of water particles, which transit within the four layers of the system, even though some parts of the curve attest to some mixing effects (the density of probability is not zero between two peaks). It can be expected that if the function $\varphi(t)$ would have been calculated by considering the breakthroughs at outlet only, then important information could have been lost. With the RT, we ensure that each contribution to the outflow rate is accounted for.

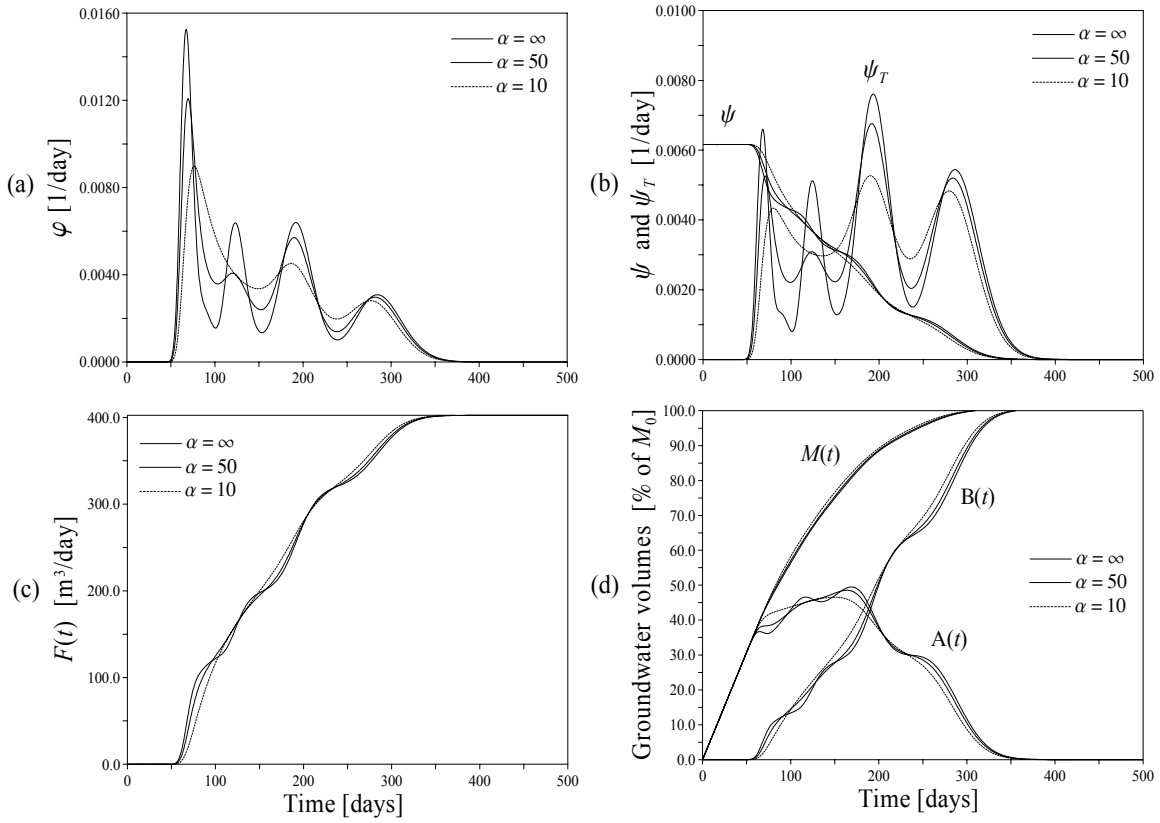

Fig. 3.21. Calculated pdfs, cdfs and groundwater volumes for the 2D vertical multi-layered aquifer as a function of the ratio $\alpha = \alpha_L/\alpha_T$: (a) Outlet transit time pdf; (b) Internal age pdf and internal total transit time pdf; (c) Outlet transit time cdf (scaled by F_0); (d) Groundwater volumes versus time deduced from the outlet transit time cdf.

Table 2
Dispersive parameters related to Fig. 3.20 and 3.21, and calculated pdf statistics (units in meters and days).

Parameters	**Fig. 3.20**				**Fig. 3.21**			
α	10	–	–	–	∞	50	10	5
α_L	5.0	10.0	20.0	30.0	5.0	5.0	5.0	5.0
α_T	0.5	1.0	2.0	3.0	0.0	0.1	0.5	1.0
Statistics								
$\sigma[\varphi]$	75.710	75.955	79.871	89.113	81.766	79.786	75.940	72.482
τ_i	98.902	98.915	101.010	105.091	102.156	100.905	98.916	97.311
τ_{it}	197.804	197.830	202.020	210.183	204.313	201.811	197.833	194.623

This simple theoretical example shows the complexity that is to be expected for the nature of the age and transit time distributions. It underlines how the significance of average age, or average transit time, can lead to erroneous interpretations, regarding the system dynamics (e.g. inferences on average velocity) or hydrogeological problems related to risk and vulnerability assessment. Whenever the outlet transit time pdf is multi-modal, then the average transit time, or turnover time, can definitely not be used as a reliable quantity representative of the groundwater age distribution. With this theoretical example, it is clear that the average age values at outlet hardly represent secure information, since they are mostly related to low densities of probability (see Fig. 3.20 and Fig. 3.21, Table 2). Once more this consideration points out to the interpretation of average age measurements (or mean age simulations) that should be done very carefully. Generally, attention is given to hydrodynamic dispersion, heterogeneity, and long distance travelling induced mixing [Goode, 1996, 1998; Varni & Carrera, 1998; Weissmann *et al.*, 2001], which are factors that represent a source of uncertainty for the age dating methods and environmental tracer data

interpretations. Here one can see that the geological, the structural and the hydraulic boundary configurations can by themselves be responsible of unrepresentative mean ages, even in advection-dominated transport regimes. Mean ages should a priori not represent an absolute simulation answer, and the knowledge of the entire age distribution should be of prime interest in most cases.

3.5. Analysis of boundary condition effects

3.5.1. Cauchy type condition versus Dirichlet type condition to derive the RT

To derive the RT formulation (3.21), the Cauchy type condition has been used at inlet (age problem) and outlet (life expectancy problem), to simplify the integrated forward and backward ADEs. If instead, a Dirichlet type boundary condition is used to solve Eqs. (3.12) and (3.16), then Eq. (3.21) takes the form:

$$\varphi(t) + \tau_0 \frac{\partial \tilde{\psi}(t)}{\partial t} = \delta(t) \tag{3.42}$$

with

$$\tilde{\psi}(t) = \psi(t) - \frac{1}{M_0} \int_0^t J_d(\tau) d\tau \tag{3.43}$$

$$J_d(t) = \int_{\Gamma_-} \mathbf{D} \nabla C_A(\mathbf{x},t) \cdot \mathbf{n} \, d\Gamma = \int_{\Gamma_+} \mathbf{D} \nabla C_A(\mathbf{x},t) \cdot \mathbf{n} \, d\Gamma \tag{3.44}$$

The scalar quantity $J_d(t)$ is the sum of the age dispersive fluxes projected on the inlet limit Γ_-, or equivalently the sum of the life expectancy dispersive fluxes projected on the outlet limit Γ_+. Since $J_d(t)$ is negative at $t = 0^+$, it accounts for a mass loss by dispersion at inlet or outlet, and is therefore expected to mainly affect the short times for a relative low level of dispersion. The function $\tilde{\psi}(t)$ is the internal age (or life expectancy) pdf, corrected by the total cumulated dispersive mass flux of water particles that exit Ω through Γ_-, or amount of particles that will not reach Γ_+. The dispersive term in Eq. (3.43) has the drawback that the integral of $\tilde{\psi}(t)$ from 0 to infinity is less than unity, unless $J_d(t) = 0$. This correction is, however, necessary when using the Dirichlet type boundary condition to calculate resident concentrations, in order to ensure that the function $\varphi(t)$ is related to the considered outlet zone Γ_+ only. The value at the origin of the function $\psi(t)$ in (3.43) accounts for the loss of water by dispersion on Γ_-, with $\psi(0) \geq \tilde{\psi}(0)$, as shown in Fig. 3.22b (to be compared to Fig. 3.3b). As a matter of fact, the probability of finding elements in the reservoir per unit time that reach an age smaller than the minimum transit time is not constant anymore, since water particles with very small ages exit the system through the inlet boundary.

The age loss by upstream dispersion may be interpreted as a consequence of the Fickian transport model used in this analysis. With such a model, water particles can indeed exit the system by backward dispersion/diffusion through the same boundary where they have been injected. More formally speaking, it is a fact that, in multi-dimensional domains, the Dirichlet type condition prescribed on a inflowing or outflowing hydraulic boundary, is not properly posed with respect to the representation of boundaries in mathematical continua [Parker & van Genuchten, 1984]. Considering the forward equation (3.12) with a Cauchy type boundary condition at inlet, each water particle on Γ_- is forced to enter the system, and the internal age pdf $\psi(t)$ does not need to be corrected to evaluate the outlet transit time pdf ($\tilde{\psi} = \psi$). As discussed by Parker & van Genuchten

[1984], Bear & Verruijt [1987], this kind of boundary condition simulates the presence of a very small transition zone within which the medium dispersivity and concentration vary continuously, ensuring macroscopic solute mass balance and a self-consistent definition of the resident concentration. The Dirichlet type boundary condition comes with the additional assumption of a zero concentration gradient inside the boundary transition zone, and since this is not necessarily always the case, the consequence is a loss of mass flux, evaluated by the function $J_d(t)$ in Eq. (3.44). This mass loss problem concerns the advective-dispersive contaminant transport in general, for which the total flux boundary condition should be used at hydraulic inlet limits rather than the imposed concentration condition, to ensure a correct solute mass balance.

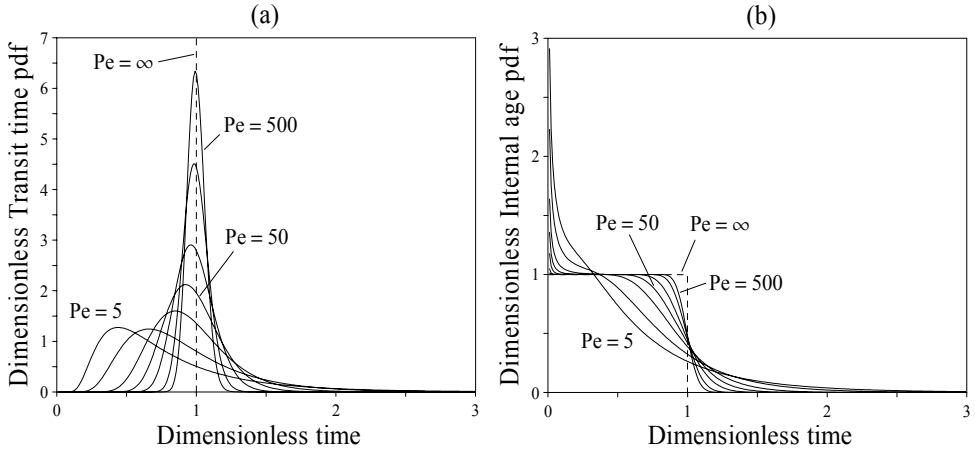

Fig. 3.22. Outlet transit time pdf and internal age pdf for a 1D semi-infinite flow domain, as a function of the Peclet number for $\mathrm{Pe} = 5, 10, 25, 50, 100, 250, 500$, using a Dirichlet condition for calculating resident concentrations: (a) Outlet transit time pdf; (d) Internal age pdf. Time is normalized by the average turnover time $\tau_0 = L/v$, x by L, and $\mathrm{Pe} = Lv/D$.

For the case of the 1D semi-infinite domain presented in section 3.2.2, the Dirichlet type condition induces a lowering of the average transit time relative to the turnover time τ_0 by the flow rate-normalized mean age dispersive flux D/v^2 at inlet, while the average internal total transit time τ_{it} and the average internal age τ_{i} do not depend on the dispersion coefficient D. Since $\psi(t)$ and $\psi_T(t)$ are defined from resident concentrations, their temporal moments should be dispersion-dependent. Hence, the non-dependency of τ_{it} and τ_{i} with D indicates the erroneous choice of a Dirichlet type condition for solving the ADE if resident concentrations are expected. The internal age pdf $\psi(t)$ also shows an anomalous behaviour at early times and with an undefined value at origin (Fig. 3.22b), due to the dispersive losses at $x = 0$ which cause very short residence times that increase the amount of water with very small ages (water particles that flow out by the inlet). The dispersion-corrected average internal age (mean of the function $\tilde{\psi}$) is dispersion dependent, indicating that $\tilde{\psi}(t)$ should be taken as the correct internal age pdf when the Dirichlet type boundary condition is used, although the overall problem is ill-posed.

When the outlet transit time probability function is modelled with Eq. (3.42), the effect of dispersion is a decrease of the average transit time. The age mass flux that exits the system at its hydraulic inlets by dispersion and diffusion is a quantity that will not reach the outlets, and therefore the resulting average transit time becomes younger. Evaluating the first moment of $\varphi(t)$ using Eqs. (3.42) – (3.43) yields

$$\tau_{\mathrm{t}} = \tau_0 + \frac{1}{F_0}\int_{\Gamma_-} \mathbf{D}\nabla\langle A\rangle\cdot\mathbf{n}\,d\Gamma = \tau_0 + \frac{1}{F_0}\int_{\Gamma_+} \mathbf{D}\nabla\langle E\rangle\cdot\mathbf{n}\,d\Gamma = \frac{\tilde{M}_0}{F_0} \tag{3.45}$$

The average transit time at the outlet equals the turnover time reduced by the flow rate-normalized mean age dispersive flux at the inlet, or equivalently by the flow rate-normalized mean life expectancy dispersive flux at the outlet. Due to the negative sign of the boundary integrals in Eq. (3.45), the effect of dispersion is a decrease of the average transit time, accounting for the loss of age mass that will not reach the considered outlet, as it has been shown with the 1D example in Fig. 3.22b. The quantity $\tilde{M}_0$ relates to a reduced aquifer porous volume that corresponds to the effective porous volume contributing to the flow rate at the boundary Γ_+:

$$\tilde{M}_0 = F_0 \tau_t = M_0 + \int_{\Gamma_-} \mathbf{D}\nabla\langle A\rangle \cdot \mathbf{n}\, d\Gamma = M_0 + \int_{\Gamma_+} \mathbf{D}\nabla\langle E\rangle \cdot \mathbf{n}\, d\Gamma \le M_0 \tag{3.46}$$

The difference between M_0 and $\tilde{M}_0$ corresponds to the total amount of water which exits the system by dispersion through the boundaries. It is measured by the sum of the dispersive fluxes of average age on Γ_-, or equivalently by the sum of the dispersive fluxes of average life expectancy on Γ_+. The quantity $\tilde{M}_0$ can be used to give a measure of the mass balance error induced by the use of the Dirichlet type boundary condition when the ADE is solved for resident concentrations. Fig. 3.23 illustrates for the aquifer of section 3.4.1 the error induced by the solution resulting from a Dirichlet type boundary condition, when the age pdf is wrongly taken as a resident concentration. The average transit time at the outlet is linearly decreasing with respect to its physical value (turnover time τ_0) when α_L increases, in relation to the loss of age mass by backward dispersion on the inlet limit Γ_-. This loss reaches about 5% of the total porous volume M_0 ($\tilde{M}_0 \approx 0.95 M_0$) for the maximum tested value of α_L, as shown by the value at the origin of the function C(t).

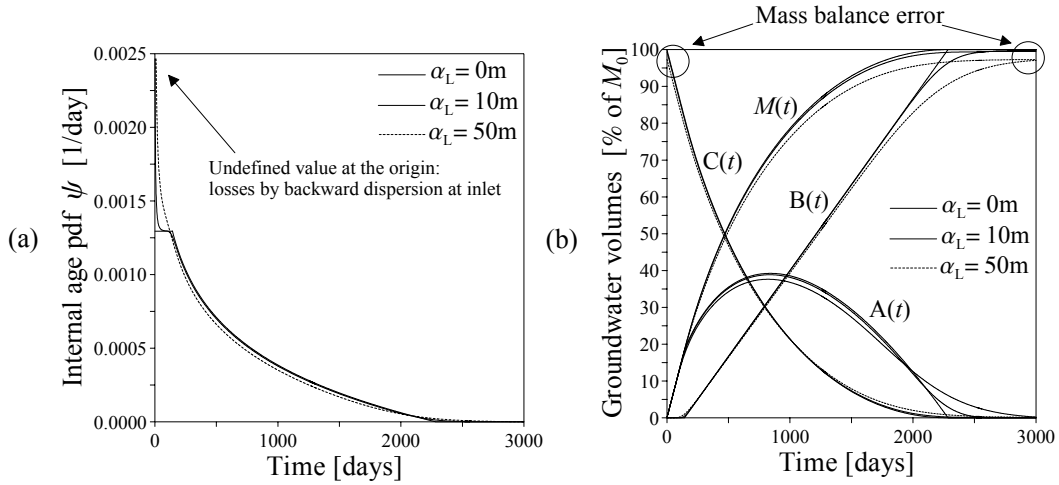

Fig. 3.23. RT solutions for the 2D vertical half-circular aquifer (see section 3.4.1) as a function of the α_L coefficient ($\alpha_T = D_m = 0$), when a Dirichlet condition is used for calculating resident concentrations: (a) Internal age pdf ψ; (b) Internal groundwater volume functions A, B, M, and C.

3.5.2. The Implicit Neumann boundary condition

In this work, the *Implicit Neumann condition* is used to allow natural outflowing age and life expectancy gradients, instead of prescribing the classical homogeneous Neumann condition (also called natural or Danckwerts condition), which forces concentration gradients to vanish. Since no clear physical evidence can support this assumption, we adopted an implicit procedure of gradient projection evaluation at inlet and outlet, in order to ensure total mass flux continuity along these limits. Backward movement of particles by dispersion is then also made possible. The implementation of the *Implicit Neumann condition* in finite element matrices is described in Appendix B. Basically, the method is based on an upstream evaluation of the dependent variable

gradient along the concerned boundaries. Boundary normal unit vectors and gradient operators must be properly evaluated. The normal projection of the gradients results in element vectors which are used to update the finite element matrices.

The effect of the *Implicit Neumann condition* is illustrated in Fig. 3.24. Three models are considered to calculate the internal distribution ψ. The reference model is indicated in Fig. 3.24a. The inlet is recharged by fluxes of constant intensity, and a hydraulic head is prescribed at outlet. The coefficient of longitudinal dispersivity α_L is fixed to the mesh size, and the transverse coefficient of dispersivity α_T is ten times smaller than α_L. The results of the FRT and of the BRT without using the *Implicit Neumann condition* to solve the forward and backward ADEs are compared. Theoretically, the FRT and the BRT must yield the same results, although significant differences exist between ψ_A and ψ_E (Fig. 3.24d). The second model (Fig. 3.24b) is similar to the reference model, but the upper left part has been truncated, such that the inlet is now at the altitude z_0. The calculated hydraulic heads of the reference at the position of the new inlet are assigned. The third model (Fig. 3.24c) is issued from the truncation of the upper right part of the reference model, the outlet being now at the altitude z_0. Similarly, the calculated hydraulic heads of the reference at the position of the new outlet are assigned.

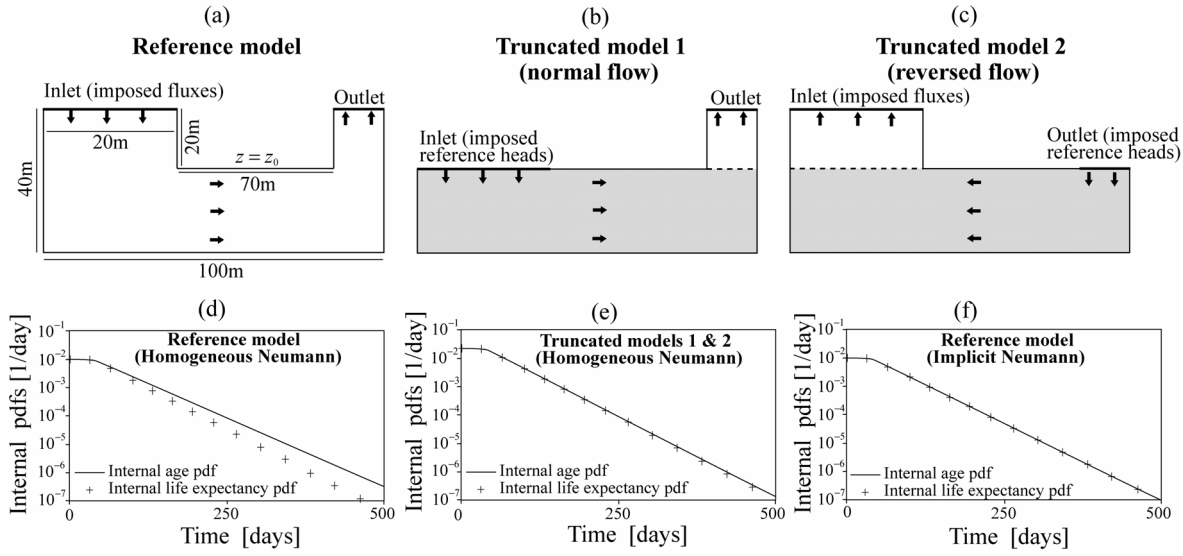

Fig. 3.24. Theoretical models that reveal the negative effects to the homogeneous Neumann condition at inlet and outlet: (a) Reference model; (b) First truncated model; (c) Second truncated model; (d) ψ_A and ψ_E for the reference with Homogeneous Neumann condition; (e) ψ_A and ψ_E for the two truncated models with Homogeneous Neumann condition; (f) ψ_A and ψ_E for the reference with Implicit Neumann condition.

For the two truncated model, the integration of concentration to evaluate ψ_A and ψ_E (see Eqs. (3.3) and (3.5)) has been performed on the sub-region indicated in grey in Fig. 3.24b and c, still without using the *Implicit Neumann condition* to solve the forward and backward ADEs. The pdf ψ_A is evaluated with the first truncated model, and the pdf ψ_E is evaluated with the second truncated model. In this way, it is expected that the effects of the inlet and outlet boundaries on the simulated concentrations should be lowered, and that ψ_A and ψ_E should be comparable. This is what effectively happen (see Fig. 3.24e), since the two simulated curves are now quasi identical, except for some small differences at large time values, showing that the errors noted with the reference model were caused by the effect of the homogeneous Neumann condition. Finally, the *Implicit Neumann condition* is used to solve the ADEs in the reference model, and the two pdfs ψ_A and ψ_E are identical (Fig. 3.24f).

3.6. Is groundwater age a paradox?

In recent articles, Bethke & Johnson [2002a, 2002b] introduced the concept of paradox in the framework of groundwater age, by manipulating the one-dimensional mean age equation [Goode, 1996]. In summary, their results relate to how, at steady-flow regime, the presence of aquitards in contact with aquifers contribute by mixing to an age mass increase in the aquifer at a rate that is unrelated to the mixing rate, but which only depends on the ratio of the fluid volume in aquitards to the fluid volume in aquifers. According to these authors, this is the paradox of groundwater age, through which the mixing of old waters from aquitards with younger waters of aquifers not only increases the age in the aquifer medium, but also decreases the age in the aquitard medium. A highly impermeable aquitard would be expected to little affect the age within an aquifer, but at the contrary its aging effect would be the same as with a more permeable aquitard, for unchanged water content in both aquitards. To obtain these results, the authors derived a one-dimensional solution of the age equation, by considering the water exchange between an aquifer horizon confined by aquitards.

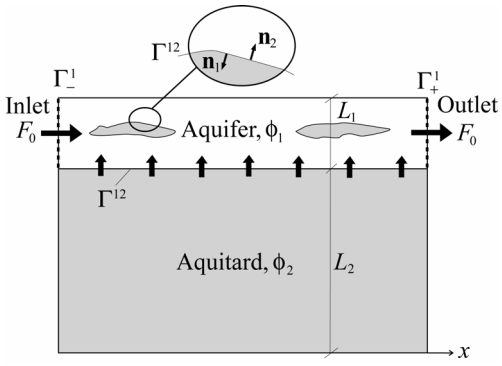

Fig. 3.25. Schematic illustration of a contact aquifer – aquitard.

In the following we wish to obtain the same mathematical result as Bethke & Johnson [2002a] through a more general approach, and discuss their vision of age paradox. Let us consider an hydro-geological domain Ω bounded by $\Gamma = \Gamma_- \cup \Gamma_0 \cup \Gamma_+$, which owns two main classes of permeability/porosity such that Ω can be decomposed into a rapid flow domain Ω_1 and low flow domain Ω_2, $\Omega = \Omega_1 \cup \Omega_2$. This configuration could correspond to a quite homogeneous sandy aquifer containing disseminated clay lenses, or to an aquifer body in contact with an aquitard (Fig. 3.25). The domains Ω_1 and Ω_2 are bounded by Γ^1 and Γ^2, respectively, and the contact between the two media is figured by Γ^{12}. The age pdf continuity equations for the media Ω_1 and Ω_2 may be written as

$$\frac{\partial \phi_1 C_1}{\partial t} = -\nabla \cdot \mathbf{q}_1 C_1 + \nabla \cdot \mathbf{D}_1 \nabla C_1 \qquad \text{in} \quad \Omega_1 \tag{3.47}$$

$$\frac{\partial \phi_2 C_2}{\partial t} = -\nabla \cdot \mathbf{q}_2 C_2 + \nabla \cdot \mathbf{D}_2 \nabla C_2 \qquad \text{in} \quad \Omega_2 \tag{3.48}$$

with the boundary condition

$$\mathbf{J}_1 \cdot \mathbf{n}_1 = \mathbf{q}_1 \cdot \mathbf{n}_1 \delta(t) \qquad \text{on} \quad \Gamma^1_- \tag{3.49}$$

In Eqs. (3.47) to (3.49), C_i is the age resident pdf in medium i, $\mathbf{q}_i$ is the fluid flux vector in medium i, ϕ_i the porous medium porosity of medium i, $\mathbf{J}_i = \mathbf{q} C_i - \mathbf{D} \nabla C_i$ is the age mass flux vector in medium i, and $\mathbf{D}_i$ is the tensor of macro-dispersion of medium i. Between the stagnant and the flowing water, continuity requires

$$C_1 = C_2 \qquad \text{on} \quad \Gamma^{12} \tag{3.50}$$

$$\int_{\Gamma^{12}} \mathbf{J}_1 \cdot \mathbf{n}_1 \, d\Gamma = -\int_{\Gamma^{12}} \mathbf{J}_2 \cdot \mathbf{n}_2 \, d\Gamma \qquad \text{on} \quad \Gamma^{12} \tag{3.51}$$

where $\mathbf{n}_i$ are unit vectors normal to the boundary Γ^{12}. Integrating Eqs. (3.47) and (3.48) over Ω_i, applying the divergence theorem, summing up and accounting for (3.49), (3.50) and (3.51) yields

$$\int_{\Gamma_+} \mathbf{J}_1 \cdot \mathbf{n}_1 \, d\Gamma + \int_{\Gamma^{12}} \mathbf{J}_2 \cdot \mathbf{n}_1 \, d\Gamma - \int_{\Gamma^{12}} \mathbf{J}_1 \cdot \mathbf{n}_1 \, d\Gamma + \frac{\partial}{\partial t} \int_{\Omega_1} \phi_1 C_1 \, d\Omega + \frac{\partial}{\partial t} \int_{\Omega_2} \phi_2 C_2 \, d\Omega = 0 \tag{3.52}$$

Since $\mathbf{n}_1 = -\mathbf{n}_2$, Eq. (3.51) is equivalent to

$$\int_{\Gamma^{12}} \mathbf{J}_1 \cdot \mathbf{n}_1 \, d\Gamma = \int_{\Gamma^{12}} \mathbf{J}_2 \cdot \mathbf{n}_1 \, d\Gamma \qquad \text{on} \quad \Gamma^{12} \tag{3.53}$$

Inserting Eq. (3.53) into Eq. (3.52), using the definitions (3.3) and (3.8), and re-arranging, leads to

$$\varphi(t) + \frac{M_1}{F_0} \frac{\partial \psi_1(t)}{\partial t} + \frac{M_2}{F_0} \frac{\partial \psi_2(t)}{\partial t} = \delta(t) \tag{3.54}$$

where M_1 and M_2 are the porous volumes of Ω_1 and Ω_2, respectively, ψ_1 and ψ_2 are the internal age pdfs of Ω_1 and Ω_2, respectively, and φ is the transit time pdf of the system outlet, through which the flow rate F_0 exits. Taking the first temporal moment of φ gives the average transit time τ_t at outlet:

$$\tau_t = \frac{M_1}{F_0}\left(1 + \frac{M_2}{M_1}\right) \tag{3.55}$$

Eq. (3.55) matches the 1D result of Bethke & Johnson [2002a]. It relates to the piston-flow model for average age, corrected by the term M_2/M_1. Eq. (3.55) shows that an increase of (average) age at the aquifer outlet is not related to mass fluxes transporting old water molecules from aquitards, but only depends on the ratio of the aquitard porous volume relative to the aquifer porous volume, as stated by Bethke & Johnson [2002a]. From Eq. (3.55), one can deduce the following 1D equation:

$$\tau(x) = \frac{x}{v}\left(1 + \frac{L_2 \phi_2}{L_1 \phi_1}\right) \tag{3.56}$$

where $\tau(x)$ denotes the mean age at the position x, v is the average pore velocity in the aquifer, L_1 and L_2 are the thicknesses of the aquifer and the aquitard, respectively (see Fig. 3.25). Eqs. (3.55) and (3.56) have important implications for interpreting radiometric age determinations, when the classical piston-flow model $\tau(x) = x/v$ is used. However, one must consider that the average age at outlet τ_t in Eq. (3.55) simply corresponds to the ratio of the system total porous volume ($M_1 + M_2$) to the steady flow rate F_0, i.e. the reservoir turnover time τ_0. Its value would be unchanged when considering a single-continuum equation instead of Eqs. (3.47) and (3.48), to characterize age transport in $\Omega = \Omega_1 \cup \Omega_2$. Eqs. (3.55) and (3.56) are equivalent to the average turnover time and the average age issued from a dual – porosity transport model, or mobile – immobile water transport model. These models were originally used to simulate solute transport in soils, where a bimodal pore size distribution exists, inducing the identification of interdependent regions, one region with mobile water and one region with stagnant water. The derivation of the RT for mobile – immobile domains is given in Excursus 3.3. Such models are based on the assumption of a simplified exchange of first order in and out the immobile region. If no diffusive process appears in the formulations (3.55) and (3.56), the distribution of age or transit time is, however, conditioned by a

diffusive exchange (the exchange between the mobile and the immobile regions is ruled by the law of Fick, see Eq. (E3.3.3)). Consequently, what looks like a paradox only concerns the mean of the age distribution. It is clear that only a small amount of stagnant water is needed to drastically shift the mean of the age distribution towards older age values. This effect is accounted for by the first moment in Eqs. (3.55) and (3.56). But in this case, what is the average of the distribution representative of ?

Considering the 1D process behind Eq. (3.56), the rate at which groundwater ages as it flows along the aquifer in contact with an aquitard can be expressed by the Eulerian derivative $d\tau/dx = (1+r)/v$, with $r = (L_2\phi_2)/(L_1\phi_1)$. Bethke & Johnson [2002a] considered two ideal radiometric age measurements τ_1 and τ_2 at two points x_1 and x_2 along the 1D axis of the considered aquifer medium. Letting $\Delta\tau = \tau_2 - \tau_1$ and $\Delta x = x_2 - x_1$, the rate of aging can be rearranged to give a measure of the average flow pore velocity between x_1 and x_2, $v = (1+r) \times (\Delta x/\Delta\tau)$. The latter equation has been tested numerically with the 2D-vertical conceptual model of the aquifer – aquitard system given in Fig. 3.25, by solving the mean age equation (2.45) and the age pdf equation (2.20). The model size is indicated in Fig. 3.26. The aquifer is 100m thick, and the aquitard 600m thick. A constant head $H = 10$m is imposed along the vertical of the aquifer at X = 0 from Z = 0 to −100m (inlet), and a constant head $H = 0$m is prescribed at X = 10'000m from Z = 0 to −100m (outlet). Hydraulic conductivity is 10^{-3} m/s in the aquifer and 10^{-8} m/s in the aquitard. Porosity is 0.1 in the aquifer and 0.3 in the aquitard. The dispersive parameters are $\alpha_L = 0.5\Delta\mathbf{x} = 10\alpha_T = 5$m for the aquifer, and $\alpha_L = \alpha_T = 0$ for the aquitard. The calculated horizontal pore velocity v_x in the aquifer is 315.359m/y, flow being fully horizontal ($v_z = 0$). Mean ages have been monitored at the two doublets $\{A_1, B_1\}$ and $\{A_2, B_2\}$, has shown in Figure 3.26, and velocity has been post-processed using the formula $v = (1+r) \times (\Delta x/\Delta\tau)$ for comparison with the 'true' velocity of 315.359m/y.

Simulation results are given in Table 3 for two values of the coefficient of molecular diffusion: $D_m = 2.3\times10^{-9}$ m^2/s (~ self-diffusion of water) and $D_m = 2.3\times10^{-8}$ m^2/s. With the coefficient of self-diffusion of water, $D_m = 2.3\times10^{-9}$ m^2/s, the age pdfs show two distinct modes, one being related to the flow in the aquifer, and the second being the contribution from the under laying aquitard. The velocity evaluation is very bad for the doublet $\{A_1,B_1\}$, and much better for $\{A_2,B_2\}$. With a coefficient of molecular diffusion 10 times higher, $D_m = 2.3\times10^{-8}$ m^2/s, the age pdfs show only one single mode, followed by a very long tail due to the contribution from the under laying aquitard. The velocity evaluation is in this case very acceptable for the two doublets, but it is still worst upstream than downstream, in relation to the apparent dispersion growing spatially and thus temporally in accordance with the generic data on α_L, α_T and D_m. A 50km×3.5km similar model (with still 100m of aquifer) has also been tested with $D_m = 2.3\times10^{-9}$ m^2/s, yielding same results than with the 10'000m×700m model. Consequently, Eqs. (3.55) and (3.56) would then hold in the long-term limit, for the ideal cases when transverse dispersion and diffusion cause a complete and perfect equalization of ages across both the aquitard and the aquifer (compare the two mean age distributions in Fig. 3.26). Moreover, sensitivity analysis showed that small changes in the coefficients of longitudinal and transverse dispersivity in the aquitard (originally set to zero in the aquitard) alter drastically the validity of Eq. (3.56), in relation to the non-purely 1D transport behaviour induced by the effect of the couple $\alpha_L - \alpha_T$ on the spatial distribution of mean age. In this case, the age pdfs within the aquifer can have three modes, depending on the horizontal position.

Table 3
Simulation results related to Fig. 3.26 (units in meters and years).

$D_m = 2.3\times10^{-9}$ m^2/s	$\Delta\tau$	Δx	$v_{calc.}$	Relative error [%]
$\{A_1,B_1\}$	20.922	500	454.061	**43.98**
$\{A_2,B_2\}$	29.289	500	324.354	2.85
$D_m = 2.3\times10^{-8}$ m^2/s	$\Delta\tau$	Δx	$v_{calc.}$	Relative error [%]
$\{A_1,B_1\}$	29.729	500	319.553	1.33
$\{A_2,B_2\}$	30.129	500	315.311	0.01

To our point of view, the concept of groundwater age paradox is more linked to the conceptual representation of the groundwater system than to particular physical processes. The so-called paradox could be a result of an insufficient one-dimensional conceptualization of age modelling in aquitard-aquifer systems. In so far, if groundwater age represents a paradox, then solute transport must also represent a paradox. The works of Bethke & Johnson [2002a, 2002b] have pointed out important restrictions on the interpretation of radiometric age evaluations, but their analysis may remain confined to very few cases, when a perfect and uniform mixing of ages between aquitard and aquifer stands. Therefore, it is crucial to calculate the full age distribution, rather than average ages only, in order to be able to evaluate if the mean age is misleading or not, and to accurately establish the relationship between age transport and the distribution of a decaying isotope.

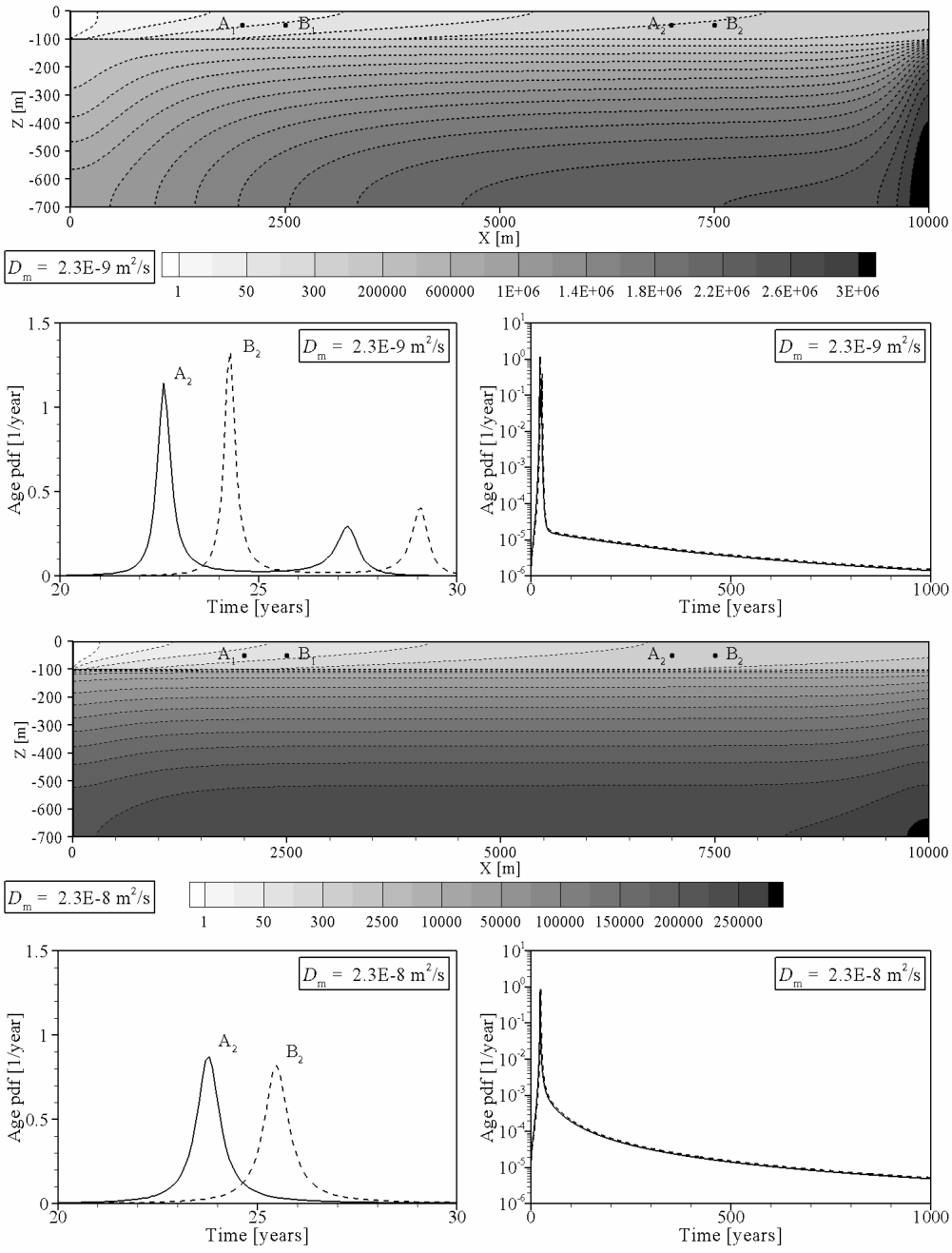

Fig. 3.26. Mean age and age pdf simulations within an aquifer – aquitard groundwater system.

It seems also important to consider what kind of system is to be treated, and furthermore, what model must be chosen to solve the age transport problem. If it is acceptable that the system corresponds to $\Omega = \Omega_1$, then applying the piston-flow model might be valid. If the system really

corresponds to $\Omega = \Omega_1 \cup \Omega_2$, then one can expect to under-estimate the mean groundwater velocity with the piston-flow model.

We extend this discussion by asking the question of what the limits of an aquifer are, or in other words, until where the concept of no-flow boundary can hold in nature? Does a no-flow boundary really exist if the geological material owns significant water content, since diffusion effects from stagnant water zones to more mobile water zones occur, diffusion being driven by the concentration gradients from old ages towards young ages, and by molecular diffusion? The age pdf equation (3.12) is used to simulate the age growth of water particles in an aquifer, by assuming that an age zero is assigned to each inflowing limit. The age in the aquifer is then relative to the age zero on the inflowing limits. In so doing, we must be confident of the zero condition on age along these limits, which is equivalent to be sure, that the limit corresponds effectively to a hydraulic limit of the system. However, in practical modelling of real hydrogeological systems, it is common to draw the limits of what one considers as the aquifer system, although it is known that other groundwater systems partially recharge the aquifer system that is intended to be modelled. For example, consider the classical setting of an alluvial plain in contact on its sides with aquiferous formations. Classically, the flow model of this alluvial aquifer could contain prescribed fluxes or hydraulic heads along some portions of the chosen boundaries, to account for the recharge from bordering aquiferous systems. At these limits, the age would be nil with the boundary value problem (3.12), although the recharging groundwater would contain a non-zero age distribution. In this case, a specific age distribution, which would result from older recharge events, should be assigned instead of a Dirac-type distribution. Otherwise, a more regional model should be envisaged. We can also consider the particular case of internal production of water, e.g. when crystallized water changes to liquid phase (e.g. presence of evaporites, anhydrites), as well as the diffusion of old waters confined in low permeability material. Therefore, we could envision adapting Eq. (3.12) to the following:

$$\frac{\partial \phi C_A}{\partial t} = -\nabla \cdot \mathbf{q} C_A + \nabla \cdot \mathbf{D} \nabla C_A + m_o(t)\delta(\mathbf{x} - \mathbf{x}_o) + Q_1 \delta(t) \qquad \text{in} \quad \Omega \tag{3.57}$$

$$\mathbf{J}_A(\mathbf{x},t) \cdot \mathbf{n} = 0 \qquad \text{on} \quad \Gamma_0$$

$$\mathbf{J}_A(\mathbf{x},t) \cdot \mathbf{n} = \mathbf{q} \cdot \mathbf{n}\, g_A(t) \qquad \text{on} \quad \Gamma_-$$

with $m_o(t)\,\delta(\mathbf{x} - \mathbf{x}_o)$ being a load term characterizing an internal source of old waters, and with $Q_1\,\delta(t)$ acting as an internal production of water. Along the recharging limits Γ_-, the function $g_A(t)$ is the time-Dirac distribution for the meteoric and superficial waters which recharge the modelled system, and $g_A(t)$ is the age distribution of the water coming from other aquifer systems in contact with the modelled aquifer. In this case, $g_A(t)$ is generally unknown, as well as the source $m_o(t)$. As a first approximation, the average date τ of a past recharge could be used, in which case we would have $g_A(t) = \delta(t - \tau)$.

Excursus 3.3. Mobile – Immobile Reservoir Theory.

The resident age distribution continuity equation in a saturated medium $\Omega^{m/im}$ describing the two sites mobile – immobile water for a conservative tracer that is non-adsorbing and non-decaying may be written as

$$\frac{\partial \phi_m C_m^r}{\partial t} + \frac{\partial \phi_{im} C_{im}^r}{\partial t} = -\nabla \cdot \mathbf{q} C_m^r + \nabla \cdot \mathbf{D}_m \nabla C_m^r \qquad \text{in} \quad \Omega^{m/im} \tag{E3.3.1}$$

with the initial and boundary conditions

$$C_m^r(\mathbf{x},0) = C_m^r(\mathbf{x},\infty) = 0 \qquad \text{in} \quad \Omega^m \tag{E3.3.2}$$

$$C_{im}^r(\mathbf{x},0) = C_{im}^r(\mathbf{x},\infty) = 0 \qquad \text{in} \quad \Omega^{im}$$

$$[\mathbf{q} C_m^r(\mathbf{x},t) - \mathbf{D}_m \nabla C_m^r(\mathbf{x},t)] = \mathbf{q} \cdot \mathbf{n}\, \delta(t) \qquad \text{on} \quad \Gamma_-^m$$

Implicit Neumann condition on Γ_+^m

The subscripts ^{m} and ^{im} denote the mobile and immobile media respectively, and $\mathbf{D}_m$ is the mobile medium dispersion tensor. Eq. (E3.3.1) is a general form of the classical equation describing the two regions, mobile – immobile water [see e.g. De Smedt & Wierenga, 1979; Jury & Roth, 1990]. Assuming a simplified exchange of first order in and out of the immobile region, we may write

$$\frac{\partial \phi_{im} C_{im}^r}{\partial t} = -\alpha (C_{im}^r - C_m^r) \tag{E3.3.3}$$

with α [1/T] being a mass transfer coefficient between the mobile and the immobile media. The s-Laplace transforms of Eqs. (E3.3.1) and (E3.3.3) are

$$s(\phi_m \hat{C}_m^r + \phi_{im} \hat{C}_{im}^r) = -\nabla \cdot \mathbf{q} \hat{C}_m^r + \nabla \cdot \mathbf{D}_m \nabla \hat{C}_m^r \tag{E3.3.4}$$

$$\hat{C}_{im}^r = \frac{1}{1 + s\dfrac{\phi_{im}}{\alpha}} \hat{C}_m^r = \hat{\beta}(s) \hat{C}_m^r \tag{E3.3.5}$$

Substitution of Eq. (E3.3.5) into Eq. (E3.3.4) and the Laplace transform of Eq. (E3.3.2) give the following boundary value problem:

$$s\hat{\theta}\hat{C}_m^r = -\nabla \cdot \mathbf{q} \hat{C}_m^r + \nabla \cdot \mathbf{D}_m \nabla \hat{C}_m^r \qquad \text{in} \quad \Omega^m \tag{E3.3.6}$$

$$[\mathbf{q}\hat{C}_m^r(\mathbf{x},s) - \mathbf{D}_m \nabla \hat{C}_m^r(\mathbf{x},s)] = \mathbf{q} \cdot \mathbf{n} \qquad \text{on} \quad \Gamma_-^m$$

Implicit Neumann condition $\qquad$ on $\quad \Gamma_+^m$

with

$$\hat{\theta} = \hat{\theta}(\mathbf{x},s) = \phi_m + \hat{\beta}(\mathbf{x},s)\phi_{im} \tag{E3.3.7}$$

The coefficient θ acts as a time-dependent capacitive parameter, which depends on the exchange coefficient α. Applying the inverse Laplace transform to Eq. (E3.3.7) yields

$$\theta(\mathbf{x},t) = \phi_m(\mathbf{x})\,\delta(t) + \alpha\, e^{-\frac{\alpha}{\phi_{im}}t} \tag{E3.3.8}$$

The total porosity ϕ_{tot} accounting for the two media is found to be the sum of ϕ_m and ϕ_{im} by calculating the mass of θ:

$$\phi_{tot}(\mathbf{x}) = \int_0^{+\infty} \theta(\mathbf{x},\tau)\, d\tau = \hat{\theta}(\mathbf{x}, s=0) = \phi_m(\mathbf{x}) + \phi_{im}(\mathbf{x}) \tag{E3.3.9}$$

Consequently, the system total porous volume is the sum of the mobile and immobile sites porous volumes:

$$M_0 = \int_{\Omega^{m/im}} \phi_{tot}(\mathbf{x}) d\Omega = \int_{\Omega^m} \phi_m(\mathbf{x}) d\Omega + \int_{\Omega^{im}} \phi_{im}(\mathbf{x}) d\Omega = M_0^m + M_0^{im} \tag{E3.3.10}$$

The quantity β [-] in Eq. (E3.3.7) is an exchange function that rules the dynamics of the mass exchanges between the mobile and the immobile phase, by convolution with the age pdf in the mobile phase. The Laplace inversion L^{-1} yields

$$\beta(t) = \lambda\, \mathrm{L}^{-1}\left\{\frac{1}{\lambda + s}\right\} = \lambda e^{-\lambda t} \tag{E3.3.11}$$

with

$$\lambda = \frac{\alpha}{\phi_{im}} \tag{E3.3.12}$$

The coefficient λ [1/T] is similar to a constant of decay. Eq. (E3.3.11) attests of the linear exchange between the mobile and the immobile phase, at the rate λ. The decreasing exponential (E3.3.11) is responsible of the high magnitude exchanges at early times ($\beta(0) = \lambda$), creating very short arrival times, and of the very low magnitude exchanges at late times ($\beta(\infty) = 0$), creating old arrival times and thus important tails of the simulated pdfs. By considering only the age resident concentration in the mobile site, the dual-porosity behaviour is simulated by convoluting C_m^r with the exponential exchange model (E3.3.11):

$$C_{im}^r(\mathbf{x},t) = \lambda \int_0^t e^{-\lambda\tau} C_m^r(\mathbf{x}, t-\tau)\, d\tau \tag{E3.3.13}$$

The application of the reservoir theory to the boundary value problem (E3.3.6) yields

$$\hat{\varphi}(s) = \frac{1}{F_0} \int_{\Gamma_+} [\mathbf{q}\hat{C}_m^r - \mathbf{D}_m \nabla \hat{C}_m^r] \cdot \mathbf{n}\, d\Gamma = 2 - \tau_0\, s\, \hat{\psi} \tag{E3.3.14}$$

$$\hat{\psi}(s) = \frac{1}{M_0} \int_{\Omega^{m/im}} \hat{\theta}(\mathbf{x},s) \hat{C}_m^r(\mathbf{x},s) d\Omega \tag{E3.3.15}$$

The turnover time τ_0 in Eq. (E3.3.14) is defined by:

$$\tau_0 = \frac{M_0}{F_0} = \frac{M_0^m + M_0^{im}}{F_0} = \tau_0^m \left(1 + \frac{M_0^{im}}{M_0^m}\right) \tag{E3.3.16}$$

with $\tau_0^m = M_0^m / F_0$ being the turnover time of the immobile medium. The one-site mobile groundwater internal age pdf is the total porous volume-normalized domain integral of the quantity $\phi_m C_m^r$. When the immobile water is taken into account, the internal age pdf is then defined as the normalized domain integral of the convolution of the mobile age pdf $C_m(\mathbf{x}, t)$ with the capacitive parameter $\theta(\mathbf{x}, t)$:

$$\psi(t) = \frac{1}{M_0} \int_{\Omega^{m/im}} \left(\int_0^t \theta(\mathbf{x},\tau) C_m^r(\mathbf{x}, t-\tau) d\tau \right) d\Omega \tag{E3.3.17}$$

Inserting Eq. (E3.3.7) into Eq. (E3.3.15) and developing results in

$$\hat{\psi}(s) = \frac{1}{M_0} \int_{\Omega^m} \phi_m(\mathbf{x}) \hat{C}_m^r(\mathbf{x}, s) d\Omega + \frac{1}{M_0} \int_{\Omega^{m/im}} \hat{\beta}(\mathbf{x}, s) \phi_{im}(\mathbf{x}, s) \hat{C}_m^r(\mathbf{x}, s) d\Omega \tag{E3.3.18}$$

When accounting for Eq. (E3.3.5), Eq. (E3.3.18) simplifies in

$$\hat{\psi}(s) = \frac{1}{M_0} \int_{\Omega^m} \phi_m(\mathbf{x}) \hat{C}_m^r(\mathbf{x}, s) d\Omega + \frac{1}{M_0} \int_{\Omega^{im}} \phi_{im}(\mathbf{x}) \hat{C}_{im}^r(\mathbf{x}, s) d\Omega \tag{E3.3.19}$$

Eq. (E3.3.19) shows that the mobile – immobile internal age pdf ψ is the sum of the internal age pdf ψ_m in the mobile region and the internal age pdf ψ_{im} in the immobile region, such that the mobile – immobile reservoir theory may be formalized as follows:

$$\varphi(t) + \tau_0 \frac{\partial \psi(t)}{\partial t} = \delta(t) \tag{E3.3.20}$$

$$\psi(t) = \psi_m(t) + \psi_{im}(t) = \frac{1}{M_0} \int_{\Omega^m} \phi_m C_m^r d\Omega + \frac{1}{M_0} \int_{\Omega^{im}} \phi_{im} C_{im}^r d\Omega \tag{E3.3.21}$$

3.7. Specific 2D horizontal formulations

The general 3D formulations (3.12) and (3.16) can be used for modelling 2D vertical situations. Vertically averaged 2D formulations are very common in practical modelling, but they require particular attention. We consider the common case of a 3D aquifer system partially recharged by an infiltration of intensity Q_I on top and/or bottom of the body. The flux intensity Q_I on top of the 3D aquifer would e.g. represent natural recharge from rain infiltration, while a flux intensity Q_I on the bottom would e.g. represent leakage from lower aquifer horizons. The steady-state vertically averaged flow equation can therefore be expressed by $\nabla \cdot \mathbf{q} = Q_\mathrm{I}$, with the flux vector $\mathbf{q} = -\mathbf{K}B\nabla H$. The aquifer thickness is $B = z_\mathrm{T} - z_\mathrm{B}$ for confined conditions, and $B = H - z_\mathrm{B}$ for unconfined conditions, with z being the vertical coordinate, H is the hydraulic head and $\mathbf{K}$ is the tensor of hydraulic conductivity. To obtain vertically averaged equivalent horizontal formulations from the 3D continuum ADEs (3.12) and (3.16), we make use of the theorems rigorously established by Gray [1982], which enable averaging gradient operators and time derivatives. The averaging concepts used by Gray [1982] are based on the representative elementary volume (REV) averaging ideas of Hassanizadeh & Gray [1979]. The averaging-volume size, shape and orientation, which are taken as constant in space, are assumed to be identical to the cylindrical REV illustrated in Fig. 3.27. The vertical integration of Eqs. (3.12) and (3.16) over a depth B, which may vary in space ($B = B(\mathbf{x})$), can be expressed by

$$\frac{\partial \langle\phi\rangle C_A}{\partial t} = -\nabla \cdot \langle\mathbf{q}\rangle C_A + \nabla \cdot \langle\mathbf{D}\rangle \nabla C_A + B q_{\mathrm{T/B}} \tag{3.58}$$

$$\frac{\partial \langle\phi\rangle C_E}{\partial t} = \nabla \cdot \langle\mathbf{q}\rangle C_E + \nabla \cdot \langle\mathbf{D}\rangle \nabla C_E + B q_{\mathrm{T/B}} \tag{3.59}$$

with the symbols ⟨⟩ indicating that a quantity has been multiplied by the thickness $B(\mathbf{x})$, and the subscript $_{T/B}$ denoting the top or the bottom of the aquifer. The additional exchange term $q_{T/B}$ accounts for the addition or removal of mass at the upper and lower surfaces of the aquifer. In Eqs. (3.58) and (3.59), the term $q_{T/B}$ is defined by

$$q_{T/B} = \frac{1}{B\delta S}\int_{\delta S_{T/B}} [\mathbf{D}\nabla C_A + (\mathbf{w}-\mathbf{q})C_A]\cdot \mathbf{n}_{T/B}\, dS \tag{3.60}$$

$$q_{T/B} = \frac{1}{B\delta S}\int_{\delta S_{T/B}} [\mathbf{D}\nabla C_E + (\mathbf{w}+\mathbf{q})C_E]\cdot \mathbf{n}_{T/B}\, dS \quad , \tag{3.61}$$

The differential $\delta S_{T/B}$ is a projected element of surface at the top or the bottom of the aquifer (see Fig. 3.27), $\mathbf{n}_{T/B}$ is the top or bottom surfaces outward pointing normal unit vector, and $\mathbf{w}$ is the velocity vector of the surface. Since the boundary $S_{T/B}$ is the material surface of the solid body (ground surface or aquifer bottom), one can assume in Eq. (3.60) that the term $(\mathbf{w}-\mathbf{q})\cdot\mathbf{n}_{T/B}$, which defines the normal projection of the apparent velocity $\boldsymbol{\omega} = \mathbf{q} - \mathbf{w}$ of the fluid phase with respect to the solid phase, can be replaced by $-\mathbf{q}\cdot\mathbf{n}_{T/B}$. Consequently, we also have $(\mathbf{w}+\mathbf{q})\cdot\mathbf{n}_{T/B} \approx \mathbf{q}\cdot\mathbf{n}_{T/B}$ in Eq. (3.61). By using the flux definitions in Eqs. (2.16) and (2.18), Eqs. (3.58) and (3.59) simplify in

$$\frac{\partial\langle\phi\rangle C_A}{\partial t} = -\nabla\cdot\langle\mathbf{q}\rangle C_A + \nabla\cdot\langle\mathbf{D}\rangle\nabla C_A - \frac{1}{\delta S}\int_{\delta S_{T/B}} \mathbf{J}_A\cdot\mathbf{n}_{T/B}\, dS \tag{3.62}$$

$$\frac{\partial\langle\phi\rangle C_E}{\partial t} = \nabla\cdot\langle\mathbf{q}\rangle C_E + \nabla\cdot\langle\mathbf{D}\rangle\nabla C_E - \frac{1}{\delta S}\int_{\delta S_{T/B}} \mathbf{J}_E\cdot\mathbf{n}_{T/B}\, dS \tag{3.63}$$

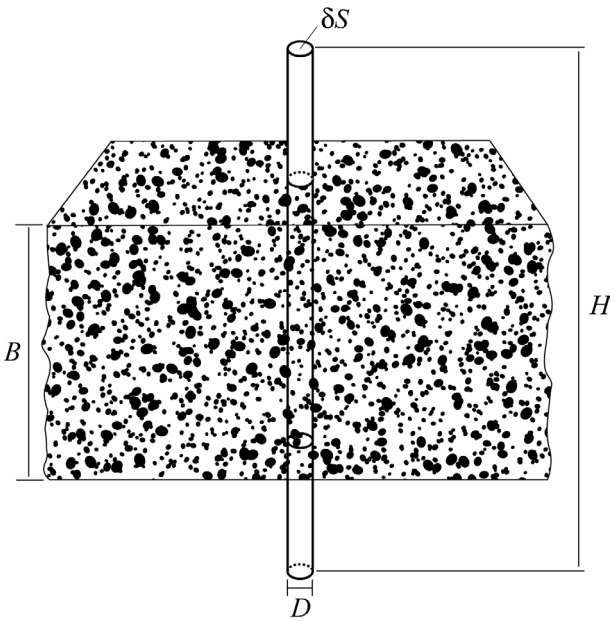

Fig. 3.27. Cylindrical REV of total length H and diameter D, used for the vertical averaging procedure. In the horizontal directions, the REV must satisfy the constraint $l \ll D \ll L$, where l is the characteristic length of a pore diameter and L is a characteristic of the horizontal extend of the aquifer. In the vertical direction, the REV must satisfy the constraint $H > B \gg D$. Adapted from Gray [1982].

From the flux boundary condition at the inlet zones Γ_- in Eq. (3.12), we have $\mathbf{J}_A\cdot\mathbf{n}_{T/B} = \mathbf{q}\cdot\mathbf{n}_{T/B}\,\delta(t)$, with $\mathbf{q}\cdot\mathbf{n}_{T/B}$ being negative. In the backward equation (3.16), we also need the flux continuity $\mathbf{J}_E\cdot\mathbf{n}_{T/B} = -\mathbf{q}\cdot\mathbf{n}_{T/B}\,C_E$ at inlet zones, with $-\mathbf{q}\cdot\mathbf{n}_{T/B}$ being positive. Consequently, the surface integrals in Eqs. (3.62) and (3.63) can be simplified to yield the following 2D divergence form of the forward and backward equations:

$$\frac{\partial \langle \phi \rangle C_A}{\partial t} = -\nabla \cdot \langle \mathbf{q} \rangle C_A + \nabla \cdot \langle \mathbf{D} \rangle \nabla C_A + Q_\mathrm{I} \delta(t) \tag{3.64}$$

$$\frac{\partial \langle \phi \rangle C_E}{\partial t} = \nabla \cdot \langle \mathbf{q} \rangle C_E + \nabla \cdot \langle \mathbf{D} \rangle \nabla C_E - Q_\mathrm{I} C_E \tag{3.65}$$

from which the following equivalent convective forms can be deduced [see Diersch, 2002]:

$$\langle \phi \rangle \frac{\partial C_A}{\partial t} = -\langle \mathbf{q} \rangle \cdot \nabla C_A + \nabla \cdot \langle \mathbf{D} \rangle \nabla C_A + Q_\mathrm{I} (\delta(t) - C_A) \tag{3.66}$$

$$\langle \phi \rangle \frac{\partial C_E}{\partial t} = \langle \mathbf{q} \rangle \cdot \nabla C_E + \nabla \cdot \langle \mathbf{D} \rangle \nabla C_E \tag{3.67}$$

Note that the convective forms of the forward and backward ADEs are not useful in our case, since they cannot handle the third-kind boundary condition. They can be used when the ADEs are associated to the Dirichlet type condition. Eq. (3.65) is consistent with the analysis of Neupauer & Wilson [2001, 2002]. In this backward equation, recharge by areal fluxes is introduced by the first-order decay type term $-Q_\mathrm{I} C_E$, as a consequence of the reversed flow field. Internal sources produce a sink of life expectancy probability, while internal sinks do not appear in the backward model since a fluid sink may not influence the life expectancy pdf. The assumption of divergence-free flow field used until this section can finally be omitted, and source/sink terms can be accounted for in the forward and backward ADEs.

From the age and life expectancy fields C_A and C_E obtained by solving the ADEs (3.64) and (3.65), the general RT formulation (3.21) can be applied to evaluate the outlet transit time pdf and the inlet life expectancy pdf φ. Note the important fact that the probability sink term $-Q_\mathrm{I} C_E$ in the backward equation (3.65) does not induce an additional term in the RT formulation (3.21), since it is included in the inlet life expectancy pdf φ, so that one can write:

$$F_0 \varphi(t) = \int_{\Gamma_-} \mathbf{J}_E(\mathbf{x},t) \cdot \mathbf{n} \, d\Gamma + \int_\Omega Q_\mathrm{I}(\mathbf{x}) C_E(\mathbf{x},t) \, d\Omega \tag{3.68}$$

For the 2D horizontal aquifer configuration, the FRT and the BRT can still be expressed by

$$\varphi(t) + \tau_0 \frac{\partial \psi(t)}{\partial t} = \delta(t) \tag{3.69}$$

The equivalence between the forward and backward ADEs (3.64) and (3.65) for the application of the RT is illustrated in Fig. 3.28, which gives the results for the case of a perfectly mixed reservoir, represented in the (x, y)-plane (see Fig 3.28a). For such a hydraulic configuration, when lateral dispersion is negligible the transit time pdf φ and the internal age pdf ψ both equal the exponential model (see Eq. (3.34) and Fig. 3.28b, c and d). When perfect mixing is assumed, which excludes the possibility of lateral exchanges of water particles between the flow lines, then at each position in the reservoir the age pdf is the same exponential function, $C_A(x, y, t) = \varphi(t)$ (see Fig. 3.28b), as shown in section 3.2.3, and the probability of having an age t or less at any position x is $\int_t \varphi(t) \, dt = 1 - \exp(-t/\tau_0)$. For any position in the reservoir each water particle will reach the exit zone an equal number of times per unit time, or, in other words, all water particles have a constant probability of being removed per unit time. The water particles life expectancy $C_E(x, y, t)$ shows a different behaviour, since the probability for a water particle of having infiltrated at x differs from the probability of having infiltrated at $x + dx$ (see Fig. 3.28b), as stated by the decay-type term $-Q_\mathrm{I} C_E$ in the backward model (3.65). Theoretically, the life expectancy varies in space from zero, downstream, to infinity, upstream (zero velocities). Consequently, the total transit time pdf

$C_T(x, y, t)$ as defined by Eq. (2.11) differs from one place to another, and the internal total transit time pdf ψ_T shows an increasing part from the zero total transit time probability (infiltration at $x = 0$, age zero) to the maximum total transit time probability ($t = \tau_0$), followed by a decreasing part until the maximum age (Fig. 3.28e). According to Eq. (3.28), the average internal total transit time is $\tau_{it} = 2\tau_t = 2\tau_i$, and from Eqs. (3.29) and (3.32), one can deduce the standard deviation of φ or ψ, $\sigma^2 = (\tau_0)^2$, and of ψ_T, $\sigma^2 = 2(\tau_0)^2$.

This simple example provides a good demonstration of the validity of Eqs. (3.64) and (3.65), but also of the equivalence between the FRT and BRT formulations.

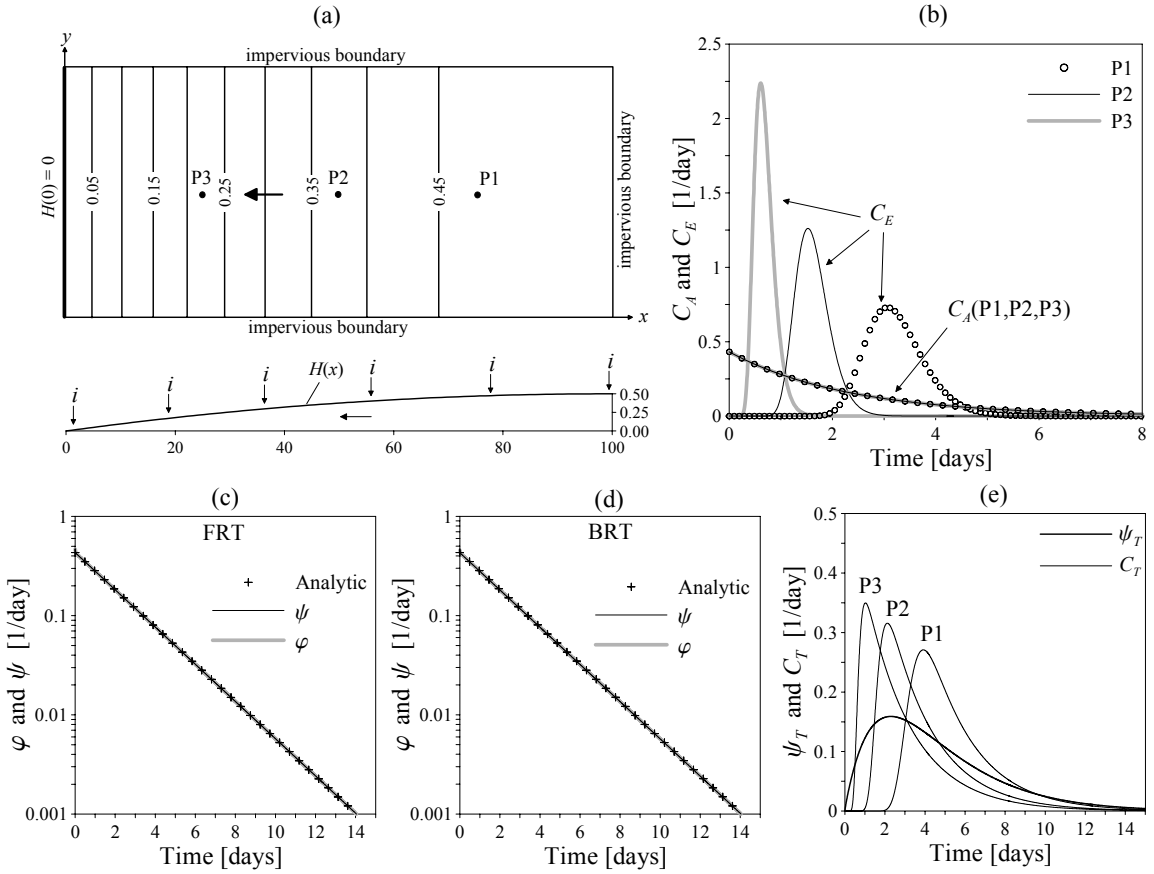

Fig. 3.28. Perfectly mixed reservoir: (a) Plan and vertical views with heads distribution, with indicated locations of the observation points P1, P2, and P3; (b) Numerical solutions of the age and life expectancy pdfs at the observations points; (c) and (d) Numerical solutions of the FRT and BRT compared to the exponential model; (e) Numerical solutions of ψ_T and C_T at the observation points. The model size is 100×50m, the infiltration rate is $i = 1.0\times10^{-6}$ m/s, transmissivity is $T = 1.0\times10^{-2}$ m^2/s, porosity is $\phi = 0.2$, longitudinal dispersivity is $\alpha_L = \Delta\mathbf{x}/5 = 0.1$m ($\alpha_T = D_m = 0$), $M_0 = 1000$m^3, $F_0 = 432$m^3/day, $\tau_0 = 2.315$days.

3.8. Summary

In this Chapter the results of Eriksson [1961, 1971] have been recovered by manipulating the advection-dispersion equation, thus extending the reservoir theory to systems with significant dispersive components. The outlet transit time distribution is derived from the internal age distribution, and has therefore a far more refined resolution. In so doing, mixing of converging flow patterns near the outlet is ignored, and the maximum transit time is never smaller than the maximum age in the reservoir. The RT formulation also applies to the internal distribution of life expectancy, and can be used to evaluate recharge zones life expectancy pdfs. To derive the RT, the integration of the age or life expectancy occurrence in the aquifer must be performed. Consequently, the third-

kind boundary condition is the right condition for age and life expectancy transport that ensures a correct solute mass balance. From the reservoir characteristic distributions, fundamental additional transient information on water volumes and water fluxes can be gained. From the outlet transit time cdf, specific groundwater porous volumes can directly be identified and quantified with respect to age, life expectancy and transit time. These functions can be very useful for aquifer characterization and intrinsic vulnerability assessments. They can be used to easily evaluate the magnitudes of young and old groundwater volumes in the aquifer.

Using analytical and numerical solutions for theoretical aquifer configurations, some effects of macro-dispersion on simulated age and transit time distributions could be underlined. For instance, longitudinal dispersion has a significant aging effect, while lateral dispersion rejuvenates the system. As in previous studies, it has been shown that the average age resulting from dating-methods or direct simulations, can lead to erroneous interpretations. It is a well-known fact that dispersion can induce a high variability of the age distribution around the average. Here we have shown that not only mixing processes could make the average age meaningless, but also the geological structure and the geometry of the flow patterns.

The proposed methodology can equivalently be implemented in one-, two-, and three-dimensions, and presents considerable technical and numerical advantages, which may be pivotal in handling very large natural systems. In fact, when the outlet transit time pdf is defined by integrating all hydro-dispersive properties over the entire flow field, the level of refinement required by a stable transport model is generally sufficient. The RT ensures that the minimum and the maximum ages in the reservoir are captured at the outlet, which is hardly ever the case with traditional methods, mainly due to the numerical mixing of converging fluxes in the vicinity of the outlet.

In practical transport modelling, the horizontal formulation of the advection-dispersion equation is very often used. To adapt the reservoir theory to more specific horizontal configurations, the forward and backward ADEs have been vertically averaged. We found that, when flow is not divergence free, a sink of probability appears in the backward model with the form of a first-order decay term, as consequence of the reversed velocity in the backward equation.

In this preliminary approach of the RT, the presented models have been developed for the global aquifer system, with respect to the inlet and outlet zones only. At this stage, the applicability of the RT is restricted to systems with single outlet and inlet zones. In the following Chapter, we generalize the RT to any observation zone and sub-system, and to systems with multiple inlets and outlets.

References

[1] Bear J. and Verruitj A. Modeling Groundwater Flow and Pollution. Kluwer Academic Publ.; 1987.

[2] Bethke C.M. and Johnson T.M. Paradox of groundwater age: Correction. *Geology* 2002a;30(4):385–388.

[3] Bethke C.M. and Johnson T.M. Groundwater age. *Ground Water* 2002b;40(4):337–339.

[4] Bolin B. and Rodhe H. A note on the concept of age distribution and transit time in natural reservoirs. *Tellus* XXV 1973;1:58–62.

[5] Cornaton F. and Perrochet P. Analytical 1D dual-porosity equivalent solutions to 3D discrete single-continuum models. Application to karstic spring hydrograph modelling. *J Hydrol* 2002;262:165–176.

[6] Danckwerts P.V. Continuous flow systems: distribution of residence times. *Chem Eng Sci* 1953;2(1):93–102.

[7] Danckwerts P.V. The effect of incomplete mixing on homogeneous reactions. *Chem Eng Sci* 1958;8:93–102.

[8] De Smedt F. and Wierenga P.J. A Generalized Solution for Solute Flow in Soils With Mobile and Immobile Water. *Water Resour Res* 1979;15(5):1137–1141.

[9] Diersch H.-J. About the difference between the convective form and the divergence form of the transport equation. FEFLOW Software White Papers Vol. 1, 2002, WASY GmbH Berlin, 119–129.

[10] Eriksson E. The possible use of Tritium for estimating groundwater storage. *Tellus* 1958;10:472–478.

[11] Eriksson E. and Welander P. On a mathematical model of the carbon cycle in nature. *Tellus* 1956;8:115–175.

[12] Eriksson E. Natural reservoirs and their characteristics. *Geofisica International* 1961;1(2):27–43.

[13] Eriksson E. Compartment models and reservoir theory. *Annual Review of Ecology and Systematics* 1971;2:67–84.
[14] Etcheverry D. and Perrochet P. Reservoir theory, groundwater transit time distributions and lumped parameter models. IAEA-SM-361/44, Vienna;1999.
[15] Etcheverry D. and Perrochet P. Direct simulation of groundwater transit time distributions using the reservoir theory. *Hydrogeology Journal* 2000;8:200–208.
[16] Etcheverry D. Une approche déterministe des distributions des temps de transit de l'eau souterraine par la théorie des réservoirs. Ph.D. Thesis, Centre of Hydrogeology, University of Neuchâtel, 2001, 118 pp.
[17] Flynn R., Cornaton F., Hunkeler D. and Rossi P. Virus Transport in a Fining-Upwards Sedimentary Sequence: Laboratory Experiments and Simulation. *Submitted (June 2003) to J. of Cont. Hydrology*.
[18] Flynn R. Virus transport and attenuation in perialpine gravel aquifers. Ph.D. Thesis, Centre of Hydrogeology, University of Neuchâtel, 2003.
[19] Goode D.J. Direct simulation of groundwater age. *Water Resour Res* 1996;32:289–296.
[20] Goode D.J. Ground-water age and atmospheric tracers: Simulation studies and analysis of field data from the Mirror Lake site, New Hampshire. Ph.D. thesis, Princeton University, Department of Civil Engineering and Operations Research, 1998, 194 pp.
[21] Hassanizadeh M. and Gray W.G. General conservation equations for multiphase systems, 1, Averaging procedure. *Advan Water Resour* 1979;2:131–144.
[22] Jury W.A. Simulation of Solute transport Using a Transfer Function Model. *Water Resour Res* 1982;18(2):363–368.
[23] Jury W.A., Sposito G. and White R.E. A Transfer Function Model of Solute Transport through Soil, 1, Fundamental Concepts. *Water Resour Res* 1986;22(2):243–247.
[24] Jury W.A. and Roth K. Transfer Functions and Solute Movement Through Soil: Theory and Applications. Birkhauser Boston, Cambridge, Mass, 289 pp.; 1990.
[25] Kreft A. and Zuber A. On the physical meaning of the dispersion equation and its solutions for different initial and boundary conditions. *Chem Eng Sci* 1978;33:1471–1480.
[26] Kreft A. and Zuber A. Comments on "Flux-Averaged and Volume-Averaged Concentrations in Continuum Approaches to Solute Transport" by J. C. Parker and M. Th. van Genuchten. *Water Resour Res* 1986;22(7):1157–1158.
[27] Luther K.H. and Haitjema H.M. Numerical experiments on the residence time distributions of heterogeneous groundwatersheds. *J Hydrol* 1998;207:1–17.
[28] Maloszewski P. and Zuber A. Influence of matrix diffusion and exchange reactions on radiocarbon ages in fissured carbonate aquifers. *Water Resour Res* 1991;27:1937–1945.
[29] Nauman E.B. and Buffham B.A. Mixing in Continuous Flow Systems. John Wiley, New York, 1983.
[30] Neumann S.P., Winter C.L. and Newman C.M. Stochastic theory of field-scale Fickian dispersion in anisotropic porous media. *Water Resour Res* 1987;23:453–466.
[31] Neupauer R. and Wilson J.L. Adjoint method for obtaining backward-in-time location and travel time probabilities of a conservative groundwater contaminant. *Water Resour Res* 1999;35(11):3389–3398.
[32] Neupauer R. and Wilson J.L. Adjoint-derived location and travel time probabilities for a multidimensional groundwater system. *Water Resour Res* 2001;37(6):1657–1668.
[33] Parker J.C. and van Genuchten M. Th. Flux-averaged and volume-averaged concentrations in continuum approaches to solute transport. *Water Resour Res* 1984;20(7):866–872.
[34] Parker J.C. and van Genuchten M. Th. Reply. *Water Resour Res* 1986;22(7):1159–1160.
[35] Schnegg P. and Doerfliger N. An inexpensive flow-through field fluorometer. *Proceedings of the 6th 'Colloque d'hydrologie en pays calcaire et milieu fissuré'*, Chaux-de-Fonds, August, 1997.
[36] Sposito G., White R.E., Darrah P.R, Jury W.A. A Transfer Function Model of Solute Transport Through Soil 3. The Convection-Dispersion Equation. *Water Resour Res* 1986;22(2):255–262.
[37] Sposito G. and Barry D.A. On the Dagan model of solute transport in groundwater: Foundational aspects. *Water Resour Res* 1987;23(10):1867–1875.
[38] Sudicky E.A. The Laplace transform Galerkin technique: A time-continuous finite element theory and application to mass transport in groundwater. *Water Resour Res* 1989;25(8):1833–1846.
[39] Varni M. and Carrera J. Simulation of groundwater age distributions. *Water Resour Res* 1998;34(12):3271–3281.
[40] Weissmann G. S., Zhang Y., LaBolle E. and Fogg G.E. Dispersion of groundwater age in an alluvial aquifer system. *Water Resour Res* 2002;38(10):doi:10.1029/2001WR000907.
[41] White R.E., Dyson J.S., Haigh R.H., Jury W.A., Sposito G. A Transfer Function Model of Solute Transport Through Soil 2. Illustrative applications. *Water Resour Res* 1986;22(2):248–254.
[42] Zwietering T.N. The degree of mixing in continuous flow systems. *Chem Eng Sci* 1953;11:1–15.

CHAPTER 4

Reservoir Theory for aquifers of arbitrary configuration: From water molecule age transport to contaminant transport

Abstract

In this Chapter, we extend the RT to arbitrary aquifer configurations by treating groundwater flow systems as compartments which transfer the water fluxes from recharge zones to a particular discharge zone, and inside and between which mixing and dispersion processes can take place. In this way, we make the RT applicable to any sub-drainage system of an aquifer of arbitrary complexity and configuration. The backward transport of the life expectancy pdf is then combined with the forward transport of a contaminant, in order to predict, with one single realization of the life expectancy field, the concentration breakthrough curve at an outlet, which would result from the transport of unit and instantaneous mass release at any upstream point. The usefulness of the method is illustrated with two-dimensional synthetic examples, which particularly address the well-head vulnerability and protection problem, as well as the problem of underground storage of high-level nuclear waste.

4.1. Groundwater flow systems and outlet drainage basins

The fundamental concept of groundwater flow systems originates from the works of Hubbert [1940] and Tóth [1962, 1963]. The groundwater flow systems are separated into different categories, mainly in relation to their spatial extend. The regional flow systems extend both from regionally and topographically elevated areas to lower regions, and beneath overlying local shallower watersheds within which smaller flow systems can further be distinguished. Regional flow systems are important in areas where the topographic gradients are significant, where recharge is limited, or where the rock basement has still a good permeability. Most of the time, the deep regional flow systems do not interact with surface waters. Since the water particles in these deep flow systems follow long travel paths, involving long contact time with geological materials, dissolved chemicals are more abundant in groundwater.

The local flow systems are generally shallow, and the recharge waters often rapidly reach the downstream discharge zones. In such flow systems, the interactions with the surface waters can prevail. These systems are often underlain by intermediate and regional flow systems. An outlet drainage basin can cover local and intermediate flow systems, but also regional flow systems. The discharge of the outlet is then possibly constituted of groundwater particles which have experienced various travel histories, from the restricted movement within the local flow system, to the long circulations within the regional flow system.

Following the concepts of Tóth [1962, 1963], Kiraly [1978] defined the flow system as a fundamental hydrogeological unit. According to Kiraly [1978], the hydrogeological unit can be compared to an equivalence class spatially connected (continuous) in the field of a dependent variable that characterizes the quality, the quantity, or the movement of groundwater. To characterize this hydrogeological unit, the equivalence class in the field of the flow parameters, and the equivalence class in the field of the boundary conditions, must be properly defined. In the definition of Tóth, the flow system is defined as a set of flow lines for which any two adjacent flow lines at any point of the flow region remain adjacent throughout the whole domain. The

hydrogeological flow system thus corresponds to an equivalence class in the set of the flow lines. This concept is fundamental, and has provided many insights in hydrogeology. However, it corresponds to a purely advective vision of the dynamics of groundwater flow. Since dispersion can move water particles laterally from a flow line towards another, the jump from a flow system to an other is more than possible. An advective-dispersive vision of a drainage basin is more appropriate to characterize the processes of groundwater movement towards an outlet. In the sense of Kiraly's equivalence classes, one can also define an equivalence class in the field of the advective and dispersive-diffusive parameters.

An outlet drainage basin, or capture zone, can be assimilated to the domain in space within which water particles have some chances to be absorbed by the outlet. This domain can penetrate through different flow units. The backward probability approach represents an interesting alternative to the pure advective definition of outlet drainage basins. Backward ADEs have already been used for delineating pumping well capture zones [see e.g. Uffink, 1989; Wilson & Liu, 1997; Neupauer & Wilson, 1999; 2001]. Generally, a capture zone is defined in terms of probability of absorption of the water particles by a given outlet. In this Chapter, we will also make use of the backward transport modelling approach to delineate probabilistic drainage basins, for which the RT is developed to characterize the outlet transit time pdf, as well as the internal distribution of age within the probabilistic drainage basin.

4.2. Reservoir theory in aquifers of arbitrary complexity

In Chapter 3, the reservoir theory was applied to open reservoirs with single recharge and discharge zones. In this Chapter, we show how complex reservoirs of arbitrary configuration, and with various flow systems in connection with several distinct outlets and inlets, can be characterized with the RT approach by treating each sub-system as a compartment model. In a first step the applicability of the RT for aquifer sub-drainage systems is theoretically demonstrated. In a second step, an appropriate backward boundary value problem is defined in order to derive the RT for a given outlet drainage basin, and this aquifer specific sub-system, or flow unit, is characterized in terms of probability for the water particles to reach the outlet.

4.2.1. Reservoir theory for compartmented aquifer systems

For a sub-divided reservoir with several internal flow units, the transit time pdf φ is related to all the discharge (FRT) or recharge (BRT) areas of the aquifer. In the following, we demonstrate that the global distributions φ and ψ can be regarded as a flux- and porous volume-weighted linear combination of the intrinsic distributions of each sub-drainage basin and associated outlet. Consider the example of a reservoir Ω with n discharge areas, and let $p_n(\mathbf{x}, t)$ be the field of probability that a water particle located at the position $\mathbf{x}$ have a life expectancy t or less before being absorbed by the outlet n. The field p_n corresponds to the life-expectancy-to-outlet cdf, $p_n(\mathbf{x}, t) = G_E(\mathbf{x}, t)$. The cumulative mass of age t or less in the sub-system Ω_n is the cdf m_n of the internal age pdf ψ_n, scaled by the corresponding porous volume $M_{0,n}$, $M_n(t) = M_{0,n}\, m_n(t)$. The function M_n, or m_n, can be calculated if the field $p_n(\mathbf{x}, t)$ for the outlet n is known [see Chapter 3]:

$$M_n(t) = M_{0,n}\, m_n(t) = \int_\Omega \phi\, p_n(\mathbf{x},t)\, d\Omega = \int_\Omega \phi \left(\int_0^t C_E(\mathbf{x},\tau)\, d\tau \right) d\Omega \tag{4.1}$$

with $M_{0,n}$ being the total porous volume of the sub-system Ω_n, and with $\phi = \phi(\mathbf{x})$. According to Eqs. (3.5) and (3.20), we can write for $t > 0$ the RT formulation for the sub-system Ω_n:

$$\psi_n(t) = \frac{\partial m_n(t)}{\partial t} = \frac{1}{M_{0,n}} \frac{\partial M_n(t)}{\partial t} \tag{4.2}$$

$$\varphi_n(t) = -\tau_{0,n} \frac{\partial \psi_n(t)}{\partial t} = -\frac{1}{F_{0,n}} \frac{\partial^2 M_n(t)}{\partial t^2} \tag{4.3}$$

where $F_{0,n}$ and $\tau_{0,n} = M_{0,n}/F_{0,n}$ stand for the steady flow rate and the turnover time of sub-system Ω_n, respectively. Since the cumulated mass of age t or less in the reservoir Ω is simply

$$M(t) = \sum_n M_n(t) \tag{4.4}$$

taking the first and second derivatives of Eq. (4.4) and using Eqs. (4.2) and (4.3) yields

$$\frac{\partial M(t)}{\partial t} = \sum_n \frac{\partial M_n(t)}{\partial t} = \sum_n M_{0,n} \psi_n(t) \tag{4.5}$$

$$\frac{\partial^2 M(t)}{\partial t^2} = \sum_n \frac{\partial^2 M_n(t)}{\partial t^2} = -\sum_n F_{0,n} \varphi_n(t) \tag{4.6}$$

Inserting Eqs. (4.5) and (4.6) into the general RT formulation (3.1), given that $M_0 = \sum M_{0,n}$ and $F_0 = \sum F_{0,n}$, is thus:

$$\psi(t) = \frac{\sum_n M_{0,n} \psi_n(t)}{\sum_n M_{0,n}} = \frac{1}{M_0} \sum_n M_{0,n} \psi_n(t) \tag{4.7}$$

$$\varphi(t) = \frac{\sum_n F_{0,n} \varphi_n(t)}{\sum_n F_{0,n}} = \frac{1}{F_0} \sum_n F_{0,n} \varphi_n(t) \tag{4.8}$$

Eqs. (4.7) and (4.8) show that the pdfs calculated with the RT applied to the entire aquifer correspond to the superposition of each pdf calculated with the RT applied to each sub-system of the reservoir. The internal residence time distribution of the entire flow domain corresponds to porous volume-weighted mean of each internal residence time distribution of each sub-drainage basin, and the transit time distribution of the union of all outlets corresponds to flow rate-weighted mean of each outlet transit time distribution. A direct consequence of Eqs. (4.7) and (4.8) is that the global reservoir turnover time is $\tau_0 = (\sum F_{0,n}\tau_{0,n})/F_0$ and the global reservoir internal age is $\tau_i = (\sum M_{0,n}\tau_{i,n})/M_0$. Eqs. (3.10) and (3.22) can be used to define the transit time cdf $f(t)$ as a function of the linear combination of each φ_n or each ψ_n. Furthermore, the internal groundwater volume functions defined Chapter 3.2.4 can also be characterized for each sub-system Ω_n.

A drainage basin is considered here as a compartment within which the input amounts of age mass are transferred to its outlet. The compartment, therefore, is defined with respect to one of the global reservoir outlets, since the rate of mass transfer out of the compartment depends on the different possible paths of water particles within the compartment. It may be assimilated to an internal flow unit that connects a set of recharge zones to a specific discharge zone, and inside which the water particles motion is ruled by advection and dispersion processes. The limits of this compartment inside Ω are not clearly defined, unlike in Eriksson [1971], but they rather enclose a specific property. This property is chosen as the occurrence of water particles with respect to the time they need to reach the outlet, sooner or later, so that the compartment corresponds to a field of probability of exit. This field of probability can include dispersion-induced mixing processes, within the compartment and between compartments, which means that two different compartments can share their mass, as illustrated in Fig. 4.1.

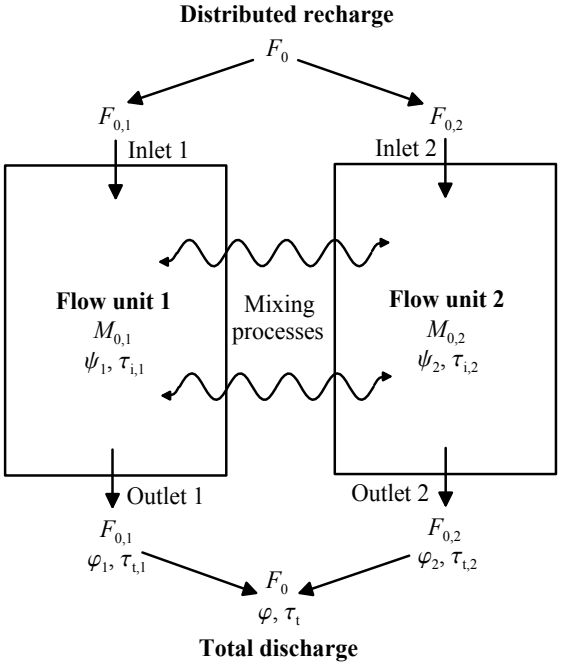

Fig. 4.1. Schematic illustration of a two-compartments reservoir.

Due to the fact that the exit probability field can be considered as time-dependent, the drainage basin characterizes a transport domain within which the transported property gives the fractions of water particles that will contribute to the compartment outflow rate. The uncertainty in the position of the groundwater particles is characterized by a general spreading of the location probability. This spreading itself depends on dispersion, and therefore two compartments (or transport domains) corresponding to two distinct outlet zones can exchange their amounts of age mass. This exchange is considered within the field $p_n(\mathbf{x}, t) = G_E(\mathbf{x}, t)$. In the sense of Kiraly's definition of a flow system as an equivalent class, as above-mentioned, the outlet drainage basin is defined here as an equivalence class in the field of probability of absorption at outlet, for which and equivalence class in the field of velocity and dispersion tensor can also be defined.

4.2.2. Reservoir theory for sub-drainage basins

The functions φ_n and ψ_n in Eqs. (4.7) and (4.8) characterize a sub-system Ω_n of the global reservoir Ω, corresponding to the drainage basin of a given natural or artificial outlet symbolized by Γ_n. To evaluate these two pdfs, we consider the backward ADE (3.16) with the additional sink of life expectancy related to a potential fluid source Q_I in the flow equation ($\nabla \cdot \mathbf{q} = Q_\mathrm{I}$), and adapt the boundary conditions in such a way that the dependent variable characterizes the density of probability that the water particles will exit the system at Γ_n, exclusively. This pdf can be calculated as a solution of the following boundary value problem:

$$\begin{aligned}
&\frac{\partial \phi C_E}{\partial t} = \nabla \cdot \mathbf{q} C_E + \nabla \cdot \mathbf{D} \nabla C_E - Q_\mathrm{I} C_E && \text{in} && \Omega \\
&\mathbf{J}_E(\mathbf{x}, t) \cdot \mathbf{n} = -\mathbf{q} \cdot \mathbf{n} \delta(t) && \text{on} && \Gamma_n \\
&\mathbf{J}_E(\mathbf{x}, t) \cdot \mathbf{n} = 0 && \text{on} && \Gamma_+ \\
&\textit{Implicit Neumann condition} && \text{on} && \Gamma_- \\
&\mathbf{D} \nabla C_E \cdot \mathbf{n} = 0 && \text{on} && \Gamma_0
\end{aligned} \tag{4.9}$$

The Cauchy type conditions on Γ_n and Γ_+ ensure that the calculated life-expectancy-to-outlet solution $C_E(\mathbf{x}, t)$ gives the intensity of probability that the water particles situated at the position $\mathbf{x}$ will be absorbed by Γ_n at time t. On any other outlet boundary Γ_+, this intensity of flux probability of exit is fixed to zero. Note that the sink term $-Q_I C_E$ has a real physical meaning for two-dimensional horizontal configurations (cf. Section 3.7).

Now let ψ_n be the internal life expectancy pdf of the sub-system Ω_n:

$$\psi_n(t) = \frac{1}{M_{0,n}} \int_\Omega \phi\, C_E(\mathbf{x},t)\, d\Omega \tag{4.10}$$

with $M_{0,n}$ the sub-system Ω_n porous volume. The transit time pdf φ_n of the outlet Γ_n can be obtained by evaluating the inlet life expectancy pdf [see section 3.2.2 in Chapter 3]:

$$\varphi_n(t) = \frac{1}{F_{0,n}} \int_{\Gamma_n} \mathbf{J}_A(\mathbf{x},t)\cdot\mathbf{n}\, d\Gamma = \frac{1}{F_{0,-}} \int_{\Gamma_-} \mathbf{J}_E(\mathbf{x},t)\cdot\mathbf{n}\, d\Gamma \tag{4.11}$$

where $F_{0,-}$ is the sum of the inflow rates on the inlet limits Γ_- that contribute to the outflow $F_{0,n}$ through Γ_n. The derivation of the BRT from Eq. (4.9) yields

$$\varphi_n(t) + \tau_{0,n} \frac{\partial \psi_n(t)}{\partial t} = \delta(t) \tag{4.12}$$

with the observation zone drainage basin turnover time $\tau_{0,n} = M_{0,n}/F_{0,n}$. The transit time cdf f_n of the outlet Γ_n is defined by the integral of φ_n:

$$f_n(t) = \int_0^t \varphi_n(\tau) d\tau = 1 - \tau_{0,n}\, \psi_n(t) \tag{4.13}$$

With the boundary conditions associated to Eq. (4.9), the outlet Γ_n of a reservoir sub-system is identified with a maximum probability flux of exit for the water particles that pertain to its drainage basin, while a zero probability of exit is assigned on every other outlet. For the flow unit corresponding to the outlet Γ_n, the life expectancy occurrence is given by ψ_n, and its outflow is decomposed with respect to the arrival time using the RT formulation (4.13).

The porous volume in Eq. (4.10) can be evaluated by integrating over all time values:

$$M_{0,n} = \frac{\int_0^\infty \int_\Omega \phi\, C_E(\mathbf{x},t)\, d\Omega\, dt}{\int_0^\infty \psi_n(t) dt} = \int_\Omega \phi \int_0^\infty C_E(\mathbf{x},t) dt\, d\Omega = \int_\Omega \phi\, p_n^\infty(\mathbf{x})\, d\Omega \tag{4.14}$$

where $p_n^\infty(\mathbf{x}) = p_n(\mathbf{x},\infty)$ is the asymptotic limit of the life-expectancy-to-outlet cdf. Because in both 2D and 3D domains there is a non-zero probability that the water particles will *not* be intercepted by the outlet Γ_n (the only location where this probability is zero), then $p_n^\infty(\mathbf{x})$ in Eq. (4.14) is less than one, $\int_t C_E(\mathbf{x},t)dt < 1$ for any $\mathbf{x}$. It follows that the quantity $1 - \int_t C_E(\mathbf{x},t)dt$ corresponds to the probability that the water particles located at the position $\mathbf{x}$ will not reach Γ_n.

4.2.3. Sub-drainage basin characterization and outlet cumulated outflow distribution of transit times

The internal life-expectancy-to-outlet distribution function ψ_n is found by integrating each breakthrough curve $C_E(\mathbf{x}, t)$ over the entire aquifer Ω. This pdf characterizes the internal organization of life expectancy within the specific sub-domain Ω_n that is drained by the outlet Γ_n. This is implicitly done with Eq. (4.11) since zero probabilities to reach Γ_n are present in the aquifer, and the outlet transit time pdf φ_n can be evaluated without the knowledge of the porous volume $M_{0,n}$, by calculating the function $M_{0,n}\psi_n$. But if one needs to evaluate $M_{0,n}$, the field $p_n^\infty(\mathbf{x})$ must be known. The probability P_n that water particles exit through the boundary portion $\delta\Gamma_n$ prior to time t is related to the time integral of the probability flux [Gardiner, 1983]:

$$P_n(\mathbf{x}_n, t)\left|\delta\Gamma_n\right| = \int_0^t \left[\mathbf{J}(\mathbf{x}_n, \tau \mid \mathbf{x}, 0)\cdot \delta\Gamma_n\right] d\tau \tag{4.15}$$

where the probability flux $\mathbf{J}$ on an element $\mathbf{x}_n$ of $\delta\Gamma_n$ is conditional on the initial state $(\mathbf{x},0)$ in Ω. The total probability Π_n of exit through Γ_n is:

$$\Pi_n(t) = \int_{\Gamma_n} \left(\int_0^t \mathbf{J}(\mathbf{x}_n, \tau \mid \mathbf{x}, 0)\cdot \mathbf{n}\, d\tau \right) d\Gamma_n \tag{4.16}$$

Following Gardiner [1983], P_n also obeys the adjoint backward equation. Accordingly, we can formulate the following boundary value problem for the life-expectancy-to-outlet cdf $p_n(\mathbf{x}, t)$:

$$\begin{array}{lll}
\dfrac{\partial \phi p_n}{\partial t} = \nabla\cdot\mathbf{q}\, p_n + \nabla\cdot\mathbf{D}\nabla p_n - Q_1 p_n & \text{in} & \Omega \\
[\mathbf{q}\, p_n(\mathbf{x},t) + \mathbf{D}\nabla p_n(\mathbf{x},t)]\cdot\mathbf{n} = \mathbf{q}\cdot\mathbf{n} & \text{on} & \Gamma_n \\
[\mathbf{q}\, p_n(\mathbf{x},t) + \mathbf{D}\nabla p_n(\mathbf{x},t)]\cdot\mathbf{n} = 0 & \text{on} & \Gamma_+ \\
\textit{Implicit Neumann condition} & \text{on} & \Gamma_- \\
\mathbf{D}\nabla p_n(\mathbf{x},t)\cdot\mathbf{n} = 0 & \text{on} & \Gamma_0
\end{array} \tag{4.17}$$

The boundary conditions in (4.17) ensure a maximum flux probability of exit at Γ_n (with $p_n = 1$ on the right-hand side of the Cauchy condition formulation on Γ_n), and a minimum flux probability of exit at each other outlet Γ_+. Since the flow velocity $\mathbf{q}$ and the dispersion tensor $\mathbf{D}$ are assumed to be independent of time, the function $p_n(\mathbf{x}, t)$ approaches a limit at infinity. For the ultimate probability of exit $p_n^\infty(\mathbf{x})$, one has to make the temporal derivative in Eq. (4.17) vanish. The total flux boundary condition in Eq. (4.17) ensures that the probability $P_n|\delta\Gamma_n|$ of exit through Γ_n is certain. The function $p_n(\mathbf{x}, t)$ can also be assimilated to the fraction of the water particles situated at the position $\mathbf{x}$ that will reach Γ_n before time t, and consequently $p_n^\infty(\mathbf{x})$ represents the fraction of the water particles that will reach Γ_n sooner or later. With Eq. (4.17), we have defined the drainage basin corresponding to the outlet Γ_n, or the probabilistic capture zone $p_n(\mathbf{x}, t_r)$ relative to a particular transit time t_r. The ultimate, or steady-state drainage basin is the field p_n^∞.

Integrating Eq. (4.17) and applying the divergence theorem ($\int_\Omega \nabla\cdot\mathbf{u}\, d\Omega = \int_\Gamma \mathbf{u}\cdot\mathbf{n}\, d\Gamma$) yields

$$F_{0,n} - M_{0,n}\psi_n(t) = -\sum_k \int_{\Gamma_-^k} [\mathbf{q}\, p_n(\mathbf{x},t) + \mathbf{D}\nabla p_n(\mathbf{x},t)]\cdot\mathbf{n}\, d\Gamma^k + \int_\Omega Q_1(\mathbf{x}) p_n(\mathbf{x},t)\, d\Omega \tag{4.18a}$$

The left-hand side of Eq. (4.18a) corresponds to the integral formulation of the RT, as given in Eq. (4.13), if Eq. (4.13) is scaled by the outlet steady discharge rate $F_{0,n}$. Consequently, one can substitute Eq. (4.13) into Eq. (4.18a) to obtain

$$F_n(t) = -\sum_k \int_{\Gamma_-^k} [\mathbf{q}\, p_n(\mathbf{x},t) + \mathbf{D}\nabla p_n(\mathbf{x},t)] \cdot \mathbf{n}\, d\Gamma^k + \int_\Omega Q_I(\mathbf{x}) p_n(\mathbf{x},t)\, d\Omega \tag{4.18b}$$

With Eq. (4.18b) one can decompose the cumulated outflow distribution of the arrival times at Γ_n into distinct flow rate fractions of various origins of infiltration. The surface/line boundary portions Γ_-^k account for distinct natural (areal recharge fluxes, rivers, lakes, etc) and/or artificial (injection wells, irrigation and infiltration areas, etc) inflowing limits, and the domain integral term evaluates the outlet flow rate fraction from internal or areal sources. Since each flow rate fraction is represented by an independent space integral, Eq. (4.18) provides a powerful quantitative means for separating the different fractions of the flow rate of a particular outlet, with respect to their different origins, for a given arrival time t at Γ_n. For example, the first term on the right-hand side of (4.18b) is the fraction of the outlet flow rate which originates from infiltrations by the limits, and which transits to the outlet at a time t or less.

If we consider the particular case of the vertically averaged aquifer with natural recharge of intensity Q_I, with inlet limit Γ_-, and with $\Gamma_n = \Gamma_w$ being an extraction well (see Fig. 4.2), one can decompose the well steady-state discharge rate $F_{0,w}$ by taking the limit of (4.18) at infinity ($F_n(\infty) = F_{0,n}$ and $\psi_n(\infty) = 0$):

$$F_{0,w} = F_{\text{limits}} + F_{\text{pluvial}} = -\int_{\Gamma_-} [\mathbf{q}\, p_w^\infty(\mathbf{x}) + \mathbf{D}\nabla p_w^\infty(\mathbf{x})] \cdot \mathbf{n}\, d\Gamma + \int_\Omega Q_I(\mathbf{x}) p_w^\infty(\mathbf{x})\, d\Omega \tag{4.19}$$

Eq. (4.19) provides an accurate way of separating the exclusive pluvial origin of the extracted groundwater at a pumping-well, from any other kind of infiltrated waters, as illustrated in Fig. 4.2.

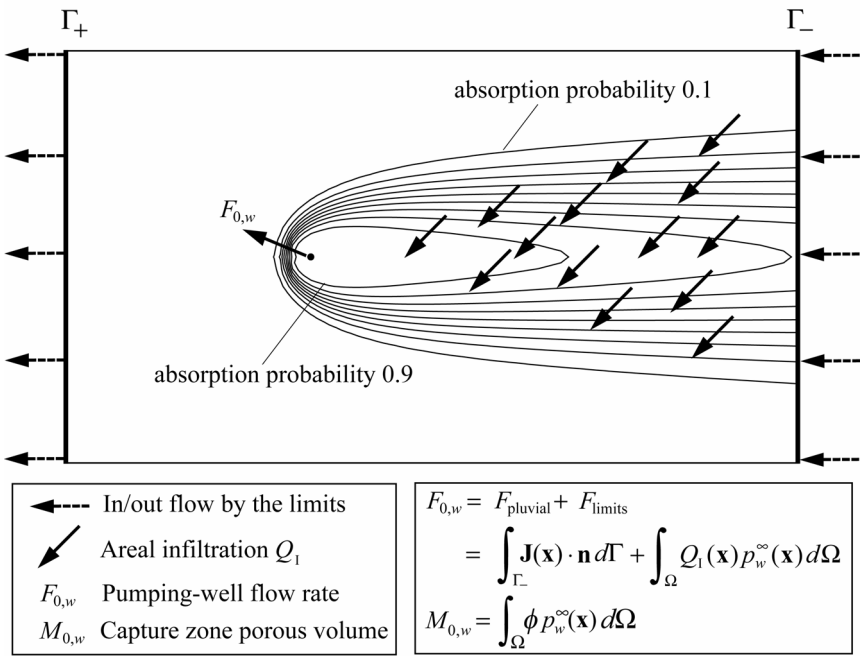

Fig. 4.2. Example of a pumping-well absolute capture zone from which the extracted flow rate at the well can be decomposed into flow rates from different origins of the infiltration. **J** denotes the total mass flux of probability of being absorbed by the well.

4.3. Example: Analysis of pore velocity effects on simulated ages at a pumping-well

In Chapter 3 (see section 3.4), sensitivity analysis has been carried out to analyze the effects of dispersion on the simulated age and transit time distributions in reservoirs and at specific outlets, for given velocity fields. In this section, we want to focus on the exclusive effect of velocity on the calculated transit time pdf at a pumping-well.

4.3.1. Random generation of velocity fields

To analyse the sensibility of the transit time pdf to the spatial variations of velocity, hundred realizations of an unconditional Log-normal random hydraulic conductivity field $\mathrm{Log}\,K$ have been performed, following the spectral generation procedure of Mejía & Rodríguez-Iturbe [1974]. The method makes use of a stationary random phase model to obtain asymptotically Gaussian and ergodic processes, by addition of harmonics of random frequencies, which are sampled from a spectral density function. The number of harmonics is the main factor that governs the quality of the generated process.

The geometry of the model is similar to the one used by Neupauer & Wilson [2001], who considered a 600×350m flow domain with a single pumping-well. The flow boundary conditions are somehow modified; they are indicated in Fig. 4.3. On the western outflowing boundary a constant hydraulic head is assigned ($H = 40$m). The pumping-well is located at $\mathbf{x}_w = (200; 175)$ with an extraction flow rate $Q(\mathbf{x}_w) = 8.64\mathrm{m}^3/\mathrm{day}$. On the eastern inflowing boundary, a constant flux intensity of $q = 0.1728$m/day is imposed, rather than a prescribed hydraulic head, to ensure that the aquifer turnover time remains unchanged between each realization of the K-field. The northern and southern boundaries are impervious. Dispersion is uniformly fixed to the minimum acceptable, in relation to the possible numerical instabilities (longitudinal dispersivity $\alpha_\mathrm{L} = \Delta\mathbf{x}/2 = 0.25$m, transverse dispersivity $\alpha_\mathrm{T} = \alpha_\mathrm{L}/10$, and molecular diffusion $D_\mathrm{m} = 2.3\times10^{-9}\,\mathrm{m}^2/\mathrm{s}$). The $\mathrm{Log}\,K$ generations were carried out for two relative separation distances $\zeta = L/\xi$, with L being the characteristic domain length in the x- and y-directions, and ξ being the correlation length. One example of generation is given in Fig. 4.3. The pumping well transit time pdf φ is calculated for each realization using the BRT formulation (4.12). The groundwater volumes A, B and M relative to age and transit time within the well capture zone Ω_w are also evaluated by post-processing the transit time cdf f (see Chapter 3). We recall that the function $\mathrm{A}(t)$ characterizes the groundwater volume in Ω_w with an age t or less, but with a transit time superior to t. It corresponds to the difference between the cumulated amount $M(t)$ of groundwater with an age t or less (cdf of the function ψ times the porous volume $M_{0,w}$) and the cumulated amount $\mathrm{B}(t) = M_T(t)$ of groundwater with a total transit time t or less (cdf of the function ψ_T times the porous volume $M_{0,w}$), which characterizes the amount of water with total transit time t or less from recharge to the well.

For each realization of the $\mathrm{Log}\,K$ field, the functions φ, f, A, B and M were calculated by assuming a physical dependency between the hydraulic conductivity K and the porosity ϕ. To do so, we considered the well-known Hagen-Poiseuille law, which expresses the geometric permeability κ in granular media by the following general formulation:

$$\kappa = \frac{\phi^3}{\omega\theta^2\mathrm{A}_s^2} \tag{4.20}$$

where ω is a dimensionless geometrical factor depending on the morphology and distribution of the grains, θ is tortuosity, ϕ is porosity, and A_s is the specific surface of the grains, which can be defined by (according to Perrochet, 2003, personal communication):

$$A_s = \frac{3(1-\phi)}{G_0}\int_0^{+\infty}\frac{1}{r}\frac{\partial G_{\text{cum}}(r)}{\partial r}dr = 3(1-\phi)\int_0^{+\infty}\frac{g(r)}{r}dr \tag{4.21}$$

with $G_{\text{cum}}(r)/G_0$ being the grain size cdf (G_0 is the total dry soil weight), and thus the function $g(r)$ being the corresponding grain size pdf. Once the κ-field has been generated, the medium porosity is calculated by solving

$$\kappa = \gamma\frac{\phi^3}{(1-\phi)^2} \tag{4.22a}$$

for ϕ, with the important assumption that the factor γ,

$$\gamma = 9\omega\theta^2\left(\int_0^{+\infty}\frac{g(r)}{r}dr\right)^2, \tag{4.22b}$$

is a constant over the entire domain. This assumption implies that the grain-size distribution, the shape and arrangement of the grains are uniform functions of space. However, for Log K fields showing variations up to four orders of magnitude, we verified that Eq. (4.22) yields smoothly varying porosity fields (e.g. between 15% and 25%), which belong to an acceptable range of porosity in porous medium. The mean of the calculated heterogeneous porosity fields were used in the simulations with uniform porosity. Note that Eq. (4.22) is close to the Fair-Hatch equation for non-uniform soils [see e.g. Todd, 1959], although it is expressed in a more general form.

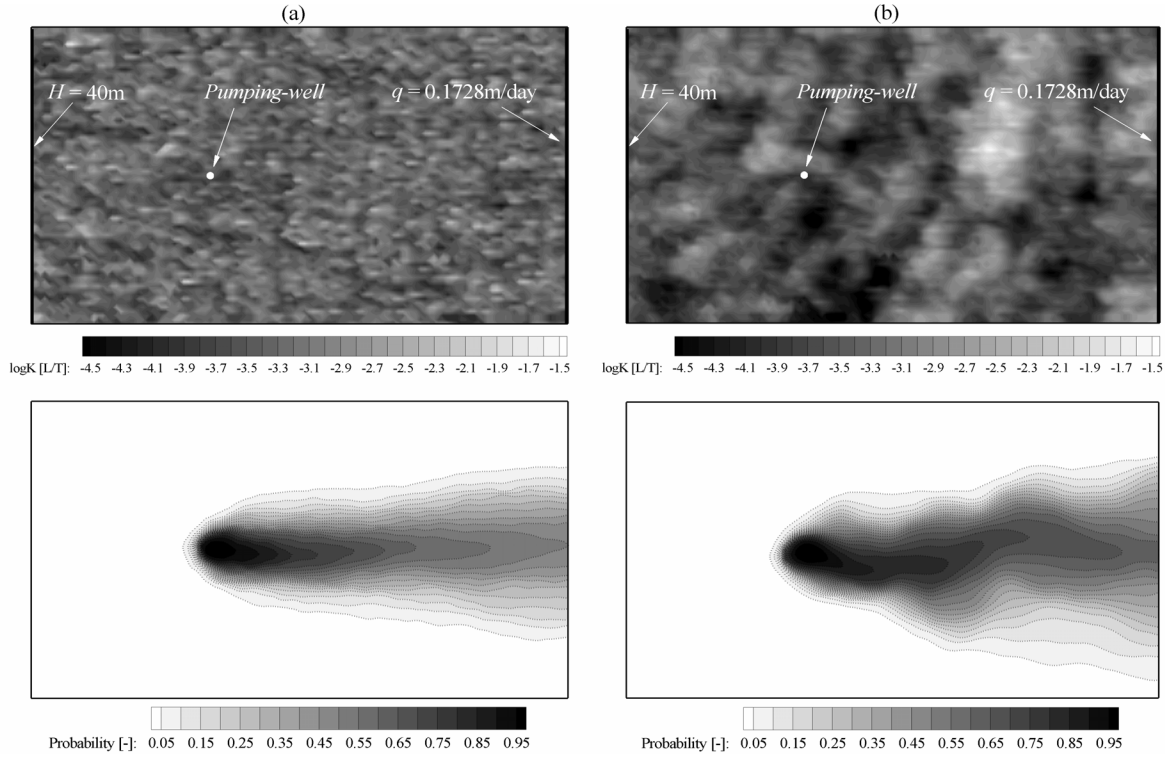

Fig. 4.3. Example of Log K hydraulic conductivity field realization (in m/s) with simulated mean $\mu_{\text{Log10}(K)} = -3.5$ and standard deviation $\sigma = 0.5$ (Top), and corresponding well absolute capture zones (Bottom) (a) Relative separation distance $\zeta = 2$; (b) Relative separation distance $\zeta = 20$.

4.3.2. Pumping-well age pdf simulations

The simulations for the relative separation distance $\zeta = 2$ show very small fluctuation of the calculated well transit time pdfs and groundwater volume functions, as illustrated in Fig. 4.4a and b. Including the $K - \phi$ relationship (4.22) has the effect of reducing the differences between the simulated curves (Fig. 4.4c and d). Since pore velocity is proportional to the ratio K/ϕ, using Eq. (4.22) instead of a uniform porosity has the effect of homogenising the velocity field, and consequently the spreading of the results is minimized. The results of the simulations with the relative separation distance $\zeta = 20$ show far more important differences between the calculated curves (Fig. 4.5). This was expected because of the different types of generated $\mathrm{Log}\,K$ fields, depending on ζ. The case $\zeta = 20$ results in marked zones of permeability, which can easily create separated preferential flow paths, as attested by the disturbed shape of the pumping-well capture zone in Fig. 4.3b. The case $\zeta = 2$ presents more local permeability contrasts, which induce more homogeneous transport behaviour. The pumping-well capture zone in Fig. 4.3a has a smoother and more regular shape than the capture zone in Fig. 4.3b. The effect of the $K - \phi$ relationship (4.22) for the case $\zeta = 20$ is even more pronounced than for the case $\zeta = 2$. When a uniform porosity is used, the simulated transit time pdfs and groundwater volume functions have contrasted shapes between each realization, and they all present important tails. When Eq. (4.22) is used, tailing is highly diminished, and the differences between the realizations are far less apparent.

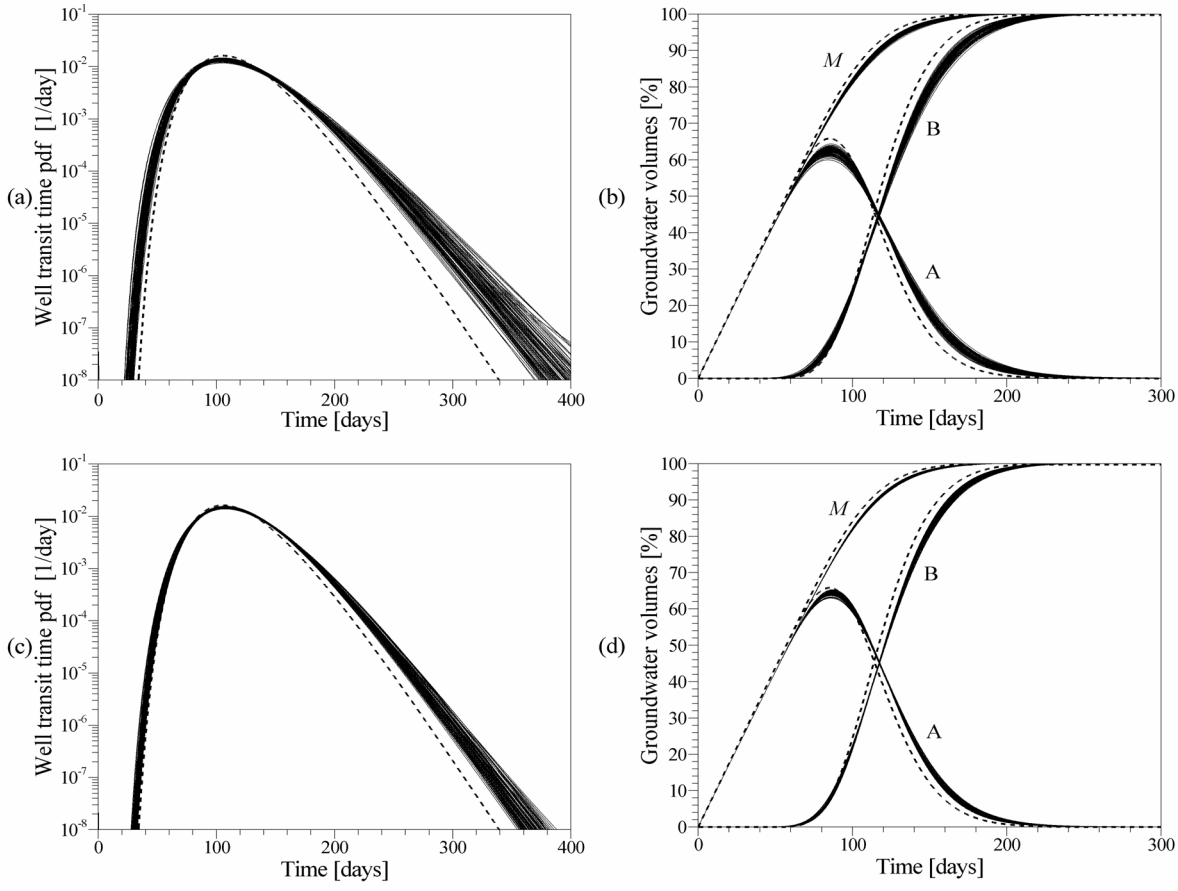

Fig. 4.4. BRT for the randomly generated $\mathrm{Log}\,K$ field with the relative separation distance $\zeta = 2$: (a) and (b) Uniform porosity; (c) and (d) $K - \phi$ relationship. The dashed lines are the results for the homogeneous case.

The differences between the heterogeneous case and the homogeneous case (with uniform hydraulic conductivity $K = 10^{-\mu}$ m/s) are given in Fig. 4.4 and Fig 4.5. The effect of the $K - \phi$ relationship on the dispersion of the results is obvious, when the tail of the curves simulated with a uniform porosity are compared to the tail of the curves simulated with the $K - \phi$ dependency, and when both cases are compared to the homogeneous solutions. The solutions with the $K - \phi$

relationship are always closer to the homogeneous reference, for the two tested separation distances. Note that the homogeneous solution with the geometric mean for permeability does not exactly fall within the cluster of the lines representing the heterogeneous realizations, in relation to the non purely horizontal nature of flow in the domain (effect of the well on velocity fluctuations), the geometric mean for an effective equivalent permeability being valid in uni-directional flow domains.

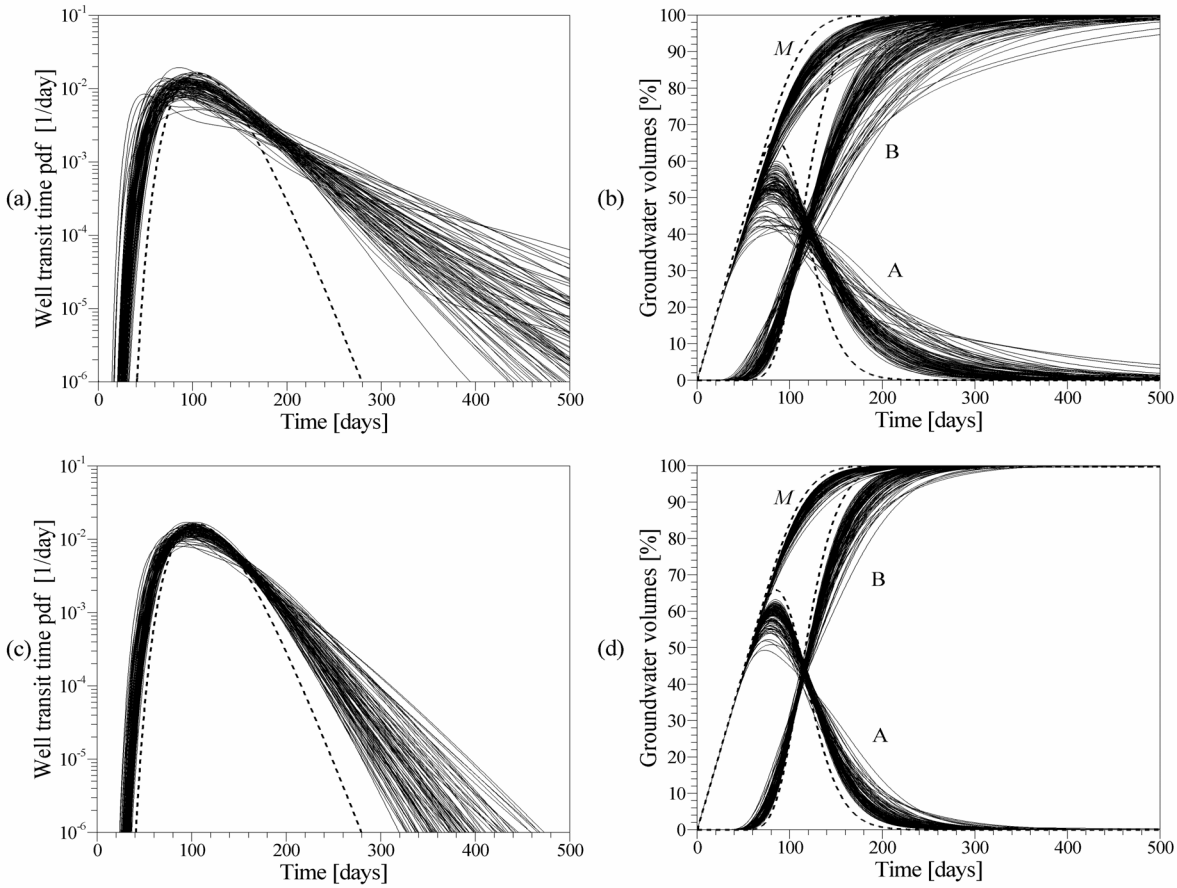

Fig. 4.5. BRT for the randomly generated Log K field with the relative separation distance $\zeta = 20$: (a) and (b) Uniform porosity; (c) and (d) $K - \phi$ relationship. The dashed lines are the results for the homogeneous case.

In this section, we have shown by means of numerical experiments, that a correlation between porosity and hydraulic conductivity has striking effects on age transport, particularly through the smoothing effect that this correlation induces on the age distribution, yielding more homogeneous-like transport phenomena. With even small spatial variations in porosity, the resulting velocity fields produce far less different age transport solutions than velocity fields which are only proportional to the Darcy flux vector. In porous media settings, it is reasonable to consider that the solutions which account for a $K - \phi$ dependency are physically more consistent. In such cases, pore velocity will depend only on the hydraulic gradient as in homogeneous medium, which is a much smoother function than hydraulic conductivity, in relation to the diffusive nature of the flow equation. We may argue that since porosity is generator of age during the water particles travel history, the ratio K/ϕ is a main factor that governs age transport. The knowledge of the spatial distribution of porosity is of high importance when dealing with age transport processes, because the uncertainty on porosity distribution has a direct effect on the uncertainty of the results. For mean age simulations which are carried out using a uniform distribution of porosity, one must be aware of the fact that multiplying porosity by two will yield simulated ages twice older, or similarly dividing porosity by two will yield simulated ages twice younger. In some cases the number of parameters may be reduced by one, depending on the available field data information on the couples $K - \phi$.

4.4. Backward Reservoir Theory and outlet protection zone and intrinsic vulnerability mapping

The outlet transit time pdf $\varphi(t)$ formulates the transport process of groundwater particles in terms of an integral property of the aquifer. It is defined in terms of the unit response of the reservoir to a unit flux input at the limits, which is mathematically equivalent to the Dirac pulse distribution. The parameters, the structural characteristics and heterogeneities of the entire reservoir that influence transport are incorporated when $\varphi(t)$ is evaluated with the RT. With the pdf $\varphi(t)$, or also with the pdfs $C_A(\mathbf{x}, t)$ and $C_E(\mathbf{x}, t)$, a 'static' vision of age transport was adopted, in the sense that these functions can be correlated with the water particles age distribution within a groundwater sample. However, this 'static' vision can take the form of a 'dynamic' vision of water particles transport, if these pdfs are compared to a breakthrough curve. By using the principle of superposition, the pdf $\varphi(t)$, which can be assimilated to the transfer function of the considered system, can be used to model the outflow concentration of a conservative tracer, with a transfer function representation of solute transport [Jury & Roth, 1990]. This procedure has already been illustrated in section 3.3.2, where the transit time pdf at the outlet of an experimental column was used to model a monitored outflow concentration breakthrough. Therefore, there is a relationship between the outflow concentration at an outlet and the distribution of the arrival times of a tracer.

In this section, the BRT and the backward life-expectancy-to-outlet pdf and cdf equations (4.9) and (4.17) are combined with the aim of characterizing the protection zones and the intrinsic vulnerability of artificial and natural outlets. In a first step, the utility of the BRT for defining the age of groundwater particles in drainage basins and at outlets is illustrated. In a second step, we discuss some approaches of definition and quantification of specific outlet protection zones. Finally, we show how the transport of a contaminant source from any point can be predicted with one single realization of the backward life expectancy equation, thus allowing the mapping of the outlet intrinsic vulnerability to source contamination.

For these purposes, we use the same geometry as in Section 4.3. The model is now homogeneous with respect to hydraulic conductivity ($K = 5.0\times10^{-5}$ m/s), porosity ($\phi = 0.3$), longitudinal dispersivity ($\alpha_L = 10$m), and transverse dispersivity ($\alpha_T = 2$m). The prescribed fluxes on the natural inlet limit Γ_- are converted into a prescribed hydraulic head $H = 50$m. The pumping-well is still at the position $\mathbf{x}_w = (200; 175)$ with the flow rate $Q(\mathbf{x}_w) = 8.64\ \mathrm{m}^3$/day. An additional infiltration zone of finite size ($40\mathrm{m}\times 40\mathrm{m}$) is simulated here, which implies that the correct forward and backward ADEs for simulating the age and life expectancy pdfs are (3.64) and (3.65). This infiltration zone could represent an irrigation area. Three observation points are used in the following (Fig. 4.6a), the first one (P1) being within the irrigation area at the position $(x, y) = (120\mathrm{m}, 220\mathrm{m})$, the second one (P2) being laterally displaced on the opposite side of P1 with respect to the N-S line passing through the well, and the third one (P3) being 100m upstream P1 and P2 in the N-S axis through the well. The irrigation waters contribute to the total inflow into the system, and the well flow rate contains a fraction of infiltrated water by irrigation, and a fraction of infiltrated water by the natural inlet limit Γ_-. The aquifer porous volume being $M_0 = 63000\mathrm{m}^3$, and the steady flow rate being $F_0 = 30.45\mathrm{m}^3$/day, the aquifer turnover time τ_0 is thus 2068.56days.

4.4.1. Pumping-well transit time pdf and capture zone internal age pdf

The probabilistic well capture zone relative to a given temporal reference t_r is obtained by solving the boundary value problem (4.9), and by evaluating the life-expectancy-to-well cdf $p_w(\mathbf{x}, t_r)$ at each node for time t_r. This can also be achieved by direct resolution of the boundary value problem (4.17). The pumping-well steady-state capture zone porous volume $M_{0,w}$ calculated with Eq. (4.14)

is ~16.35% of M_0, and the corresponding turnover time $\tau_{0,w}$ is 1191.71days. By enforcing Eq. (4.19), we find that 61.07% of the water extracted at the well originates from the natural inlet limit Γ_-, and that 38.93% originates from the irrigation area. Fig. 4.6b shows the 3-years capture zone (or life-expectancy-to-well cdf field at $t = 3$years), and Fig. 4.6c gives the distribution of the life-expectancy-to-well pdf for the corresponding date. These two distributions are deformed by the presence of the infiltration area. Note the effect of the *Implicit Neumann* condition which permits a natural outflowing life expectancy gradient on the inlet boundary Γ_-. Generally, the concentration gradients are assumed to be zero at exit zones (here at the inlet zone in the backward model), yielding unphysical solutions at the boundary surroundings, since the iso-lines of concentration are forced to be perpendicular to the boundary. The induced errors can be important, when e.g. too coarse meshes are used. But above any consideration of numerical nature, the backward problems are very often more concerned than the forward problems by the assumption of a zero concentration gradient at inlet limits, since a free exit of the fluxes is required at the inlet boundary portions, which generally occupy more space than the outlet limits. The case of the free exit of life expectancy fluxes on top of a 3D aquifer, where natural recharge is reversed, is a good example.

In addition to the probabilistic well capture zone, Frind *et al*. [2002] have calculated the arrival times at the well by using a backward particle-tracking method to perform the statistics on the computed ages intercepting the ground surface. This procedure is conceptually right in the sense that the transit time distribution of the water particles at the ground surface is the life-expectancy-to-well of the particles, which again is equivalent to the age distribution at the well. However, the particle-tracking method does not associate the water fluxes to computed ages, with the result that the calculated distribution cannot be taken as the 'true' transit time pdf at the well. In Fig. 4.6d and e, the solutions of Eq. (4.10) and of the BRT formulation (4.12) are given. The circles are the verification of Eqs. (4.7) and (4.8). The BRT was applied to the natural outlet (Γ_+) capture zone, and the resulting pdfs were combined to the BRT results for the well (Γ_w), by enforcing Eqs. (4.7) and (4.8) to evaluate the global reservoir pdfs. The comparison with the FRT results for the global reservoir (considering the transit time pdf of the union $\Gamma_+ \cup \Gamma_w$ and the entire aquifer internal age pdf), shows a perfect agreement between the global reservoir pdfs, and the result of the superposition of the two flow units pdfs (well and natural outlet drainage basins), using Eqs. (4.7) and (4.8). The FRT applied to the global system characterizes the entire environment in terms of residence and arrival times, by including each groundwater recharge and discharge zone. The BRT enables the characterization of each specific outlet and associated drainage basin, in terms of arrival times and residence times, respectively.

The well transit time pdf shows two modes that are related to the two sources of infiltration. The irrigation area produces short transit times to the well (the minimum is ~200days), and corresponds thus to the major contribution to the first mode of the curve at t~500days. The second mode (at t~1450days) is mainly due to infiltration by the natural inlet Γ_-. The intersection of the life-expectancy-to-well pdf field at time $t = 3$years with the inlet limit Γ_- (Fig. 4.6c) contains values up to 3.5×10^{-4}days^{-1}. This probability density magnitude must be present in the age distribution curve at the well, as shown in Fig. 4.6d. In a similar way, the point P1 is concerned by a life expectancy value around 8.5×10^{-5}days^{-1} and P2 is around 1.0×10^{-4}days^{-1}, while P3 is around 9.5×10^{-4}days^{-1}. This shows that the effect of the irrigation area on the transit time distribution at the well is limited for ages superior to 3years, and that the natural inlet limit is the main origin for the high probability of having arrival times at the well superior to this date.

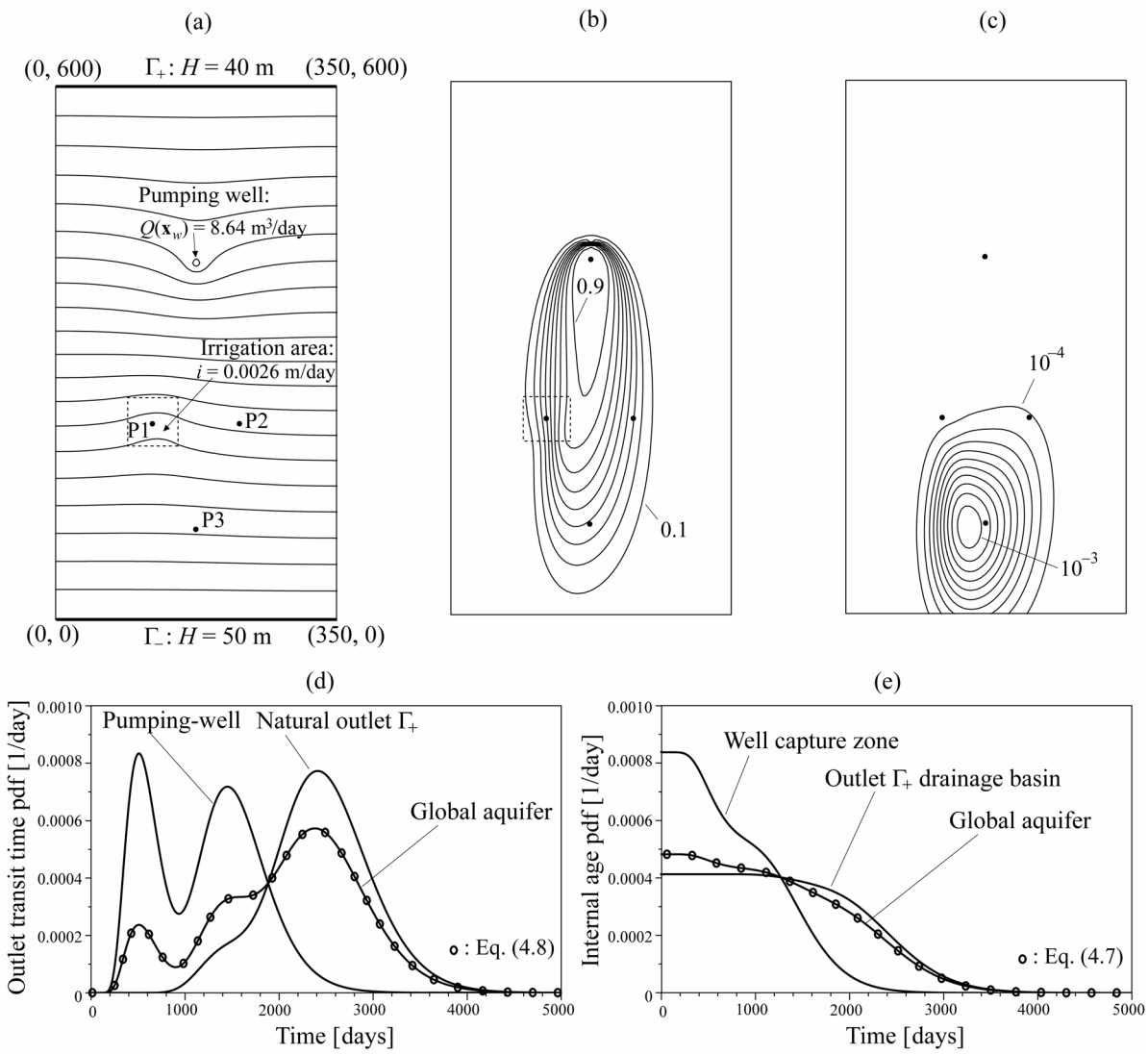

Fig. 4.6. RT for a theoretical pumping-well field. (a) Geometry, flow boundary conditions, Hydraulic head field, and observation points location; (b) Well 3-years capture zone, or life-expectancy-to-well cdf distribution, with contour interval 0.1; (c) Life-expectancy-to-well pdf field in days^{-1} at time $t = 3$years; (d) Transit time pdf for the pumping-well (BRT), the outlet Γ_+ (BRT), and the whole aquifer domain (FRT); (e) Internal age pdf for the pumping-well (BRT), the outlet Γ_+ (BRT), and the whole aquifer domain (FRT).

The analysis of the well transit time cdf $f(t)$ (Fig. 4.7a) indicates e.g. that 63.10% of the well outflow is concerned by water particles of 3.95 years of age or less (second mode of the well transit time pdf), 50% by water particles of 3.42 years of age or less (median of the well transit time pdf), 46.75% by water particles of 3.26 years of age or less (average age at the well), 42.25% by particles of 3 years of age or less, 14.15% by particles of 500 days of age or less (first mode of the well transit time pdf), and only 4.25% by particles of 1year of age or less. The functions derived from the transit time cdf $f(t)$, and that describe the groundwater volumes in the reservoir as a function of age (or life expectancy), and transit time (see Chapter 3), provide interesting complementary information on the dynamics of the system, in terms of groundwater volumes. Particularly the function A(t) informs on the quantities of water that contribute to the renewal of the groundwater stocks, and at the same time on the quantities which remain a long time within the system prior to exit. The function A(t) relative to the pumping-well capture zone (Fig. 4.7b) equals the function $M(t)$ (volume of age t or less) up to the approximate minimum transit time $t \sim 200$ days, indicating that the minimum arrival time at the well is close to this date. Note that dispersion does not allow the identification of an absolute numeric value of the minimum transit time at the well. The

maximum of A(t) is at time t =3 years (53% of M_0), and the relative rapid decrease that follows indicates that the water particles with an age superior to 3 years will not remain very long in the system, but will rather be rapidly absorbed by the well. An important tailing of the function A(t) would at the contrary indicate that significant groundwater volumes remain a long time in the system before exit. The value of the function B(t) at time t =3 years is 22% of M_0. The drastic increase of this function after 3 years indicates also that important amounts of groundwater flow rapidly to the well with a transit time superior to 3 years.

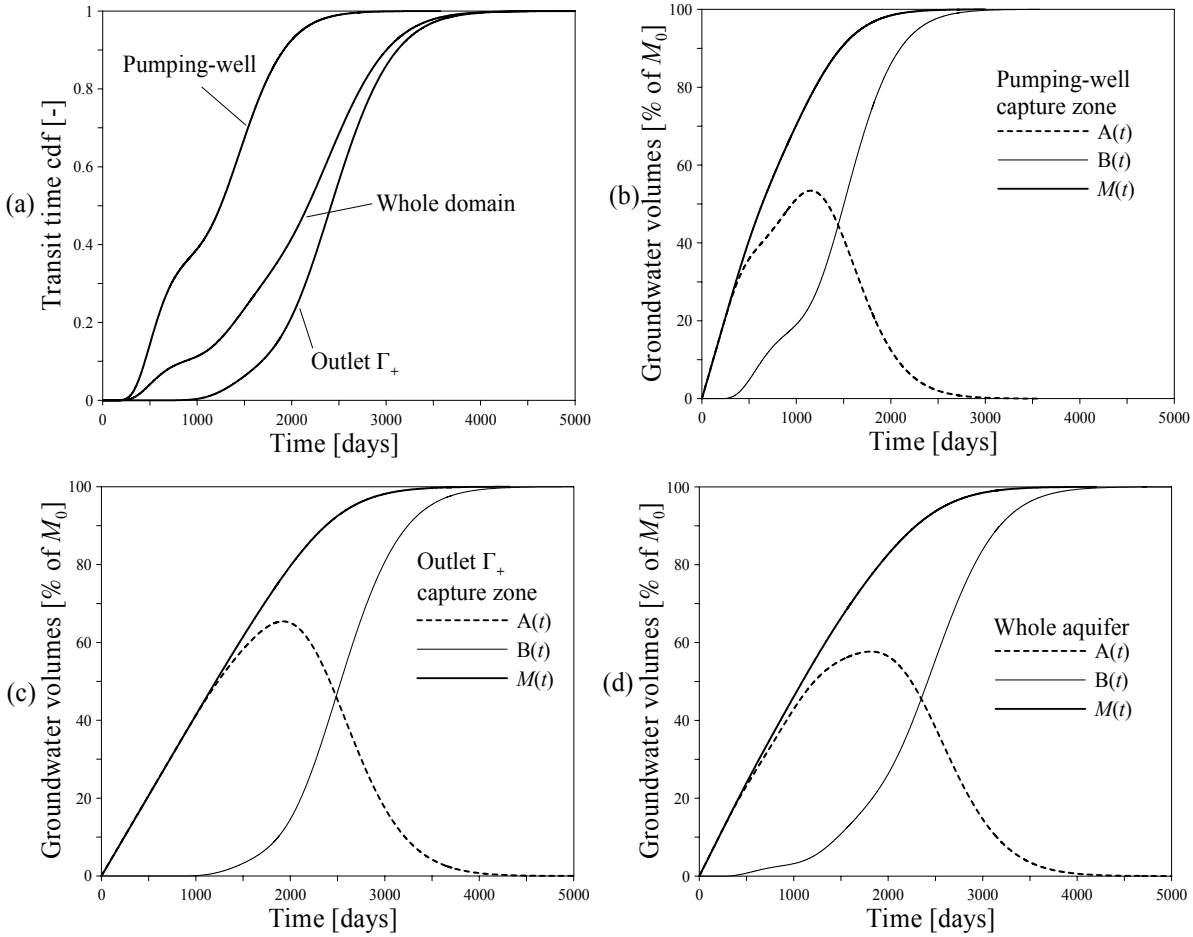

Fig. 4.7. RT for a theoretical pumping-well field. (a): Transit time cdf for the pumping-well, the natural outlet Γ_+ (see Fig. 4.6a) and the whole aquifer domain; (b), (c) and (d): Internal groundwater volumes.

4.4.2. Well-head protection zones definition

Various countries have their own conventions for the definition of the different well-head and spring protection zones. The definition of these zones is generally linked to the notion of transit time to the outlet, and of surface area within which natural infiltration balances a given percentage of the outlet discharge. By using Eqs. (4.18) or (4.19) to separate the fractions of infiltration fluxes that contribute to a given outlet flow rate, one can easily define the exact surface area (i.e. enclosing surface within a given iso-level of probability) that corresponds to the zone which ensures that a desired percentage of the outlet discharge is sufficiently secured by natural recharge by rain infiltration, e.g. during low water periods. To evaluate this zone in a 2D horizontal case and by considering the absolute capture-zone, we can look for the p^{∞} iso-line that satisfies:

$$\epsilon Q_w = \int_{\Omega} Q_I(\mathbf{x}) p_w^{\infty}(\mathbf{x}) d\Omega \tag{4.23}$$

where ϵ is a factor between 0 and 1 that defines a given fraction of the well discharge Q_w, e.g. $\epsilon = 0.9$. The corresponding iso-line of probability defines the zone for which the fraction ϵQ_w of the well discharge is exclusively sustained by recharge from rain infiltration. Such an operation is illustrated in Fig. 4.8, where we have made use of one of the realization of composite porous medium described in Section 4.3. The flow boundary conditions were once again modified to simulate pseudo steady-state low water conditions. The eastern inflowing limit is now impervious, and a uniform fluid source term of low intensity ($Q_I = 2.0\times10^{-9}$ m/s) is used to simulate areal recharge. The conditions along the western limit and at the pumping-well are unchanged. Fig. 4.8a shows the ultimate capture zone for the adopted low water conditions, and Fig. 4.8b shows the reduced capture zone corresponding to the surface within which 90% of the well discharge is balanced by areal infiltration. Fig. 4.8c and d give the same results for the 200-days capture zone.

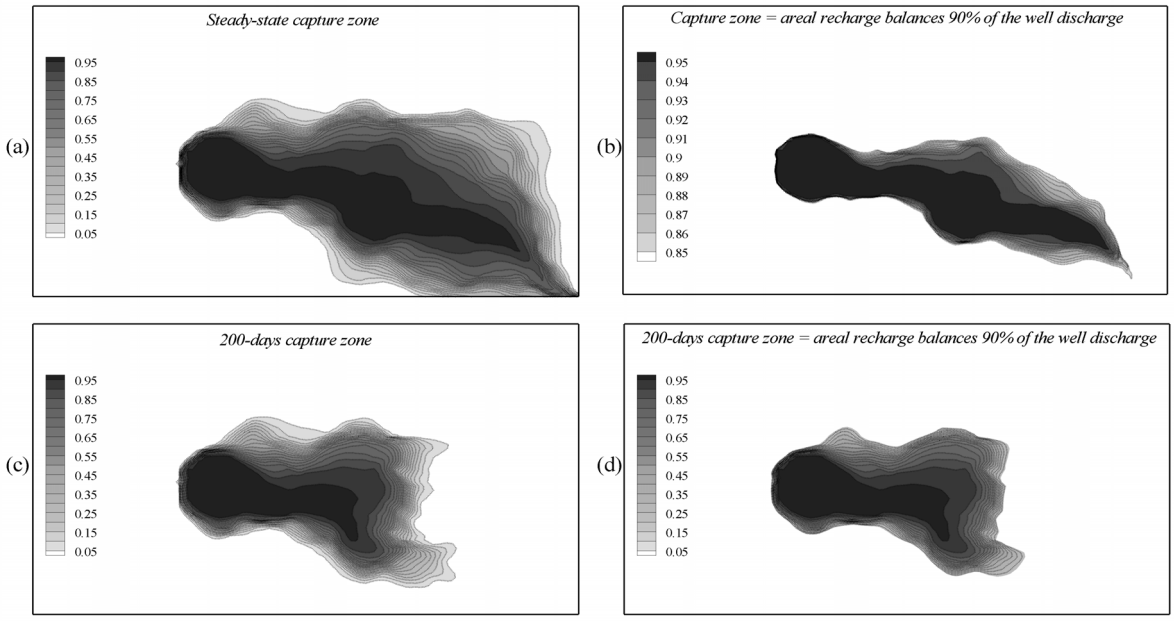

Fig. 4.8. Well capture zones in composite porous medium ($\mu_{\mathrm{Log10}(K)} = -3.5$, $\sigma = 0.5$, $\zeta = 20$) with the uniform fluid source intensity of 2.0×10^{-9} m/s: (a) Steady-state capture zone; (b) Surface area with which 90% of the well discharge is balanced by natural recharge from rain infiltration; (c) Well 200-days capture zone; (d) Surface area in the 200-days capture zone with which 90% of the well discharge is balanced by natural recharge from rain infiltration.

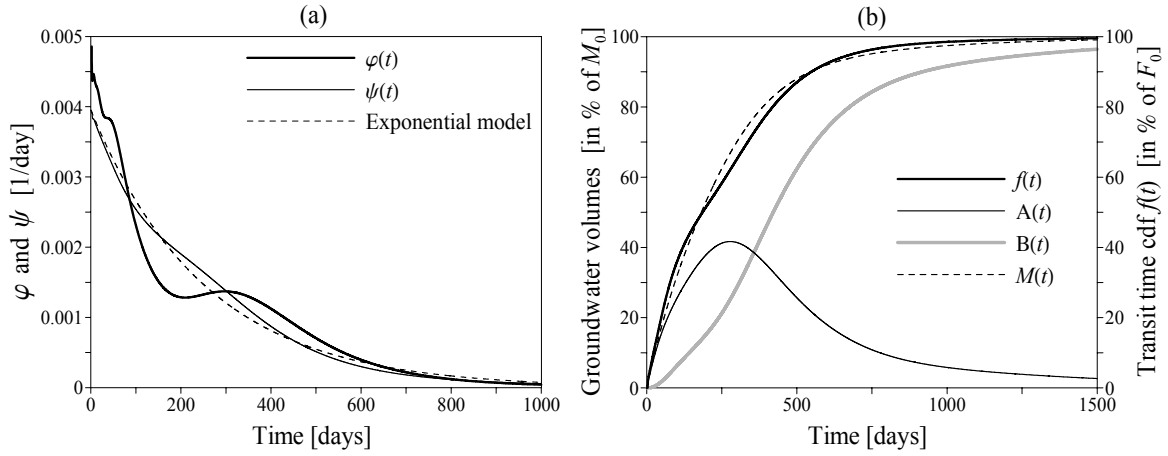

Fig. 4.9. BRT results for the example of Fig. 4.8: (a) Well transit time pdf and capture zone internal age pdf, compared to the exponential model applied to the well capture zone ($\tau_0 = 253$days); (b) Well transit time cdf and capture zone groundwater volumes as a function of age and transit time.

Under these hydraulic conditions, the well capture-zone internal age pdf ψ shows more or less an exponential-like behaviour (Eq. (3.34) is enforced for comparison by using the well capture zone mean transit time $\tau_t = \tau_0 = 253$days), unlike the well transit time pdf φ which can definitely not be simulated by the exponential model (Fig. 4.9a). The function A(t) diverges from the function $M(t)$, from the earliest calculated time, showing that the minimum transit time at the well approaches zero (Fig. 4.9b). This is in accordance with the fact that the uniform infiltration source is responsible of nearly zero ages at the well. The maximum of A(t) occurs 25days after time $t = \tau_0$ (for the pure exponential model, it is exactly at $t = \tau_0$).

The example of the Z_u protection zone

According to the Swiss law on groundwater protection, the Z_u-zone corresponds to the area generating 90% of the total well discharge rate under low water conditions, by precipitation infiltration and/or infiltration along hydraulic limits. The main objective of the Z_u-zone is to protect drinking-water extraction points with respect to contamination, e.g. the diffuse contamination induced by the flushing of the soil by rain infiltrations (e.g. nitrates and pesticides flush). The Z_u-zone definition can be obtained by adapting Eq. (4.19) as follows:

$$F_{0,w} = 0.9F_{0,w} + 0.1F_{0,w} = \left(\int_{\Omega=Z_u} Q_I(\mathbf{x}) p_w^{\infty}(\mathbf{x}) d\Omega + \int_{\Gamma_-^{Z_u}} \mathbf{J}\cdot\mathbf{n}\, d\Gamma \right) + \int_{\Gamma_{+/-}^{Z_u}} \mathbf{J}\cdot\mathbf{n}\, d\Gamma \qquad (4.24)$$

with **J** being the total mass flux of absolute probability of absorption by the well. The terms inside parentheses on the right-hand side of (4.24) must provide 90% of the well flow rate $F_{0,w}$. To obtain the probability isoline that defines the Z_u-zone domain, the pluvial contribution and the contribution from the limits are summed up from the maximum probability at the well until the probability level for which this flow rate fraction is attained (Fig. 4.10). The second term on the right-hand side of (4.24) characterizes the 10% missing, which must cross the Z_u-zone domain limit. Through this limit, the fluxes can enter and exit by dispersion (the normal to that isoline points towards lower probability values).

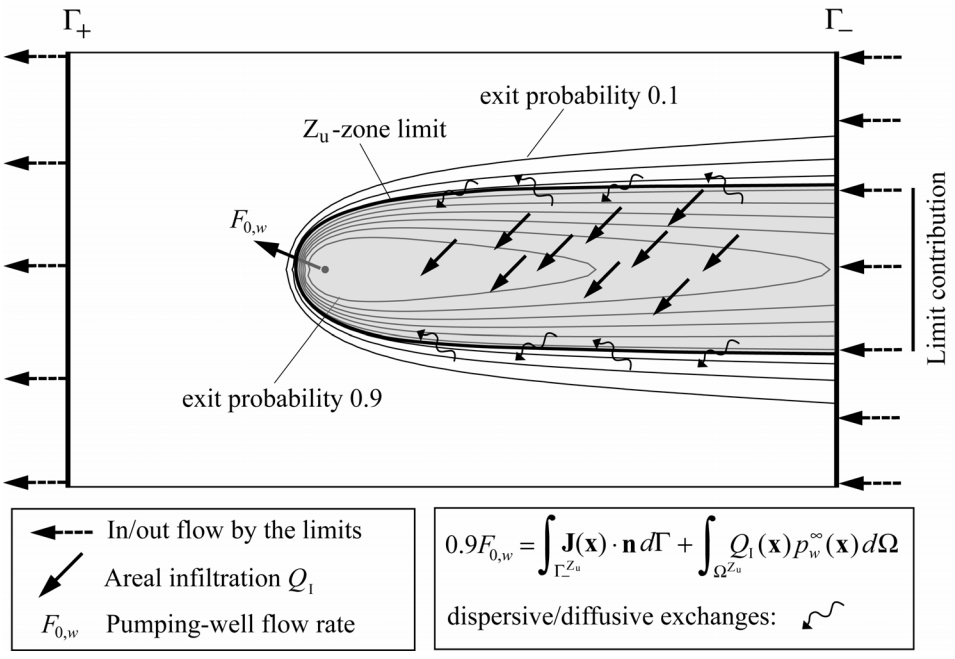

Fig. 4.10. Principle of a Z_u-zone delineation, using the absolute probability field of exit.

4.4.3. Outlet intrinsic vulnerability to source contamination

According to Gogu & Dassargues [2000], the actual intrinsic vulnerability index mapping methods suffer from a lack of inclusion of physical processes that lead to the groundwater resources contamination. Numerical models are good actors for the intrinsic vulnerability assessment that aims at including the quantification of the major physical transport processes in groundwater. The intrinsic vulnerability is often defined by some criteria like the maximum concentration that is expected at the outlet, the time to reach this maximum, or the time to reach a reference level of concentration at the outlet. The criterion of contamination duration can also be added, in order to modulate between the concepts of a rapid and concentrated contamination, and of a long but more diluted contamination [Brouyère *et al.*, 2001]. The life-expectancy-to-outlet pdf and cdf fields can provide robust answers to the questions of transit time to the outlet, and of vulnerability to an upstream contamination event.

Theoretical approach

The spatial distribution of the life-expectancy-to- outlet pdf can be post-processed with the aim of mapping the outlet vulnerability to an upstream pollution event that may lead to a contamination within a critical time-span. As it was shown in previous works [Wilson & Liu, 1997; Neupauer & Wilson, 1999, 2001], the expected concentration at an outlet resulting from a unit mass input at an upstream source, is predicted with one single resolution of the backward equation.

In Fig. 4.11 we have verified this interesting property of the backward model by comparing three scenarios of the well contamination originating from the forward transport of an instantaneous input of contaminant at the three observation points, to one single realization of the backward life expectancy equation. To do so, the ADE has been solved for resident concentration with the initial condition $C^r(\mathbf{x}, 0) = m^* \delta(\mathbf{x} - \mathbf{x}_i)/B(\mathbf{x}_i)$ at the points P1, P2, P3, with m^* being the injected mass at $\mathbf{x}_i$ and B the aquifer thickness, and the resulting breakthrough curves at the well have been monitored. The three plumes of contamination issued from these three distinct forward simulations are superimposed in Fig. 4.11a, for time $t = 200$days.

The unit response function at the well resulting from the contaminant input at $\mathbf{x}_i$ is deduced by normalizing the resident concentration breakthrough $C^r(\mathbf{x}_w, t)$ by the injected mass m^*. The resulting function is the travel distance pdf (or location pdf) at the well, $g_{\mathbf{x}}(\mathbf{x}_w, t) = C^r(\mathbf{x}_w, t)/m^*$ (to be compared with Eq. (2.12)). The pdf $g_{\mathbf{x}}(\mathbf{x}_w, t)$ can be approximated by the life-expectancy-to-well pdf at the three injection points:

$$g_{\mathbf{x}}(\mathbf{x}_w, t) = \frac{C^r(\mathbf{x}_w, t)}{m^*} = \frac{C_E(\mathbf{x}_i, t)}{Q_w} \tag{4.25}$$

The flow rate scaled life-expectancy-to-well pdf at the injection point is thus equivalent to the travel distance pdf at the well. This property is demonstrated for a general case in Excursus 4.1. In Fig. 4.11e, the scaled life-expectancy-to-well pdf curves for the three observation points are compared to the travel distance pdfs at the well, following Eq. (4.25). The crosses correspond to the three travel distance pdfs $g_{\mathbf{x}}(\mathbf{x}_w, t)$ monitored at the well. They are in perfect agreement with the flow rate normalized life-expectancy-to-well pdfs $C_E(\mathbf{x}_i, t)/Q_w$, which have been evaluated with one single backward run at the three injection points. The same comparison is given in Fig. 4.11f for the natural outlet Γ_+, for which Eq. (E4.1.6) was used.

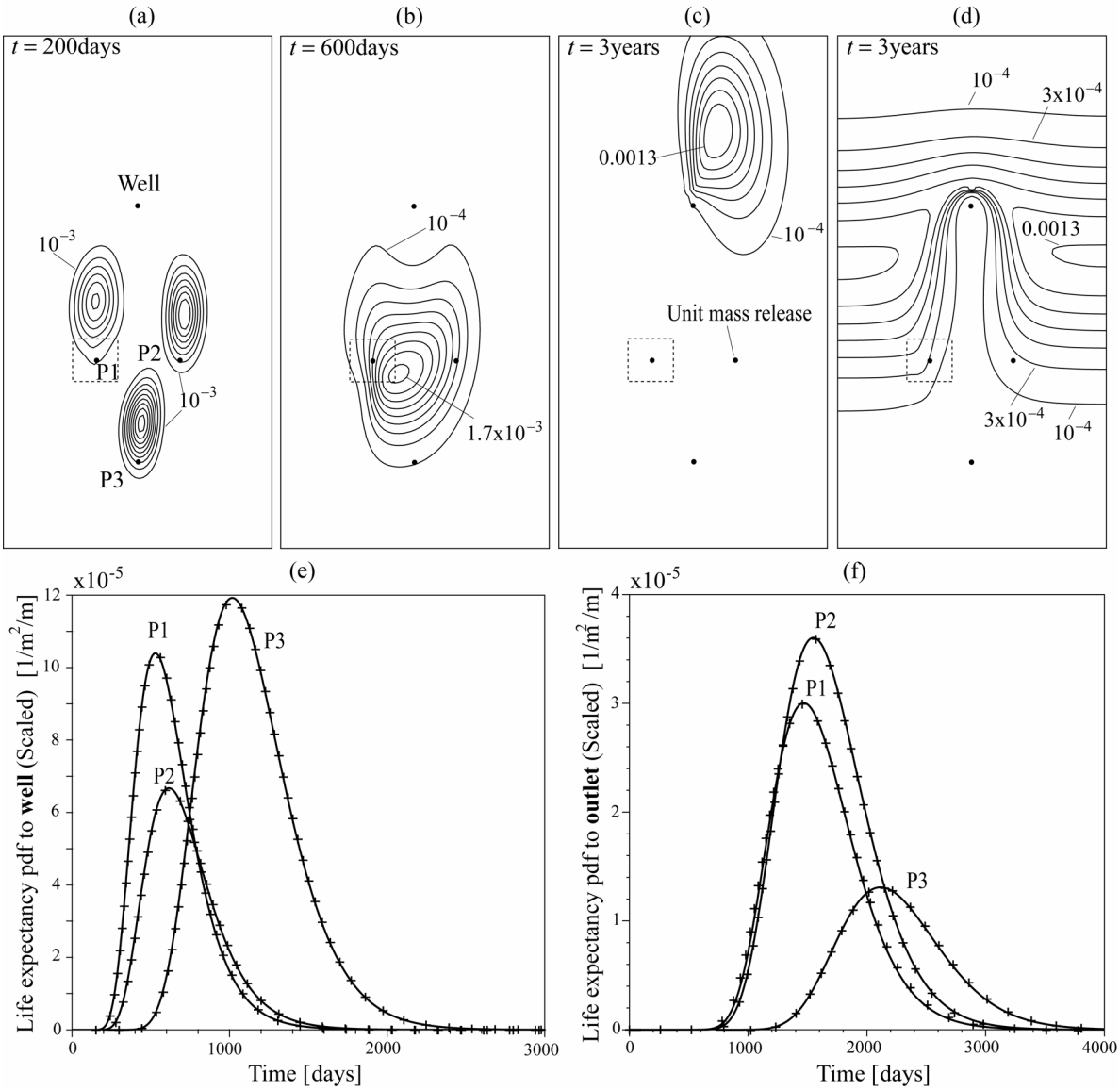

Fig. 4.11. Forward and backward modelling of a contamination of the well and the natural outlet. (a) Superimposed plumes of resident concentration at time $t = 200$days (contour interval 1.0×10^{-3} mg/l), originating from three forward simulations of a unit mass instantaneous release at P1, P2 and P3; (b) Life-expectancy-to-well pdf field at time $t = 600$days (contour interval 2.0×10^{-4} days^{-1}); (c) Plume of resident concentration at time $t = 3$years (contour interval 2.0×10^{-4}), originating from a unit instantaneous mass release at P2; (d) Life-expectancy-to-outlet pdf field at time $t = 3$years; (e) Scaled life-expectancy-to-well pdfs (in m^{-2}) at the three observation points (solid lines), fitting the normalized resident concentration breakthrough curves at the well (crosses); (f) Scaled life-expectancy-to-outlet pdf at the three observation points (solid lines), fitting the normalized resident concentration breakthrough curves at the natural outlet (crosses).

The field C_E at a fixed time t_r permits identification of the most likely spatial origin of a contamination source that may be detected at the well, and that would need the amount of time t_r to travel from its initial position to the well (Fig. 4.11b). The probability that the water particles will be absorbed by the well is $\int_t C_E(\mathbf{x}, t)dt$. The probability of being absorbed downstream at Γ_+ is thus the complement $1 - \int_t C_E(\mathbf{x}, t)dt$. The point P1 has a higher probability per unit time of being absorbed by the well than point P2, since the irrigation area increases the velocities in the vicinity of P1. The probability of being absorbed by the well is 40.97% for P1, 30.1% for P2, and 71.83% for P3.

The map of life-expectancy-to-well pdf for a given time value t_r, divided by the well flow rate Q_w, can directly be taken as a map of the relative contamination level one can expect at the well at time t_r, if a contamination event occurs somewhere upstream within the well capture zone. Since the life expectancy pdf at any position in the capture zone is related to the concentration at the ultimate point (pumping-well), the bigger the value of the density of probability of C_E in Fig. 4.11b, the higher the level of contamination that is to be expected at the well.

Outlet vulnerability mapping

By using the fact that the life-expectancy-to-well pdf at a position $\mathbf{x}_i$ within the capture zone is proportional to the concentration that one could observe at the well if some source contamination may occur at $\mathbf{x}_i$ (see Eq. (4.25)), more specific protection maps, which account for the groundwater resource vulnerability to source contamination, can be established by post-processing the life expectancy breakthrough curves. This post-process can correspond to the evaluation at each point of the maximum concentration that is expected at the well, together with the corresponding required times. The times to reach a given threshold concentration at the well, and the contamination duration, or spreading, which can e.g. be assimilated to the life-expectancy-to-well curves variance, can also be evaluated and mapped.

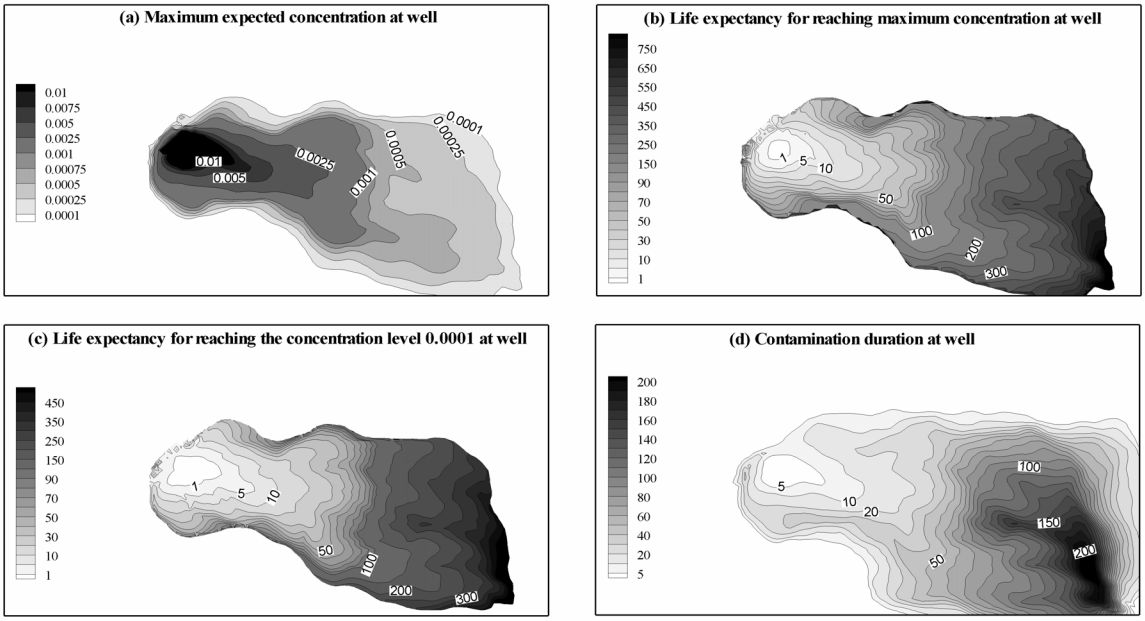

Fig. 4.12. Well vulnerability to source contamination in composite porous medium ($\mu_{\mathrm{Log10}(K)} = -3.5$, $\sigma = 0.5$, $\zeta = 2$): (a) Map of maximum expected relative concentration at the well; (b) Map of life expectancy to reach the maximum concentration at the well (in days); (c) Map of life expectancy to reach the relative concentration of 1.0×10^{-4} at the well (in days); (d) Map of contamination duration at the well (in days).

In Fig. 4.12 these vulnerability maps are given for the case of the model of Fig. 4.8. The life-expectancy-to-well pdf distribution has been calculated by solving the backward boundary value problem (4.9). The life expectancy pdfs have then been scaled by the well discharge rate to obtain the equivalent expected concentration at the well, following Eq. (4.25). The maximum concentrations (Fig. 4.12a) and corresponding life expectancies (Fig. 4.12b) are identified at each point, as well as the times to reach a threshold relative concentration of 10^{-4} (Fig. 4.12c). The contamination duration map in Fig. 4.12d is defined by the standard deviation of the scaled life-expectancy-to-well pdfs. It gives a measure of the tail of the breakthrough curves at the well, and must therefore be compared to the maps of maximum concentration and life expectancy for maximum concentration. The contamination duration map could be defined according to different

criteria than the standard deviation of the scaled life-expectancy-to-well pdfs. For ideal uni-modal breakthroughs, the contamination duration could e.g. be defined as the time-span between the time of apparition of a threshold concentration (which is followed by an increase of concentration until the maximum), and the time at which this threshold concentration is found again during the decrease of concentration.

From the vulnerability maps presented in Fig. 4.12, a critical zone can easily be identified. For example, one could consider more particularly the zone enclosed by the l00-days life expectancy for reaching the maximum concentration at the well (Fig. 4.12b), or the l00-days life expectancy for reaching the threshold relative concentration of 10^{-4} at the well (Fig. 4.12c).

The RT can help to refine the outlet vulnerability study, by adding information obtained on the outlet and its drainage basin, to the outlet time-dependent and steady-state capture zones delineation. With the function φ, we are informed on the age distribution of the extracted water at the outlet, by considering the intersection of the life expectancy cdf field with every recharging boundary. This information permits the evaluation of the possible 'groups of arrival times' at the outlet, allowing subsequent focus on specific critical times. The functions A(t), B(t) and $M(t)$ allow the characterization of the internal organization of age and of transit time to outlet, within the considered aquifer sub-domain. With one simulation of the life expectancy field, one can delineate capture zones relative to a given time of travel to the outlet, and one can also design intrinsic vulnerability maps for a source of contamination that may occur within the capture zone. By combining each above-described information, the outlet capture zone extend for protection and intrinsic vulnerability are defined. Field tracer tests can be envisaged for calibration of the life expectancy model.

The methodology does not present limiting factors due to the considered space dimension, and can therefore face the commonly encountered complicated geometries and hydraulic conditions. A good example of complex 3D shapes of the capture zones, in relation to the geological and hydrogeological configurations of the site, is given in Frind *et al.* [2002]. The above outlined approach for the system outlet represented by a pumping-well can equivalently be used to treat natural aquifer outlets like springs, lakes or rivers. The specific vulnerability to a contamination source of arbitrary input in time can also be characterized, as shown in Excursus 4.1. The life-expectancy-to-outlet pdf can also be useful for planning of the location of potentially contaminating sites, like e.g. waste disposals, since the site location can be optimized in space and time to protect water supply wells by using the field $C_E(\mathbf{x}, t = t_r)$. The LTG technique allows easy post-processing to obtain capture zones and vulnerability maps. For example, the calculation of the life expectancy cdf field for a reference time t_r, is a straightforward operation in the Laplace domain by making use of the Laplace transform property (E2.2.4).

Excursus 4.1. Backward problem equivalent to forward problem

We consider the resident concentration resulting from the transport of the initial condition $C^r(\mathbf{x},0)=m^*\delta(\mathbf{x}-\mathbf{x}_i)$, as shown in Fig. 4.13a. This initial value problem can be equivalently formulated as a boundary value problem with source term:

$$\frac{\partial\phi C^r}{\partial t}=-\nabla\cdot\mathbf{q}C^r+\nabla\cdot\mathbf{D}\nabla C^r+m^*\delta(\mathbf{x}-\mathbf{x}_i)\delta(t) \quad \text{in} \quad \Omega \qquad \text{(E4.1.1)}$$

$$[\mathbf{q}C^r-\mathbf{D}\nabla C^r]\cdot\mathbf{n}=0 \quad \text{on} \quad \Gamma_-\cup\Gamma_0$$

Implicit Neumann condition on $\Gamma_+\cup\Gamma_n$

where m^* is the injected mass at $\mathbf{x}=\mathbf{x}_i$. The Cauchy type boundary condition at $\mathbf{x}=\Gamma_-$ prevents solute from migrating upgradient, and the time Dirac delta function $\delta(t)$ allows an instantaneous mass release at $t=0$. The life-expectancy-to-outlet problem is defined according to the backward model (4.9) for the supposed outlet Γ_n, and is theoretically illustrated in Fig. 4.13b. We transform Eqs. (E4.1.1) and (4.9) by applying a Laplace transform, as defined in the Excursus 2.2. The transformed ADEs and boundary conditions are

$$s\phi\hat{C}^r=-\nabla\cdot\mathbf{q}\hat{C}^r+\nabla\cdot\mathbf{D}\nabla\hat{C}^r+m^*\delta(\mathbf{x}-\mathbf{x}_i) \quad \text{in} \quad \Omega \qquad \text{(E4.1.2)}$$

$$[\mathbf{q}\hat{C}^r-\mathbf{D}\nabla\hat{C}^r]\cdot\mathbf{n}=0 \quad \text{on} \quad \Gamma_-\cup\Gamma_0$$

Implicit Neumann condition on $\Gamma_+\cup\Gamma_n$

for equation (E4.1.1), and

$$s\phi\hat{C}_E=\nabla\cdot\mathbf{q}\hat{C}_E+\nabla\cdot\mathbf{D}\nabla\hat{C}_E-Q_I\hat{C}_E \quad \text{in} \quad \Omega \qquad \text{(E4.1.3)}$$

$$[\mathbf{q}\hat{C}_E+\mathbf{D}\nabla\hat{C}_E]\cdot\mathbf{n}=\mathbf{q}\cdot\mathbf{n} \quad \text{on} \quad \Gamma_n$$

$$[\mathbf{q}\hat{C}_E+\mathbf{D}\nabla\hat{C}_E]\cdot\mathbf{n}=0 \quad \text{on} \quad \Gamma_+$$

Implicit Neumann condition on Γ_-

$$\mathbf{D}\nabla\hat{C}_E\cdot\mathbf{n}=0 \quad \text{on} \quad \Gamma_0$$

for the backward equation (4.9). Note that flow is non necessary divergence-free, $\nabla\cdot\mathbf{q}=Q_I$.

We now multiply Eq. (E4.1.2) with $\hat{C}_E$ and Eq. (E4.1.3) with $-\hat{C}^r$, add the resulting expressions, integrate by parts over the domain and explicit each boundary integral:

$$\begin{aligned}&\int_{\Gamma_n}\hat{C}^r[\mathbf{q}\hat{C}_E+\mathbf{D}\nabla\hat{C}_E]\cdot\mathbf{n}d\Gamma+\int_{\Gamma_+}\hat{C}^r[\mathbf{q}\hat{C}_E+\mathbf{D}\nabla\hat{C}_E]\cdot\mathbf{n}d\Gamma+\int_{\Gamma_-}\hat{C}^r[\mathbf{q}\hat{C}_E+\mathbf{D}\nabla\hat{C}_E]\cdot\mathbf{n}d\Gamma\\&+\int_{\Gamma_n}\hat{C}_E[\mathbf{q}\hat{C}^r-\mathbf{D}\nabla\hat{C}^r]\cdot\mathbf{n}d\Gamma+\int_{\Gamma_+}\hat{C}_E[\mathbf{q}\hat{C}^r-\mathbf{D}\nabla\hat{C}^r]\cdot\mathbf{n}d\Gamma+\int_{\Gamma_-}\hat{C}_E[\mathbf{q}\hat{C}^r-\mathbf{D}\nabla\hat{C}^r]\cdot\mathbf{n}d\Gamma\\&=\int_\Omega\hat{C}_E m^*\delta(\mathbf{x}-\mathbf{x}_i)d\Omega+\int_\Gamma\mathbf{q}(\hat{C}^r\hat{C}_E)\cdot\mathbf{n}d\Gamma-\int_\Omega(\hat{C}^r\hat{C}_E)\nabla\cdot\mathbf{q}d\Omega+\int_\Omega(\hat{C}^r\hat{C}_E)Q_I d\Omega\end{aligned} \qquad \text{(E4.1.4)}$$

The first and second lines of Eq. (E4.1.4) are simplified by accounting for the boundary conditions of Eq. (E4.1.3) on Γ_+ (zero flux) and Γ_n, and for the boundary condition of Eq. (E4.1.2) on Γ_- (zero flux), and by neglecting C^r on Γ_- and C_E on Γ_+. We also assume that for short times the resident concentration C^r can be neglected at the outlet Γ_n, and that C_E vanishes rapidly on Γ_n, since the Cauchy type boundary condition in Eq. (E4.1.3) is homogeneous for $t>0$. The first term of the second line of Eq. (E4.1.4) is then neglected. The first domain integral on the right-hand side of Eq. (E4.1.4) is simply the life expectancy $C_E(\mathbf{x}_i,t)$ at the source location times the injected mass m^*. The second term can be neglected by assuming that C^r is zero on Γ_n and Γ_+ for short times, but also on Γ_- at $t>0$, and that C_E is also zero on Γ_+ and Γ_n for larger times. The last two terms also vanish since $\nabla\cdot\mathbf{q}=Q_I$. Finally, after simplification and inversion of the Laplace transforms, Eq. (E4.1.4) becomes:

$$\int_{\Gamma_n}\mathbf{q}C^r(\mathbf{x},t)\cdot\mathbf{n}d\Gamma=m^*C_E(\mathbf{x}_i,t) \qquad \text{(E4.1.5)}$$

Normalizing Eq. (E4.1.5) by the steady flow rate $F_{0,n}$ yields

$$\bar{C}_n^r(t) = \frac{1}{F_{0,n}} \int_{\Gamma_n} \mathbf{q} C^r(\mathbf{x},t) \cdot \mathbf{n} d\Gamma = \frac{m^* C_E(\mathbf{x}_i,t)}{F_{0,n}} = m^* C_E^{\mathbf{x}}(\mathbf{x}_i,t) \tag{E4.1.6}$$

where $C_E^{\mathbf{x}}(\mathbf{x},t)$ is the life-expectancy-to-outlet pdf scaled by the outlet flow rate, which at the source injection location $\mathbf{x} = \mathbf{x}_i$ equals the flow rate normalized flux-weighted relative resident concentration $\bar{C}_n^r(t)$ at the outlet Γ_n. If the outlet is a pumping-well ($\Gamma_n = \Gamma_w$, $F_{0,n} = Q_w$), then for a unit mass input ($m^* = 1$) Eq. (E4.1.6) simplifies in

$$C^r(\mathbf{x}_w,t) = \frac{C_E(\mathbf{x}_i,t)}{Q_w} = C_E^{\mathbf{x}}(\mathbf{x}_i,t) \tag{E4.1.7}$$

Eq. (E4.1.7) shows that the expected resident concentration at the pumping-well, resulting from an instantaneous unit mass release, is predicted by the life expectancy pdf at the injection point, scaled by the pumping-well flow rate. The function $g_{\mathbf{x}}(\mathbf{x}_w, t) = C^r(\mathbf{x}_w, t)/m^*$ at the well is the travel distance pdf (see Eq. (2.12)), and is equivalent to the flow rate normalized life-expectancy-to-well pdf at the injection point $\mathbf{x} = \mathbf{x}_i$:

$$g_{\mathbf{x}}(\mathbf{x}_w,t) = C_E^{\mathbf{x}}(\mathbf{x}_i,t) \tag{E4.1.8}$$

The flow rate scaled life-expectancy-to-outlet pdf $C_E^{\mathbf{x}}(\mathbf{x},t)$ can be compared to the backward location probability in the sense of Neupauer & Wilson [1999, 2001, 2002].

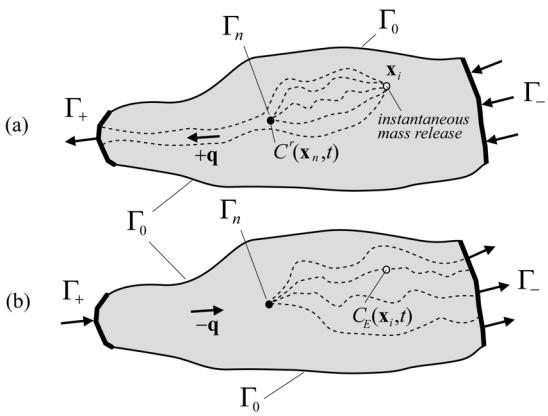

Fig. 4.13. Schematic illustration of the backward transport problem equivalent to the forward transport problem: (a) Forward transport of an instantaneous mass release; (b) Backward transport of the life-expectancy-to-outlet Γ_n.

If the mass release at $\mathbf{x} = \mathbf{x}_i$ is not instantaneous, but dependent on time t such that the source term in Eq. (E4.1.1) may be formalized by $S(t) = \delta(\mathbf{x} - \mathbf{x}_i)\, m^*(t)$, then Eq. (E4.1.6) takes the form:

$$\bar{C}_n^r(t) = \int_0^t C_E^{\mathbf{x}}(\mathbf{x}_i,u) m^*(t-u) du \tag{E4.1.9}$$

With Eq. (E4.1.9), the concentration at outlet is approximated by the convolution integral of the scaled life-expectancy-to-outlet pdf at $\mathbf{x} = \mathbf{x}_i$ with the transient input function. If the mass is distributed over a region of finite size Δ, then Eq. (E4.1.6) takes the form:

$$\bar{C}_n^r(t) = \frac{1}{F_{0,n}} \int_{\Omega} \left(\int_0^t C_E(\mathbf{x}_i,u) m^*(t-u) du \right) \delta(\mathbf{x} - \mathbf{x}_i)\, d\Omega \quad , \quad \mathbf{x}_i \in \Delta \tag{E4.1.10}$$

Note that Eqs. (E4.1.6)–(E4.1.10) are approximations, since some boundary integral terms in Eq. (E4.1.4) have been neglected. It can be expected that in highly dispersive systems, if the injection is located too close to inflowing limits, then the backward movement effects by dispersion may induce some differences between the forward solution and the proposed approximations. However, we have verified that Eqs. (E4.1.6)–(E4.1.10) still yield very good approximations of the forward solution when a high level of dispersion is used, and when the source location is close to the boundaries. For a 1D configuration, one can show that (E4.1.8) is exact. We consider a 1D semi-infinite domain $x \in [0;\infty[$. We apply a double Laplace transform L^2 (see E2.2.6) to the 1D form of (E4.1.1) for eliminating the variables x and t:

$$s\tilde{C} = -rv\tilde{C} + r^2 D\tilde{C} - rD\hat{C}(0,s) + \tilde{m}^*(r) \tag{E4.1.11}$$

with r denoting the Laplace variable for the transformation with respect to x. By letting

$$\omega = \sqrt{1+\frac{4Ds}{v^2}} \qquad \alpha_1 = \frac{v(1-\omega)}{2D} \qquad \alpha_2 = \frac{v(1+\omega)}{2D} \quad ,$$

one can write (E4.1.11) according to the following:

$$s\tilde{C}(r,s) = \frac{1}{D(\alpha_2-\alpha_1)}\left(\frac{D\alpha_2\hat{C}(0,s)-\tilde{m}^*(r)}{r-\alpha_2} - \frac{D\alpha_1\hat{C}(0,s)-\tilde{m}^*(r)}{r-\alpha_1}\right) \quad , \tag{E4.1.12}$$

and since $\mathrm{L}\{e^{-ax}, x, r\} = 1/(r+a)$, Eq. (E4.1.12) can be inverted for x to give

$$\hat{C}(x,s) = \frac{1}{D(\alpha_2-\alpha_1)}\left(e^{\alpha_2 x}\left[D\alpha_2\hat{C}(0,s) - \int_0^x e^{-\alpha_2 y}m(y)dy\right] - e^{\alpha_1 x}\left[D\alpha_1\hat{C}(0,s) - \int_0^x e^{-\alpha_1 y}m(y)dy\right]\right) \tag{E4.1.13}$$

where use has been made the convolution theorem (E2.2.5). Using the Cauchy condition in (E4.1.1), and accounting for the fact that $\alpha_2 > 0$, we have:

$$\hat{C}(0,s) = \frac{1}{D\alpha_2}\int_0^\infty e^{-\alpha_2 y}m(y)dy \tag{E4.1.14}$$

By substituting ω, α_1, α_2 and (E4.1.14) into (E4.1.13), and by making use of the shifting theorem for inverting the Laplace transforms with respect to s, Eq. (E4.1.13) becomes:

$$C(x,t) = \int_0^\infty \frac{m(y)}{\sqrt{4\pi Dt}}e^{-\frac{(x-y+vt)^2}{4Dt}}dy + \int_0^\infty \frac{m(y)}{\sqrt{4\pi Dt}}e^{-\frac{-xy}{Dt}}e^{-\frac{(x-y-vt)^2}{4Dt}}dy - \frac{v}{2D}e^{\frac{vx}{D}}\int_0^\infty m(y)\,\mathrm{erfc}\left(\frac{(y+x+vt)}{2\sqrt{Dt}}\right)dy \tag{E4.1.15}$$

for which the following Laplace transforms have been used:

$$\mathrm{L}\left\{\frac{1}{\sqrt{\pi t}}e^{-\frac{a^2}{4t}}\right\} = \frac{1}{\sqrt{s}}e^{-a\sqrt{s}} \quad \text{and} \quad \mathrm{L}^1\left\{\frac{1}{\sqrt{\pi t}}e^{-\frac{b^2}{4t}} - a\exp\left(a^2t+ab\right)\mathrm{erfc}\left(\frac{b}{2\sqrt{t}}+a\sqrt{t}\right)\right\} = \frac{1}{a+\sqrt{s}}e^{-b\sqrt{s}}$$

Finally, since $m^*(y) = \delta(y-x_i)/\phi$ the integrals in (E4.1.15) can be solved to give

$$C(x,t) = \frac{1}{\phi\sqrt{\pi Dt}}\exp\left(-\frac{1}{4}\frac{(x-x_i-vt)^2}{Dt}\right) - \frac{v}{2\phi D}\exp\left(\frac{v(x-x_i)}{D}\right)\mathrm{erfc}\left(\frac{x-x_i+vt}{2\sqrt{\pi Dt}}\right) \tag{E4.1.16}$$

The life expectancy resident pdf $C_E(x,t)$ is given by Eq. (E2.3.1), after substitution of x by $L-x$, if L is a characteristic length (supposed outlet position). Comparing it with (E4.1.16), one can see that (E4.1.8) is exact:

$$g_{\mathbf{x}}(L,t) = C(L,t) = C_E^{\mathbf{x}}(x_i,t) = \frac{C_E(x_i,t)}{\phi v} \tag{E4.1.17}$$

4.4.4. Example: Well-head protection zones and intrinsic vulnerability assessment in the Seeland aquifer (North-West Switzerland)

The unconfined Seeland aquifer is situated in the north-western part of Switzerland, on the molassic plateau in the region of Bienne (Fig. 4.14). This alluvial aquifer of Quaternary deposits covers approximately 70km^2, and consists mainly of a heterogeneous set of well sorted gravels, sandy gravels and silty sands. The average thickness of the aquifer is about 20 to 30m, and the maximum thickness is about 50m.

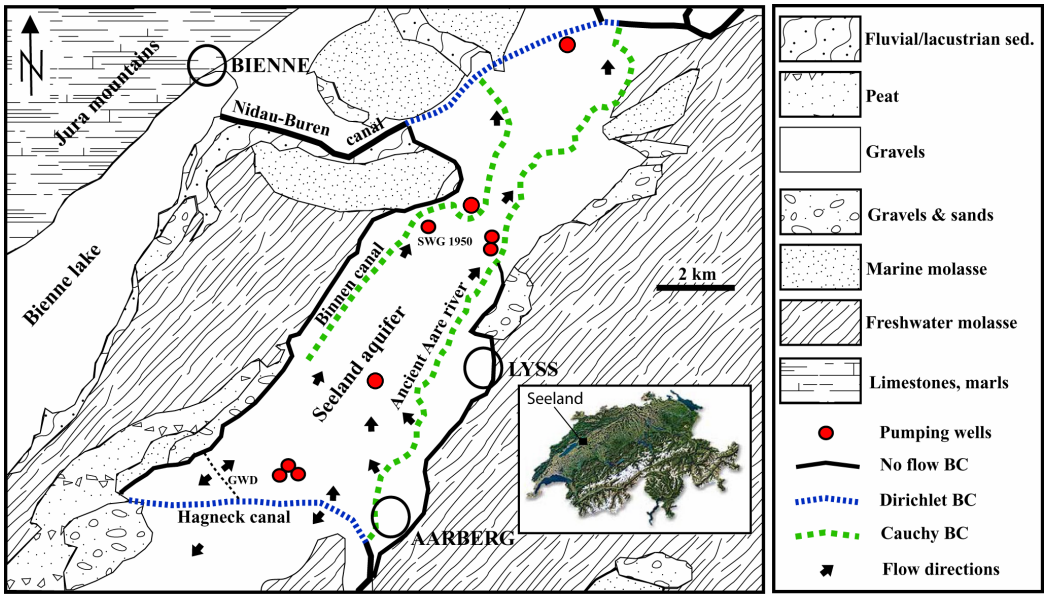

Fig. 4.14. Situation map of the Seeland aquifer (North-Western part of Switzerland) with indicated flow boundary conditions (The Cauchy BC relates to a transfer-type condition on rivers or canals).

A 2D horizontal finite element flow model was built by Jordan [2000] with the FEFLOW4.8 software package, and calibrated under both steady- and transient-state flow regimes. With this model, Jordan [2000] also designed the Z_u protection zone of the SWG1950 pumping well (location in Fig. 4.14).

The absolute and temporal capture zones, Z_u-zones, and intrinsic vulnerability maps for the SWG1950 pumping-well have been performed in the present work by using the hydraulic model designed by Jordan [2000] with, however, a refined mesh in order to work with average element sizes of 25-50m. The coefficient of longitudinal dispersivity α_L is fixed at 20m ($\alpha_T = 0.1\alpha_L$), and a porosity of 15% is uniformly distributed. To design the Z_u-zone, Jordan [2000] considered pseudo-steady state low water conditions corresponding to the mean annual effective infiltration intensity of 1 mm/d, which he also compared to the infiltration intensity of 0.1 mm/d. The calculated hydraulic heads corresponding to these two recharge conditions are shown in Fig. 4.15.

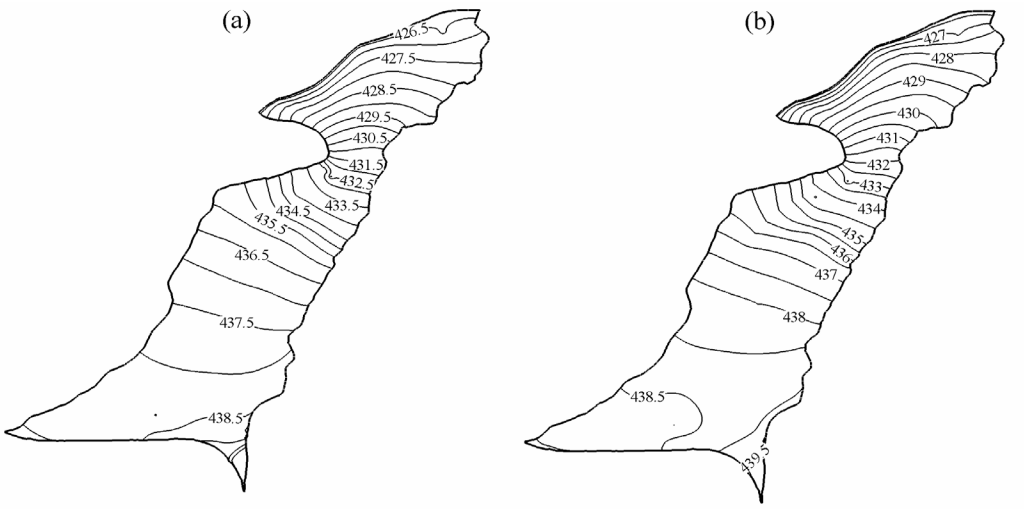

Fig. 4.15. Finite element flow model of the Seeland aquifer. Hydraulic head distribution in masl: (a) Infiltration rate $Q_I = 0.1$ mm/d; (b) Infiltration rate $Q_I = 1$ mm/d.

Fig. 4.16 shows the absolute capture zone for the two tested infiltration intensities ($Q_I = 0.1$ mm/d and $Q_I = 1$ mm/d), computed with the steady-state form of the boundary value problem (4.17). From these probability fields of exit at the SWG1950 pumping-well, the pluvial and river/canals contributions to the well outflow are separated and evaluated by enforcing Eq. (4.19) (see Table 1). For increasing values of the infiltration rate, the lateral extend of the absolute capture zone decreases. A consequence is the decreasing contribution along the limits to the outflow at the well. For the low infiltration intensity $Q_I = 0.1$ mm/d, the pluvial contribution is only 13.916% of the well discharge rate, the capture zone is wide and intersects inflowing portions of the ancient Aare river, as well as some inflowing portions of the Binnen and Hagneck canals (see Fig. 4.14 for their location).

For the mean annual infiltration intensity $Q_I = 1$ mm/d, the pluvial contribution is 79.388% of the well discharge rate, the capture zone is much thinner and shows quite clearly the portion of the ancient Aare river which infiltrates the water that can be pumped at the well. The corresponding Z_u protection zones are also given in Fig. 4.16. For the lowest tested infiltration rate $Q_I = 0.1$ mm/d, the Z_u-zone is contained within the probability iso-line 45.375% (6.3% of the total area of the absolute capture zone), and has still an important lateral extend in relation to the small contribution from rain infiltration. For the infiltration rate $Q_I = 1$ mm/d, the Z_u-zone is contained within the probability iso-line 59.35% (7.1% of the total area of the absolute capture zone). Since the flow rate provided by the areal infiltrations is still not sufficient to balance 90% of the well flow rate, some inflowing portions of the ancient Aare river must be included into the Z_u-zone.

Table 1
Capture zones and Z_u-zones extend [m^2], and evaluation of the pluvial and limits contributions [%] to the SWG1950 pumping-well discharge ($Q_w = 3600$ m^3/d).

Q_I	Capture zone area	Z_u-zone area	Limits contribution	Pluvial contribution
0.1 mm/d	7.14×10^7	4.51×10^6	86.084	13.916
1.0 mm/d	3.60×10^7	2.57×10^6	20.612	79.388

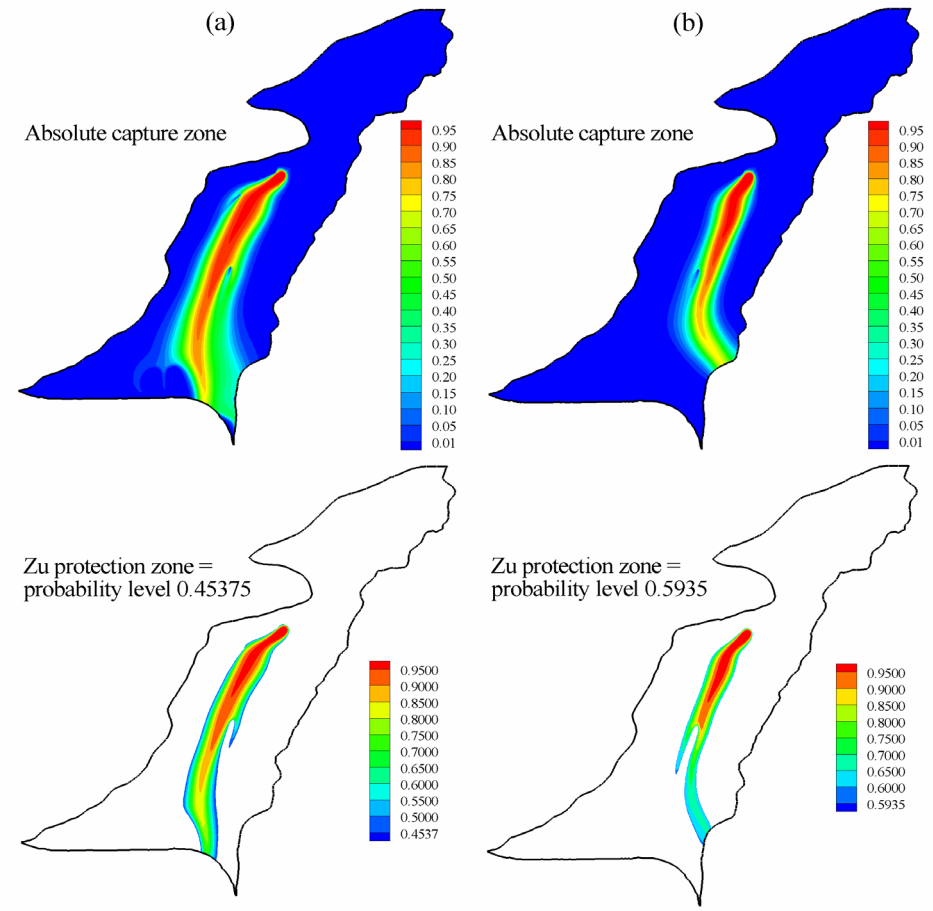

Fig. 4.16. SWG1950 pumping-well absolute capture zones and Z_u-zones: (a) Infiltration rate $Q_I = 0.1$ mm/d; (b) Infiltration rate $Q_I = 1$ mm/d.

The temporal capture zones as well as the life-expectancy-to-well pdf field are given in Fig. 4.17, for the infiltration rate $Q_I = 1$ mm/d. The one-year and three-years capture zones have a relatively small extend. They are not connected to the inflowing limits of the aquifer (except a little with the Binnen canal in the neighbourhood of the well). This observation is correlated with the information given by the well transit time pdf φ in Fig. 4.18a, which shows that the major contribution is of pluvial origin until 3years, the rest of the curve with the series of peaks being a mixture of the limits and the pluvial contributions. The strong pluvial contribution to the well outflow rate is marked by high density values for the transit time pdf φ at origin. For the infiltration rate $Q_I = 0.1$ mm/d, the well transit time pdf is principally bimodal, which attests of the main contribution of the canals and rivers to the well outflow rate. The origin of the first peak can be attributed to the water particles infiltrated by the Binnen canal, while the second peak is due to the infiltrations of the ancient Aare river. For the two tested infiltration rates, significant water quantities with age dates up to 25years can be found at the pumping-well.

The functions A(t) and $M(t)$ in Fig. 4.18b diverge at early times, in relation to the imposed areal infiltration which creates short travel times to the pumping-well. The important tailing effect on the function A(t) for the low infiltration rate $Q_I = 0.1$ mm/d is related to the large extend of the absolute well capture zone, causing collection of water particles with very different infiltration locations. At the contrary, for the case $Q_I = 1$ mm/d the function A(t) does not show important tailing effects, since the origin of the infiltrations by the limits is confined along a single continuous portion of the ancient Aare river (see Fig. 4.16b).

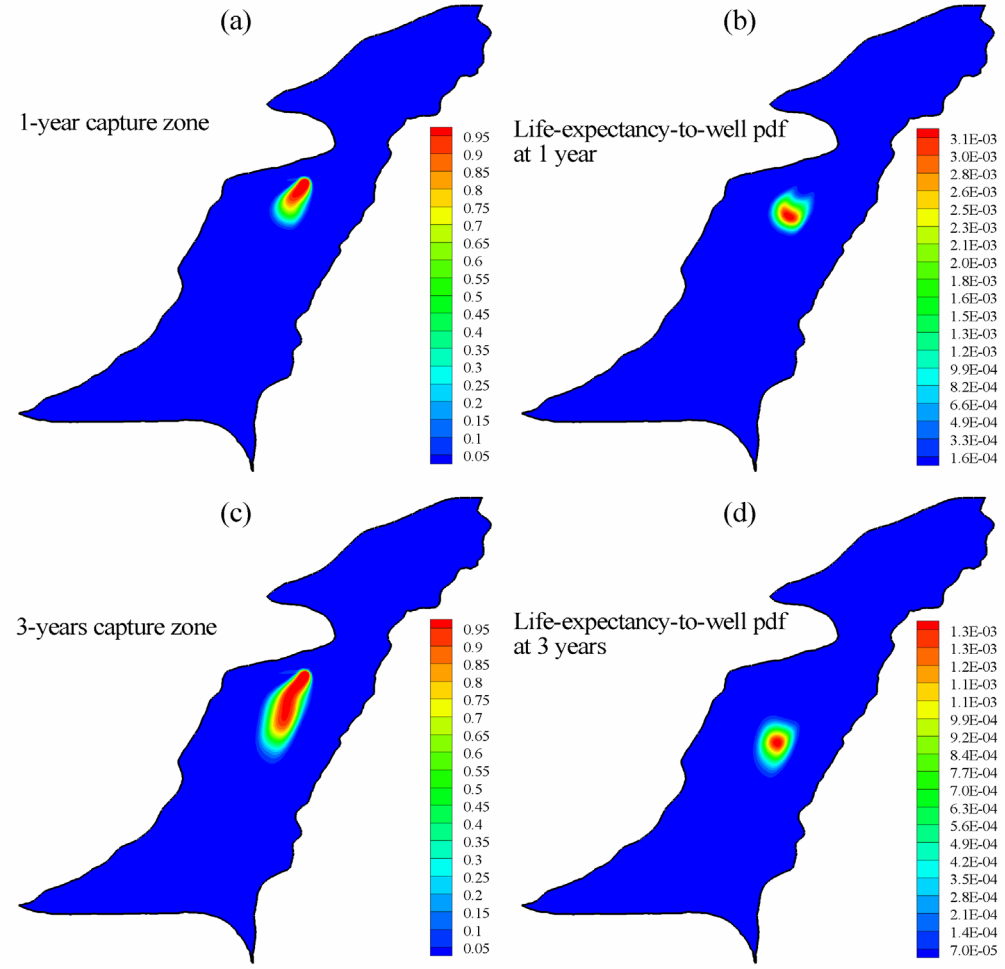

Fig. 4.17. Life-expectancy-to-well pdf and cdf fields for the SWG1950 pumping-well (Q_I = 1 mm/d): (a) One-year capture zone; (b) Life-expectancy-to-well pdf at one year; (c) Three-years capture zone; (d) Life-expectancy-to-well pdf at three years.

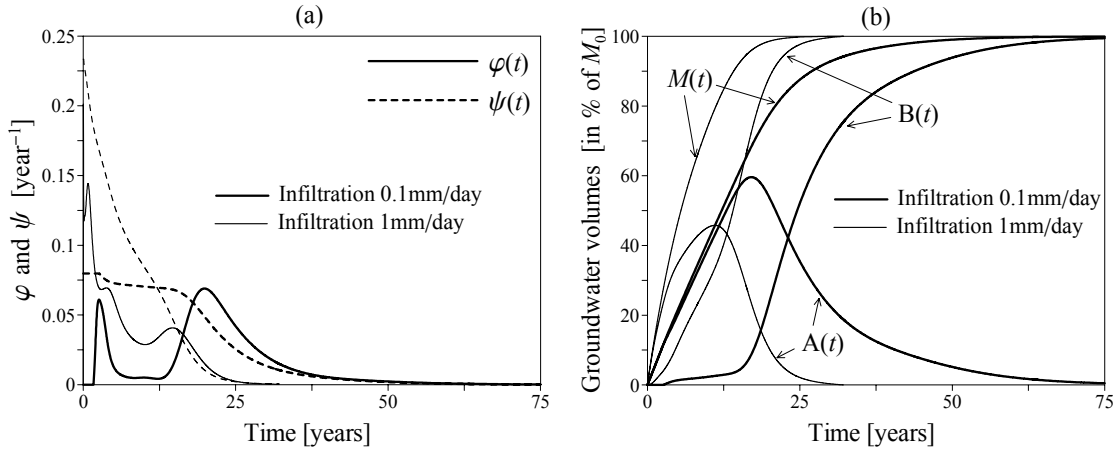

Fig. 4.18. BRT functions and internal groundwater volumes for the SWG1950 pumping-well: (a) Internal age pdf ψ and well transit time pdf φ; (b) Internal groundwater volume functions.

The intrinsic vulnerability maps to source contamination resulting from the post-processes described in section 4.4.3 and Excursus 4.1 are presented in Fig. 4.19. The maximum relative concentration expected at the SWG1950 pumping-well does not exceed the level 1.0×10^{-5}, which however must not be taken as a sign of low vulnerability. On the other hand, the times required to reach the maximum concentration at the well are considerably high, as predicted by the well transit time pdf. For many reasons, of course these maps are simply a rough image of reality. The aquifer is generally unconfined with relatively small saturated thicknesses. A 2D horizontal model can then be acceptable, although the aquifer thickness may attain 50m at some locations (mostly in the southern extremity). However, no transport processes within the unsaturated zone can be simulated. Also, the heterogeneity of permeability is badly known, yielding uncertainties in the simulated velocity fields. Field tracer tests could represent a means to calibrate the protection zones and vulnerability maps.

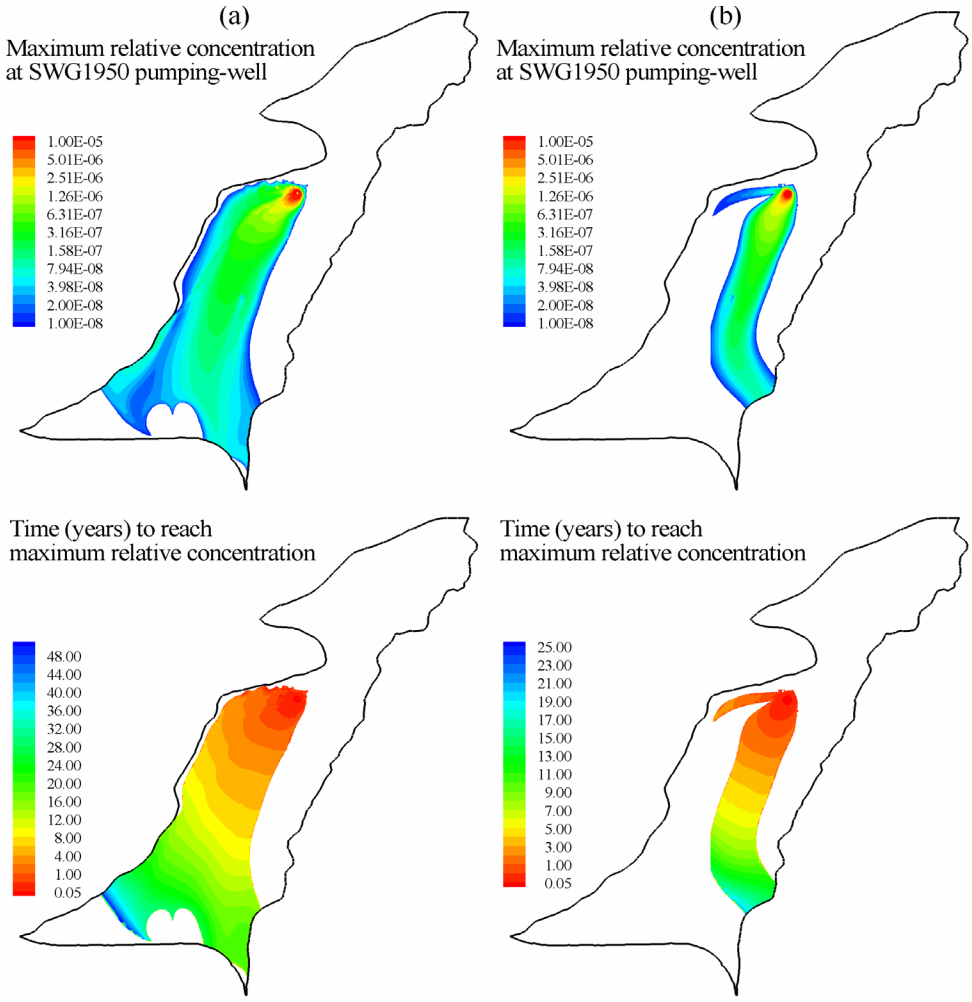

Fig. 4.19. Vulnerability maps for the SWG1950 pumping-well: (a) Infiltration rate $Q_I = 0.1$ mm/d; (b) Infiltration rate $Q_I = 1$ mm/d.

The groundwater of the Seeland aquifer suffers from a diffuse nitrate contamination, which in many parts of the plain exceeds the threshold value of 40mg/l, like e.g. in the extracted water of the SWG1950 pumping-well. The calculated average age at the SWG1950 pumping-well varies between approximately 4.2 years ($Q_I = 1$ mm/d, second peak of the curve in Fig. 4.18a) and 11 years ($Q_I = 0.1$ mm/d, in between the two peaks of the curve in Fig. 4.18a). Significant densities of probability for the arrival times at this well can also be found for ages superior to 40 years. If we consider that the sources of nitrates and fertilizers were massively introduced since the 1960s, one

might expect steadily declining water quality some decades from now, even if the diffuse application of chemicals is nowadays reduced or stopped.

The vulnerability to diffuse contamination could be simulated by post-processing Eq. (E4.1.10), which allows the prediction of the concentration at the well with respect to a diffuse input of contaminants over a region of finite size. With this equation, future evolution of nitrate concentration at the well could be predicted by taking the spatial organization of the agricultural activity of the plain into account. The most influential agricultural zones could also be identified with such easy post-processes, and in this way improve the fertilizing practises in the plain.

Eq. (E4.1.10) can also be used as a means to optimize the planning of potential polluting installations (rubbish dumps, chemical industries, sewage plants, etc…). Once the life-expectancy-to-well field C_E is known, a production function $m^*(t)$ can be chosen, and integration performed on the sub-domain of the potential site to evaluate the expected resident concentration at the well. This point will be further developed in the next section.

4.5. Large space- and time-scale forward and backward modelling of contaminant transport: the problem of the underground storage of high-level nuclear waste.

Large scale simulations in space and time are generally not easily handled by numerical codes. Particularly the time-stepping procedure quickly becomes a limiting factor and reveals to be intensive CPU-time consuming, when the simulated periods exceed the order of decades. The LTG technique [Sudicky, 1989] presents the considerable advantage that the computational burden for a thousands of years simulation is comparable to the one of a ten years simulation. Moreover, it can handle coarser meshes than conventional simulation codes.

In the planning of an underground nuclear waste repository, the indubitable release of radioactive contaminants from the repository and their migration within the groundwater reservoir to the biosphere must be considered. In Chapter 3, we have seen that the LTG can handle the backward transport of the life expectancy pdf within a network of discrete pipes embedded in a 3D continuum matrix (see section 3.3.3). The LTG technique proved to be very efficient in large scale aquifer formations containing complex discrete features, like faults and fractures [Sudicky & McLaren, 1992]. In the following, we show the advantages provided by the forward and backward transport modelling approaches in combination with the LTG technique, when dealing with the problem of underground storage of radioactive waste. This problem involves simulation over very large space and time scales of reservoirs within which high parameter contrasts exist.

4.5.1. Modelling approaches

Forward approach

For the proposed problem of the impact of a nuclear waste repository, the forward transport modelling approach is suitable for the prediction of the future position of the contaminants, given the location of the repository. In the present analysis, the transport of radioactive contaminants is simulated by the following form of the ADE:

$$\frac{\partial \phi R C}{\partial t} = -\nabla \cdot \mathbf{q} C + \nabla \cdot \mathbf{D} \nabla C + m^*(t) - \phi R \lambda C \qquad \text{in} \quad \Omega \tag{4.26}$$

$$C(\mathbf{x},0) = C(\mathbf{x},\infty) \qquad \text{in} \quad \Omega$$

$$[\mathbf{q}C - \mathbf{D}\nabla C]\cdot \mathbf{n} = 0 \qquad \text{on} \quad \Gamma_0 \cup \Gamma_-$$

where C is resident concentration, λ is the first-order decay constant [T^{-1}], and where $m^*(t)$ is a time-dependent source [$M/L^3/T$] distributed over the waste repository region, which corresponds to the production function of the nuclear repositories. The retardation factor R [−] is assumed to be dependent on the linear adsorption law of Henry, $R = 1 + \beta(1-\phi)/\phi$, with β [−] denoting the slope of Henry's isotherm. In Eq. (4.26), the *Implicit Neumann* condition can be used on Γ_+. In the following, the forward transport LTG solutions will be denoted as FLTG.

Backward approach

The backward transport modelling approach proved to be efficient for the prediction of past contaminant source locations, given the future positions [Wilson & Liu, 1997; Neupauer & Wilson, 1999, 2001]. For the present problem, the backward approach can help to optimize the planning of future waste repository locations, by considering the groundwater contamination they will induce.

With Eq. (3.65), we have seen that a source of age probability in the forward equation becomes a sink of life expectancy probability in the backward equation. In adjoint operator theory, linear processes in the forward model, such as linear decay, remain unchanged in the backward model. The effect of decay during the evolution of a contaminant particle forward-in-time from one point to one other must be the same as during the evolution backward-in-time, the travel path and distance being identical in both cases. Letting L^f be the linear forward operator, in which case Eq. (4.26) is $L^f(C^r) = m^*(t)$, then the backward operator L^b is

$$L^b() = \frac{\partial \phi R()}{\partial t} - \nabla \cdot \mathbf{q}() - \nabla \cdot \mathbf{D} \nabla() + \phi R \lambda() \tag{4.27}$$

Consequently, the adjoint backward boundary value problem is:

$$\begin{aligned}
&\frac{\partial \phi R C_E}{\partial t} = \nabla \cdot \mathbf{q} C_E + \nabla \cdot \mathbf{D} \nabla C_E - \phi R \lambda C_E && \text{in} \quad \Omega \\
&C_E(\mathbf{x}, 0) = C_E(\mathbf{x}, \infty) && \text{in} \quad \Omega \\
&\mathbf{J}_E(\mathbf{x}, t) \cdot \mathbf{n} = -\mathbf{q} \cdot \mathbf{n} \delta(t) && \text{on} \quad \Gamma_n \\
&\mathbf{J}_E(\mathbf{x}, t) \cdot \mathbf{n} = 0 && \text{on} \quad \Gamma_+ \\
&\mathbf{D} \nabla C_E \cdot \mathbf{n} = 0 && \text{on} \quad \Gamma_0
\end{aligned} \tag{4.28}$$

In Eq. (4.28), the *Implicit Neumann* condition can be used on Γ_-. The dependent variable C_E does not characterize the groundwater particles life expectancy, as it used to be previously. The variable C_E characterizes the pdf for the time required for a decaying contaminant initially situated at a given point within the repository site location to reach the outlet Γ_n. The travel times from the initial point to the outlet are the same as with a conservative substance (except for $R \neq 1$), but the corresponding density of probability decays over time. Consequently, we still use the symbol C_E to characterize the life-expectancy-to-outlet pdf of a specific substance. In the forward model, the contamination is decaying with time. In the backward model, the probability that the contaminant particle has decayed before reaching the outlet Γ_n increases with backward time [Neupauer & Wilson, 2003], i.e. the time required by the particles to travel from the outlet Γ_n ($t = 0$) to the repository site location.

To evaluate the resident concentration at the outlet Γ_n, which would result from the release of radio-nuclides at the repository site location (i.e. a solution of Eq. (4.26)), the post-process given by Eq. (E4.1.10) is realized. Note that the decay terms in the forward and backward equations (4.26) and (4.28) annihilate when the procedure described in Excursus 4.1 is applied, such that Eq. (E4.1.10) can still be used for decaying substances:

$$C_E^{\mathbf{x}}(\mathbf{x},t)=\frac{C_E(\mathbf{x},t)}{F_{0,n}} \tag{4.29a}$$

$$\bar{C}_n^r(t)=\int_\Delta\int_0^t C_E^{\mathbf{x}}(\mathbf{x},u)\,m^*(\mathbf{x},t-u)\,du\,d\mathbf{x}=\mathrm{L}^{-1}\left\{\int_\Delta \hat{C}_E^{\mathbf{x}}(\mathbf{x},s)\,\hat{m}^*(\mathbf{x},s)\,d\mathbf{x}\right\} \tag{4.29b}$$

with Δ representing the repository site spatial extend, L^{-1} the inverse Laplace operator, and $\mathbf{x}=(x,y,z)$.

Eq. (4.29) is comparable to a transfer function equation. The flow rate normalized life-expectancy-to-outlet (4.29a) is the same function as in section 4.4. The life expectancy pdf C_E at a position $\mathbf{x}$ in Δ acts as the transfer function of the transport domain relative to the transport of a unit and instantaneous mass release at $\mathbf{x}$, towards Γ_n. By convolution with the transient input function $m^*(t)$, and by summation of each contribution in Δ, the flux-weighted resident concentration at Γ_n is predicted. As discussed in Excursus 4.1, Eq. (4.29) is an approximation, since some boundary integrals have be neglected.

However, the errors induced by this approximation can only be significant when the situation of a high dispersion and Δ being close to an inflowing boundary is encountered. An obvious advantage of Eq. (4.29) is that the outlet concentration is calculated without any operation along the outflowing boundary, so that the gain in accuracy can be compared to the one obtained with the RT, when the internal age or life expectancy occurrence is integrated to evaluate an outlet transit time pdf (see Chapter 3). The principle of superposition inherent in Eq. (4.29) holds as long as the velocity field and the diffusive parameters are assumed to be time-independent, which is the case in the present work. In the following, the solutions derived from the LTG solution of (4.28) and of the post-process (4.29) will be denoted as BLTG.

4.5.2. Example

We make use of a theoretical 2D vertical reservoir to illustrate the application of the post-process (4.29). The computational benefits of the LTG technique are also compared to the classical solution of the ADE with time-stepping procedure. The system is schematized in Fig. 4.20a, with indicated flow boundary conditions. The system contains four layers with high hydraulic conductivity contrasts. Two radioactive waste repositories are situated within the third layer (R1 and R2 in Fig. 4.20a), which could be compared to a clay formation, and are supposed to produce a specific radionuclide according to a triangle-shaped production function $m^*(t)$.

The hydraulic head distribution is given in Fig. 4.20c. The two main outlets of the system (at $\mathrm{X}=0$ in Fig. 4.20a) are the outlets of layer2 (steady flow rate $Q_2=8.33298\,\mathrm{m^3/y}$) and of layer3 (steady flow rate $Q_3=0.58463\,\mathrm{m^3/y}$). The outlet of layer1 produces the small flow rate $Q_1=0.02991\,\mathrm{m^3/y}$. The Darcy fluxes are horizontal within layer2 (max. $q_\mathrm{X}=-3\times10^{-2}\,\mathrm{m/y}$) and layer3 (max. $q_\mathrm{X}=-3\times10^{-3}\,\mathrm{m/y}$). Within the low-permeability host unit, the Darcy fluxes are vertically descending (max. $q_\mathrm{Z}=-7\times10^{-7}\,\mathrm{m/y}$) in the neighbourhood of the repositories, and vertically ascending downstream of the repositories (max. $q_\mathrm{Z}=3\times10^{-6}\,\mathrm{m/y}$), as a consequence of the gradient inversion between layer2 and layer3. The flow and transport parameters are given in Table 2. Note that the porosity of the host layer varies with the type of contaminant (different sorption effects), and must therefore be viewed as a transport porosity, or effective porosity. The transport problem is numerically unstable, particularly due to the zero longitudinal and lateral dispersivities in the host layer and in layer1.

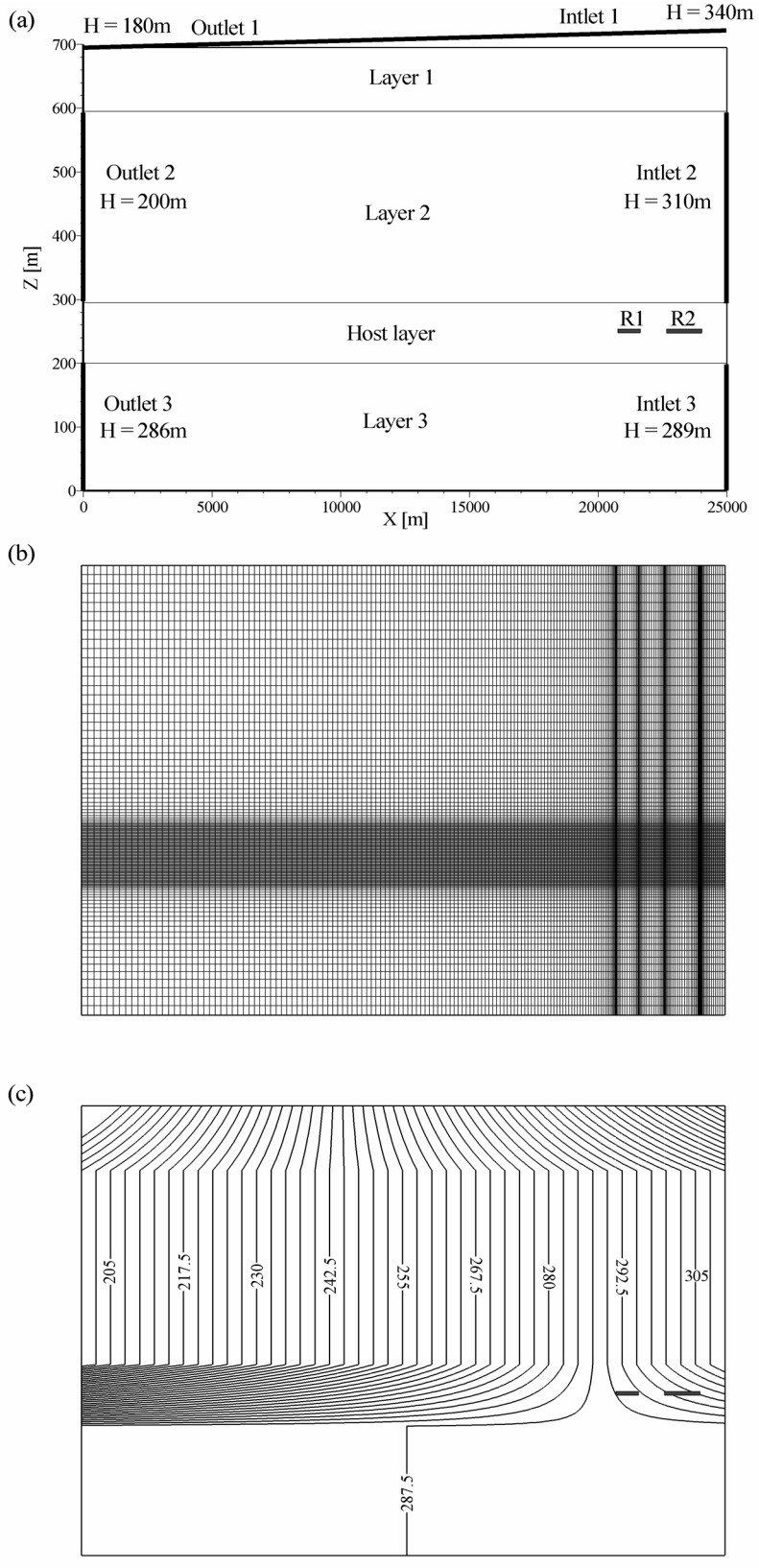

Fig. 4.20. Hypothetical 2D vertical aquifer: (a) Geometry, flow boundary conditions and location of the depositories R1 and R2; (b) Finite element mesh (27392 linear quadrangles; $\Delta x_{min} = \Delta z_{min} = 1.5$m, $\Delta x_{max} = 250$m, $\Delta z_{max} = 15$m); (c) Hydraulic heads in meters. Vertical exaggeration: 25.

Table 2
Flow and transport parameters for the hypothetical aquifer of Fig. 4.20.

Layer	1	2	Host	3
K [$\times 10^{-4}$ m/s]	10^{-8}	2×10^{-3}	10^{-9}	8×10^{-3}
ϕ [−]	0.100	0.100	0.001	0.100
α_L [m]	0	50	0	50
α_T [m]	0	1	0	1
D_m [$\times 10^{-9}$ m^2/s]	0.159	0.159	0.030	0.159
R [−]	1	1	1	1
λ [$\times 10^{-4}$ 1/s]	1.4×10^{-11}	1.4×10^{-11}	1.4×10^{-11}	1.4×10^{-11}

In Fig. 4.21 we compare the solution of the FLTG to the solution of the BLTG. The forward ADE (4.26) was also solved with a time-stepping procedure, by using the software FEFLOW 5.0. The non-diffusive Crank-Nicholson scheme is used for the temporal integration. The time-step is 100y for a simulation period of 10My, i.e. 100'000 time-steps. This time-step is still adequate if we consider the 1D stability criteria of Péclet (Pe) and Courant (Cu), although these criteria are theoretically valid only for a homogeneous 1D advective-diffusive transport. For layer2 and layer3, inside which flow is generally horizontal, the product Pe Cu is 0.6 (max. Pe and max. Cu), and in the host layer, this product is $\mathrm{Pe}\,\mathrm{Cu} = 0.05$. The resolution of the linear system is iterative for the three simulations. Since the *Implicit Neumann* condition is not handled by FEFLOW, Eqs. (4.26) and (4.28) were solved with the homogeneous Neumann condition $\mathbf{D}\nabla C \cdot \mathbf{n} = 0$ on Γ_+ and Γ_-, respectively. The mass fluxes at outlet2 and outlet3 are compared (convective part $\mathbf{q}C \cdot \mathbf{n}$ only, since $\mathbf{D}\nabla C \cdot \mathbf{n} = 0$ on Γ_+). The solutions for the three simulations are all in very good agreement. However, the durations of the simulations are incomparable, as attested by the CPU-time in Table 3. This CPU contains the transport solution plus the post-process of the mass fluxes and the cumulated mass for the forward simulations, and the transport solution plus the post-process in Eq. (4.29) for the backward simulation. A number of 25 ($= 2n + 1$) discrete Laplace variables were sufficient to obtain an accurate solution with the LTG scheme.

The discussion of these theoretical results is not the concern of this section. We can note some minor differences between the mass fluxes issued from the FLTG and the ones issued from the BLTG. The FLTG solution must be more affected than the BLTG solution by the high parameter contrasts between the host layer and the aquifer layers (layer 2 and layer 3), and by the fact that $\alpha_L = \alpha_T = 0$ in the host layer. In fact, the resident concentration fronts along these interfaces are sharper than the life-expectancy-to-outlet fronts, since the time to reach the repositories neighbourhood in the backward model is longer than in the forward model (Fig. 4.23). During the early evolution of the concentration plume in the forward model, the extremely low dispersion in the host layer cannot develop its smoothing effect. The time-marching solution is far more concerned by numerical instabilities than the LTG solution, particularly in the neighbourhood of the repositories, where important oscillations are visible (Fig. 4.22). The three simulations also yield slightly different mass budgets (see Table 3). Since these budgets include the mass losses by decay, the mass balance comparison is ambiguous. However, we have verified with similar runs without decay, that the BLTG, with which no post-process along the outlet line is required, provides the best mass restitutions. Note that the injected mass differs a bit in the forward time-marching solution compared to the LTG solutions, caused by a slightly inaccurate input of the temporal function into FEFLOW. This can also explain the very small differences between the shapes of the simulated curves as can be noted in Fig. 4.21.

Table 3
Comparison of the forward and backward computational burden and accuracy.
Mass unit in mol.

Results at t = 10My	FLTG	BLTG	FEFLOW
CPU-time in hours	0.058	0.055	27.124
Total injected mass	11.08759	11.08759	11.03654
Cumulated mass at outlet 2	0.53039	0.52795	0.51281
Cumulated mass at outlet 3	10.12129	10.13063	10.07703
Total	10.65168	10.65862	10.58984

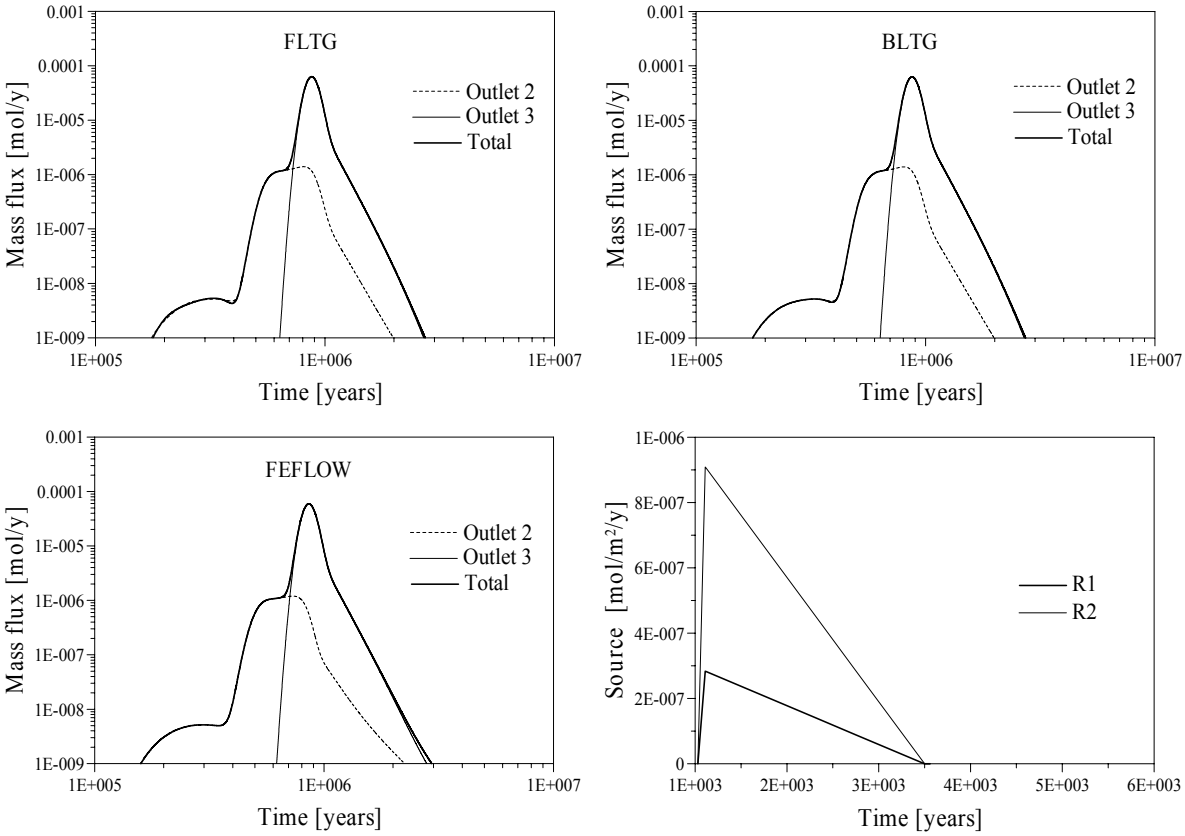

Fig. 4.21. Comparison of results from the FLTG, the BLTG and the time-marching procedures. The triangle-shaped production function in the Laplace domain is obtained by superposition of Heaviside step functions: $\hat{m}^*(s) = \frac{m_0 \exp(-su)}{s^2 t_1 (t_2 - t_1)}[t_2 - t_1 + t_1 \exp(-st_2) - t_2 \exp(-st_1)]$, where u is the time-span before the starting of the signal, t_1 is the time-span between u and the time at which the peak of the production m_0 is reached, and t_2 is the total duration of the production. The total produced mass is $0.5 m_0 t_2$ times the volume of the repository site Δ.

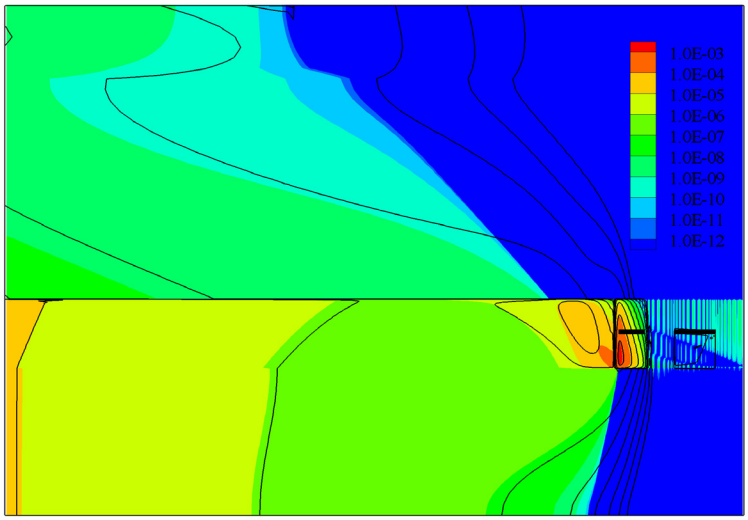

Fig. 4.22. Time marching solution (fringes) versus LTG solution (solid lines) at t = 1My.

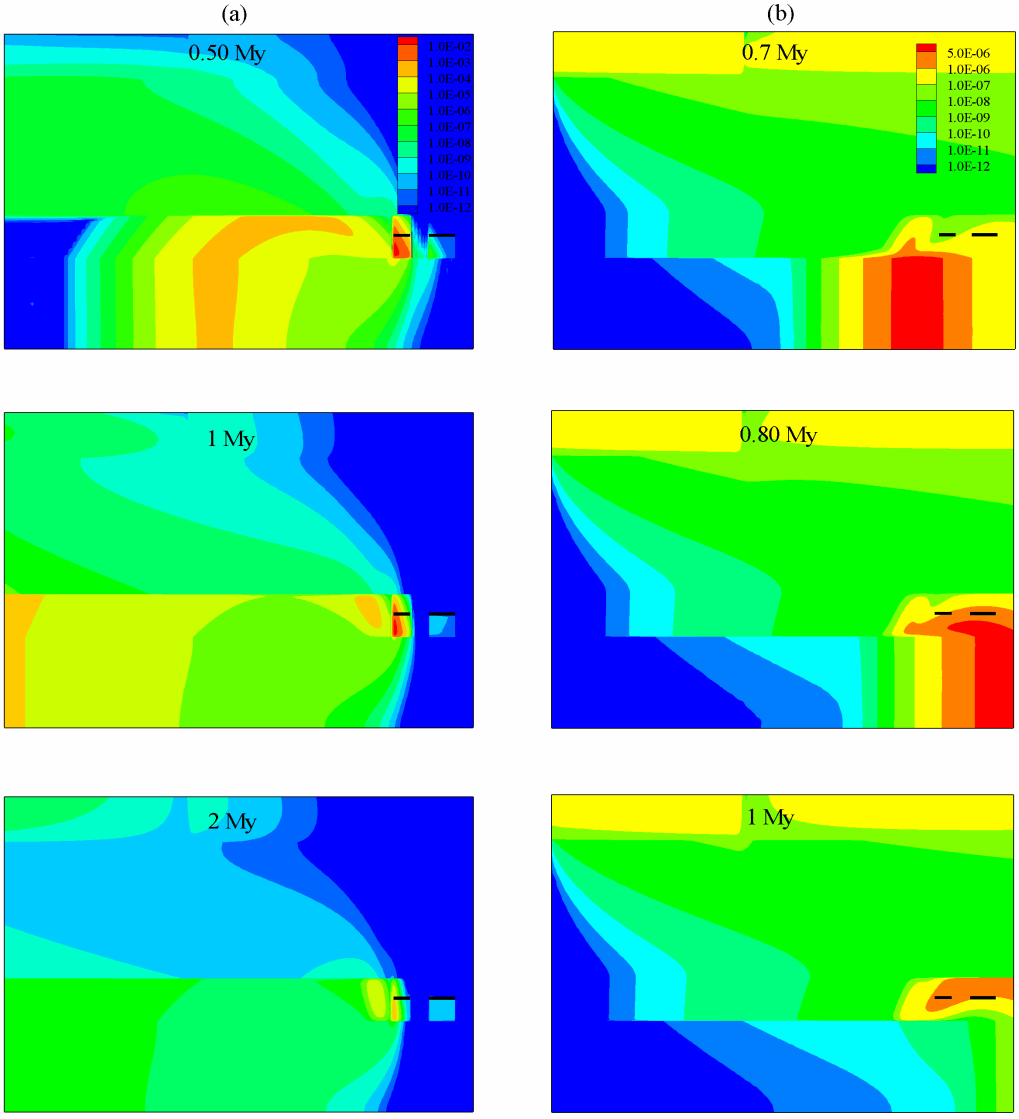

Fig. 4.23. Plot of resident concentration and life-expectancy-to-outlets pdf (outlets 2 and 3) at different times: (a) Resident concentration in mol/m^3; (b) Life-expectancy-to-outlets 2 & 3 pdf in year^{-1}.

One of the major advantages of the LTG method is that the simulation durations are extremely reduced compared to classical time-stepping procedures. It was demonstrated [Sudicky, 1989; Sudicky & McLaren, 1992] that the LTG scheme is able to provide very accurate and stable solutions for coarse grids and meshes (with Péclet numbers up to 30), which might contain discrete feature elements such as fractures or pipes. The large scale and large time capabilities of the LTG technique are indubitable.

The presented BLTG approach may have some positive implications for the assessment of groundwater contamination risk, and in particular for the problem of underground disposal of nuclear waste. The disintegration of the radionuclides being extremely long (e.g. the isotope I^{129} has a half-life of about 17My) and generally longer than the time a groundwater system needs for renewing its stocks, it is of major importance to evaluate the future evolution of the radionuclides towards the biosphere. With the BLTG approach, one can easily evaluate a global concentration (relative to all land outlets) one can expect from any source location. If a good accuracy is required in such simulations, a good representation of the structural characteristics and parameters distribution of the system is also of importance.

Considering the enormous saving of time provided by the FLTG and BLTG, multiple realizations of the models can be envisaged (e.g. Monte Carlo procedures). These methods are very well-suited for realizing the first phase of a modelling work, prior to inclusion of more complex non-linear physico-chemical processes affecting the transport of radionuclides, such as chain reactions, higher-order sorption kinetics, or phase changes. If the FLTG and BLTG techniques allow rapid simulations over millions of years, the sense of a simulation over so long periods is, however, questionable. For example, the simple consideration of an erosion rate of e.g. 1mm/y, which is reasonable, would bring the repositories (if situated 500m under the ground surface) to the ground surface in less than 500'000 years.

References

[1] Brouyère S., Jeannin P-.Y., Dassargues A., Goldscheider N., Popescu I-.C., Sauter M., Vadillo I. and Zwahlen F. Evaluation and validation of vulnerability concepts using a physically based approach. *Proceedings of the 7th Conference on Limestone Hydrology and Fissured Media*, 20th-22nd September, Besançon, France, 2001:67–76.

[2] Diersch H.-J. FEFLOW Reference Manual, 1998, WASY GmbH Berlin.

[3] Frind E., Muhammad D.S., Molson J.W. Delineation of Three-Dimensional Well Capture Zones for Complex Multi-Aquifer Systems. *Ground Water* 2002;40(6):586–598.

[4] Gardiner C.W. Handbook of Stochastic Methods for Physics, Chemistry and Natural Sciences. Berlin: Springer, 672 pp.; 1983.

[5] Gogu R.C. and Dassargues A. Current trends and future challenges in groundwater vulnerability assessment using overlay and index methods. *Environmental Geology* 2000;39(6):549–559.

[6] Hubbert M.K. The theory of ground-water motion. *Journal of Geology* 1940;48: 785–944.

[7] Jordan P. Modélisation de la partie nord de l'aquifère du Seeland (BE). Méthode de détermination des aires d'alimentation Z_u en milieu poreux. Master thesis, Centre of Hydrogeology, University of Neuchâtel, 2000.

[8] Kiraly L. La notion d'unité hydrogéologique. Essai de définition. Ph.D. thesis, Centre of Hydrogeology, University of Neuchâtel, 1978.

[9] Mejía J.M., Rodríguez-Iturbe I. On the Synthesis of Random Field Sampling From the Spectrum: An Application to the Generation of Hydrologic Spatial Processes. *Water Resour Res* 1974;10(4):705–711.

[10] Neupauer R. and Wilson J.L. Adjoint method for obtaining backward-in-time location and travel time probabilities of a conservative groundwater contaminant. *Water Resour Res* 1999;35(11):3389–3398.

[11] Neupauer R. and Wilson J.L. Adjoint-derived location and travel time probabilities for a multidimensional groundwater system. *Water Resour Res* 2001;37(6):1657–1668.

[12] Neupauer R. and Wilson J.L. Backward probabilistic model of groundwater contamination in non-uniform and transient flow. *Adv Water Res* 2002;25:733–746.

[13] Neupauer R. and Wilson J.L. Backward location and travel probabilities for a decaying contaminant in an aquifer. *J. Cont. Hydrol.* 2003;66:39–58.
[14] Sudicky E.A. The Laplace transform Galerkin technique: A time-continuous finite element theory and application to mass transport in groundwater. *Water Resour Res* 1989;25(8):1833–1846.
[15] Sudicky E.A. and McLaren R.G. The Laplace transform Galerkin Technique for Large-Scale Simulation of Mass Transport in Discretely Fractured Porous Formations. *Water Resour Res* 1992;28(2):499–514.
[16] Todd D.K. Ground Water Hydrology. New York: John Wiley, 535 pp.; 1959.
[17] Tóth J. A theory of groundwater motion in small drainage basins in central Alberta. *J Geophys Res* 1962;67:4375–4387.
[18] Tóth J. A theoretical analysis of groundwater flow in small drainage basins. *J Geophys Res* 1963;68:4795–4812.
[19] Varni M. and Carrera J. Simulation of groundwater age distributions. *Water Resour Res* 1998;34(12):3271–3281.
[20] Weissmann G. S., Zhang Y., LaBolle E. and Fogg G.E. Dispersion of groundwater age in an alluvial aquifer system. *Water Resour Res* 2002;38(10):doi:10.1029/2001WR000907.
[21] Wilson J.L. and Liu J. Field Validation of the Backward-in-Time Advection Dispersion Theory. In *Proceedings of the 1996 HSRC/WERC Joint Conference on the Environment*, Great Plains-Rocky Mountain Hazard. Substance Cent., Manhattan, Kansas;1997.

CHAPTER 5

Conclusions and perspectives

5.1. Summary

The main objective of this work was the development of deterministic mathematical approaches for the simulation of groundwater age and transit time distributions in hydro-dispersive aquifer systems. As a result of previous works [Etcheverry, 2001], the reservoir theory (RT) was successfully utilized for characterizing aquifer outlet transit time distributions with refined accuracy. However, this approach considered purely advective motion of water particles in aquifers, and was unable to deal with aquifers with multiple outlets and inlets. These limitations have motivated further investigations, in order to generalize the RT to systems with significant dispersive components, and of arbitrary hydraulic configuration. This was the second goal of the present work. The sensibility of age and transit time distributions to the aquifer structure and the transport parameters was also a purpose, and a further link between age transport and contaminant transport in groundwater was envisaged.

In the first place, the probability distributional evolution of groundwater age was evaluated by means of the classical forward advection-dispersion, according to proper boundary conditions (Chapter 2). The time-Dirac delta function is suitable for a mathematical representation of the nil age of groundwater at inlet. The life expectancy of water particles in the aquifer was then modelled by means of an adjoint backward equation. If age is defined as a relative measure of the time elapsed since recharge, life expectancy was defined as the time required for groundwater particles before they exit the aquifer. For a given position in space, the age and life expectancy probability density functions (pdf) were found to be complementary distributions. A direct application of the principle of superposition to these functions, i.e. by means of a convolution integral of the age pdf and the life expectancy pdf, resulted in an integrated distribution of total transit times, which characterizes the intensity of probability of having a given transit time from the recharge zone to the discharge zone. Thus, the total transit time pdf yields information on the entire history of water particles from recharge until discharge. Age, life expectancy, and total transit time pdfs provide different kinds of information, and each of them can reveal to be more advantageous than the other one depending on the hydrogeological question to be treated. On the one side, life expectancy and total transit time distributions are well suited for intrinsic vulnerability assessment problems, allowing mapping different regions within a recharge zone, in terms of residence time in the aquifer and associated properties. On the other hand, the simulated age distributions can be used for making inferences on internal aquifer characteristics, such as mixing processes, but also as a cross-validation tool of age-dating methods.

In the second section (Chapter 3), the RT was recovered by manipulating the forward and backward advection-dispersion equations, thus extending the reservoir theory to systems with significant dispersive components. The outlet transit time distribution was derived from the internal age distribution, and was therefore obtained with a far more refined resolution. In so doing, mixing of converging flow patterns near the outlet is ignored, and the maximum transit time is never smaller than the maximum age in the reservoir. The RT was then also derived from the internal distribution of life expectancy, in which case it allowed evaluation of recharge zones life

expectancy pdfs. From these reservoir characteristic distributions, i.e. the internal age and life expectancy pdfs, and the transit time pdf at inlet and outlet, fundamental additional transient information on water volumes and water fluxes can be gained. From the outlet transit time cdf, specific groundwater porous volumes could directly be identified and quantified with respect to age, life expectancy and transit time. These functions were found to be very useful for aquifer characterization and intrinsic vulnerability assessments. They can be used to easily evaluate the ratios of young and old groundwater volumes in the aquifer.

On the basis of analytical and numerical solutions for theoretical aquifer configurations, some effects of macro-dispersion on simulated age and transit time distributions could be underlined. For instance, longitudinal dispersion was found to have a significant aging effect, while lateral dispersion rejuvenates the system. It was shown that the average age resulting from dating-methods or direct simulations, can lead to erroneous interpretations, since dispersion can induce a high variability of the age distribution around the average. Moreover, it was shown that not only mixing processes can make the average age meaningless, but also the geological structure, which can yield complicated shapes of the transit time distribution, even without the need of complicated geometries of the flow patterns.

In practical transport modelling, the horizontal formulation of the advection-dispersion equation is very often used. To adapt the reservoir theory to more specific horizontal configurations, the forward and backward ADEs were vertically averaged. It was found that, when flow is not divergence free, a water source in the forward model yields a sink of probability in the backward model, with the form of a first-order decay term. This probability sink is a consequence of the reversed velocity in the backward equation, and reflects the addition of water by natural or artificial areal infiltration (with age zero in the forward model) that influences the life expectancy of water particles.

For the application of the RT, based on the advective-dispersion simulation of age transport, the third-kind boundary condition (prescribed total mass flux) was found to be the appropriate condition that ensures correct mass balances. Moreover, a total flux continuity of the age total fluxes at outlet (but also of the life expectancy total fluxes at inlet) was found to be of high importance. Specific formulations for the conservation of these quantities at the boundaries were consequently developed. The proposed models for age, life expectancy and total transit time from recharge to discharge, can equivalently be implemented in one-, two-, and three-dimensions, and present considerable technical and numerical advantages, which may be pivotal in handling very large natural systems. In fact, when the outlet transit time pdf is defined by integrating all hydro-dispersive properties over the entire flow field, the level of refinement required by a stable transport model is generally sufficient. The RT ensures that the minimum and the maximum ages in the reservoir are captured at the outlet, which is hardly ever the case with traditional methods, mainly due to the mixing of converging fluxes in the vicinity of the outlet. The LTG technique [Sudicky, 1989] was adopted to solve the equations with low computational burden.

In the last section (Chapter 4), the applicability of the RT (which had been derived for the global aquifer irrespective of any particular outlet) was extended to any internal flow unit of a reservoir, by using the backward transport modelling approach. For any natural or artificial outlet of a reservoir of arbitrary geometry and flow complexity, the transit time distribution could then be calculated by relating the life expectancy occurrence at inlet to the life expectancy occurrence in the outlet drainage basin. The capture zone of any outlet was defined with respect to a time value, and characterized in terms of probability.

The application of this generalized reservoir theory was illustrated with synthetic numerical experiments related to the well-head protection problem, by considering homogeneous and heterogeneous velocity fields. The spatial heterogeneity of velocity was modelled by generating lognormal random permeability fields, and by adopting a physical relationship between porosity and

permeability. Simulation results for the well transit time pdf illustrate the effects of velocity fluctuations on the arrival times. Under advection-dominated regimes, the simulations generally showed important tailing effects. This joins the idea already forwarded by several authors who considered the effects of dispersion on age transport, that the representation of groundwater age by a single date value (generally this date is a mean age) can be misleading. However, as illustrated in the second section, dispersion is only one factor among others that creates unrepresentative mean ages. The spreading of the results for the well transit time pdf, based on hundreds of realizations of the velocity field, is very much lowered when permeability and porosity are linked by a physical relationship. This points out the importance of the porosity since it is a governing parameter for age transport, since it acts as an age generator. Therefore, particular attention should be given to the spatial distribution of this parameter.

The backward transport modelling approach was used to define capture zones, and additionally linked to the RT approach. The combination of both approaches can be helpful in aquifer and outlet vulnerability studies, allowing vulnerability mapping by post-processing the life-expectancy-to-outlet pdf field. Since the resident concentration that is expected at an outlet as a result of an instantaneous release of mass somewhere within the domain can be predicted with one single realization of the backward transport equation, the outlet specific vulnerability to source contamination was easily characterized and quantified. Robust post-processes of the life-expectancy-to-outlet pdf field were proposed for predicting the resident concentration at a given outlet, which might result from the release of an arbitrary source function that may be distributed over a region of finite size. Decay and first order sorption processes can also be taken into account.

The usefulness of such post-processes, in combination with the LTG technique, was finally illustrated on an example of an underground storage of high-level nuclear waste. The results of theoretical simulations have, on the one hand confirmed the efficiency of the LTG technique, with which a 5 minutes real-time simulation replaces a 36 hours real-time simulation, and on the other hand proved the robustness and utility of the proposed post-processes. The saving of time obtained with the LTG technique can allow additional simulations to be carried out, in order to refine the quality of a model and of its predictions, e.g. by adopting Monte Carlo procedures.

5.2. Limitations and perspectives

The transport models developed in this work are based on the assumption of a time-independence of the velocity fields. The transit time distribution at an aquifer outlet was discussed by considering the transfer of matter (age mass) through a groundwater reservoir at steady and stationary state, i.e. the amount of mobile water is considered constant. However, aquifers are by nature non-stationary reservoirs, since they exhibit fluctuations in the flow rate of their discharge and recharge zones, and frequent changes in the mass of groundwater. Fluctuations of the water levels are observed in every aquifers, however with different magnitudes, in relation to the nature of the system and recharge conditions. The transit time distribution $\varphi(t)$ derived from steady-state velocity fields can be assimilated in a reasonable manner to a mean distribution corresponding to smoothly varying hydraulic annual conditions. When the flow rate fluctuations are important, one can expect that the transit time response $\varphi(t)$ is very dependent on the level of the outflow rate, in which case $\varphi(t)$ should be replaced by $\varphi(t, \tau)$. An addition of energy (potential) is dissipated along the flow, but the response in flow rate to this addition is not necessarily related to the transit time within the aquifer of the added water amounts. In other words, the classes of transit time in $\varphi(t)$ might not be modified under transient flow regimes, since they mainly depend on the aquifer structure and on the organization of its hydraulic boundaries, but the corresponding intensities of probability could, however, be modified. Precipitation is often quantified as an uncorrelated stochastic process. Highly heterogeneous rainfall conditions in space could induce significant modifications of the age distribution in a groundwater sample. The impact on the transit time distribution of long-term

modifications of the recharge patterns, e.g. due to global climate changes, could represent a first step for a further research. One-dimensional solutions of inflow-dependent transit time distributions have been developed by soil scientists [see e.g. Jury & Roth, 1990]. At aquifer scale, this task must be far more complicated.

The LTG method was found to be the appropriate solution technique for performing the RT formulation. However, it is not appropriated for non-linear problems and when velocity varies in time. The simulation of transit time distributions under time-varying flow conditions would require a time-marching solution procedure, but in this case the pure unit impulse Dirac function at the boundaries, which is simply one in the Laplace domain, could not properly be handled.

Further investigations of reservoir theory-type formulations could be of interest. To evaluate an aquifer outlet transit time distribution $\varphi(t)$, the reservoir theory makes use of a differentiation operator which applies to the internal age distribution $\psi(t)$. In Chapter 3, specific internal volume properties have been defined on the basis of the outlet transit time cumulative distribution function $f(t)$. In particular, the cumulative distribution function of the internal total transit times $m_T(t)$ could be deduced from $f(t)$. A simple differentiation of the relationship between $m_T(t)$ and $f(t)$ links the internal total transit time distribution function $\psi_T(t)$ to the function $\varphi(t)$ by the simple relation of proportionality $\varphi(t) \sim \psi_T(t)/t$, which presents the considerable advantage that no differentiation is required compared to the classical reservoir theory formulation. If this formulation works for pure advective to low-level dispersive systems, it is not the case when dispersion is significantly added. Further investigations could help to define if a correction is missing in this formulation, or if the definition of the function $\psi_T(t)$ has not been rigorously posed.

This works suffers from the lack of field data that can support the developed models. The advantages of the RT formulation compared to other evaluation methods of outlet transit time pdfs should be validated by means of experimental and field data.

The age of groundwater calls for the knowledge of its origins. The origins of the water quantities passing through a given portion of an aquifer, like an outlet, are of prime importance for many hydrogeological problems. For example, one could be interested in the quantification of the percentage of the water passing through a given region, which has previously passed through an upstream given portion of a specific layer. To our point of view, the backward transport equation owns the capacity of providing answers to such questions, but requires further elaboration.

References

[1] Etcheverry D. Une approche déterministe des distributions des temps de transit de l'eau souterraine par la théorie des réservoirs. Ph.D. Thesis, Centre of Hydrogeology, University of Neuchâtel, 2001, 118 pp.
[2] Jury W.A. and Roth K. Transfer Functions and Solute Movement Through Soil: Theory and Applications. Birkhauser Boston, Cambridge, Mass, 289 pp.; 1990.
[3] Sudicky E.A. The Laplace transform Galerkin technique: A time-continuous finite element theory and application to mass transport in groundwater. *Water Resour Res* 1989;25(8):1833–1846.

REFERENCES

Abramowitz M., Stegun I.A. Handbook of Mathematical Functions. Dover Publishing Co., New-York, 1970.

Amin I.E. and Campana M.E. A general lumped parameter model for the interpretation of tracer data and transit time calculation in hydrologic systems. *J Hydrol* 1996;179:1–21.

Arnold L. Stochastic Differential Equations: Theory and Applications. New York: John Wiley, 228 pp.; 1974.

Balderer W. Signification de l'âge moyen de l'eau souterraine donné par les isotopes radioactifs. *Bulletin du Centre d'Hydrogéologie* 1986;6:43–66.

Bath A.H., Edmunds W.M. and Andrews J.N. Paleoclimatic trends deduced from hydrochemistry of a Triassic sand-stone aquifer, United Kingdom. Int. At. Energy, Vienna 1979. Isotope Hydrology 1978;2:545–568.

Bear J. and Verruitj A. Modeling Groundwater Flow and Pollution. Kluwer Academic Publ., 414 pp.; 1987.

Benjamin J.R. and Cornell C.A. Probability, Statistics, and Decision for Civil Engineers. New York: McGraw-Hill Book Co.; 1970.

Bethke C.M. and Johnson T.M. Paradox of groundwater age: Correction. *Geology* 2002;30(4):385–388.

Bethke C.M. and Johnson T.M. Groundwater age. *Ground Water* 2002;40(4):337–339.

Boehlke J.K. and Denver J.M. Combined use of groundwater dating, chemical, and isotopic analysis to resolve the history and fate of nitrate contamination in two agricultural watersheds, Atlantic Coastal Plain, Maryland. *Water Resour Res* 1996;31(9):2319–2339.

Bolin B. and Rodhe H. A note on the concept of age distribution and transit time in natural reservoirs. *Tellus* XXV 1973;1:58–62.

Brouyère S., Jeannin P-.Y., Dassargues A., Goldscheider N., Popescu I-.C., Sauter M., Vadillo I. and Zwahlen F. Evaluation and validation of vulnerability concepts using a physically based approach. *Proceedings of the 7th Conference on Limestone Hydrology and Fissured Media*, 20th-22nd September, Besançon, France, 2001:67–76.

Busenberg E. and Plummer L.N. Use of chlorofluoromethanes (CCL3F and CCL2F2) as hydrologic tracers and age-dating tools; The alluvium and terrace system of central Oklahoma. *Water Resour Res* 1992;28(9):2257–2283.

Campana M.E. and Simpson E. Groundwater residence times and recharge rates using a discrete-state compartment model and ^{14}C data. *J Hydrol* 1984;72:171–185.

Campana M.E. Generation of Ground-Water Age Distributions. *Ground Water* 1987;25(1):51–58.

Cordes C. and Kinzelbach W. Continuous groundwater velocity fields and path lines in linear, bilinear, and trilinear finite elements. *Water Resour Res* 1992;28:2903–2911.

Cornaton F. and Perrochet P. Analytical 1D dual-porosity equivalent solutions to 3D discrete single-continuum models. Application to karstic spring hydrograph modelling. *J Hydrol* 2002;262:165–176.

Cook P.G. and Solomon D.K. Recent advances in dating young groundwater: chlorofluorocarbons, $^{3}H/^{3}He$ and ^{85}Kr. *J Hydrol* 1997;191:245–265.

Dagan G. Stochastic modelling of groundwater flow by unconditional and conditional probabilities, 2, The solute transport. *Water Resour Res* 1982;18(4):835–848.

Dagan G. Solute transport in heterogeneous porous formations. *J Fluid Mech* 1984;145:151–177.

Dagan G. Theory of solute transport by groundwater. *Ann Rev Fluid Mech* 1987;19:183–215.

Dagan G. Flow and Transport in Porous Formations. Springer, Berlin, Heidelberg, Germany; 1989.

Dagan G. and Nguyen V. A comparison of travel time and concentration approaches to modelling transport by groundwater. *J Contam Hydrol* 1989;4:79–91.

Danckwerts P.V. Continuous flow systems: distribution of residence times. *Chem Eng Sci* 1953;2(1):93–102.

Danckwerts P.V. The effect of incomplete mixing on homogeneous reactions. *Chem Eng Sci* 1958;8:93–102.

Davis S.N. and Bentley H.W. Dating groundwater, a short review, In *Nuclear and Chemical Dating Techniques*, Ed. Lloyd Curie, Am. Chem. Soc. Symp. Ser. 176, 187–222;1982.

De Smedt F. and Wierenga P.J. A Generalized Solution for Solute Flow in Soils With Mobile and Immobile Water. *Water Resour Res* 1979;15(5):1137–1141.

Diersch H.-J. FEFLOW Reference Manual, 1998, WASY GmbH Berlin.

Diersch H.-J. An efficient method for computing groundwater residence times. FEFLOW Software White Papers Vol. 1, 2002, WASY GmbH Berlin, 137–145.

Diersch H.-J. About the difference between the convective form and the divergence form of the transport equation. FEFLOW Software White Papers Vol. 1, 2002, WASY GmbH Berlin, 119–129.

Dunkle S.A., Plummer L.N., Busenberg E., Phillips P.J., Denver J.M., Hamilton P.A., Michel R.L. and Coplen T.B. Chlorofluorocarbons (CCl3F and ClCl2F2) as dating tools and hydrologic tracers in shallow groundwater of the Delmarva Peninsula, Atlantic Coastal Plain, United States. *Water Resour Res 1993*;29:3837–3860.

Eriksson E. and Welander P. On a mathematical model of the carbon cycle in nature. *Tellus* 1956;8:115–75.

Eriksson E. The possible use of Tritium for estimating groundwater storage. *Tellus* 1958;10:472–478.

Eriksson E. Natural reservoirs and their characteristics. *Geofisica International* 1961;1(2):27–43.

Eriksson E. Compartment models and reservoir theory. *Annual Review of Ecology and Systematics* 1971;2:67–84.

Etcheverry D. Valorisation des méthodes isotopiques pour les questions pratiques liées aux eaux souterraines. Isotopes de l'oxygène et de l'hydrogène. *Berichte des BWG*, Serie Geologie 2002; 71 pp.

Etcheverry D. and Perrochet P. Reservoir theory, groundwater transit time distributions and lumped parameter models. IAEA-SM-361/44, Vienna;1999.

Etcheverry D. and Perrochet P. Direct simulation of groundwater transit time distributions using the reservoir theory. *Hydrogeology Journal* 2000;8:200–208.

Etcheverry D. Une approche déterministe des distributions des temps de transit de l'eau souterraine par la théorie des réservoirs. PhD Thesis, Centre of Hydrogeology, University of Neuchâtel, 2001, 118 pp.

Flynn R. Virus transport and attenuation in perialpine gravel aquifers. Ph.D. Thesis, Centre of Hydrogeology, University of Neuchâtel, 2003.

Flynn R., Cornaton F., Hunkeler D. and Rossi P. Virus Transport in a Fining-Upwards Sedimentary Sequence: Laboratory Experiments and Simulation. *Submitted (June 2003) to Journal of Contaminant Hydrology*.

Frind E., Muhammad D.S., Molson J.W. Delineation of Three-Dimensional Well Capture Zones for Complex Multi-Aquifer Systems. *Ground Water* 2002;40(6):586–598.

Garabedian P.R. Partial Differential Equations. New York: John Wiley, 672 pp.; 1964.

Gardiner C.W. Handbook of Stochastic Methods for Physics, Chemistry and Natural Sciences. Berlin: Springer, 672 pp.; 1983.

Gelhar L.W. and Axness C.L. Three-dimensional stochastic analysis of macro dispersion in aquifers. *Water Resour Res* 1983;19(1):161–180.

Gelhar L.W. Stochastic Subsurface Hydrology, Prentice-Hall, Inc., Englewood Cliffs, NJ, 1993.

Ginn T.R. On the distribution of multicomponent mixtures over generalized exposure time in subsurface flow and reactive transport: Fundations, and formulations for groundwater age, chemical heterogeneity, and biodegradation. *Water Resour Res* 1999;35(5):1395–1407.

Gogu R.C. and Dassargues A. Current trends and future challenges in groundwater vulnerability assessment using overlay and index methods. *Environmental Geology* 2000;39(6):549–559.

Goode D.J. Direct simulation of groundwater age. *Water Resour Res* 1996;32:289–296.

Goode D.J. Ground-water age and atmospheric tracers: Simulation studies and analysis of field data from the Mirror Lake site, New Hampshire. Ph.D. thesis, Princeton University, Department of Civil Engineering and Operations Research, 1998, 194 pp.

Haitjema H.M. On the residence time distributions in idealized groundwatersheds. *J Hydrol* 1995;172:127–146.

Harvey C.F. and Gorelick S.M. Temporal moment generating equations: Modeling transport and mass transfer in heterogeneous aquifers. *Water Resour Res* 1995;31:1895–1912.

Hassanizadeh M. and Gray W.G. General conservation equations for multiphase systems, 1, Averaging procedure. *Advan Water Resour* 1979;2:131–144.

Hubbert M.K. The theory of ground-water motion. *Journal of Geology* 1940;48: 785–944.

Jordan P. Modélisation de la partie nord de l'aquifère du Seeland (BE). Méthode de détermination des aires d'alimentation Z_u en milieu poreux. Master thesis, Centre of Hydrogeology, University of Neuchâtel, 2000.

Jury W.A Simulation of Solute transport Using a Transfer Function Model. *Water Resour Res* 1982;18(2):363–368.

Jury W.A., Sposito G. and White R.E. A Transfer Function Model of Solute Transport through Soil, 1, Fundamental Concepts. *Water Resour Res* 1986;22(2):243–247.

Jury W.A. and Roth K. Transfer Functions and Solute Movement Through Soil: Theory and Applications. Birkhauser Boston, Cambridge, Mass, 289 pp.; 1990.

Kiraly L. La notion d'unité hydrogéologique. Essai de définition. Ph.D. thesis, Centre of Hydrogeology, University of Neuchâtel, 1978.

Kolmogorov A.N. Über die analytischen Methoden in der Wahrscheilichkeitsrechnung. *Math Anal* 1931;104:415–458.

Kreft A. and Zuber A. On the physical meaning of the dispersion equation and its solutions for different initial and boundary conditions. *Chem Eng Sci* 1978;33:1471–1480.

Kreft A. and Zuber A. Comments on "Flux-Averaged and Volume-Averaged Concentrations in Continuum Approaches to Solute Transport" by J. C. Parker and M. Th. van Genuchten. *Water Resour Res* 1986;22(7):1157–1158.

LaBolle E.M., Quastel J. and Fogg G.E. Diffusion theory for transport in porous media : Transition-probability densities of diffusion processes corresponding to advection-dispersion equations. *Water Resour Res* 1998;34(7):1685–1693.

Luther K.H. and Haitjema H.M. Numerical experiments on the residence time distributions of heterogeneous groundwatersheds. *J Hydrol* 1998;207:1–17.

Maloszewski P. and Zuber A. Determining the turnover time of groundwater systems with the aid of environmental tracers, 1, Models and their applicability. *J Hydrol* 1982;57:207–231.

Maloszewski P. and Zuber A. Influence of matrix diffusion and exchange reactions on radiocarbon ages in fissured carbonate aquifers. *Water Resour Res* 1991;27:1937–1945.

Maloszewski P. and Zuber A. Principles and practice of calibration and validation of mathematical models for the interpretation of environmental tracer data in aquifers. *Adv Water Res* 1993;16:173–190.

Mejía J.M., Rodríguez-Iturbe I. On the Synthesis of Random Field Sampling From the Spectrum: An Application to the Generation of Hydrologic Spatial Processes. *Water Resour Res* 1974;10(4):705–711.

Nauman E.B. and Buffham B.A. Mixing in Continuous Flow Systems. John Wiley, New York, 1983.

Neumann S.P., Winter C.L. and Newman C.M. Stochastic theory of field-scale Fickian dispersion in anisotropic porous media. *Water Resour Res* 1987;23:453–466.

Neupauer R. and Wilson J.L. Adjoint method for obtaining backward-in-time location and travel time probabilities of a conservative groundwater contaminant. *Water Resour Res* 1999;35(11):3389–3398.

Neupauer R. and Wilson J.L. Adjoint-derived location and travel time probabilities for a multidimensional groundwater system. *Water Resour Res* 2001;37(6):1657–1668.

Neupauer R. and Wilson J.L. Backward probabilistic model of groundwater contamination in non-uniform and transient flow. Adv Water Res 2002;25:733–746.

Neupauer R. and Wilson J.L. Backward location and travel probabilities for a decaying contaminant in an aquifer. *J Cont Hydrol* 2003;66:39–58.

Oster H., Sonntag C. and Munnich, K.O. Groundwater age dating with chlorofluorocarbons. *Water Resour Res* 1996;32(10):2989–3001.

Parker J.C. and van Genuchten M. Th. Flux-averaged and volume-averaged concentrations in continuum approaches to solute transport. *Water Resour Res* 1984;20(7):866–872.

Parker J.C. and van Genuchten M. Th. Reply. *Water Resour Res* 1986;22(7):1159–1160.

Plummer L.N., Michel R.L., Thurman E.M. and Glynn P.D. Environmental tracers for age dating young ground water. In *Regional ground-water quality* 1993, Ed. Alley W.M., New York, Van Nostrand Reinhold,255–294.

Reilly T.E., Plummer L.N., Phillips P.J. and Busenberg E. The use of simulation and multiple environmental tracers to quantify groundwater flow in a shallow aquifer. *Water Resour Res* 1994;30:421–433.

Richter J., Szymezak P., Abraham T. and Jordan H. Use of combination of lumped parameter models to interpret groundwater isotopic data. *J Cont Hydrol* 1993;14(1):1–13.

Robertson W.D. and Cherry J.A. Tritium as an indicator of recharge and dispersion in a groundwater system in Central Ontario. *Water Resour Res* 1989;25:1097–1109.

Schnegg P. and Doerfliger N. An inexpensive flow-through field fluorometer. *Proceedings of the 6th 'Colloque d'hydrologie en pays calcaire et milieu fissuré',* Chaux-de-Fonds, August, 1997.

Shapiro A.M. and Cvetkovic V.D. Stochastic analysis of solute arrival time in heterogeneous porous media. *Water Resour Res* 1988;24(10):1711–1718.

Smith D.B., Downing R.A., Monkhouse R.A, Otlet R.L. and Pearson F.J. The age of groundwater in the Chalk of the London Basin. *Water Resour Res* 1976;12:392–404.

Solomon D.K., Poreda R.J., Schiff S.L. and Cherry J.A. Tritium and Helium 3 as groundwater-age tracers in the Borden aquifer. *Water Resour Res* 1992;28:741–755.

Sonntag C., Klitzch E., Lohnert E.P., El-Shazly E.M, Munich K.O., Junghans C., Thorweike U., Weistroffer K. and Swailem F.M. Paleoclimatic information from deuterium and oxygen-18 in carbon-14 dated north Saharian groundwaters. *Isotope Hydrology* 1979;2:569–580, Int. At. Energy Agency, Vienna.

Spalding D.B. A note on mean residence-times in steady flows of arbitrary complexity. *Chem Eng Sci* 1958;9:74–77.

Sposito G., White R.E., Darrah P.R, Jury W.A. A Transfer Function Model of Solute Transport Through Soil 3. The Convection-Dispersion Equation. *Water Resour Res* 1986;22(2):255–262.

Sposito G. and Barry D.A. On the Dagan model of solute transport in groundwater: Foundational aspects. *Water Resour Res* 1987;23(10):1867–1875.

Sudicky E.A. and Frind E. Carbon 14 dating of groundwater in confined aquifers: Implication of aquitard diffusion. *Water Resour Res* 1981;17:1060–11064.

Sudicky E.A. A natural-gradient experiment on solute transport in a sand aquifer: spatial variability of hydraulic conductivity and its role in the dispersion process. *Water Resour Res* 1986;22:2069–2082.

Sudicky E.A. The Laplace transform Galerkin technique: A time-continuous finite element theory and application to mass transport in groundwater. *Water Resour Res* 1989;25(8):1833–1846.

Sudicky E.A. and McLaren R.G. The Laplace transform Galerkin Technique for Large-Scale Simulation of Mass Transport in Discretely Fractured Porous Formations. *Water Resour Res* 1992;28(2):499–514.

Todd D.K. Ground Water Hydrology. New York: John Wiley, 535 pp.; 1959.

Tóth J. A theory of groundwater motion in small drainage basins in central Alberta. *J Geophys Res* 1962;67:4375–4387.

Tóth J. A theoretical analysis of groundwater flow in small drainage basins. *J Geophys Res* 1963;68:4795–4812.

Uffink G.J.M. Application of the Kolmogorov's backward equation in random walk simulation of groundwater contaminant transport. In *Contaminant Transport in Groundwater* 1989;ed. H.E. Kobus & Kinzelbach, Balkema, Rotterdam, 283–289.

Van Herwaarden O.A. Spread of pollution by dispersive groundwater flow. *SIAM J Appl Math* 1994;54(1):26–41.

Van Kooten J.J.A. An asymptotic method for predicting the contamination of a pumping well. *Adv Water Res* 1995;18(5):295–313.

Varni M. and Carrera J. Simulation of groundwater age distributions. *Water Resour Res* 1998;34(12):3271–3281.

Weissmann G. S., Zhang Y., LaBolle E. and Fogg G.E. Dispersion of groundwater age in an alluvial aquifer system. *Water Resour Res* 2002;38(10):doi:10.1029/2001WR000907.

White R.E., Dyson J.S., Haigh R.H., Jury W.A., Sposito G. A Transfer Function Model of Solute Transport Through Soil 2. Illustrative applications. *Water Resour Res* 1986;22(2):248–254.

Wilson J.L. and Liu J. Field Validation of the Backward-in-Time Advection Dispersion Theory. In P*roceedings of the 1996 HSRC/WERC Joint Conference on the Environment*, Great Plains-Rocky Mountain Hazard. Substance Cent., Manhattan, Kansas;1997.

Woodbury A.D. and Rubin Y. A full-Bayesian approach to parameter inference from tracer travel time moments and investigation of scale effects at the Cape Cod experimental site. *Water Resour Res* 2000;36(1):159–171.

Zuber A. Mathematical models for the interpretation of environmental radioisotopes in groundwater systems. In *Handbook of Environmental Isotope Geochemistry 2*, Fritz P. and Fontes J.-Ch. (Eds);1986.

Zwietering T.N. The degree of mixing in continuous flow systems. *Chem Eng Sci* 1953;11:1–15.

APPENDIX A

Technical aspects of the developed programs

The programs developed in this work have been written in FORTRAN90. They correspond to a portable finite element library allowing one-, two, and three-dimensional simulation of variably saturated flow and transport. In this appendix, the computational aspects related to the implementation of the Laplace Transform Galerkin technique [Sudicky, 1989] are briefly described.

Transport equation:

The divergence form of the transport equation can be written as [Diersch, 2002]:

$$\frac{\partial(\phi RC)}{\partial t} = -\nabla\cdot(\mathbf{q}C - \mathbf{D}\nabla C) - \phi R\lambda C + S \tag{A.1}$$

where **q** is the fluid flux vector [L/T], ϕ is porosity [−], **D** is the tensor of macro-dispersion [L^2/T], λ the decay rate [T^{-1}], R the retardation factor [−], and S a source term [$M/L^3/T$].

Laplace Transformation:

When a Laplace transform (see Excursus 2.2) is applied to Eq. (A.1), the time-derivative is eliminated:

$$s\phi R\hat{C} = -\nabla\cdot(\mathbf{q}\hat{C} - \mathbf{D}\nabla\hat{C}) - \phi R\lambda\hat{C} + \hat{S} \tag{A.2}$$

where $\hat{C}$ denotes the s-transformed state of the dependent variable C. Eq. (A.2) has the form of a steady-state equation, with an additional term on the left-hand side, which is similar to a first-order decay term. Note that a zero initial condition is supposed in the formulation (A.2). The number s is complex, and its dimension is the inverse of time.

Finite element formulations:

Using the classical Galerkin formulation, and introducing $\mathbf{N} = [N_1,\ldots,N_{node}]$ as the element shape functions vector (with *node* denoting the number of nodes in the element), the weak form of Eq. (A.2) can be synthesized by

$$\begin{aligned}&\int_\Omega [\mathbf{N}\phi R(\lambda+s)\hat{C} - \nabla\mathbf{N}(\mathbf{q}\hat{C} - \mathbf{D}\nabla\hat{C})]\,d\Omega + \int_{\Gamma_2}\mathbf{N}(\alpha+\mathbf{q}\cdot\mathbf{n})\hat{C}\,d\Gamma \\ &= \int_\Omega \mathbf{N}\hat{S}\,d\Omega + \int_{\Gamma_2}\mathbf{N}(\alpha\hat{C}_2 - \beta)\,d\Gamma\end{aligned} \tag{A.3}$$

In Eq. (A.3), **n** is a normal positive outward unit vector, α and β are constants. The normal dispersive flux is expressed, and the case $\alpha = \beta = 0$ yields boundaries impermeable to the normal dispersive flux (Neumann homogeneous), but not necessarily boundaries impermeable to the normal convective flux. The left-hand side of Eq. (A.3) exhibits the capacity of conserving the total flux on boundaries, and in turn is equivalent to the following set of boundary conditions:

$$\hat{C} = \hat{C}_1 \qquad \text{on} \quad \Gamma_1 \tag{A.4}$$

$$-(\mathbf{D}\nabla\hat{C} - \mathbf{q}\hat{C})\cdot\mathbf{n} + \alpha(\hat{C}_2 - \hat{C}) = \beta \qquad \text{on} \quad \Gamma_2 \tag{A.5}$$

where Γ_1 and Γ_2 are the boundaries of the domain along which the conditions (A.4) and (A.5) are prescribed. Equation (A.4) is the classical Dirichlet boundary condition with $\hat{C}_1$ being a prescribed value of the unknown function. Eq. (A.5) has the form of a Robin boundary condition from which more specific Neumann and Cauchy type conditions can be derived. At outlet boundary portions, Eq. (A.5) requires technical manipulation to handle the normal diffusive term $-\mathbf{D}\nabla\hat{C}\cdot\mathbf{n}$. This point is detailed in Appendix B.

On any finite element domain Ω_e, the unknown complex variable is replaced by a continuous approximation of the form:

$$\bar{\hat{C}}(s) = \sum_{n=1}^{node} \hat{C}_n(\mathbf{x}, s) N_n(\mathbf{x}) \tag{A.6}$$

where $\hat{C}_n(\mathbf{x}, s)$ are the concentration spectra nodal unknowns. After substitution of the trial solution (A.6) into (A.3), and after dividing the domain and boundary integrals into piecewise elemental contributions over an element Ω_e, the following global matrix system of *m* algebraic equations is obtained:

$$\left([\mathbf{A}] + s[\mathbf{M}]\right)\left\{\hat{C}\right\} = \left\{\hat{F}\right\} \tag{A.7}$$

with

$$\begin{aligned}
[\mathbf{A}] &= \sum_{e=1}^{nelm} \int_{\Omega_e} [\nabla\mathbf{N}\mathbf{D}\nabla\mathbf{N}^T - \nabla\mathbf{N}\mathbf{q}\mathbf{N}^T + \mathbf{N}R\phi\lambda\mathbf{N}^T]\, d\Omega_e \\
[\mathbf{M}] &= \sum_{e=1}^{nelm} \int_{\Omega_e} \mathbf{N}\phi R\mathbf{N}^T d\Omega_e \\
\left\{\hat{F}\right\} &= \sum_{e=1}^{nelm} \int_{\Omega_e} \mathbf{N}\hat{S}\, d\Omega_e + \int_{\Gamma_2^e} \mathbf{N}(\mathbf{D}\nabla\mathbf{N}^T - \mathbf{q}\mathbf{N}^T)\cdot\mathbf{n}\, d\Gamma^e
\end{aligned} \tag{A.8}$$

where *nelm* denotes the number of elements in the finite element mesh. The convective term in the matrix [**A**] can easily be evaluated by using the property $\nabla\mathbf{N}\mathbf{q}\mathbf{N}^T = [\mathbf{N}\mathbf{q}\nabla\mathbf{N}^T]^T$. The global matrices [**A**] and *s*[**M**] are complex. The calculation of the coefficients of these two matrices is done a single time, and the coefficients of the matrix [**M**] are simply scaled during the incrementing of the Laplace variable *s*.

Solution techniques:

Calculation and assembling of finite element matrices

The element matrices in (A.8) are evaluated according to the method of Perrochet [1995] (see Appendix B for more details), in order to mix elements of different dimensions within the same mesh. For the assembling of the global matrices, the Compressed Sparse Row format [CSR format; Saad, 1994] has been adopted for the matrix storage. The CSR format allows the storage of big sparse matrices by means of one real (or complex) array *da* for the non-zero coefficients, associated to two integer pointer arrays: the integer array *ja* (dimension of *da*) points to the columns of the global $n \times n$ matrix, and the integer array *ia* (dimension $n+1$) points to the beginning of each row. The following example summarizes the CSR format for a real-argument arbitrary matrix:

$$\begin{pmatrix} 1 & -1 & 0 & 0 & 0 \\ -1 & 2 & -2 & 3 & 0 \\ 0 & -2 & 2 & -1 & 0 \\ 0 & 3 & -1 & 2 & -2 \\ 0 & 0 & 0 & -2 & 1 \end{pmatrix} \equiv \begin{bmatrix} da: & 1 & -1 & -1 & 2 & -2 & 3 & -2 & 2 & -1 & 3 & -1 & 2 & -2 & -2 & 1 \\ ja: & 1 & 2 & 1 & 2 & 3 & 4 & 2 & 3 & 4 & 2 & 3 & 4 & 5 & 4 & 5 \\ ia: & 1 & 3 & 7 & 10 & 14 & 16 & & & & & & & & & \end{bmatrix}$$

Array *ia* has the properties: $ia(1) = 1$, $ia(n+1) - ia(1) = \dim(da) = \dim(ja)$. Matrix-vector operations are particularly straightforward with the CSR format.

Solving

The assembled linear system of equations (A.7) is solved by a version with complex arguments of the accurate *ILUT*-based sparse iterative solver [Saad, 1994], with *BiCGSTAB* acceleration [van der Vorst, 1992]. The well-known matrix-preconditioning *LU* procedure performs an incomplete factorization of an assembled finite element matrix **A**, in order to make the linear system $\mathbf{A}\{C\} = \{F\}$ easier to solve by a given iterative method. The *LU* method realizes a decomposition of the form $\mathbf{A} = \mathbf{LU} - \mathbf{R}$, where **L** and **U** are sparse triangular matrices which have the same non-zero structure as the lower and upper parts of **A**, respectively. The matrix **R** is the residual of the factorization, and must satisfy certain constraints, such as the presence of zero elements at some locations. The *ILUT* method is one of the variants that allow some fill-in elements to appear in **L** and **U**, creating additional diagonals in the **LU** product. A particularity of *ILUT* is the dual-threshold strategy that is applied for dropping small elements, instead of considering the structure of **A** only.

In order to solve the linear system iteratively, the Biconjugate Gradient Stabilized procedure *BiCGSTAB* is used. *BiCGSTAB* is a transpose-free variant of the well-known Biconjugate Gradient algorithm, and is known to yield smoother convergence.

Inversion of the Laplace transforms

The numerical inversion of the Laplace transformed functions is performed by the algorithm of Crump [1976], which is based on Fourier series approximation of the inverse function, and on a trapezoidal approximation of the inverse integral procedure L^{-1} (see Excursus 2.2):

$$C(t) = \frac{1}{T}\exp(\gamma t)\left[\frac{\hat{C}(\gamma)}{2} + \sum_{k=1}^{2n+1} \mathrm{Re}[\hat{C}(s_k)]\cos(\frac{k\pi t}{T}) - \mathrm{Im}[\hat{C}(s_k)]\sin(\frac{k\pi t}{T})\right] + E$$
$$s_k = \gamma + j\frac{k\pi}{T} \quad , \quad k = 1,\ldots,2n+1 \quad , \quad j = \sqrt{-1} \tag{A.9}$$

where $2T$ is the period of the Fourier series approximating the inverse function on the interval $[0, 2T]$, E is the error induced by the truncation of the series after $2n+1$ terms, and where γ is the real part of the discrete Laplace variable s_k. Experiments on several functions [Crump, 1976; Sudicky, 1989] have shown that the values $E = 10^{-6}-10^{-7}$ and $T = 0.8t_{max}$ (t_{max} is the maximum simulation time) can be used in (A.9), and that the k discrete values of the Laplace variable s_k can be approximated by:

$$s_k = -\frac{\ln(E)}{1.6t_{\max}} + j\frac{k\pi}{0.8t_{\max}} \quad , \quad k = 1,\ldots,2n+1 \tag{A.10}$$

where E is the absolute error tolerance.

In order to reduce the truncation error in Eq. (A.9), and thus accelerate the series convergence, additional algorithms are required. To accelerate the convergence of the Fourier series, the algorithm of Crump is often coupled with two accelerators, the epsilon algorithm and the quotient-difference algorithm (QD) [De Hoog *et al.*, 1982]. The QD algorithm was preferred here, since it proved to be very efficient to treat inversion in the neighbourhood of discontinuities or sharp fronts, and the required computational effort, which is linearly proportional to the $2n+1$ number of discrete Laplace variables, is highly diminished with respect to the epsilon algorithm. The QD algorithm can be summarized by the following. The un-accelerated estimate (A.9) is issued from the truncation of the following original complex power series:

$$\begin{cases} C(t) = \dfrac{\hat{C}(\gamma)}{2} + \displaystyle\sum_{k=1}^{\infty} \hat{C}(\gamma + \frac{jk\pi}{T}) \exp\left(\frac{jk\pi t}{T}\right) = \sum_{k=0}^{\infty} a_k z^k \\ a_0 = \dfrac{\hat{C}(\gamma)}{2} \quad , \quad a_k = \hat{C}(\gamma + \frac{jk\pi}{T})\Big|_{k=1,\ldots,\infty} \quad , \quad z^k = \exp\left(\frac{j\pi t}{T}\right) \end{cases} \tag{A.11}$$

The De Hoog method provides an estimate of the power series (A.11). The approximated solution $C(t,\gamma,T,n)$ is given by the following trigonometric rational approximation of the series (A.11):

$$C(t) = \frac{1}{T}\exp(\gamma t)\,\mathrm{Re}\left(\frac{A_{2n}}{B_{2n}}\right), \quad v(z,n) = \frac{A_{2n}}{B_{2n}} \tag{A.12}$$

where A_{2n} and B_{2n} are the successive convergents of the continued fraction estimator of the Fourier series. The continued fraction corresponding to the power series (A.11), and yielding an estimator $v(z,n)$, is

$$\begin{aligned} &u(z,n) = \sum_{k=0}^{2n} a_k z^k \\ &v(z,n) = d_0 / (1 + d_1 z / (1 + d_2 z / (1 + \cdots + d_{2n} z))) \\ &u(z,n) - v(z,n) = \mathrm{O}(z^{2n+1}) \end{aligned} \tag{A.13}$$

The continued fraction coefficients d_k are calculated with the QD algorithm as follows:

$$\begin{cases} A_k = A_{k-1} + d_n z A_{k-2} \\ B_k = B_{k-1} + d_n z B_{k-2} \end{cases} \quad , \quad k = 1,\ldots,2n \tag{A.14}$$

where

$$A_{-1} = 0\,, \quad A_0 = d_0\,, \quad B_{-1} = B_0 = 1$$
$$d_0 = a_0\,, \quad d_{2m-1} = -q_m^{(0)}\,, \quad d_{2m} = -e_m^{(0)}\,, \quad m = 1,\ldots,n$$
$$e_j^{(k)} = q_j^{(k+1)} - q_j^{(k)} + e_{j-1}^{(k+1)} \quad \text{for} \quad j = 1,\ldots,n \quad \text{with} \quad k = 0,\ldots,2(n-j)$$
$$q_j^{(k)} = q_{j-1}^{(k+1)}\, e_{j-1}^{(k+1)} \big/ e_{j-1}^{(k)} \quad \text{for} \quad j = 2,\ldots,n \quad \text{with} \quad k = 0,\ldots,2(n-j)-1$$
$$e_0^{(k)} = 0 \quad \text{for} \quad k = 0,\ldots,2n \quad \text{and} \quad q_1^{(k)} = a_{k+1}/a_k \quad \text{for} \quad k = 0,\ldots,2n-1$$
$$a_0 = \frac{1}{2}\hat{C}(\gamma) \quad , \qquad a_k = \hat{C}(s_k)$$

A double acceleration is obtained if for the last evaluation of the recurrence relations in (A.14), the term $d_{2n}z$ is replaced by R_{2n},

$$R_{2n}(z) = -h_{2n}[1 - \sqrt{1 + d_{2n}z/h_{2n}}]$$
$$h_{2n} = \frac{1}{2}[1 + z(d_{2n-1} - d_{2n})] \qquad ,$$

in which case the estimators A_{2n} and B_{2n} in (A.12) are replaced by

$$A'_{2n} = A_{2n-1} + R_{2n}A_{2n-2}$$
$$B'_{2n} = B_{2n-1} + R_{2n}B_{2n-2}$$

With the recurrence relations in (A.14), the calculation of the coefficients of the continued fractions is realized for a single value of z. For the convective-diffusive transport problems presented in the present work, we have found that the minimum n for an acceptable accuracy is 5, and that very accurate solutions can be obtained with $n = 12$, $0.8t_{max} \le T \le 1.0t_{max}$ and $E = 10^{-8}$–10^{-7}.

References

[1] Crump K.S. Numerical Inversion of Laplace Transforms Using Fourier Series Approximation. J Ass Comp Mech 1976;23(1):89–96.

[2] De Hoog F.R., Knight J.H., Stokes A.N. An improved method for numerical inversion of Laplace transforms. SIAM J Sci Stat Comput 1982;3:357–366.

[3] Diersch H.-J. About the difference between the convective form and the divergence form of the transport equation. FEFLOW Software White Papers Vol. 1, 2002, WASY GmbH Berlin, 119–129.

[4] Perrochet P. Finite hyper-elements: a 4D geometrical framework using covariant bases and metric tensors. Com. in Num. Meth. in Eng. 1995;11:525–534.

[5] Sudicky E.A. The Laplace transform Galerkin technique: A time-continuous finite element theory and application to mass transport in groundwater. Water Resour Res 1989;25(8):1833–1846.

[6] Saad Y. ILUT: A dual threshold incomplete ILU factorization. Linear Algebra Appl. 1994; 1:387–402.

[7] van der Vorst H.A. Bi-CGSTAB: A fast and smoothly converging variant of Bi-CG for the solution of non-symmetric linear systems. SIAM Journal on Scientific and Statistical Computing 1992;12:631–644.

APPENDIX B

A finite element formulation of the outlet gradient boundary condition for convective-diffusive transport problems

SUMMARY

A simple finite element formulation of the outlet gradient boundary condition is presented in the general context of convective-diffusive transport processes. Basically, the method is based on an upstream evaluation of the dependent variable gradient along open boundaries. Boundary normal unit vectors and gradient operators are evaluated using covariant bases and metric tensors, which allow handling finite elements of mixed dimensions. Even though the presented method has implications for many fields where diffusion processes are involved, discussion and illustrative examples address more particularly the framework of contaminant transport in porous media, in which the outlet gradient concentration is classically, but wrongly assumed to be zero.

KEY WORDS: finite elements; open boundary problem; upstream gradient evaluation; implicit Neumann condition

1. INTRODUCTION

Convective-diffusive transport simulations require the prescription of specific boundary conditions. Particularly the inlet and outlet limits of a given reservoir often lead to boundary condition effects on the behaviour of the conserved property. Boundary conditions are obtained from the flux conservation principle accounting for the fact that there cannot be accumulation at the boundary [1]. The outcome of the transported dependent variable is partially linked to the kind of boundary condition that is used at inflow and outflow boundaries of the dynamic system. The latter boundary, which in many cases corresponds to an open boundary of the reservoir, is often the most delicate to handle because the convective and dispersive quantities cannot be specified a priori. In practice, a direct consequence is that outflow boundaries are often subject to the assumption that the gradient is zero [2], with the consequence that the boundary is impermeable to the normal diffusive (or dispersive) fluxes. Usually, the assignment of such condition at outlet derives from technical advantages of resolution or intuitive choices, rather than from physical considerations and field observations. However, for finite reservoirs one must evaluate the influence of the exit boundary on the upstream behaviour of the transported property.

Various transport column experiments in porous media clearly showed that the physical meaning of convective flux permeable and dispersive flux impermeable limits is not always obvious [3-8]. More formally speaking, the representation of boundaries in mathematical continua put forward the presence of a finite and very small transition zone (Figure 1) within which the medium properties vary continuously, ensuring macroscopic mass balance and a self-consistent definition of the transported property [3], provided the fact that a total flux is prescribed. Integration of the mass conservation equation over the finite transition zone leads to continuity of the total flux [3]. As discussed by Nauman and Buffham [9], the formulation of boundaries permeable to both the convective and the dispersive parts of the total flux permits upgradient solute movement by dispersion. Parker [6] and Novakowski [7,8] provided experimental data supporting the meaning of a total flux formulation at outflow boundaries.

The conceptualization of a zero gradient or homogeneous Neumann condition at outlet boundaries, which is also called the ‘natural’ or also the Danckwerts condition [10], comes together with the assumption that the existence of a boundary layer at the outlet may not be realistic, and that

the effluent boundary should not influence the property within the medium. However, the macroscopic treatment of boundaries implies that continuity of the transported property at a microscopic level has poor relevance when volume-averaged equations are used. The irregularity of the medium structure at a microscopic level may alter the validity of the Danckwerts condition, which assumes that the volume-averaged property is equivalent to the flux-averaged property. When dispersion processes are included into transport phenomena, no clear physical evidence can support the idea of a zero concentration gradient at the interface between the considered medium and the surroundings. Moreover, the diffusive component of the flux at the outlet cannot be dropped without losing the generality of the transport equations. As example consider the common situations encountered in sub-surface hydrology, of groundwater volumes flowing out in reservoirs of free water like lakes. If the effluent concentration is perfectly mixed we might accept the possibility of no gradient within the transition zone. Such a situation may be encountered at ponds or mass accumulation areas due to extensive evaporation. But as long as smooth variability of parameters and conserved property can occur, a discontinuity may generally exist and permit non-zero gradient. Moreover, a property discontinuity at the outlet boundary has sense when diffusivity in the medium is important. The high diffusive effects, which are known to induce upstream mixing, could not be simulated if the gradient is forced to be zero.

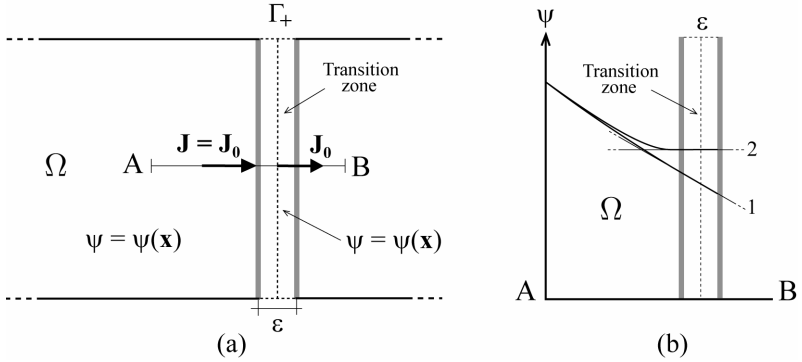

Figure 1. Finite transition zone representation of the out flowing open boundary Γ_+ of a medium Ω: (a) Continuity of the mass flux $\mathbf{J}$ within the transition zone of infinitesimal size ε, inside which the property $\psi = \psi(\mathbf{x})$ may vary continuously; (b) Profile showing the behaviour of the property when it varies continuously (1) and when gradient is forced to zero (2).

As will be shown in the following, the hypothetic behaviour of a property in the neighbourhood of outlet boundaries can be a priori estimated by an upstream formulation of the normal gradients, allowing the classical assumption of a zero gradient to be removed. In Section 2 we set the considered mathematical models and boundary conditions. In Section 3 we derive finite element formulations for the outlet normal diffusive flux vector. Finally, a theoretical illustration of the effects of the outlet boundary condition on the distribution of a solute concentration is given in Section 4. The proposed finite element formulation is expected to be applicable to a wide range of engineering modelling problems where gradient-type boundary conditions require special attention.

2. BASIC EQUATIONS

Let us consider a bounded domain $\Omega \subset \mathbb{R}^d$, $d = 1$, 2 or 3. The domain boundary $\partial\Omega = \Gamma_1 \cup \Gamma_2 \cup \Gamma_3$ is decomposed into portions with essential (Dirichlet) and natural (Neumann) boundary conditions on Γ_1 and Γ_2, respectively, with $\Gamma_3 \neq \emptyset$ being the open boundary part of $\partial\Omega$ (see Figure 2). The classical convection-diffusion-reaction equation for a scalar space-time property $\psi = \psi(\mathbf{x}, t)$ can be expressed in three dimensions by

$$\frac{\partial \psi}{\partial t} + \mathbf{v} \cdot \nabla\psi - \nabla \cdot \mathbf{D}\nabla\psi + \alpha\psi = f \qquad \text{in} \quad \Omega, \;\; t \in (0, T] \tag{1}$$

where t is time in the time interval of interest $(0, T]$, and where ∇ denotes the gradient, $\mathbf{v}$ is the advection velocity, $\mathbf{D}$ is a symmetric positive dispersion-diffusion tensor, α is a reaction function, and f stands for a source/sink term. Initial conditions and standard boundary conditions yielding solutions of (1) can be formalized by the following:

$$\psi = \psi_0 \qquad \text{in} \quad \Omega, \ t = 0 \qquad (2)$$

$$\psi = \psi_1 \qquad \text{on} \quad \Gamma_1 \qquad (3)$$

$$\mathbf{D}\nabla\psi \cdot \mathbf{n} + \gamma\psi = g \qquad \text{on} \quad \Gamma_2 \qquad (4)$$

Equation (3) is the classical Dirichlet boundary condition, with ψ_1 being a prescribed value of the unknown function ψ. Equation (4) has the form of a Robin boundary condition from which more specific Neumann and Cauchy type conditions can be derived. In Equation (4), $\mathbf{n}$ is a normal positive outward unit vector, γ and g are functions on Γ_2. The unknown term $\mathbf{D}\nabla\psi \cdot \mathbf{n}$ at open outflow boundaries is explicitly formulated in the following using a finite element analysis.

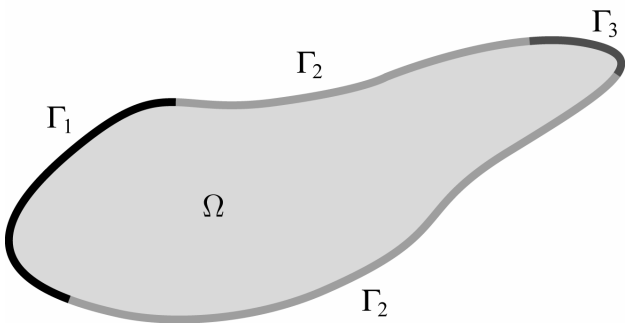

Figure 2. Schematic illustration of the considered single domain Ω and its boundary parts. Γ_1 and Γ_2 represent the boundary portions of $\partial\Omega$ where Dirichlet and Neumann conditions, respectively, are prescribed, and Γ_3 represents the open boundary portion of $\partial\Omega$.

3. FINITE ELEMENT FORMULATIONS

3.1. Weak form of the transport equation

In preparation to the formulation of normal gradients at open outflow boundaries, we proceed to formulate the transport equation in weak form. To obtain a weak form of the boundary value problem defined by the differential equation (1), with the initial conditions (2) and the boundary conditions (3) – (4), we consider the two following spaces of weighting functions η and solution functions ψ:

$$V = \left\{ \eta \in H^1(\Omega) \;\middle|\; \eta = 0 \ \text{ on } \Gamma_1 \right\}$$

$$S = \left\{ \psi \in H^1(\Omega) \;\middle|\; \psi = \psi_1 \text{ on } \Gamma_1 \right\}$$

where $H^1(\Omega)$ is the usual Sobolev space of functions which are square integrable, and which have square integrable first derivatives. The weak form is obtained by finding $\psi \in S$ such that for all $\eta \in V$

$$\left(\frac{\partial\psi}{\partial t}, \eta \right) + a(\psi, \eta) = \phi(\eta) \qquad \text{in} \quad \Omega \qquad (5)$$

with

$$\left(\frac{\partial\psi}{\partial t},\eta\right)=\int_\Omega \frac{\partial\psi}{\partial t}\eta\, d\Omega \tag{6}$$

$$a(\psi,\eta)=\int_\Omega [(\mathbf{v}\cdot\nabla\psi)\eta+\mathbf{D}\nabla\psi\nabla\eta]d\Omega-\int_{\Gamma_3}(\mathbf{D}\nabla\psi\cdot\mathbf{n})\eta\, d\Gamma+\int_\Omega \alpha\psi\eta\, d\Omega \tag{7}$$

$$\phi(\eta)=\int_\Omega f\eta\, d\Omega+\int_{\Gamma_2}(g-\gamma\psi)\eta\, d\Gamma \tag{8}$$

where use has been made of the Green's theorem for integrating by parts the diffusive term. A standard Galerkin finite element formulation is used to obtain a discrete problem of the weak form (5). The Dirichlet constraint in Equation (3) must be imposed on Γ_1 to Equation (8). The second term in Equation (7) exhibits the normal diffusive term $-\mathbf{D}\nabla\psi\cdot\mathbf{n}$ on the open boundary Γ_3. In the following, we propose an evaluation method of the diffusive term on the open boundary Γ_3. Usually, the outflow diffusive flux is not known necessarily, and one uses the homogeneous condition $-\mathbf{D}\nabla\psi\cdot\mathbf{n}=0$ as a way of truncating the physical domain at a substantial distance from the zone of interest.

3.2. Normal gradient evaluation along open boundaries

We evaluate the normal projection of the diffusive flux $\mathbf{J}_\mathrm{D}=-\mathbf{D}\nabla\psi$ approaching the open boundary Γ_3 from the interior of the considered domain Ω. The projection of the total diffusive flow leaving a boundary element e can be implicitly formulated as a function of the m nodal unknowns $\boldsymbol{\psi}=[\psi_1\,\psi_2\ldots\psi_m]^\mathrm{T}$ of the element:

$$Q_\mathrm{D}^e=\sum_{1\le n\le n_b}\int_{\Gamma_e}N_n\mathbf{J}_\mathrm{D}\cdot\mathbf{n}\,d\Gamma=\sum_{1\le n\le n_b}\int_{\Gamma_e}N_n\mathbf{D}\mathbf{B}^\mathrm{T}\boldsymbol{\psi}\cdot\mathbf{n}\,d\Gamma=\sum_{1\le n\le n_b}\mathbf{q}_n\boldsymbol{\psi} \tag{9}$$

with $\mathbf{B}^\mathrm{T}=\nabla\mathbf{N}^\mathrm{T}$ denoting the transpose of the gradient matrix, and n_b being the number of nodes of the considered element boundary. The nodal shape functions $\mathbf{N}=[N_1\,N_2\ldots N_m]^\mathrm{T}$ are defined with respect to the local coordinates s^k ($s^1=s, s^2=t, \ldots$), as well as their partial derivatives $\nabla\mathbf{N}$ and the differential surface (3-D) or length (2-D) $d\Gamma$. Equation (9) evaluates the contribution of element e to the control volumes of the n_b nodes on the element boundary Γ_e. The projected diffusive out flux at a node n is the product $\mathbf{q}_n\boldsymbol{\psi}$ of the vector $\mathbf{q}_n=[q_1\,q_2\ldots q_m]^\mathrm{T}$ with the vector of the element m nodal unknowns $\boldsymbol{\psi}$. The vector $\mathbf{q}_n$ stores the m components of the projected gradient vector $-\mathbf{D}\nabla()$ contributing to the out flux at node n. The components of $\mathbf{q}_n$ are only functions of the global coordinates of the m nodes, and of the medium diffusive property $\mathbf{D}$.

To solve Equation (9) one must identify the boundary normal vector $\mathbf{n}$, which is by definition orthogonal to the element edge or face Γ_e. The gradient matrix $\mathbf{B}^\mathrm{T}$ and the diffusion tensor $\mathbf{D}$ also require evaluation at the same points. To do so, it is convenient to operate in the local coordinate space. To describe these operations we make use of the geometrical framework of covariant bases and contravariant metric tensors, as described in books like Ciarlet [11], or more recently in the finite hyper-elements framework proposed by Perrochet [12]. This gradient generalized mapping method, which allows handling finite elements of mixed dimensions, is described in detail in Perrochet [12], and has been recently discussed by Juanes *et al.* [13]. We recall here the main results that are used in the present work, and restrict the method to the three dimensions of space only.

The gradient operator ∇ in a curvilinear element is expressed by the tensor product of the element covariant base $\mathbf{a}$ and the contravariant components of the gradient $\ddot{\nabla}$ in the curvilinear system. The contravariant components of $\ddot{\nabla}$ are themselves obtained by transformation of its covariant components ∇^* in the element orthogonal local system. From the covariant base

$$\mathbf{a} = \mathbf{x}^{\mathrm{T}}\nabla^{*}\mathbf{N} = [a_{ik}] \quad , \quad a_{ik} = \frac{\partial x^{i}}{\partial s^{k}} = \sum_{m}\frac{\partial N_{m}}{\partial s^{k}}x^{i}_{m} \quad , \quad k_{\max} \le i_{\max} \tag{10}$$

which is the differentiation of the global coordinates of the m nodes $\mathbf{x} = [x_{mi}] = [x^{i}_{m},\ i = 1, 2, 3]$ with respect to the k local coordinates s^{k}, and from the covariant metric tensor $\mathbf{h} = \mathbf{a}^{\mathrm{T}}\mathbf{a}$, the gradient matrix and the differential volume $d\Omega$ are fully defined according to

$$\mathbf{B}^{\mathrm{T}} = \nabla\mathbf{N}^{\mathrm{T}} = \mathbf{a}\,\mathbf{g}\nabla^{*}\mathbf{N}^{\mathrm{T}} = \mathbf{a}(\mathbf{a}^{\mathrm{T}}\mathbf{a})^{-1}\nabla^{*}\mathbf{N}^{\mathrm{T}} \tag{11}$$

$$d\Omega = \sqrt{\det\mathbf{h}}\,d\Omega^{*} \tag{12}$$

with the superscript * indicating operations in the local domain, and $\mathbf{g} = \mathbf{h}^{-1}$ being the contravariant metric tensor. The gradient operator in the curvilinear system is given by $\ddot{\nabla} = \mathbf{g}\nabla^{*}$.

Since the element boundary dimension is one lower than the dimension of the element, the differential $d\Omega$ is to be replaced by the differential $d\Gamma$ when evaluated at element boundaries. Thus, for a 2-D problem the differential $d\Gamma$ is a curve, and for a 3-D problem a surface. Considering the element boundary Γ_{e}, its normal unit vector $\mathbf{n}$ and differential $d\Gamma_{e}$ in the global space can be expressed by mapping the corresponding normal unit vector and differential in the local space:

$$\mathbf{n} = \frac{\mathbf{a}\,\mathbf{g}\,\mathbf{n}^{*}_{\xi}}{\left\|\mathbf{a}\,\mathbf{g}\,\mathbf{n}^{*}_{\xi}\right\|} \tag{13}$$

$$d\Gamma_{e} = \sqrt{\det\mathbf{h}}\,d\Gamma^{*}_{\xi} = \sqrt{\det\mathbf{h}}\,ds^{i}ds^{j} \tag{14}$$

with $\mathbf{n}^{*}_{\xi}$ denoting the outward unit vector in the local space, oriented in the ξ^{th} local coordinate direction, and $d\Gamma^{*}_{\xi}$ being the differential of the line or surface element in the local space, for which s^{ξ} is the orthogonal local coordinate. Using Equations (11), (13) and (14) we can formulate the normal dispersive flux $\mathbf{q}_{n}$ of Equation (9) for node n by the following:

$$\begin{aligned}\mathbf{q}_{n} &= \int_{\Gamma_{e}} N_{n}\mathbf{D}\mathbf{B}^{\mathrm{T}}\cdot\mathbf{n}\,d\Gamma_{e} = \int_{\Gamma_{e}} N_{n}[\mathbf{D}\mathbf{a}\mathbf{g}\nabla^{*}\mathbf{N}^{\mathrm{T}}]\cdot\mathbf{n}\sqrt{\det\mathbf{h}}\,d\Gamma^{*}_{\xi}\\ &= \lim_{s^{\xi}=\pm 1}\iint_{s^{k=i,j}} N_{n}[\mathbf{D}\mathbf{a}\mathbf{g}\nabla^{*}\mathbf{N}^{\mathrm{T}}]\cdot\frac{\mathbf{a}\,\mathbf{g}\,\mathbf{n}^{*}_{\xi}}{\left\|\mathbf{a}\,\mathbf{g}\,\mathbf{n}^{*}_{\xi}\right\|}\sqrt{\det\mathbf{h}}\,\mathrm{d}s^{i}\mathrm{d}s^{j}\\ &= \lim_{s^{\xi}=\pm 1}\iint_{s^{k=i,j}} N_{n}[\mathbf{D}\mathbf{a}\mathbf{g}\nabla^{*}\mathbf{N}^{\mathrm{T}}]\cdot(\mathbf{a}_{i}\times\mathbf{a}_{j})\mathrm{d}s^{i}\mathrm{d}s^{j}\end{aligned} \tag{15}$$

In Equation (15) $\mathbf{a}_{i}$ and $\mathbf{a}_{j}$ are the boundary tangential covariant vectors. Since integration is performed on the fictive one-dimension reduced element that belongs to the outlet boundary portion, each quantity is evaluated by fixing the ξ^{th} local coordinate. Once $\mathbf{q}_{n}$ is known for node n, it can easily be handled during the assembling procedure like a reaction term, with the result that the coefficients in line n of the global stiffness matrix $\mathbf{A} = [A_{i,j}]$ are updated according to the m coefficients of $\mathbf{q}_{n}$:

$$A_{i=n,j} = A_{i=n,j} - q_{j} \quad , \quad j = 1,\ldots,m \tag{16}$$

If one takes the example of Figure 3a, node 5 will induce a correction of line 5 in the global matrix, accounting for the contributions of the two elements which have node 5 in common. If the

edges 3−6 and 1−4 are supposed impervious, then node 4 and node 6 will receive contribution of their own element only.

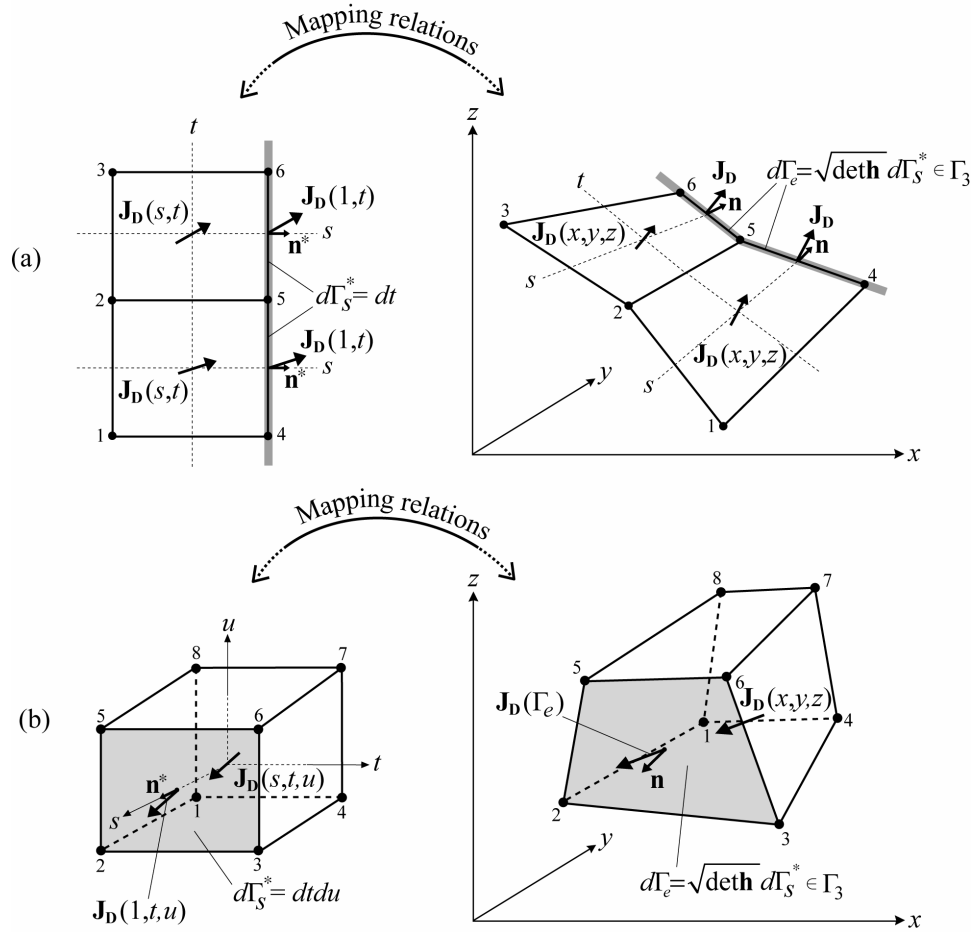

Figure 3. Examples of finite elements in the local space $(s,t,u) = (s^1, s^2, s^3)$ and the global space $(x,y,z) = (x^1, x^2, x^3)$: (a) 2-D Q_1 elements; (b) 3-D Q_1 element.

Equation (15) performs an upstream evaluation of the gradient projection along open boundaries. Therefore it comes with the implicit assumption of smooth spatial evolution of the gradients between the interior and the outside of the element. This assumption is coherent with the continuity of total flux at macroscopic level and continuity of the property at microscopic level at the boundary layer, but it also implies that beyond the medium boundary, in its neighbourhood, the gradient should be a continuation of the gradient inside the medium. The accuracy of the gradient evaluation will of course be dependent on the refinement at the boundary.

Since no specific value is prescribed for the dispersive out fluxes, and since their formulation is made implicitly, we may refer this formulation of flux condition on open boundaries to as *implicit Neumann* condition. A simple example with an explicit resolution of Equation (15) is given in the Appendix, for the specific case of bilinear Q_1 elements.

3. APPLICATION

To illustrate the proposed method of implementation of realistic gradient boundary condition on open boundaries, we simulate the transport of a conservative tracer resulting from a solute and water injection. The flow and convection-dispersion equations are solved within a 2-D (x, y) horizontal domain, $\Omega = [0, 500]\times[0, 500]$ (see Figure 4a), discretized using homogeneous bilinear Q_1 elements of size $\Delta x = \Delta y = 2\text{m}$. The boundary portion Γ_0 is a no-flow boundary ($\Gamma_2 = \Gamma_0$). Dirichlet type conditions are prescribed on the inlet boundaries Γ_- and Γ_w ($\Gamma_1 = \Gamma_- \cup \Gamma_w$), for both the flow and transport equations. A nil concentration is fixed on Γ_- and a unit concentration is fixed on Γ_w. The outlet boundary Γ_+ is the open boundary, $\Gamma_3 = \Gamma_+$. A hydraulic head difference of 5m is maintained constant between Γ_- ($H = 5\text{m}$) and Γ_+ ($H = 0\text{m}$), and $H = 3\text{m}$ on Γ_w. Flow is divergence-free, $\nabla \cdot \mathbf{v} = 0$. The hydraulic head field is given in Figure 4b, and a representation of the steady-state flow velocity field is given in Figure 4c, as well as a set of path lines in Figure 4d. The velocity norm varies between 0.8 and 1m/day in undisturbed regions.

The solutions of the convection-dispersion equation are tested for two situations: (*i*) with the classical homogeneous Neumann condition at outlet; (*ii*) with the *implicit Neumann* condition at outlet. The corresponding boundary value problems can be formalized by:

$$\begin{aligned}
&\frac{\partial C}{\partial t} + \mathbf{v}\cdot\nabla C - \nabla\cdot\mathbf{D}\nabla C = 0 && \text{in } \Omega \\
&C(\mathbf{x}, t=0) = 0 && \forall \mathbf{x} \in \Omega \\
&C = 1 && \text{on } \Gamma_w \\
&C = 0 && \text{on } \Gamma_- \\
&\text{and} \\
&(i)\quad \mathbf{D}\nabla C\cdot\mathbf{n} = 0 && \text{on } \Gamma_+ \cup \Gamma_0 \\
&\text{or} \\
&(ii)\quad \mathbf{D}\nabla C\cdot\mathbf{n} = 0 && \text{on } \Gamma_0 \\
&\quad\ \textit{implicit Neumann} && \text{on } \Gamma_+
\end{aligned} \tag{17}$$

In Equation (17), C is relative concentration [−], $\mathbf{v}$ is the velocity field vector [m/s], and $\mathbf{D}$ [m^2/s] is the time-independent macro-dispersion tensor

$$\mathbf{D} = (\alpha_\text{L} - \alpha_\text{T})\frac{\mathbf{v}\otimes\mathbf{v}}{\|\mathbf{v}\|} + \alpha_\text{T}\|\mathbf{v}\|\mathbf{I} + D_\text{m}\mathbf{I} \tag{18}$$

where α_L [m] and α_T [m] are the longitudinal and transversal coefficients of dispersivity, respectively, D_m is the coefficient of molecular diffusion [m^2/s], and $\mathbf{I}$ is the identity matrix.
The time discretization for the simulations makes use of a standard Crank–Nicholson finite-difference scheme with a constant time-step $\Delta t = 1\text{day}$.

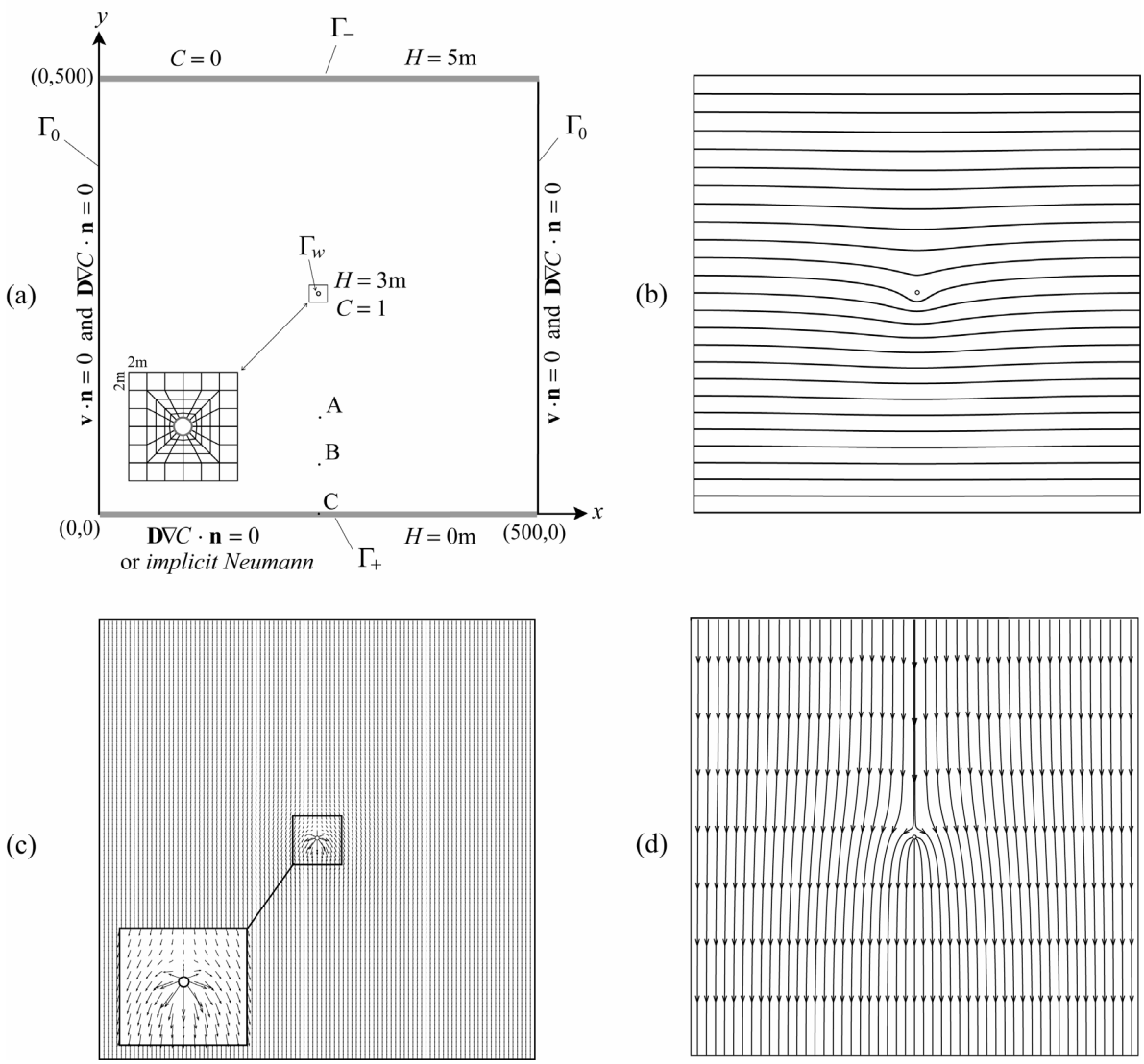

Figure 4. Definition of the 2-D (x, y) flow and chemical transport problem: (a) Domain definition with its specific boundary portions and associated boundary conditions for flow and transport. A zoom of the finite element mesh around Γ_w is given. The points $A = (250, 100)$, $B = (250, 50)$ and $C = (250, 0)$ are three observation points; (b) Hydraulic heads distribution with 0.2m increments; (c) Pore velocity field; (d) Path line representation of the velocity field.

The distribution of concentration in space at time $t = 300$days is given in Figure 5. Four levels of dispersion are tested, by keeping the ratio α_L/α_T equal to 10, and with a uniform coefficient of molecular diffusion $D_m = 2.3\times10^{-9}$ m^2/s ($\sim$ effective self-diffusion of water). The effect of the classical homogeneous Neumann boundary condition at outlet is clearly apparent; the iso-contours of concentration approaching $\Gamma_3 = \Gamma_+$ are forced to become perpendicular to the boundary. Without this constraint (with *implicit Neumann* on Γ_3), the same iso-contours naturally intercept the outlet boundary. The effect of the homogeneous Neumann condition on Γ_3 on the calculated concentration distribution becomes important when dispersion is increased. A direct consequence of this condition is an artificial mass accumulation at the outlet surroundings.

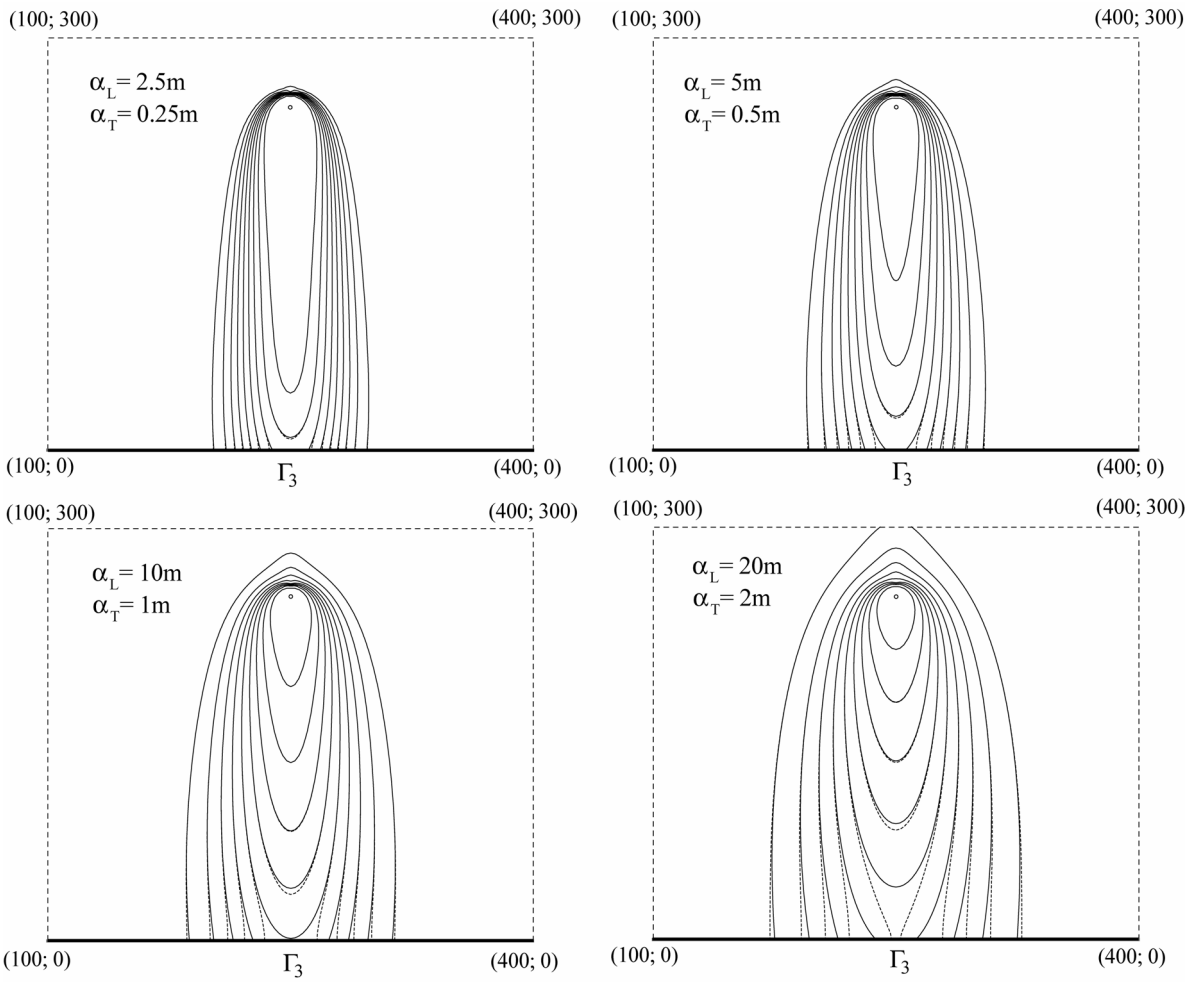

Figure 5. Compared transport solutions at time $t = 300$days, for four levels of dispersion (with $D_m = 2.3\times10^{-9}$ m^2/s). The solid lines are the solution with homogeneous Neumann condition at outlet, and the dashed lines are the solution with *implicit Neumann* condition at outlet. Iso-contours of concentration from 0.1 to 0.9 with 0.1 of increment.

Observed breakthrough curves are given in Figure 6, at the three observation points A, B and C (see Figure 4a for their location). They show the effect of the homogeneous Neumann condition on the temporal evolution of concentration, at the outlet boundary and upstream inside the medium. When dispersion increases, the homogeneous Neumann condition modifies significantly the behaviour of concentration at the outlet boundary and within the flow domain. For the maximum tested dispersion case ($\alpha_L = 20$m, $\alpha_T = 0.2$m), the effect of this condition is effective until 100m upstream the outlet boundary (point A). The un-natural mass accumulation at the outlet surroundings induced by the homogeneous Neumann condition on Γ_+, is well-visible when one follows the evolution of points A, B and C against increasing dispersion. For the lowest dispersion case (Figure 6, up), the influence of the homogeneous Neumann condition does not reach point B nor A. When dispersion is increased (Figure 6, middle and down), the time-series recorded at points B and C tend to become similar.

Sensitivity analysis showed that important changes in the coefficient of molecular diffusion (from 10^{-9} to 10^{-6} m^2/s) do not change the concentration distribution significantly. The effect on transport solutions of the homogeneous Neumann condition prescribed on open boundaries can thus be expected to be important in systems with significant mechanical dispersion.

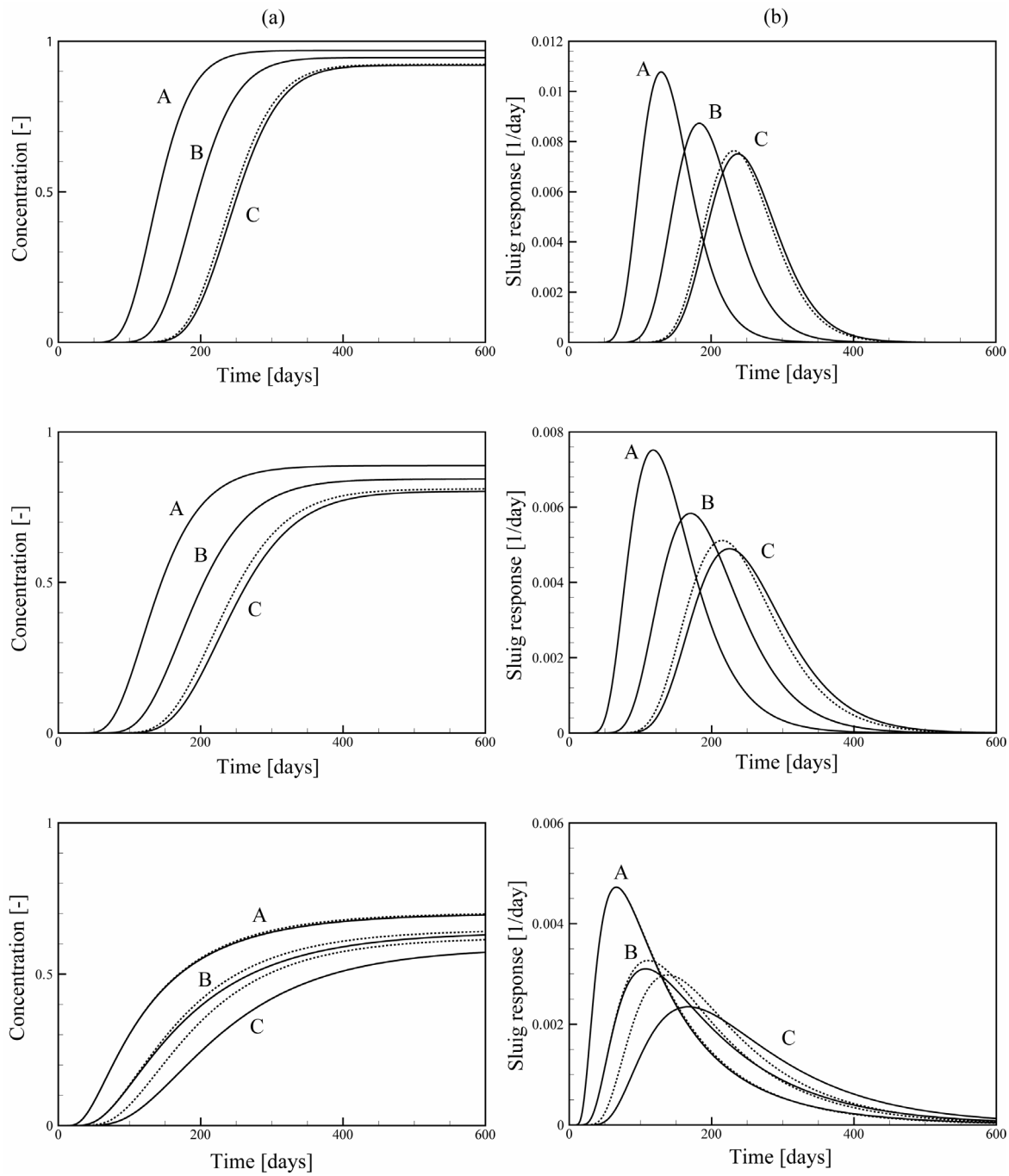

Figure 6. Compared transport solutions at the three observation points A, B and C (see Figure 4a for their location), for three levels of dispersion. From up to down: $\alpha_L = 2.5$m, $\alpha_L = 10$m, $\alpha_L = 20$m. The ratio α_L/α_T is fixed to 10. The solid lines are the solution with homogeneous Neumann condition at outlet, and the dashed lines are the solution with *implicit Neumann* condition at outlet. (a) Observed breakthrough curves; (b) Derivatives of the observed time series (slug problem equivalent solutions).

4. FINAL REMARKS

The proposed outlet gradient estimation method presents the advantage that it can directly be incorporated within an element matrix integration procedure, as it requires no more than the evaluation of the classical functions. The method is straightforward for one-, two- and three-dimensional medium configurations when using covariant basis and contravariant metric tensors, which allow working simultaneously with elements of mixed dimensions. Extension of the

presented finite element formulation to finite volume or finite difference schemes can also be considered.

This simple computational procedure can be useful to solve a large series of convective-dispersive problems, by treating outflow limits without taking the risk of making physically inconsistent hypothesis on the property behaviour at outlet, like the classical assumption of convective flux permeable and dispersive flux impermeable boundaries. For many transport settings occurring in finite reservoirs, like e.g. heat, mass, or residence time transport processes, the classical arbitrary homogeneous Neumann condition at outlet boundaries is therefore not needed anymore.

APPENDIX

An explicit resolution of Equation (15) is detailed below, using a plane domain in the Cartesian coordinate system (x, y, z). The system can be assimilated to a fracture in the three dimensional space, and is discretized using three bilinear Q_1 elements. In Figure A1, the geometry, the node numbering and the boundary conditions are indicated, as well as the nodal shape functions. The elements node spacing is fixed to Δx in the x direction and Δy in the y direction. We want to solve the following steady-state equation:

$$-\mathbf{v}\cdot\nabla\psi + \nabla\cdot\mathbf{D}\nabla\psi + 1 = 0 \qquad \text{(A1)}$$

where $\psi = \psi(x, y, z)$. The velocity $\mathbf{v} = [v_x\ v_y\ v_z]$ is assumed to be uniform in the fracture plane, with same intensity in the x and z directions ($v_x = v_z = v$ and $v_y = 0$), with the result that the system behaviour will be one-dimensional in each element. Dispersion is assumed to be only controlled by molecular diffusion $\mathbf{D} = D_m\mathbf{I}$, $\mathbf{I}$ being the identity matrix. At the two upstream nodes a Dirichlet condition is prescribed with a constant value of 0 (Γ_1 = edge 1−2 in Figure A1), $\psi(0, y, 0) = 0$. The boundary portion Γ_2 is a no-flow boundary, $\partial\psi/\partial\mathbf{n} = 0$ and $\mathbf{v}\cdot\mathbf{n} = 0$.

This problem is known as the average residence time transport, for which the exact 1-D solution $\psi(r) = r/v$ in the curvilinear coordinate r of the element (in the velocity direction) is dispersion independent. The above differential equation is discretized and solved for the cases $\partial\psi/\partial\mathbf{n} = 0$ and $\partial\psi/\partial\mathbf{n} \neq 0$ at the outlet limit (edge 7−8 in Figure A1), which is the open boundary Γ_3 of the system.

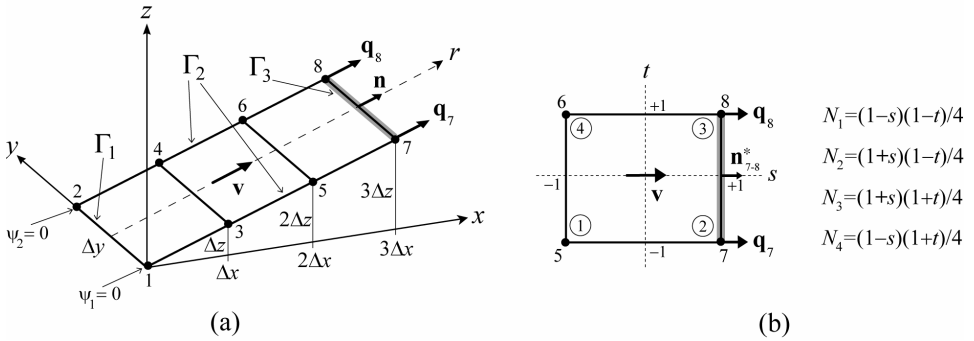

Figure A1. Discretized 2-D domain in the global Cartesian space coordinates (x, y, z): (a) Geometry made of three bilinear Q_1 elements in the global space with prescribed Dirichlet boundary conditions at nodes 1 and 2, the numbers 1 to 8 relating the node numbering; (b) Bilinear Q_1 element in the local space (s, t) with the numbers 1 to 4 into circles corresponding to the node numbering in the local space.

According to Equation (10), the element covariant base is

$$\mathbf{a}=\begin{bmatrix}\mathbf{a}_1 & \mathbf{a}_2\end{bmatrix}=\begin{bmatrix}\dfrac{\partial x}{\partial s} & \dfrac{\partial x}{\partial t}\\ \dfrac{\partial y}{\partial s} & \dfrac{\partial y}{\partial t}\\ \dfrac{\partial z}{\partial s} & \dfrac{\partial z}{\partial t}\end{bmatrix}=\begin{bmatrix}x_1 & x_2 & x_3 & x_4\\ y_1 & y_2 & y_3 & y_4\\ z_1 & z_2 & z_3 & z_4\end{bmatrix}\begin{bmatrix}\dfrac{\partial N_1}{\partial s} & \dfrac{\partial N_1}{\partial t}\\ \dfrac{\partial N_2}{\partial s} & \dfrac{\partial N_2}{\partial t}\\ \dfrac{\partial N_3}{\partial s} & \dfrac{\partial N_3}{\partial t}\\ \dfrac{\partial N_4}{\partial s} & \dfrac{\partial N_4}{\partial t}\end{bmatrix}=\begin{bmatrix}0 & \Delta x & \Delta x & 0\\ 0 & 0 & \Delta y & \Delta y\\ 0 & \Delta z & \Delta z & 0\end{bmatrix}\begin{bmatrix}-\dfrac{1-t}{4} & -\dfrac{1-s}{4}\\ \dfrac{1-t}{4} & -\dfrac{1+s}{4}\\ \dfrac{1+t}{4} & \dfrac{1+s}{4}\\ -\dfrac{1+t}{4} & \dfrac{1-s}{4}\end{bmatrix}$$

$$=\frac{1}{2}\begin{bmatrix}\Delta x & 0\\ 0 & \Delta y\\ \Delta z & 0\end{bmatrix} \tag{A2}$$

for the three elements of Figure A1. The covariant metric tensor **h** reads

$$\mathbf{h}=\mathbf{a}^{\mathrm{T}}\mathbf{a}=\frac{1}{4}\begin{bmatrix}\Delta x^2+\Delta z^2 & 0\\ 0 & \Delta y^2\end{bmatrix}\quad,\quad\sqrt{\det\mathbf{h}}=\frac{\Delta y}{4}\sqrt{\Delta x^2+\Delta z^2} \tag{A3}$$

from which the contravariant metric tensor **g** becomes

$$\mathbf{g}=\mathbf{h}^{-1}=\begin{bmatrix}\dfrac{4}{\Delta x^2+\Delta z^2} & 0\\ 0 & \dfrac{4}{\Delta y^2}\end{bmatrix} \tag{A4}$$

The normal dispersive fluxes at the two outlet nodes are calculated by straightforward application of Equation (15) in the local coordinates (s, t):

$$\begin{aligned}\mathbf{q}_{n=7,8}&=\lim_{s=+1}\int_{-1}^{+1}N_n\mathbf{D}\mathbf{B}^{\mathrm{T}}\cdot\mathbf{n}_{7-8}\sqrt{\det\mathbf{h}}\,d\Gamma_s^*=\lim_{s=+1}\int_{-1}^{+1}N_n\mathbf{D}\mathbf{B}^{\mathrm{T}}\cdot\mathbf{n}_{7-8}\left\|\mathbf{a}_2\right\|dt\\&=\lim_{s=+1}\int_{-1}^{+1}N_n\mathbf{D}\mathbf{B}^{\mathrm{T}}\cdot\mathbf{n}_{7-8}\frac{\Delta y}{2}dt\end{aligned} \tag{A5}$$

with $\mathbf{n}_{7\text{-}8}$ the unit vector normal to edge 7−8. The local coordinate s is fixed at +1 to perform integration on edge 7−8. In Equation (A5), $\sqrt{\det\mathbf{h}}$ is relative to edge 7−8 and equals the half of Δy. Enforcing Equation (13), the normal vector of edge 7−8 is

$$\mathbf{n}_{7-8}=\frac{\mathbf{a}\mathbf{g}\,\mathbf{n}_s^*}{\left\|\mathbf{a}\mathbf{g}\,\mathbf{n}_s^*\right\|}=\frac{\sqrt{\Delta x^2+\Delta z^2}}{2}\begin{bmatrix}\dfrac{2\Delta x}{\Delta x^2+\Delta z^2} & 0\\ 0 & \dfrac{2}{\Delta y}\\ \dfrac{2\Delta z}{\Delta x^2+\Delta z^2} & 0\end{bmatrix}\begin{bmatrix}1\\0\end{bmatrix}=\begin{bmatrix}\dfrac{\Delta x}{\sqrt{\Delta x^2+\Delta z^2}}\\ 0\\ \dfrac{\Delta z}{\sqrt{\Delta x^2+\Delta z^2}}\end{bmatrix} \tag{A6}$$

Following Equation (11) the product $\mathbf{D}\mathbf{B}^{\mathrm{T}}$ results in

$$\mathbf{DB}^{\mathrm{T}} = \mathbf{Dag}\nabla^{*}\mathbf{N}^{\mathrm{T}} = \frac{D_{\mathrm{m}}}{2}\begin{bmatrix} -\dfrac{\Delta x(1-t)}{\Delta x^2+\Delta z^2} & \dfrac{\Delta x(1-t)}{\Delta x^2+\Delta z^2} & \dfrac{\Delta x(1+t)}{\Delta x^2+\Delta z^2} & -\dfrac{\Delta x(1+t)}{\Delta x^2+\Delta z^2} \\ -\dfrac{1-s}{\Delta y} & -\dfrac{1+s}{\Delta y} & \dfrac{1+s}{\Delta y} & \dfrac{1-s}{\Delta y} \\ -\dfrac{\Delta z(1-t)}{\Delta x^2+\Delta z^2} & \dfrac{\Delta z(1-t)}{\Delta x^2+\Delta z^2} & \dfrac{\Delta z(1+t)}{\Delta x^2+\Delta z^2} & -\dfrac{\Delta z(1+t)}{\Delta x^2+\Delta z^2} \end{bmatrix} \tag{A7}$$

Inserting the above results into Equation (A5) and simplifying by taking the limit $s = +1$ yields

$$\mathbf{q}_7 = \frac{\Delta y D_{\mathrm{m}}}{3\sqrt{\Delta x^2+\Delta z^2}}\begin{bmatrix} -1 & 1 & \dfrac{1}{2} & -\dfrac{1}{2} \end{bmatrix}^{\mathrm{T}} \quad \text{and} \quad \mathbf{q}_8 = \frac{\Delta y D_{\mathrm{m}}}{3\sqrt{\Delta x^2+\Delta z^2}}\begin{bmatrix} -\dfrac{1}{2} & \dfrac{1}{2} & 1 & -1 \end{bmatrix}^{\mathrm{T}} \tag{A8}$$

For the sake of simplicity we consider the case $\Delta z = \Delta y = \Delta x$. The element stiffness matrices are found enforcing

$$\begin{aligned} \mathbf{A}^{e} &= \int_{-1}^{+1}\int_{-1}^{+1}[\mathbf{BDB}^{\mathrm{T}} + \mathbf{Nv}\cdot\mathbf{B}^{\mathrm{T}}]\sqrt{\det\mathbf{h}}\,dsdt \\ &= \frac{D_{\mathrm{m}}}{\sqrt{2}}\begin{bmatrix} 1-\dfrac{v\Delta x}{3D_{\mathrm{m}}} & \dfrac{v\Delta x}{3D_{\mathrm{m}}} & -\dfrac{1}{2}+\dfrac{v\Delta x}{6D_{\mathrm{m}}} & -\dfrac{1}{2}-\dfrac{v\Delta x}{6D_{\mathrm{m}}} \\ -\dfrac{v\Delta x}{3} & 1+\dfrac{v\Delta x}{3D_{\mathrm{m}}} & -\dfrac{1}{2}+\dfrac{v\Delta x}{6D_{\mathrm{m}}} & -\dfrac{1}{2}-\dfrac{v\Delta x}{6D_{\mathrm{m}}} \\ -\dfrac{1}{2}-\dfrac{v\Delta x}{6D_{\mathrm{m}}} & -\dfrac{1}{2}+\dfrac{v\Delta x}{6D_{\mathrm{m}}} & 1+\dfrac{v\Delta x}{3D_{\mathrm{m}}} & -\dfrac{v\Delta x}{3D_{\mathrm{m}}} \\ -\dfrac{1}{2}-\dfrac{v\Delta x}{6D_{\mathrm{m}}} & -\dfrac{1}{2}+\dfrac{v\Delta x}{6D_{\mathrm{m}}} & \dfrac{v\Delta x}{3D_{\mathrm{m}}} & 1-\dfrac{v\Delta x}{3D_{\mathrm{m}}} \end{bmatrix} \end{aligned} \tag{A9}$$

After assembling of the three elements and reduction of the system accounting for the Dirichlet constraints $\psi_1 = \psi_2 = 0$, the global stiffness matrix is

$$\mathbf{A} = \frac{D_m}{\sqrt{2}}\begin{bmatrix} 2 & -1 & \dfrac{v\Delta x}{3D_m} & -\dfrac{1}{2}+\dfrac{v\Delta x}{6D_{\mathrm{m}}} & 0 & 0 \\ -1 & 2 & -\dfrac{1}{2}+\dfrac{v\Delta x}{6D_{\mathrm{m}}} & \dfrac{v\Delta x}{3D_m} & 0 & 0 \\ -\dfrac{v\Delta x}{3D_m} & -\dfrac{1}{2}-\dfrac{v\Delta x}{6D_{\mathrm{m}}} & 2 & -1 & \dfrac{v\Delta x}{3D_m} & -\dfrac{1}{2}+\dfrac{v\Delta x}{6D_{\mathrm{m}}} \\ -\dfrac{1}{2}-\dfrac{v\Delta x}{6D_{\mathrm{m}}} & -\dfrac{v\Delta x}{3D_m} & -1 & 2 & -\dfrac{1}{2}+\dfrac{v\Delta x}{6D_{\mathrm{m}}} & \dfrac{v\Delta x}{3D_m} \\ 0 & 0 & -\dfrac{v\Delta x}{3D_m} & -\dfrac{1}{2}-\dfrac{v\Delta x}{6D_{\mathrm{m}}} & 1+\dfrac{v\Delta x}{3D_{\mathrm{m}}} & -\dfrac{1}{2}+\dfrac{v\Delta x}{6D_{\mathrm{m}}} \\ 0 & 0 & -\dfrac{1}{2}-\dfrac{v\Delta x}{6D_{\mathrm{m}}} & -\dfrac{v\Delta x}{3D_m} & -\dfrac{1}{2}+\dfrac{v\Delta x}{6D_{\mathrm{m}}} & 1+\dfrac{v\Delta x}{3D_{\mathrm{m}}} \end{bmatrix} \tag{A10}$$

Taking Equation (A8) to correct the lines of **A** results in

$$\mathbf{A}_c = \frac{D_m}{\sqrt{2}}\begin{bmatrix} 2 & -1 & \frac{v\Delta x}{3D_m} & -\frac{1}{2}+\frac{v\Delta x}{6D_{\mathrm{m}}} & 0 & 0 \\ -1 & 2 & -\frac{1}{2}+\frac{v\Delta x}{6D_{\mathrm{m}}} & \frac{v\Delta x}{3D_m} & 0 & 0 \\ -\frac{v\Delta x}{3D_m} & -\frac{1}{2}-\frac{v\Delta x}{6D_{\mathrm{m}}} & 2 & -1 & \frac{v\Delta x}{3D_m} & -\frac{1}{2}+\frac{v\Delta x}{6D_{\mathrm{m}}} \\ -\frac{1}{2}-\frac{v\Delta x}{6D_{\mathrm{m}}} & -\frac{v\Delta x}{3D_m} & -1 & 2 & -\frac{1}{2}+\frac{v\Delta x}{6D_{\mathrm{m}}} & \frac{v\Delta x}{3D_m} \\ 0 & 0 & \frac{1}{3}-\frac{v\Delta x}{3D_m} & -\frac{1}{3}-\frac{v\Delta x}{6D_{\mathrm{m}}} & \frac{2}{3}+\frac{v\Delta x}{3D_m} & -\frac{2}{3}+\frac{v\Delta x}{6D_{\mathrm{m}}} \\ 0 & 0 & -\frac{1}{3}-\frac{v\Delta x}{6D_{\mathrm{m}}} & \frac{1}{3}-\frac{v\Delta x}{3D_m} & -\frac{2}{3}+\frac{v\Delta x}{6D_{\mathrm{m}}} & \frac{2}{3}+\frac{v\Delta x}{3D_{\mathrm{m}}} \end{bmatrix} \tag{A11}$$

Inversion of the non-corrected matrix **A** and assembling of the global load vector **f** accounting for the unit source term, followed by the matrix-vector operation $\mathbf{A}^{-1}\mathbf{f}$ yields the diffusion-dependent solution

$$\boldsymbol{\psi} = \mathbf{A}^{-1}\frac{\Delta x^2}{\sqrt{2}}\begin{bmatrix}1\\1\\1\\1\\\frac{1}{2}\\\frac{1}{2}\end{bmatrix} = \frac{\Delta x}{v}\begin{bmatrix}c_1\\c_1\\2c_2\\2c_2\\3c_3\\3c_3\end{bmatrix} \quad , \quad \begin{aligned} c_1 &= \frac{v^3\Delta x^3 + 2v^2\Delta x^2 D_{\mathrm{m}} + 5v\Delta x D_{\mathrm{m}}^2}{(v\Delta x + D_{\mathrm{m}})^3} \\ c_2 &= \frac{v^3\Delta x^3 + 3v^2\Delta x^2 D_{\mathrm{m}} + 4v\Delta x D_{\mathrm{m}}^2}{(v\Delta x + D_{\mathrm{m}})^3} \\ c_3 &= \frac{v^3\Delta x^3 + 8v^2\Delta x^2 D_{\mathrm{m}}/3 + 3v\Delta x D_{\mathrm{m}}^2}{(v\Delta x + D_{\mathrm{m}})^3} \end{aligned} \tag{A12}$$

which is obviously not correct, while inversion of the corrected matrix $\mathbf{A}_c$ produces the diffusion-independent correct solution

$$\boldsymbol{\psi}_c = \mathbf{A}_c^{-1}\mathbf{f} = \frac{\Delta x}{v}\begin{bmatrix}1 & 1 & 2 & 2 & 3 & 3\end{bmatrix}^{\mathrm{T}} \tag{A13}$$

In Figure A2 the difference between the two schemes is illustrated. The error induced by the homogeneous Neumann condition at outlet naturally increases with dispersion.

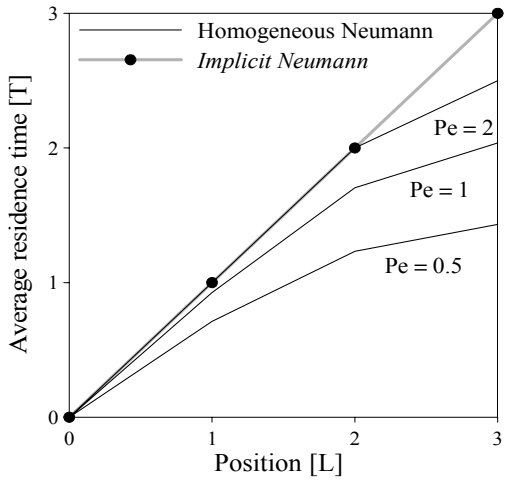

Figure A2. Convective-diffusive transport of the average residence time within a fracture in the 3-D space. Solution for three Péclet numbers $\mathrm{Pe} = v\Delta r/D_{\mathrm{m}}$ (indicated on the figure), for the case $\Delta x = \Delta y = \Delta z = 1/\sqrt{2}$, $\mathbf{v} = [1/\sqrt{2}\ \ 0\ \ 1/\sqrt{2}]$, $\Delta r = \sqrt{(\Delta x^2 + \Delta z^2)}$, $v = \|\mathbf{v}\|$.

REFERENCES

1. Kreft A. On the boundary conditions of flow through porous media and conversion of chemical flow reactors. *Bull. Acad. Pol., Ser. Sci. Tech.* 1981; **29**(9-10): 35−43.
2. Galeati G, Gambolatti G. On the boundary conditions and point sources in the finite element integration of the transport equation. *Water Resour. Res.* 1989; **25**(5): 847−856.
3. Parker J.C., van Genuchten M.Th. Flux-averaged and volume-averaged concentrations in continuum approaches to solute transport. *Water Resour. Res.* 1984; **20**(7): 866−872.
4. Schwartz R.C., McInnes K.J., Juo A.S.R., Wilding L.P. Boundary effects on solute transport in finite soil columns. *Water Resour. Res.* 1999; **35**(3): 671−681.
5. Kreft A., Zuber A. Comments on "Flux-Averaged and Volume-Averaged Concentrations in Continuum Approaches to Solute Transport" by J. C. Parker and M. Th. van Genuchten. *Water Resour. Res.* 1986; **22**(7): 1157−1158.
6. Parker J.C. Analysis of solute transport in column tracer studies. *Soil Sci. Soc. Am. J.* 1984; **48**: 719−724.
7. Novakowski K.S. An evaluation of boundary conditions for one dimensional solute transport 1. Mathematical development. *Water Resour. Res.* 1992; **28**: 2399−2410.
8. Novakowski K.S. An evaluation of boundary conditions for one dimensional solute transport 2. Column experiments. *Water Resour. Res.* 1992; **28**: 2411−2423.
9. Nauman E.B., Buffham B.A. Mixing in Continuous Flow Systems. Wiley: New York, 1983; 299 pp.
10. Danckwerts P.V. Continuous flow systems. *Chem. Eng. Sci.* 1953; **2**: 1−13.
11. Ciarlet P.G. The Finite Element Method for Elliptic Problems. North-Holland Publishing Company, 1978; Vol. 4, 530 pp.
12. Perrochet P. Finite hyper-elements: a 4D geometrical framework using covariant bases and metric tensors. *Communications in Numerical Methods in Engineering* 1995; **11**: 525−534.
13. Juanes R., Samper J., Molinero J. A general and efficient formulation of fractures and boundary conditions in the finite element method. *International Journal for Numerical Methods in Engineering* 2002; **54**: 1751−1774.